

# Electromagnetic Quantum Field Theory on Kerr-Newman Black Holes

by

Marc Casals i Casanellas

A dissertation submitted to  
the National University of Ireland  
in partial fulfilment of the requirements  
of the degree of Philosophiae Doctor

Department of Mathematical Physics  
Faculty of Science  
University College Dublin

February 23, 2004

**Supervisor:** Professor Adrian C. Ottewill

**Head of Department:** Professor Adrian C. Ottewill

## Abstract

We study classical and quantum aspects of electromagnetic perturbations on black hole space-times. We develop an elegant formalism introduced by Wald, which sets up the theory of linear perturbations in a Type-D background in a compact and transparent manner. We derive natural expressions for the electromagnetic potential in the ingoing and outgoing gauges in terms of the single Newman-Penrose (NP) scalar  $\phi_0$ . This enables the formulation of the quantum theory of the electromagnetic field as that of a complex scalar field. Unfortunately, the field equations for  $\phi_0$  in the Kerr-Newman background are non-separable, except in the Reissner-Nordström limit.

We study the separable spin-1, classical field equations obeyed by the NP scalars  $\phi_{\pm 1}$  in the Kerr-Newman background and find, for various limits, the asymptotic behaviour of the radial and angular solutions. We correct and build on a study by Breuer, Ryan and Waller to find a uniformly valid asymptotic behaviour for large frequency of the angular solutions and the eigenvalues. We complement our asymptotic analysis with the numerically obtained solution of the radial and angular differential equations.

We follow Candelas, Chrzanowski and Howard (CCH) in their canonical quantization of the electromagnetic potential and field. We study the form of the renormalized stress-energy tensor (RSET) in the past Boulware vacuum close to the horizon. In contrast with a calculation in CCH, its leading order behaviour close to the horizon corresponds to minus the stress tensor of a thermal distribution at the Hawking temperature rigidly rotating with the horizon. We prove that expressions given by CCH for the expectation value of the stress tensor in the past Boulware, past Unruh and  $|CCH^-\rangle$  states lead to a lack of symmetry under parity. We show that the origin of this asymmetry is the non-symmetrization of the quantum operators in the derivation of the expressions in CCH. We give the correct expressions, and present a detailed analysis of the resulting RSETs.

---

*Als meus avis*

## Agraïments/Acknowledgements

I wish to thank the following people, who have helped me illuminate black holes.

My supervisor, Professor Adrian Ottewill, for offering me the invaluable opportunity to take up a job that I relish doing -research in physics, and also for his ingenious advice throughout. All the other members of staff and postgraduates in the Mathematical Physics and the Mathematics departments. Gavin Duffy deserves an outstanding mention for his endless, unselfish help. I am also particularly indebted to Michael Mackey and Thomas Unger for their assistance in computer-related issues. I wish to thank Professor Valeri P. Frolov for useful comments.

All my friends, with whom I have enjoyed many dreamy conversations on merry nights. In particular, my girlfriend Siobhán, who has illuminated me on many sunny nights.

Aquesta tesi està dedicada a tots els meus avis, que amb el seu amor m'han fet veure les estrelles. Estic agraït als meus pares per haver-me transmès la curiositat d'entrar dins de forats negres i l'habilitat de saber-ne sortir. A tots els meus amics, amb qui m'he estrellat moltes nits.

This research was financially supported in part by Enterprise Ireland.

# Contents

<b>Overview</b>	<b>1</b>
<b>1 Introduction</b>	<b>5</b>
1.1 Tetrad/Newman-Penrose formalism . . . . .	5
1.2 The Kerr-Newman space-time . . . . .	13
1.3 Orthonormal and null tetrads . . . . .	23
1.4 Black hole thermodynamics . . . . .	29
1.5 Physical phenomena associated with the ergosphere . . . . .	32
<b>2 Field equations</b>	<b>35</b>
2.1 Introduction . . . . .	35
2.2 Wald's formalism . . . . .	37
2.3 Maxwell equations and gauge invariance . . . . .	38
2.4 Wald's formalism for spin-1 . . . . .	41
2.5 Wald's formalism for spin-1 in the Kerr-Newman background . . .	49
2.6 Equation for $\phi_0$ . . . . .	51
2.7 The Teukolsky equation and the homogeneous potential solution .	54

2.8	Field components and Teukolsky-Starobinskiĭ identities . . . . .	63
<b>3</b>	<b>Radial solution</b>	<b>67</b>
3.1	Introduction . . . . .	67
3.2	Short-range potentials . . . . .	69
3.3	Numerical method . . . . .	83
3.4	Numerical results . . . . .	92
3.5	Asymptotics close to the horizon . . . . .	93
3.6	Asymptotics for small frequency . . . . .	102
<b>4</b>	<b>Spin-weighted spheroidal harmonics</b>	<b>109</b>
4.1	Introduction . . . . .	109
4.2	General properties . . . . .	119
4.3	Numerical method . . . . .	122
4.4	Numerical results . . . . .	129
<b>5</b>	<b>High frequency asymptotics for the angular solution</b>	<b>133</b>
5.1	Introduction . . . . .	133
5.2	Boundary layer theory . . . . .	136
5.3	Inner solutions . . . . .	138
5.4	Outer solution . . . . .	140
5.5	Matching the solutions . . . . .	142
5.6	Calculation of $\gamma$ . . . . .	150
5.7	Numerical method . . . . .	154

5.8	Numerical results . . . . .	158
<b>6</b>	<b>Stress-energy tensor</b>	<b>173</b>
6.1	Introduction . . . . .	173
6.2	Quantization of the electromagnetic potential/field . . . . .	177
6.3	Boulware vacuum . . . . .	183
6.4	Hartle-Hawking state . . . . .	186
6.5	Unruh state . . . . .	189
6.6	Expectation value of the stress tensor . . . . .	190
6.7	Luminosity . . . . .	196
6.8	RSET close to the horizon in the Boulware vacuum . . . . .	203
6.9	Symmetry $(\theta, \phi) \rightarrow (\pi - \theta, \phi + \pi)$ . . . . .	215
6.9.1	Lack of symmetry . . . . .	226
6.9.2	New expressions for the quantization of the field . . . . .	235
6.9.3	Polarization . . . . .	243
	<b>Conclusions</b>	<b>252</b>
	<b>A Radial numerics</b>	<b>257</b>
	<b>Errata</b>	<b>272</b>

# Overview

Quantum field theory in a curved background is a semiclassical approximation to a quantum theory of gravity in which the matter fields are quantized but the gravitational field is described by a classical background space-time. The theory may be taken to include one-loop quantum gravitational effect by considering the linear perturbation of the gravitational field as a massless spin-2 field on the background space-time. In the semiclassical theory, the classical stress-energy tensor is replaced in Einstein's field equation by the renormalized expectation value of the stress-energy tensor in a suitable state  $|\Psi\rangle$  of the system:

$$R_{\mu\nu} - \frac{1}{2}Rg_{\mu\nu} + \Lambda g_{\mu\nu} = +\frac{8\pi G}{c^4} \left\langle \hat{T}_{\mu\nu} \right\rangle_{\text{ren}}^{\Psi}.$$

Quantum field theory in a curved background is the framework of this thesis. Even though this theory does not provide a full account of quantum gravity, it does provide an understanding of the influence of the gravitational field on quantum field theoretic results, which a complete quantum theory of gravitation should account for. Indeed, it is expected that this semiclassical approach is valid in the limit that the length and time scales of the quantum processes are much larger than the Planck length  $((G\hbar/c^3)^{1/2} = 1.62 \times 10^{-33}\text{cm})$  and the Planck time  $((G\hbar/c^5)^{1/2} = 5.39 \times 10^{-44}\text{s})$ .

The first important results that quantum field theory in a curved background achieved related to the discovery of particle production by rapidly varying gravitational fields. In particular, the pivotal result discovered by Hawking in 1975 [45] was that black holes radiate as black bodies due to particle creation. Many



related investigations have followed since then. Most of them, however, relate to a spherically-symmetric (Schwarzschild) black hole. Not so many relate to the more realistic case of a rotating, axially-symmetric (Kerr) black hole. The difficulty of dealing with the latter rather than the former is apparent already from noting that a spherically-symmetric black hole possesses an infinite-number of rotational symmetries whereas the axially-symmetric black hole only possesses one.

The most common field theory studied in the literature is scalar (spin-0) field theory. The main focus of this thesis is on electromagnetic (spin-1) perturbations in an electrically-charged, axially-symmetric (Kerr-Newman) background. Some of the results, however, are more general and apply to general spin theory in backgrounds of a wider type. Some other results apply to the Kerr background. We will indicate throughout this thesis what spin theory and what background the results apply to.

The algebra of general spin theory is more complicated than that for spin-0, and the Newman-Penrose formalism which exploits the underlying symmetries of the space-time is introduced in order to simplify it. It was with the use of the Newman-Penrose formalism that Teukolsky [87] decoupled the field equations for different spin fields in the Kerr background and expressed the decoupled equations into a single “master” differential equation, where the spin appeared as a parameter. More importantly, he managed to separate this equation thereby making it possible to express the general solution as a sum over generalised Fourier modes.

The content of this thesis is organized as follows:

In Chapter 1 we give an overview of the Newman-Penrose formalism and the Kerr-Newman space-time.

In Chapter 2 we study the solutions to the Maxwell equations in a curved background. We do so by developing a particularly elegant formalism, which was

presented by Wald [91]. We also suggest an approach to quantizing the electromagnetic field, different from the one commonly used in the literature, which allows the reduction of the quantum theory for the electromagnetic field to that of a complex scalar field.

Chapters 3 and 4 provide an analysis of the radial and angular differential Teukolsky equations respectively. Both chapters suggest various approaches for solving the equations and describe the methodology used to find the numerical solutions for each case. The numerical results are presented and discussed. We study the behaviour of the solutions in different asymptotic regions. In each chapter we also provide a review background of the related existing results in the literature.

In Chapter 5 we present the results of an analysis of the angular solutions in the limit of high frequency. This analysis is based on a previous one done by Breuer, Ryan and Waller [8]. Their work, however, was flawed and incomplete. This chapter corrects and completes their work and thus gives a complete account of the behaviour for large frequency of the angular functions and the eigenvalues for general integral spin, which has not been presented in the literature before. The analytic work is fully complemented with a numerical study.

The last chapter focuses on quantum field theory for the electromagnetic field in the Kerr and Kerr-Newman backgrounds. The method used follows the method of canonical quantization of the electromagnetic field used by Candelas, Chrzanowski and Howard [14]. We give an overview of the results achieved thus far in the literature in the particular problem of defining a vacuum state with certain desirable properties in the Kerr background. We present numerical results obtained for the difference of the expectation value of the stress-energy tensor between two states for spin-1. In the last three sections we deal with three separate issues. In one section, we remark on some of the differences between the spin-1 and the spin-0 cases in the calculation of flux of energy and angular momentum of a black hole, and present calculations in the cases that the field is in the past Unruh and past Boulware states. In the following section,

we rederive and review a calculation in [14] on the renormalized stress energy tensor for the past Boulware state close to the horizon. We show numerically that it corresponds to that of a rigidly rotating thermal reservoir of particles. In the last section we thoroughly discuss the apparent lack of symmetry that the expectation value of the stress tensor in different states exhibits based on the formulae of Candelas, Chrzanowski and Howard. Finally, we give for the first time in the literature the correct form of the equations for the calculation of these quantities, and give a physical interpretation of the results.

In the remainder of this thesis, we use geometrized Planck units:  $c = G = \hbar = 1$ , and follow the sign conventions of Misner, Thorne and Wheeler [66]. We follow the tetrad and Newman-Penrose formalism conventions of Chandrasekhar [20]. A Greek-letter index indicates a tensor index whereas a Latin-letter index in parentheses indicates a tetrad index.

# Chapter 1

## Introduction

### 1.1 Tetrad/Newman-Penrose formalism

Consider a 4-dimensional Riemannian space with a signature  $+2$ . A *tetrad basis* consists of four contravariant vectors  $\{e_{(a)}, a = 1, 2, 3, 4\}$  such that

$$e_{(a)}{}^\alpha e_{(b)\alpha} = \eta_{(a)(b)} \quad (1.1.1)$$

where  $(\eta_{(a)(b)})$  is a constant, symmetric matrix. The inverse to the matrix  $(e_{(a)}{}^\alpha)$  is  $(e^{(a)}{}_\alpha)$  in the sense that:  $e_{(a)}{}^\alpha e^{(b)}{}_\alpha = \delta^{(b)}_{(a)}$  and  $e_{(a)}{}^\alpha e^{(a)}{}_\beta = \delta^\alpha_\beta$ . Similarly, the inverse of the constant, symmetric matrix is given by  $\eta^{(a)(b)}\eta_{(b)(c)} = \delta^{(a)}_{(c)}$ .

The tetrad components of a tensor field are the projections of the tensor field onto the tetrad frame. They are obtained by contracting the tensor components of the field with those of the vectors in the tetrad basis:

$$\begin{aligned} A_{(a_1)\dots(a_r)} &= e_{(a_1)}{}^{\alpha_1} \dots e_{(a_r)}{}^{\alpha_r} A_{\alpha_1\dots\alpha_r} & \text{if } \mathbf{A} \in T^0_r \\ A^{(a_1)\dots(a_r)} &= e^{(a_1)}{}_{\alpha_1} \dots e^{(a_r)}{}_{\alpha_r} A^{\alpha_1\dots\alpha_r} = \eta^{(a_1)(b_1)} \dots \eta^{(a_r)(b_r)} A_{(b_1)\dots(b_r)} & \text{if } \mathbf{A} \in T^r_0 \end{aligned} \quad (1.1.2)$$

where  $T^r_s$  is a tensor field of type  $(r, s)$  on the Riemannian space. It is clear that tetrad indices are raised and lowered with  $\eta^{(a)(b)}$  and  $\eta_{(a)(b)}$  respectively.

The contravariant vectors  $e_{(a)} = e_{(a)}{}^\alpha \frac{\partial}{\partial x^\alpha}$ , considered as tangent vectors, de-

## 1.1. Tetrad/Newman-Penrose formalism

---

fine the *directional derivatives*:  $A_{(a_1)\dots(a_r),(b)} = e_{(b)}^\alpha \frac{\partial}{\partial x^\alpha} A_{(a_1)\dots(a_r)}$ . The *intrinsic derivative* of  $A_{(a_1)\dots(a_r)}$  in the direction  $e_{(b)}$  is defined in relation to the directional derivative as

$$\begin{aligned} A_{(a_1)\dots(a_r)|(b)} &\equiv A_{\alpha_1\dots\alpha_r;\beta} e_{(a_1)}^{\alpha_1} \dots e_{(a_r)}^{\alpha_r} e_{(b)}^\beta = \\ &= A_{(a_1)\dots(a_r),(b)} - \eta^{(n)(m)} \left( \gamma_{(n)(a_1)(b)} A_{(m)(a_2)\dots(a_r)} + \gamma_{(n)(a_2)(b)} A_{(a_1)(m)(a_3)\dots(a_r)} + \dots + \right. \\ &\quad \left. + \gamma_{(n)(a_r)(b)} A_{(a_1)\dots(a_{r-1})(m)} \right) \end{aligned} \quad (1.1.3)$$

where we have used the following definition of the *Ricci rotation-coefficients*:

$$\gamma_{(c)(a)(b)} \equiv e_{(a)\alpha;\beta} e_{(c)}^\alpha e_{(b)}^\beta \quad (1.1.4)$$

The Ricci rotation-coefficients are anti-symmetric in the first pair of indices:  $\gamma_{(c)(a)(b)} = -\gamma_{(a)(c)(b)}$ , due to the fact that  $\eta_{(a)(b)}$  are constant.

The *Lie bracket*  $[e_{(a)}, e_{(b)}]$  is itself a vector and can therefore be expressed as a linear combination of the basis vectors

$$[e_{(a)}, e_{(b)}] = C^{(c)}_{(a)(b)} e_{(c)} \quad (1.1.5)$$

where the coefficients  $C^{(c)}_{(a)(b)}$  are called the *structure constants*. These constants can be readily expressed in terms of the rotation coefficients as  $C^{(c)}_{(a)(b)} = \gamma^{(c)}_{(b)(a)} - \gamma^{(c)}_{(a)(b)}$  and we therefore have the *commutation relations*:

$$[e_{(a)}, e_{(b)}] = (\gamma^{(c)}_{(b)(a)} - \gamma^{(c)}_{(a)(b)}) e_{(c)} \quad (1.1.6)$$

The *Newman-Penrose (NP) formalism* [69] is a particular case of the tetrad formalism whereby the four vectors in the basis are chosen to be null, with two of the basis vectors being real and the other two complex-conjugates of each other. All four basis vectors are also chosen to be orthogonal by pairs. The remaining normalization conditions are usually chosen so that

$$(\eta_{(a)(b)}) = (\eta^{(a)(b)}) = \begin{pmatrix} 0 & 1 & 0 & 0 \\ 1 & 0 & 0 & 0 \\ 0 & 0 & 0 & -1 \\ 0 & 0 & -1 & 0 \end{pmatrix} \quad (1.1.7)$$

## 1.1. Tetrad/Newman-Penrose formalism

---

Each vector in the NP basis is designated by a specific symbol:

$$l \equiv e_{(1)} = e^{(2)}, n \equiv e_{(2)} = e^{(1)}, m \equiv e_{(3)} = -e^{(4)}, m^* \equiv e_{(4)} = -e^{(3)} \quad (1.1.8)$$

These vectors define directional derivatives which are denoted by the following symbols:

$$\begin{aligned} D &\equiv e_{(1)}^\mu \nabla_\mu = e^{(2)\mu} \nabla_\mu & \Delta &\equiv e_{(2)}^\mu \nabla_\mu = e^{(1)\mu} \nabla_\mu \\ \delta &\equiv e_{(3)}^\mu \nabla_\mu = -e^{(4)\mu} \nabla_\mu & \delta^* &\equiv e_{(4)}^\mu \nabla_\mu = -e^{(3)\mu} \nabla_\mu \end{aligned} \quad (1.1.9)$$

The Ricci rotation-coefficients, called *spin coefficients* within the NP formalism, are also given specific symbols:

$$\begin{aligned} \kappa &\equiv \gamma_{(3)(1)(1)} & \rho &\equiv \gamma_{(3)(1)(4)} & \epsilon &\equiv \frac{1}{2} (\gamma_{(2)(1)(1)} + \gamma_{(3)(4)(1)}) \\ \sigma &\equiv \gamma_{(3)(1)(3)} & \mu &\equiv \gamma_{(2)(4)(3)} & \gamma &\equiv \frac{1}{2} (\gamma_{(2)(1)(2)} + \gamma_{(3)(4)(2)}) \\ \lambda &\equiv \gamma_{(2)(4)(4)} & \tau &\equiv \gamma_{(3)(1)(2)} & \alpha &\equiv \frac{1}{2} (\gamma_{(2)(1)(4)} + \gamma_{(3)(4)(4)}) \\ \nu &\equiv \gamma_{(2)(4)(2)} & \pi &\equiv \gamma_{(2)(4)(1)} & \beta &\equiv \frac{1}{2} (\gamma_{(2)(1)(3)} + \gamma_{(3)(4)(3)}) \end{aligned} \quad (1.1.10)$$

The ten independent components of the Weyl tensor  $C_{\alpha\beta\mu\nu}$  are represented by the five complex *Weyl scalars*:

$$\begin{aligned} \psi_{-2} &\equiv -C_{(1)(3)(1)(3)} & \psi_{-1} &\equiv -C_{(1)(2)(1)(3)} \\ \psi_0 &\equiv -C_{(1)(3)(4)(2)} \\ \psi_{+1} &\equiv -C_{(1)(2)(4)(2)} & \psi_{+2} &\equiv -C_{(2)(4)(2)(4)} \end{aligned} \quad (1.1.11)$$

The other tetrad components of the Weyl tensor can be obtained from these five scalars by either using any of the symmetries it possesses ( $C_{(\alpha\beta)\gamma\delta} = 0 = C_{\alpha\beta(\gamma\delta)}$  and  $C_{\alpha\beta\gamma\delta} = C_{\gamma\delta\alpha\beta}$ ; we preferred to use tensor instead of tetrad indices for these symmetries in order to avoid mixing brackets that indicate a tetrad index with brackets that indicate symmetrization) or its trace-freeness  $C^{(a)}{}_{(b)(c)(a)} = 0$  or else the *cyclic condition*:  $C_{(1)(2)(3)(4)} + C_{(1)(3)(4)(2)} + C_{(1)(4)(2)(3)} = 0$ . Of course, in flat space-time all Weyl scalars are zero:  $\psi_h = 0, \forall h$ . Notice that the NP Weyl scalars  $\{\psi_{-2}, \psi_{-1}, \psi_0, \psi_{+1}, \psi_{+2}\}$  are respectively named  $\{\psi_0, \psi_{+1}, \psi_{+2}, \psi_{+3}, \psi_{+4}\}$

## 1.1. Tetrad/Newman-Penrose formalism

---

in most of the bibliography cited in this thesis. The index notation we use in this thesis for all NP scalars follows that of Carter [18] (a similar notation was originally used by Price [78]).

Similarly, the ten components of the Ricci tensor can be represented by four real and three complex scalars.

The anti-symmetric Maxwell tensor  $F_{\alpha\beta}$  is expressed in terms of the three complex scalars:

$$\phi_{-1} \equiv F_{(1)(3)} \quad (1.1.12a)$$

$$\phi_0 \equiv \frac{1}{2} (F_{(1)(2)} + F_{(4)(3)}) \quad (1.1.12b)$$

$$\phi_{+1} \equiv F_{(4)(2)} \quad (1.1.12c)$$

The inverse relations are given by

$$F_{(a)(b)} = \begin{pmatrix} 0 & \phi_0 + \phi_0^* & \phi_{-1} & \phi_{-1}^* \\ -\phi_0 - \phi_0^* & 0 & -\phi_{+1}^* & -\phi_{+1} \\ -\phi_{-1} & \phi_{+1}^* & 0 & -\phi_0 + \phi_0^* \\ -\phi_{-1}^* & \phi_{+1} & \phi_0 - \phi_0^* & 0 \end{pmatrix} \quad (1.1.13)$$

The commutation relations (1.1.6) are very useful and we therefore show their explicit form in the NP formalism:

$$\Delta D - D\Delta = (\gamma + \gamma^*)D + (\epsilon + \epsilon^*)\Delta - (\pi + \tau^*)\delta - (\tau + \pi^*)\delta^* \quad (1.1.14a)$$

$$\delta D - D\delta = (\alpha^* + \beta - \pi^*)D + \kappa\Delta - (\rho^* + \epsilon - \epsilon^*)\delta - \sigma\delta^* \quad (1.1.14b)$$

$$\delta\Delta - \Delta\delta = -\nu^*D + (\tau - \alpha^* - \beta)\Delta + (\mu - \gamma + \gamma^*)\delta + \lambda^*\delta^* \quad (1.1.14c)$$

$$\delta^*\delta - \delta\delta^* = (\mu^* - \mu)D + (\rho^* - \rho)\Delta + (\alpha - \beta^*)\delta + (\beta - \alpha^*)\delta^* \quad (1.1.14d)$$

The Ricci and the Bianchi identities in the NP formalism can be found in [20].

The first-order change in a basis vector  $e_{(a)}$  when it suffers an infinitesimal displacement  $\zeta$  is given by  $\delta e_{(a)\alpha}(\zeta) = e_{(a)\alpha;\beta}\zeta^\beta = -\gamma_{(a)(b)(c)}e^{(b)}_\alpha\zeta^{(c)}$ . Several consequences may be derived by studying the effect of such a displacement on the

## 1.1. Tetrad/Newman-Penrose formalism

---

vector  $\mathbf{l}$ . First of all, it is easy to see that

$$\delta l_\alpha(\mathbf{l}) = l_{\alpha;\beta} l^\beta = (\epsilon + \epsilon^*) l_\alpha - \kappa m_\alpha^* - \kappa^* m_\alpha \quad (1.1.15)$$

It is clear from (1.1.15) that the  $\mathbf{l}$ -vectors form a congruence of null geodesics if, and only if,  $\kappa = 0$ . If that is the case, they are affinely parametrized if, and only if, in addition  $\Re(\epsilon) = 0$ . The symbols  $\Re$  and  $\Im$  represent the real and imaginary parts respectively.

Furthermore, from equation (1.1.4) together with the definition (1.1.10) of the spin coefficients, it is straight-forward to prove that

$$\frac{1}{2} l^\alpha{}_{;\alpha} = -\Re(\rho) \quad (1.1.16a)$$

$$\frac{1}{2} l_{[\alpha;\beta]} l^{\alpha;\beta} = (\Im(\rho))^2 \quad (1.1.16b)$$

$$\frac{1}{2} l_{(\alpha;\beta)} l^{\alpha;\beta} = (\Re(\rho))^2 + |\sigma|^2 \quad (1.1.16c)$$

If we consider at each point of a null  $\mathbf{l}$ -ray a small circle orthogonal to  $\mathbf{l}$  with that point as its centre, and we then follow into the future null-direction the rays of the congruence  $\mathbf{l}$  which intersect the circle, the circle may become contracted or expanded, rotated or sheared. From equation (1.1.16a), the quantity  $-\Re(\rho)$  measures the possible expansion or contraction and, from (1.1.16b),  $\Im(\rho)$  measures the possible rotation of the circle. Finally, equation (1.1.16c) shows that  $|\sigma|$  is the shear of the bundle of  $\mathbf{l}$ -rays, as it measures the extent to which neighbouring  $\mathbf{l}$ -rays are sliding past each other.

Note that the full set of NP equations is invariant under the interchange  $\{\mathbf{l} \leftrightarrow \mathbf{n}, \mathbf{m} \leftrightarrow \mathbf{m}^*\}$ . Such an interchange results in the following transformations:

$$\begin{aligned} \psi_{-2} &\leftrightarrow \psi_{+2} & \psi_{-1} &\leftrightarrow \psi_{+1} & \psi_0 &\leftrightarrow \psi_0 \\ \phi_{-1} &\leftrightarrow -\phi_{+1} & \phi_0 &\leftrightarrow -\phi_0 & & \\ \kappa &\leftrightarrow -\nu & \rho &\leftrightarrow -\mu & \sigma &\leftrightarrow -\lambda \\ \alpha &\leftrightarrow -\beta & \epsilon &\leftrightarrow -\gamma & \pi &\leftrightarrow -\tau \end{aligned} \quad (1.1.17)$$



## 1.1. Tetrad/Newman-Penrose formalism

---

It is also clear that complex-conjugation of a gravitational or electromagnetic NP quantity is equivalent to swopping the tetrad indices 3 and 4.

We can subject the NP frame to a Lorentz transformation at some point and extend it continuously through all of space-time. We have six degrees of freedom to rotate the frame while keeping  $\eta_{(a)(b)}$  unchanged, corresponding to the six parameters of the group of Lorentz transformations, and we can view such a general rotation as composed of the following three classes of rotations where  $a$  and  $b$  are complex fields and  $A$  and  $\varphi$  real fields:

a) *rotation of class I:*

$$\begin{aligned} l &\rightarrow l & n &\rightarrow n + a^*m + am^* + aa^*l \\ m &\rightarrow m + al & m^* &\rightarrow m^* + a^*l \end{aligned} \quad (1.1.18)$$

The effect of such a rotation on the Maxwell scalars is:

$$\begin{aligned} \phi_{-1} &\rightarrow \phi_{-1} & \phi_0 &\rightarrow \phi_0 + a^*\phi_{-1} & \phi_{+1} &\rightarrow \phi_{+1} + 2a^*\phi_0 + a^{*2}\phi_{-1} \end{aligned} \quad (1.1.19)$$

and on the Weyl scalars:

$$\begin{aligned} \psi_{-2} &\rightarrow \psi_{-2} & \psi_{-1} &\rightarrow \psi_{-1} + a^*\psi_{-2} \\ \psi_0 &\rightarrow \psi_0 + 2a^*\psi_{-1} + a^{*2}\psi_{-2} & \psi_{+1} &\rightarrow \psi_{+1} + 3a^*\psi_0 + 3a^{*2}\psi_{-1} + a^{*3}\psi_{-2} \\ \psi_{+2} &\rightarrow \psi_{+2} + 4a^*\psi_{+1} + 6a^{*2}\psi_0 + 4a^{*3}\psi_{-1} + a^{*4}\psi_{-2} \end{aligned} \quad (1.1.20)$$

b) *rotation of class II:*

$$\begin{aligned} l &\rightarrow l + b^*m + bm^* + bb^*n & n &\rightarrow n \\ m &\rightarrow m + bn & m^* &\rightarrow m^* + b^*n \end{aligned} \quad (1.1.21)$$

The effect of a rotation of class II on the Maxwell scalars can be derived from that of a rotation of class I using the transformations (1.1.17) and including a complex-conjugation since the exchange  $m \leftrightarrow m^*$  is not being

## 1.1. Tetrad/Newman-Penrose formalism

---

performed now. The result is:

$$\begin{aligned}\phi_{-1} &\rightarrow \phi_{-1} + 2b\phi_0 + b^2\phi_{+1} & \phi_0 &\rightarrow \phi_0 + b\phi_{+1} & \phi_{+1} &\rightarrow \phi_{+1}\end{aligned}\tag{1.1.22}$$

and

$$\begin{aligned}\psi_{-2} &\rightarrow \psi_{-2} + 4b\psi_{-1} + 6b^2\psi_0 + 4b^3\psi_{+1} + b^4\psi_{+2} \\ \psi_{-1} &\rightarrow \psi_{-1} + 3b\psi_0 + 3b^2\psi_{+1} + b^3\psi_{+2} & \psi_0 &\rightarrow \psi_0 + 2b\psi_{+1} + b^2\psi_{+2} \\ \psi_{+1} &\rightarrow \psi_{+1} + b\psi_{+2} & \psi_{+2} &\rightarrow \psi_{+2}\end{aligned}\tag{1.1.23}$$

c) *rotation of class III*:

$$\begin{aligned}l &\rightarrow A^{-1}l & n &\rightarrow An \\ m &\rightarrow e^{i\varphi}m & m^* &\rightarrow e^{-i\varphi}m^*\end{aligned}\tag{1.1.24}$$

The Maxwell and Weyl scalars are respectively changed as follows under this rotation

$$\phi_{-1} \rightarrow A^{-1}e^{i\varphi}\phi_{-1} \quad \phi_0 \rightarrow \phi_0 \quad \phi_{+1} \rightarrow Ae^{-i\varphi}\phi_{+1}\tag{1.1.25}$$

and

$$\begin{aligned}\psi_{-2} &\rightarrow A^{-2}e^{2i\varphi}\psi_{-2} & \psi_{-1} &\rightarrow A^{-1}e^{i\varphi}\psi_{-1} \\ \psi_0 &\rightarrow \psi_0 \\ \psi_{+1} &\rightarrow Ae^{-i\varphi}\psi_{+1} & \psi_{+2} &\rightarrow A^2e^{-2i\varphi}\psi_{+2}\end{aligned}\tag{1.1.26}$$

These three different classes of rotation allow us to classify the Weyl tensor in four different types depending on how many of the Weyl scalars we can make zero by subjecting them to Lorentz transformations. Considering  $\psi_{+2} \neq 0$  (if it were zero we could make it non-zero with a rotation of class I unless all Weyl scalars vanished or space were conformally flat), we can make  $\psi_{-2}$  vanish by applying a rotation of class II with a parameter  $b$  satisfying:

$$\psi_{-2} + 4\psi_{-1}b + 6\psi_0b^2 + 4\psi_{+1}b^3 + \psi_{+2}b^4 = 0\tag{1.1.27}$$

## 1.1. Tetrad/Newman-Penrose formalism

---

This equation for  $b$  can have from 1 to 4 distinct solutions and the corresponding new direction(s) of the vector  $\mathbf{l}$  (given by  $\mathbf{l} + b^*\mathbf{m} + b\mathbf{m}^* + bb^*\mathbf{n}$ ) is(are) called the *principal null direction(s)* or *Debever-Penrose direction(s)* of the Weyl tensor. The Weyl tensor is called *algebraically general* if there are four distinct roots and otherwise it is called *algebraically special*. The *Petrov classification* further classifies the Weyl tensor depending on how many distinct roots equation (1.1.27) possesses:

- a) *Petrov Type I*: four distinct roots. By successively applying different classes of rotation, both  $\psi_{-2}$  and  $\psi_{+2}$  can be made to vanish but  $\psi_{\pm 1}$  and  $\psi_0$  cannot.
- b) *Petrov Type II*: one double and two single roots.  $\psi_{\pm 2}$  and  $\psi_{-1}$  can be made to vanish but  $\psi_{+1}$  and  $\psi_0$  cannot.
- c) *Petrov Type D*: two distinct double roots.  $\psi_{\pm 2}$  and  $\psi_{\pm 1}$  can be made to vanish but  $\psi_0$  cannot.
- d) *Petrov Type III*: one triple and one single root.  $\psi_{\pm 2}$ ,  $\psi_{-1}$  and  $\psi_0$  can be made to vanish but  $\psi_{+1}$  cannot.
- e) *Petrov Type N*: only one distinct root.  $\psi_{-2}$ ,  $\psi_{\pm 1}$  and  $\psi_0$  can be made to vanish but  $\psi_{+2}$  cannot.

Finally, the next theorem establishes a direct relationship between the values of certain spin coefficients and the Weyl tensor type. This theorem is restricted to the vacuum.

*Goldberg-Sachs theorem*: If the Riemann tensor is of Type II and a null basis is so chosen that  $\mathbf{l}$  is the repeated null direction and  $\psi_{-2} = \psi_{-1} = 0$ , then  $\kappa = \sigma = 0$ ; and, conversely, if  $\kappa = \sigma = 0$ , then  $\psi_{-2} = \psi_{-1} = 0$  and the Riemann tensor is of Type II.

A corollary to this theorem results from the interchange  $\mathbf{l} \leftrightarrow \mathbf{n}$  applied to the theorem. The corollary states that if the Riemann tensor is of Petrov Type D, then the congruences formed by the two principal null-directions,  $\mathbf{l}$  and  $\mathbf{n}$ , must

## 1.2. The Kerr-Newman space-time

---

both be geodesic (from (1.1.15)) and shear-free (from (1.1.16c)), i.e.,  $\kappa = \sigma = \nu = \lambda = 0$  when  $\psi_{\pm 2} = \psi_{\pm 1} = 0$ ; and conversely.

Kundt and Thompson [59] and Robinson and Schild [79] gave a generalization of the Goldberg-Sachs theorem which is not restricted to vacuum solutions. Kundt and Trümper [60] gave a generalization of the same theorem to a particular type of Einstein-Maxwell fields that includes the Kerr-Newman solution described in the following section.

All black hole solutions of general relativity are of Petrov Type D and it is therefore possible to choose a null tetrad such that the four spin coefficients  $\kappa$ ,  $\sigma$ ,  $\nu$  and  $\lambda$  and all Weyl scalars except for  $\psi_0$  are zero. Such is the case of both the Kinnersley and the Carter null tetrads, which we have chosen to use in all our calculations.

For the physically important, Petrov Type D backgrounds, the corresponding Weyl tensor and its dual satisfy the equations

$$C_{\alpha\beta\gamma[\delta}l_{\epsilon]}l^\beta l^\gamma = 0 \qquad {}^*C_{\alpha\beta\gamma[\delta}l_{\epsilon]}l^\beta l^\gamma = 0 \qquad (1.1.28)$$

where  $l$  represents any one of the two principal null congruences.

## 1.2 The Kerr-Newman space-time

The action integral

$$S = \int_{\mathcal{D}} \left( \frac{1}{16\pi} R + L_{\text{emag}} \right) \sqrt{-g} dx^4 \qquad (1.2.1)$$

corresponds to interacting gravitational and electromagnetic fields, where the integration is performed over the interior of a four-dimensional region  $\mathcal{D}$  and  $L_{\text{emag}}$  is the Lagrangian of the electromagnetic field. The result of extremizing this action integral for interacting gravitational and electromagnetic fields created by a mass  $M$ , intrinsic angular momentum per unit mass  $a$  and charge  $Q$  as seen at radial infinity, and subject to the existence of a physically nonsingular horizon

## 1.2. The Kerr-Newman space-time

---

is the *Kerr-Newman geometry* and its associated electromagnetic field. These gravitational and electromagnetic fields were first found by Newman, Couch, Chinnapared, Exton, Prakash and Torrence [67] by applying a transformation to the charged, spherical solution of Reissner-Nordström. The Kerr-Newman metric in the *Boyer-Lindquist* [7] co-ordinate system  $\{t, r, \theta, \phi\}$  is

$$\begin{aligned} ds^2 = & - \left( \frac{\Delta - a^2 \sin^2 \theta}{\Sigma} \right) dt^2 - \frac{2a \sin^2 \theta (r^2 + a^2 - \Delta)}{\Sigma} d\phi dt + \\ & + \left[ \frac{(r^2 + a^2)^2 - a^2 \Delta \sin^2 \theta}{\Sigma} \right] \sin^2 \theta d\phi^2 + \frac{\Sigma}{\Delta} dr^2 + \Sigma d\theta^2 = \\ & = - \frac{\Delta}{\Sigma} (dt - a \sin^2 \theta d\phi)^2 + \frac{\sin^2 \theta}{\Sigma} [(r^2 + a^2) d\phi - a dt]^2 + \frac{\Sigma}{\Delta} dr^2 + \Sigma d\theta^2 \end{aligned} \quad (1.2.2)$$

where

$$\Sigma \equiv r^2 + a^2 \cos^2 \theta \quad (1.2.3)$$

$$\Delta \equiv r^2 - 2Mr + a^2 + Q^2 \quad (1.2.4)$$

The associated electromagnetic field is

$$\begin{aligned} \mathbf{F} = & \frac{Q}{\Sigma^4} (r^2 - a^2 \cos^2 \theta) dr \wedge [dt - a \sin^2 \theta d\phi] + \\ & + 2 \frac{Q}{\Sigma^4} ar \cos \theta \sin \theta d\theta \wedge [(r^2 + a^2) d\phi - a dt] \end{aligned} \quad (1.2.5)$$

The co-ordinate  $\phi$  is required to be periodic with period  $2\pi$  so that the Kerr-Newman metric is asymptotically flat for large  $r$ . The metric coefficients in Boyer-Lindquist co-ordinates are independent of  $t$  and  $\phi$ . The spacetime is therefore stationary and axially symmetric. The Kerr-Newman metric possesses two Killing vectors associated with these two symmetries:

$$\xi \equiv \frac{\partial}{\partial t} \quad (1.2.6)$$

and

$$\psi \equiv \frac{\partial}{\partial \phi} \quad (1.2.7)$$

The Kerr-Newman metric is singular at

$$\Delta = 0 \quad (1.2.8)$$

## 1.2. The Kerr-Newman space-time

---

and also at

$$\Sigma = 0 \tag{1.2.9}$$

The evaluation of the curvature invariants shows that (1.2.8) is a co-ordinate singularity while (1.2.9) is a true, curvature singularity. The physical singularity is not spacelike, as it is in the Schwarzschild case, but timelike, so that the singularity may be avoided by timelike and null curves. In consequence, given any spacelike surface, it is always possible to find timelike and null curves that hit the singularity and do not cross the spacelike surface. Therefore, Cauchy surfaces do not exist for the full space-time. They do exist for the exterior region, however. The physical singularity is at  $\{r = 0, \theta = \pi/2\}$ , in Boyer-Lindquist co-ordinates. These co-ordinates, however, are not to be treated as the usual polar co-ordinates in flat space. Indeed, in the limit  $Q = M = 0$  the metric (1.2.2) would not be equal to the flat space metric if the Boyer-Lindquist co-ordinates were to be equated to the usual polar co-ordinates. Newman and Janis [68] have shown that it is instead the following set of co-ordinates  $\{\tilde{r}, \tilde{\theta}, \tilde{\phi}\}$  that correspond to polar co-ordinates in flat space-time:

$$\begin{aligned} \tilde{r}^2 &= r^2 + a^2 \sin^2 \theta \\ \tan \tilde{\phi} &= \frac{\tan \phi - a/r}{1 + (a/r) \tan \phi} \\ \cos \tilde{\theta} &= \frac{r \cos \theta}{(r^2 + a^2 \sin^2 \theta)^{1/2}} \end{aligned} \tag{1.2.10}$$

The singularity at  $\{r = 0, \theta = \pi/2\}$  corresponds to the circle  $\{\tilde{r} = a, \tilde{\theta} = \pi/2\}$  and it is therefore a *ring singularity*. Carter [19] has shown that the number of geodesics that may reach the singularity is more restricted than in the Kerr case. For Kerr-Newman, no timelike geodesics can reach the singularity and null geodesics may only reach it if they lie in the equator and have a uniquely determined angular momentum. In the Kerr background, on the other hand, both timelike and null geodesics may reach the singularity if they lie in the equator and their angular momentum lies within a finite range.

## 1.2. The Kerr-Newman space-time

---

The other type of singularity corresponds to the solutions of (1.2.8), which are

$$r_{\pm} = M \pm \sqrt{M^2 - a^2 - Q^2} \quad (1.2.11)$$

The two hypersurfaces  $r = r_{\pm}$  are event horizons, as we shall now prove. If the surface  $f(t, r, \theta, \phi) = 0$  is to be a null hypersurface containing the Killing vectors  $\xi$  and  $\psi$  then it must be:  $f(r, \theta) = 0$  and  $df_{\alpha}df^{\alpha} = 0$ . These two conditions imply

$$\frac{\Delta}{\Sigma} \left( \frac{\partial f}{\partial r} \right)^2 + \frac{1}{\Sigma} \left( \frac{\partial f}{\partial \theta} \right)^2 = 0 \quad (1.2.12)$$

The only solutions of this equation which are periodic in  $\theta$  are the null hypersurfaces  $r = r_{\pm}$ . The hypersurface  $r = r_{-}$  is called the *inner event horizon* and the hypersurface  $r = r_{+}$ , the *outer event horizon*. In the case  $Q^2 + a^2 > M^2$  there is no co-ordinate singularity and therefore the curvature singularity (1.2.9) is a naked singularity. This case does not describe black holes. The *extreme case* denotes the case  $Q^2 + a^2 = M^2$ . The inner and outer horizons then coincide at  $r_{+} = r_{-} = M$ . For the rest of this thesis we will restrict ourselves to the case  $a^2 + Q^2 < M^2$ , unless specified otherwise. The radius of the outer horizon is related to the surface area  $\mathcal{A}$  of a Kerr-Newman black hole by  $\mathcal{A} = 4\pi(r_{+}^2 + a^2)$ .

The Killing vector  $\xi$  becomes a null vector where the equation  $0 = g_{\mu\nu}\xi^{\mu}\xi^{\nu} = g_{tt}$  is satisfied, which has two roots:

$$r_{\{1\}} = M \pm \sqrt{M^2 - Q^2 - a^2 \cos^2 \theta} \quad (1.2.13)$$

The surface defined by the Boyer-Lindquist radius  $r_1$  is called the *stationary limit surface*. The stationary limit surface is timelike everywhere except at the axis, where it is null and it coincides with the surface  $r = r_{+}$ . The region between the event horizon and the stationary limit surface, i.e., for  $r_{+} < r < r_1$  is called the *ergosphere*. Within the ergosphere, the vector  $\xi$  is spacelike and therefore observers will not be able to remain at rest with respect to radial infinity. Outside the stationary limit surface, i.e., for  $r \in (r_1, +\infty)$ ,  $\xi$  is a timelike vector.

The Killing vector  $\psi$  becomes timelike close to the ring singularity for negative values of  $r$ . Because  $\phi$  is a periodic co-ordinate, the orbits of  $\psi$  are closed

## 1.2. The Kerr-Newman space-time

---

and therefore there exist closed timelike curves in a neighborhood of the ring singularity.

We can construct another Killing vector as

$$\chi \equiv \xi + \Omega_+ \psi \quad (1.2.14)$$

with

$$\Omega_+ \equiv \frac{a}{r_+^2 + a^2} \quad (1.2.15)$$

We shall see later on that  $\Omega_+$  represents the angular velocity of the horizon. The Killing vector  $\chi$  becomes null wherever  $0 = g_{\mu\nu}\chi^\mu\chi^\nu = g_{tt} + 2\Omega_+g_{t\phi} + \Omega_+^2g_{\phi\phi}$  is satisfied. Its only real root corresponds to the *speed-of-light surface* and is given by

$$r_{\text{SOL}}(\theta) = 2\sqrt{-C} \cos\left(\frac{\Theta}{3}\right) - \frac{r_+}{3} \quad (1.2.16)$$

where

$$\begin{aligned} A &= r_+^2 + a^2(2 - \sin^2 \theta) - \frac{(r_+^2 + a^2)^2}{a^2 \sin^2 \theta}; & C &= \frac{3A - r_+^2}{9} \\ B &= r_+A + 2M \left[ a^2 \sin^2 \theta - 2(r_+^2 + a^2) + \frac{(r_+^2 + a^2)^2}{a^2 \sin^2 \theta} \right] \\ D &= \frac{9r_+A - 27B - 2r_+^3}{54}; & \Theta &= \cos^{-1} \left( \frac{D}{\sqrt{-C^3}} \right) \end{aligned} \quad (1.2.17)$$

The vector  $\chi$  is timelike between the event horizon and the speed-of-light surface, and it is spacelike for a radius larger than  $r_{\text{SOL}}$ .

Figure 1.1 shows the radii of the outer event horizon, the static limit surface and the speed-of-light surface as functions of the angle  $\theta$  for various values of the intrinsic angular momentum per unit mass  $a$ . The value of the mass has been chosen to be  $M = (1 + a^2 + Q^2)/2$  so that  $r_+ = 1$ . Since  $r_{\text{SOL}}$  only depends on  $Q$  via  $r_+$ , with the chosen normalization this radius does not vary with  $Q$ . As the intrinsic angular momentum per unit mass increases,  $r_{\text{SOL}}$  diminishes whereas  $r_1$  increases, as expected. The radius of the speed-of-light surface becomes infinite at the axis of symmetry and it reaches a minimum value at the equator. The cusp observed for the speed-of-light surface at the axis of symmetry is merely a



## 1.2. The Kerr-Newman space-time

---

manifestation of the choice of co-ordinate system, rather than the geometry of the space-time.

Apart from the Killing isometries, the Kerr-Newman solution is also invariant under the discrete symmetry

$$(t, \phi) \rightarrow (-t, -\phi) \quad (1.2.18)$$

as expected from a rotational source, and under the *parity operation*  $\mathcal{P}$ :

$$\mathcal{P} \equiv (\mathbf{r} \rightarrow -\mathbf{r}) = (\theta \rightarrow \pi - \theta, \phi \rightarrow \phi + \pi) \quad (1.2.19)$$

We say that  $M$ ,  $a$  and  $Q$  are respectively the mass, intrinsic angular momentum per unit mass and charge of the black hole in the sense that

$$M = -\frac{1}{8\pi} \int_S \eta_{\alpha\beta\gamma\delta} \nabla^\gamma \xi^\delta dx^\alpha \wedge dx^\beta \quad (1.2.20a)$$

$$J \equiv Ma = \frac{1}{16\pi} \int_S \eta_{\alpha\beta\gamma\delta} \nabla^\gamma \psi^\delta dx^\alpha \wedge dx^\beta \quad (1.2.20b)$$

$$4\pi Q = \frac{1}{2} \int_S \eta_{\alpha\beta\gamma\delta} F^{\gamma\delta} dx^\alpha \wedge dx^\beta \quad (1.2.20c)$$

where  $\eta_{\alpha\beta\gamma\delta}$  are the components of the space-time's volume 4-form and  $S$  is any spacelike 2-surface which has the topology of a 2-sphere, completely surrounds the source and lies entirely in the vacuum region. By comparison with the Schwarzschild and the Reissner-Nordström solutions it can be easily seen from (1.2.2) and (1.2.5) that  $M$  and  $Q$  represent the mass and the electric charge in the limit of large positive  $r$ . Similarly, in the limit of large negative  $r$ , the mass and the charge are respectively  $-M$  and  $-Q$ . On the other hand, the parameter  $a$  is the cause for Coriolis-type forces which in the limit  $r \rightarrow +\infty$  are identical to the ones created by a rotating body with angular momentum  $Ma$  in the weak-field limit.

The *surface gravity on the outer[inner] horizon* is  $\kappa_+[\kappa_-]$  defined as

$$\kappa_\pm \equiv \frac{r_\pm - r_\mp}{2(r_\pm^2 + a^2)} \quad (1.2.21)$$

## 1.2. The Kerr-Newman space-time

---

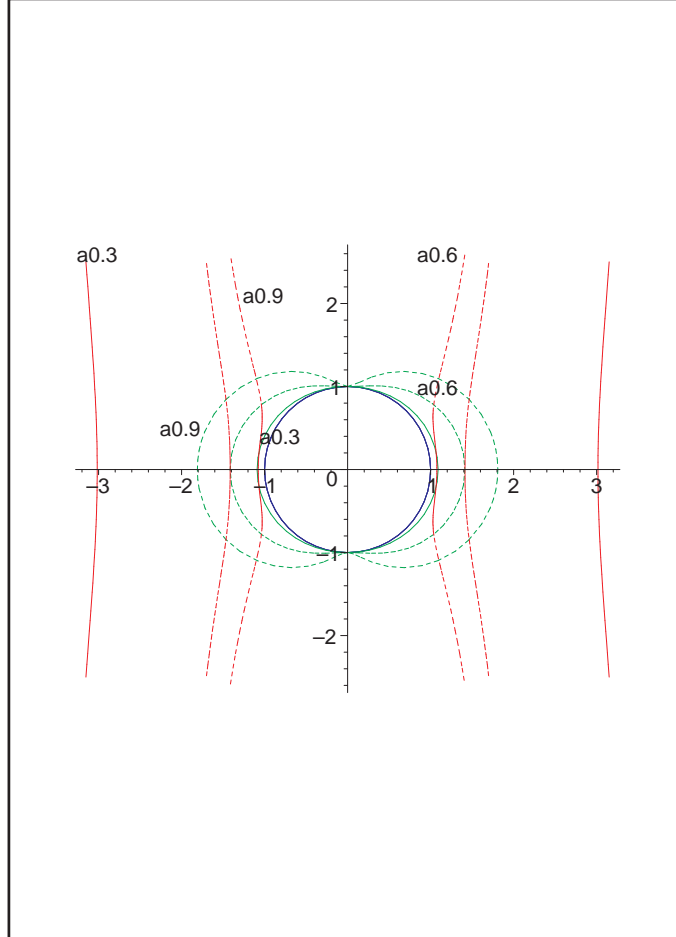


Figure 1.1: Values of the radii  $r_+$  (blue),  $r_1$  (green) and  $r_{\text{SOL}}$  (red) as functions of the angle  $\theta$ , corresponding to hypersurfaces of constant  $t$  and  $\phi$ . The parameters of the black hole are:  $Q = 0$  and  $a = 0.3$  (straight line),  $a = 0.6$  (dashed line) and  $a = 0.9$  (lighter, dashed line). Values have been normalized so that  $r_+ = 1$ . With this normalization, the radius  $r_{\text{SOL}}$  would not vary with  $Q$ .

## 1.2. The Kerr-Newman space-time

---

For a Schwarzschild black hole,  $\kappa_+$  is the value of the force that must be exerted at radial infinity to hold a unit test mass in place in the limit of it lying on the horizon.

The radial co-ordinate  $r_*$  defined by

$$\frac{dr_*}{dr} = \frac{(r^2 + a^2)}{\Delta} \quad (1.2.22)$$

is commonly known as the *tortoise* co-ordinate. We choose the constant of integration in (1.2.22) so that  $r_* = r_*(r)$  coincides with Chandrasekhar's [20], i.e.,

$$r_* = r + \frac{1}{2\kappa_+} \ln(r - r_+) + \frac{1}{2\kappa_-} \ln(r - r_-) \quad (1.2.23)$$

The *retarded*  $u$  and *advanced*  $v$  time co-ordinates are defined via

$$\begin{aligned} du &\equiv dt - dr_* \\ dv &\equiv dt + dr_* \end{aligned} \quad (1.2.24)$$

we can also define a new pair of angular co-ordinates by

$$\begin{aligned} d\bar{\phi} &\equiv d\phi + \frac{a}{\Delta} dr \\ d\bar{\phi}' &\equiv d\phi - \frac{a}{\Delta} dr \end{aligned} \quad (1.2.25)$$

The system of co-ordinates  $\{v, r, \theta, \bar{\phi}\}$  is called *Kerr system* of co-ordinates ([66]), and it is a generalization of the ingoing Eddington-Finkelstein system in the Schwarzschild space-time. The Kerr-Newman metric can be analytically extended across the horizons  $r_{\pm}$  by transforming to the Kerr system. Both the metric and the associated electromagnetic field are indeed analytic at  $r = r_{\pm}$  when expressed in these co-ordinates. In this set of co-ordinates, we denote the regions  $r_+ < r < +\infty$ ,  $r_- < r < r_+$  and  $-\infty < r < r_-$  by *I*, *II* and *III* respectively. Analogously, the metric can also be extended across the horizons by transforming to the co-ordinates  $\{u, r, \theta, \bar{\phi}'\}$ . In this set of co-ordinates, we denote the regions  $r_+ < r < +\infty$ ,  $r_- < r < r_+$  and  $-\infty < r < r_-$  by  $-I$ ,  $-II$  and  $-III$  respectively. We have assumed that the common region to both co-ordinate systems is the one for  $r > r_+$  and therefore regions *I* and  $-I$  are the same. We can now take another

## 1.2. The Kerr-Newman space-time

---

patch formed with the co-ordinates  $\{u, r, \theta, \bar{\phi}'\}$  containing regions  $I^*$ ,  $II^*$  and  $III^*$ , such that regions  $II$  and  $II^*$  coincide. Boyer and Lindquist found a system of co-ordinates, analogous to Kruskal's for the Schwarzschild solution, which spans the regions  $\{I, II, I^*, -II\}$  and such that the metric is regular throughout these regions. Similarly, they found another system of co-ordinates that spans, and is regular throughout (except at the ring singularity), regions  $II$ ,  $III$ ,  $III^*$  plus another region which, like  $II$ , is bounded by two pairs of horizons. This extension procedure can be continued indefinitely both upward and downward. The result, which is the *maximal analytic extension* of the space-time for the case  $a^2 + Q^2 < M^2$ , is depicted in figure 1.2. The surfaces  $\mathcal{H}^\pm$  are the future and past horizons respectively, and the surfaces  $\mathcal{I}^\pm$  are the future and past null infinity respectively, as shown in figure 1.2. The point  $i^0$  is spacelike infinity and the points  $i^\pm$  are future and past null infinity respectively.

Regions  $I$  and  $I^*$  are asymptotically flat regions where  $r_+ < r < \infty$ . Regions  $II$  and  $-II$ , where  $r_- < r < r_+$ , represent a black hole and a white hole respectively. Unlike the Schwarzschild space-time, they do not contain the curvature singularity, but the inner horizon instead. In these regions, the surfaces  $r = \text{const.}$  are spacelike and therefore these regions contain closed trapped surfaces.

If the inner horizon is crossed from region  $II$ , then regions  $III$  and  $III^*$ , where  $-\infty < r < r_-$  and which are identical in structure to each other, are encountered. These regions contain the curvature singularity. Since it is a ring singularity, it is possible to pass through it and enter another asymptotically flat region for  $r \rightarrow -\infty$ . Alternatively, since the singularity is timelike, it may be avoided by entering a region which is identical in structure to  $-II$ .

The global structure of the space-time in the extreme case is similar to the one for the non-extreme case, but differs in that the regions  $r_- < r < r_+$  do not exist.

## 1.2. The Kerr-Newman space-time

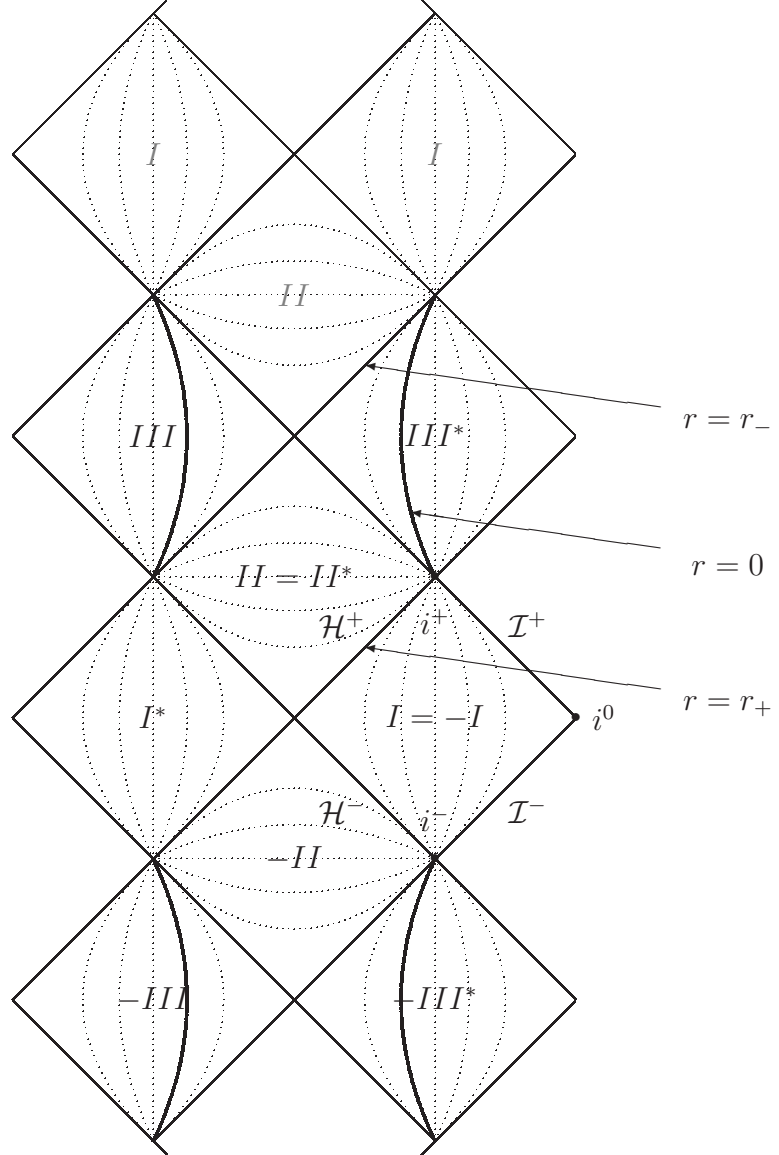


Figure 1.2: Conformal diagram (see [92]) for the extended Kerr-Newman space-time along the axis of symmetry for the case  $a^2 + Q^2 < M^2$ . The dotted lines indicate surfaces of constant  $r$ . The bold lines indicate the ring singularities, which lie on  $\theta = \pi/2$ .

### 1.3. Orthonormal and null tetrads

---

A new azimuthal angular variable  $\phi_+$  may be defined as

$$\phi_+ \equiv \phi - \Omega_+ t \quad (1.2.26)$$

It is found that in the co-ordinate system  $\{u, v, \theta, \phi_+\}$  and close to the past and future horizons:

$$\chi = \begin{cases} \frac{\partial}{\partial u} & \text{at } \mathcal{H}^- \\ \frac{\partial}{\partial v} & \text{at } \mathcal{H}^+ \end{cases} \quad (1.2.27)$$

The *rigidly rotating co-ordinate system* is given by  $\{t_+, r, \theta, \phi_+\}$ , where  $t_+ \equiv t$ .

In this system, the Killing vector  $\chi$  takes up the form

$$\chi = \frac{\partial}{\partial t_+} \quad (1.2.28)$$

Accordingly, we can construct two hamiltonians associated one with the Killing vector  $\xi$  and the other one with the Killing vector  $\chi$ :

$$\begin{aligned} \hat{H}_\xi &\equiv i\xi = i\frac{\partial}{\partial t} \\ \hat{H}_\chi &\equiv i\chi = i\frac{\partial}{\partial t_+} \end{aligned} \quad (1.2.29)$$

### 1.3 Orthonormal and null tetrads

An observer who moves along a world line of constant  $r$  and  $\theta$  with an angular velocity  $\omega \equiv d\phi/dt$  relative to the asymptotic rest frame has a tetrad  $\{\mathbf{e}_{(t)}, \mathbf{e}_{(r)}, \mathbf{e}_{(\theta)}, \mathbf{e}_{(\phi)}\}$  associated with him. Such an observer sees no local change in the geometry and is therefore considered a *stationary observer* relative to the local geometry. If his angular velocity is zero, and therefore he moves along a world line of constant  $r$ ,  $\phi$  and  $\theta$ , he is a *static observer (SO)* relative to radial infinity. A SO moves along the integral curves of  $\xi$ . If we require  $\mathbf{e}_{(r)}$  and  $\mathbf{e}_{(\theta)}$  to be parallel to  $\partial/\partial r$  and  $\partial/\partial \theta$  respectively, we then find that the vectors in the

### 1.3. Orthonormal and null tetrads

tetrad of a stationary observer are given by

$$\begin{aligned}
\mathbf{e}_{(t)} &= \frac{1}{\sqrt{|g_{tt} + 2\omega g_{t\phi} + \omega^2 g_{\phi\phi}|}} \left( \frac{\partial}{\partial t} + \omega \frac{\partial}{\partial \phi} \right) \\
\mathbf{e}_{(r)} &= \sqrt{\frac{\Delta}{\Sigma}} \frac{\partial}{\partial r} \\
\mathbf{e}_{(\theta)} &= \sqrt{\frac{1}{\Sigma}} \frac{\partial}{\partial \theta} \\
\mathbf{e}_{(\phi)} &= \frac{1}{\sqrt{|g_{tt} + 2\omega g_{t\phi} + \omega^2 g_{\phi\phi}|}} \frac{1}{\sqrt{g_{t\phi}^2 - g_{tt} g_{\phi\phi}}} \left[ -(g_{t\phi} + \omega g_{\phi\phi}) \frac{\partial}{\partial t} + (g_{tt} + \omega g_{t\phi}) \frac{\partial}{\partial \phi} \right]
\end{aligned} \tag{1.3.1}$$

Only the angular velocities  $\omega$  such that  $\mathbf{e}_{(t)}$  is a timelike vector are valid. The corresponding range of validity for  $\omega$  is  $\omega_{\min} < \omega < \omega_{\max}$  where

$$\omega_{\{\min\}^{\max}} = \Omega \mp \sqrt{\Omega^2 - \frac{g_{tt}}{g_{\phi\phi}}} \tag{1.3.2a}$$

$$\Omega \equiv \frac{1}{2} (\omega_{\min} + \omega_{\max}) = -\frac{g_{t\phi}}{g_{\phi\phi}} \tag{1.3.2b}$$

Note that at asymptotic radial infinity it is:  $r\omega_{\{\min\}^{\max}} = \mp 1$ , as it should be. As the Boyer-Lindquist radius  $r$  decreases, the value of  $\omega_{\min}$  increases until it reaches the value zero at the stationary limit surface. If  $r$  decreases below the stationary limit surface then both  $\omega_{\min}$  and  $\omega_{\max}$  are positive and all stationary observers must orbit around the black hole with positive angular velocity. Static observers cannot exist inside the ergosphere and hence the name of static limit surface for the region outside the ergosphere. As  $r$  decreases below the stationary limit surface, the two positive quantities  $\omega_{\min}$  and  $\omega_{\max}$  become larger and closer to each other until they coincide with value  $+\sqrt{g_{tt}/g_{\phi\phi}}$  at the event horizon. All timelike curves at the horizon point inside the black hole. *Dragging of inertial frames* refers to the fact that as a stationary observer approaches the horizon, the range of validity for its angular velocity as seen by an observer at infinity becomes narrower and contains ever larger values.

The quantity  $p_\phi \equiv \mathbf{p}\boldsymbol{\psi} = p_\alpha \psi^\alpha$ , where  $\mathbf{p}$  is the 4-momentum of a certain observer, is the component of angular momentum of that observer along the black hole's spin axis. This quantity is conserved for geodesic observers. The only stationary

### 1.3. Orthonormal and null tetrads

---

observers for whom this quantity is zero are those with an angular velocity  $\Omega$  (1.3.2b). These observers are the closest analogue to the static observers in Schwarzschild space-time on the Kerr-Newman space-time in the sense that their 4-velocity is orthogonal to  $\psi$ , the hypersurfaces of constant  $t$ . These observers are called *zero angular momentum observers (ZAMO)*, or alternatively, *locally non-rotating observers (LNRO)*. The angular velocity  $\omega_{ZAMO}(=\Omega)$  of the ZAMOs as they approach the horizon tends to  $\omega_{ZAMO}(r=r_+) = \Omega_+$ , which can therefore be interpreted as the angular velocity of the horizon. The stationary observers whose angular velocity is constant and equal to  $\Omega_+$  are observers that follow integral curves of  $\chi$  and are called *rigidly rotating observers (RRO)*. Their 4-velocity becomes null at the speed-of-light surface  $r=r_{\text{SOL}}$  and is spacelike for  $r > r_{\text{SOL}}$ .

The last orthonormal tetrad we wish to present is the *Carter orthonormal tetrad* [16], which corresponds to a stationary observer (1.3.1) with angular velocity

$$\omega_c = \frac{a}{r^2 + a^2} \quad (1.3.3)$$

The Carter orthonormal tetrad is given by

$$\begin{aligned} \mathbf{e}_{(t)} &= +\frac{r^2 + a^2}{\sqrt{\Delta\Sigma}} \left[ \frac{\partial}{\partial t} + \frac{a}{r^2 + a^2} \frac{\partial}{\partial \phi} \right] \\ \mathbf{e}_{(\phi)} &= \frac{1}{\sqrt{\Sigma}} \left[ a \sin \theta \frac{\partial}{\partial t} + \frac{1}{\sin \theta} \frac{\partial}{\partial \phi} \right] \end{aligned} \quad (1.3.4)$$

together with  $\mathbf{e}_{(r)}$  and  $\mathbf{e}_{(\theta)}$  of equation (1.3.1).

All the above tetrads are orthonormal, consisting of one timelike and three spacelike vectors, and they can therefore be associated to observers in some regions of exterior Kerr-Newman. The Newman-Penrose formalism, however, is constructed with a basis of four null vectors. We will next give the two null tetrads that are most commonly used, which are the only two we have made use of in this thesis.

Kerr and Schild [57] have shown that the Kerr-Newman metric can be expressed



### 1.3. Orthonormal and null tetrads

---

as

$$g_{\alpha\beta} = \eta_{\alpha\beta} + 2Hk_{\alpha}k_{\beta} \quad (1.3.5)$$

where  $H$  is a scalar field and  $k_{\alpha}$  are the covariant components of a null vector field, then the null congruence  $k_{\alpha}$  is geodesic and  $H$  can be chosen so that  $k_{\alpha}$  is an affinely-parametrized geodesic. They further showed that  $k_{\alpha}$  is then a principal null direction.

The Weyl tensor for the Kerr-Newman metric has two principal null directions; these correspond to the two different null vectors  $\mathbf{k}$  such that equation (1.3.5) for the Kerr-Newman metric is satisfied. The Kerr-Newman solution is therefore of Petrov Type D.

The *advanced Eddington-Finkelstein co-ordinate system* is defined by the set of co-ordinates  $\{\bar{t}, r, \theta, \bar{\phi}\}$  where

$$d\bar{t} \equiv dt + \frac{2Mr}{\Delta} dr \quad (1.3.6)$$

If the Kerr-Newman metric is expressed in the advanced Eddington-Finkelstein co-ordinates, we obtain in contravariant form:

$$\frac{\partial^2}{\partial s^2} = -\frac{\partial^2}{\partial \bar{t}^2} + \frac{1}{\Sigma} \left[ (r^2 + a^2) \frac{\partial^2}{\partial r^2} + 2a \frac{\partial}{\partial r} \frac{\partial}{\partial \bar{\phi}} + \frac{1}{\sin^2 \theta} \frac{\partial^2}{\partial \bar{\phi}^2} + \frac{\partial^2}{\partial \theta^2} \right] - \frac{2Mr}{\Sigma} \left( \frac{\partial}{\partial \bar{t}} - \frac{\partial}{\partial r} \right)^2 \quad (1.3.7)$$

By comparing equations (1.3.5) and (1.3.7), we can immediately see that the vector for one of the principal null congruences must be:

$$\mathbf{n} = \frac{\Delta}{2\Sigma} \left( \frac{\partial}{\partial \bar{t}} - \frac{\partial}{\partial r} \right) \quad (1.3.8)$$

in the advanced Eddington-Finkelstein co-ordinate system. The other principal null direction  $\mathbf{l}$  may be obtained by using the fact that the Kerr-Newman metric is invariant under the symmetry  $(t, \phi) \rightarrow (-t, -\phi)$ , It may alternatively be obtained by performing the transformation  $dr \rightarrow -dr$ , which interchanges ingoing and outgoing rays. The vectors  $\mathbf{l}$  and  $\mathbf{n}$  are respectively outgoing and ingoing. Their normalization is chosen so that they are regular at the inner and outer horizons when expressed in the advanced Eddington-Finkelstein system.

### 1.3. Orthonormal and null tetrads

---

The Boyer-Lindquist co-ordinates are singular at the horizon. For a particle or photon falling inward through the horizon not only the Boyer-Lindquist co-ordinate  $t$  will go to infinity as the horizon is approached, but also  $\phi$  will go to infinity, due to the dragging of inertial frames. A set of co-ordinates that remain finite as a particle or photon fall inward through the horizon will therefore need to perform an infinite untwisting of  $\phi$  as well as an infinite compression of  $t$  in the neighborhood of the horizon. The Kerr co-ordinate system achieves both objectives. The ingoing principal null congruence expressed in the Kerr co-ordinates is simply

$$\mathbf{n} = -\frac{\partial}{\partial r} \quad (1.3.9)$$

It can be shown that the only particle that can remain forever at the horizon is massless and is the one that follows the curves of the outgoing principal null congruence  $\mathbf{l}$ . We therefore say that  $\mathbf{l}$  is the generator of the horizon. These particles have angular velocity  $\Omega_+$ . The fact that their angular velocity is non-zero is another consequence of the dragging of inertial frames.

The congruences given by  $\mathbf{l}$  and the ones given by  $\mathbf{n}$  are both geodesic and are the two principal null directions of the Kerr-Newman space-time. The *Kinnersley tetrad* [58] consists in the null vectors  $\mathbf{l}$  and  $\mathbf{n}$  together with another null vector,  $\mathbf{m}$ , and its complex conjugate, chosen so that the normalization conditions correspond to those of the Newman-Penrose tetrad, i.e., (1.1.7). The Kinnersley tetrad is therefore formed with the vectors

$$\mathbf{l} = \frac{1}{\Delta} \left[ (r^2 + a^2) \frac{\partial}{\partial t} + \Delta \frac{\partial}{\partial r} + a \frac{\partial}{\partial \phi} \right] \quad (1.3.10a)$$

$$\mathbf{n} = \frac{1}{2\Sigma} \left[ (r^2 + a^2) \frac{\partial}{\partial t} - \Delta \frac{\partial}{\partial r} + a \frac{\partial}{\partial \phi} \right] \quad (1.3.10b)$$

$$\mathbf{m} = \frac{-\rho^*}{\sqrt{2}} \left[ ia \sin \theta \frac{\partial}{\partial t} + \frac{\partial}{\partial \theta} + i \operatorname{cosec} \theta \frac{\partial}{\partial \phi} \right] \quad (1.3.10c)$$

The spin coefficients with respect to this tetrad of the Kerr-Newman metric are

### 1.3. Orthonormal and null tetrads

given by (1.1.10):

$$\begin{aligned}\rho &= -\frac{1}{r - ia \cos \theta}; & \beta &= -\frac{\rho^* \cot \theta}{2\sqrt{2}}; & \pi &= \frac{ia\rho^2 \sin \theta}{\sqrt{2}}; \\ \tau &= \frac{-ia \sin \theta}{\sqrt{2}\Sigma}; & \mu &= \frac{\rho\Delta}{2\Sigma}; & \gamma &= \mu + \frac{(r - M)}{2\Sigma}; \\ \alpha &= \pi - \beta^*; & \kappa &= \sigma = \lambda = \nu = \epsilon = 0\end{aligned}\quad (1.3.11)$$

In terms of the Newman-Penrose formalism with the Kinnersley tetrad, the Weyl tensor and the electromagnetic field corresponding to the Kerr-Newman solution of the Einstein-Maxwell equations are given by

$$\psi_{\pm 2} = \psi_{\pm 1} = 0 \qquad \psi_0 = M\rho^3 + Q^2\rho^3\rho^* \quad (1.3.12a)$$

$$\phi_{\pm 1} = 0 \qquad \phi_0 = -\frac{1}{2}iQ\rho^2 \quad (1.3.12b)$$

It is easy to see that the effect of the parity operator (1.2.19) on the NP Kinnersley tetrad and spin coefficients is

$$\begin{aligned}\mathcal{P}X &= X & \mathcal{P}Y &= Y^* & \mathcal{P}Z &= -Z^* \\ X &= \mathbf{l}, \mathbf{n}, D, \Delta & Y &= \epsilon, \rho, \mu, \gamma & Z &= \mathbf{m}, \delta, \tau, \pi, \alpha, \beta\end{aligned}\quad (1.3.13)$$

Under the symmetry transformation (1.2.18), the Kinnersley tetrad transforms in the following manner:

$$\mathbf{l} \rightarrow -\frac{\Sigma}{\Delta}\mathbf{n}, \quad \mathbf{n} \rightarrow -\frac{\Delta}{\Sigma}\mathbf{l}, \quad \mathbf{m} \rightarrow \frac{\rho^*}{\rho}\mathbf{m}^* \quad \text{under} \quad (t, \phi) \rightarrow (-t, -\phi) \quad (1.3.14)$$

From their definition (1.1.12), the NP Maxwell scalars will accordingly transform under these symmetries as

$$\phi_h \rightarrow \phi_h^* \quad \forall h \quad \text{under} \quad (\theta, \phi) \rightarrow (\pi - \theta, \phi + \pi) \quad (1.3.15a)$$

$$\left. \begin{aligned}\phi_{-1} &\rightarrow \Delta^{-1}\rho^{-2}\phi_{+1} \\ \phi_0 &\rightarrow -\phi_0 \\ \phi_{+1} &\rightarrow \Delta\rho^2\phi_{-1}\end{aligned} \right\} \text{under} \quad (t, \phi) \rightarrow (-t, -\phi) \quad (1.3.15b)$$

subject to the boundary conditions being the same.

We have decided to mainly use the Kinnersley tetrad when working with the Newman-Penrose formalism because of the fact that this the null tetrad used by

## 1.4. Black hole thermodynamics

---

the overwhelming majority of the literature. The reason for this popular choice is probably that the decoupling and separability of the linear perturbations of general spin in the Kerr background discovered by Teukolsky ([86], [87]) was originally obtained using the Kinnersley tetrad. Nevertheless, the tetrad (1.3.10) does not fully exploit the symmetries of the space-time. The Carter null tetrad [18], on the other hand, does exploit the symmetries of the space-time as it does not violate the symmetry (1.2.18). The *Carter null tetrad* in the co-ordinate system  $\{r, q, \tilde{\phi}, \tilde{t}\}$  where  $q \equiv a \cos \theta$ ,  $\tilde{\phi} \equiv a^{-1}\phi$  and  $\tilde{t} \equiv t - a\phi$  is

$${}^c\mathbf{l} = \frac{1}{\sqrt{2\Delta\Sigma}} \left[ -\Delta \frac{\partial}{\partial r} + \frac{\partial}{\partial \tilde{\phi}} + r^2 \frac{\partial}{\partial \tilde{t}} \right] \quad (1.3.16a)$$

$${}^c\mathbf{n} = \frac{1}{\sqrt{2\Delta\Sigma}} \left[ +\Delta \frac{\partial}{\partial r} + \frac{\partial}{\partial \tilde{\phi}} + r^2 \frac{\partial}{\partial \tilde{t}} \right] \quad (1.3.16b)$$

$${}^c\mathbf{m} = \frac{1}{\sqrt{2(a^2 - q^2)\Sigma}} \left[ -(a^2 - q^2) \frac{\partial}{\partial q} - i \frac{\partial}{\partial \tilde{\phi}} + iq^2 \frac{\partial}{\partial \tilde{t}} \right] \quad (1.3.16c)$$

We keep the same values for  $\Sigma$  and  $\rho$  as the ones we have been using so far, which in the new co-ordinates can be written as  $\Sigma = r^2 + q^2$  and  $\rho = \frac{-1}{r - iq}$ . The spin coefficients in the Carter null tetrad are

$$\begin{aligned} {}^c\mu &= -\sqrt{\frac{\Delta}{2\Sigma}}\rho; & {}^c\rho &= {}^c\mu; \\ {}^c\epsilon &= -\frac{\Delta\rho + (r - M)}{2\sqrt{2\Delta\Sigma}}; & {}^c\gamma &= {}^c\epsilon; \\ {}^c\tau &= \sqrt{\frac{(a^2 - q^2)}{2\Sigma}}i\rho; & {}^c\pi &= -{}^c\tau; \\ {}^c\alpha &= -\frac{i(a^2 - q^2)\rho + q}{2\sqrt{2(a^2 - q^2)\Sigma}}; & {}^c\beta &= -{}^c\alpha; \\ {}^c\kappa &= {}^c\sigma = {}^c\lambda = {}^c\nu = 0 \end{aligned} \quad (1.3.17)$$

## 1.4 Black hole thermodynamics

Hawking [45] showed in 1975 that particle creation could occur at late times as a result of the collapse of a star to a Schwarzschild black hole. He also found that the nature of this radiation is thermal, black body radiation at the *Hawking*

## 1.4. Black hole thermodynamics

---

temperature

$$T_H = \frac{\kappa_+}{2\pi} \quad (1.4.1)$$

Consider the collapse of a spherical, uncharged star and the vacuum state that corresponds to quantizing the field with respect to the standard incoming exponential modes at  $\mathcal{I}^-$ . If the field is in this state, then an inertial partial detector at  $\mathcal{I}^-$  will detect no particles. As the radius of the collapsing star becomes close to the radius of its event horizon, the waves coming in from  $\mathcal{I}^-$  suffer a blue-shift as they approach the surface of the star which is much smaller than the red-shift they suffer as they emerge through the star. The Bogolubov transformation between these outgoing waves as they reach  $\mathcal{I}^+$  and the standard exponential modes at  $\mathcal{I}^+$  can be calculated. The result is that an inertial partial detector at  $\mathcal{I}^+$  will detect a flux of outgoing particles corresponding to a thermal spectrum of a black body at the Hawking temperature. This flux of particles is the *Hawking radiation*. The mass of the black hole will decrease in time due to the emission of this flux, that is, the black hole evaporates. If the black hole is rotating, more particles will be emitted by its gravitational field with angular momentum of the same sign as that of the black hole's. Similarly, if the black hole is charged, more particles will be emitted by its electromagnetic field with charge of the same sign as that of the black hole's. Both the angular momentum and charge of the black hole will also decrease in time.

Heuristically, the Hawking radiation can be explained in the following manner. Virtual particle-antiparticle pairs created with wavelength  $\lambda$  separate temporarily to a distance  $\sim \lambda$  before they are reannihilated. For those pairs of wavelength of the order of the size of the black hole,  $\lambda \sim M$ , the tidal forces between the particle and the antiparticle become so large that they separate before reannihilation. One particle escapes to infinity, thus contributing to the Hawking radiation, whilst the other particle enters the black hole following a timelike path of negative energy relative to infinity. In a strict sense, however, it is not possible to talk about particles in curved space-time, except at an asymptotically

## 1.4. Black hole thermodynamics

---

flat region. It is instead the stress energy tensor the right tool to use in order to describe the natural processes.

The above results suggest a relationship between black hole processes and thermodynamics. This relationship is at a much more essential level than the mere existence of thermal radiation emitted by black holes. Indeed, a correlation has been found between certain properties of black holes and the four laws of thermodynamics. This correlation is the following:

### 0th law

The zeroth law of thermodynamics states that the temperature is constant throughout a system in thermal equilibrium.

The black hole analogue of this law is the theorem [17] that the surface gravity parameter  $\kappa_+$ , and therefore the Hawking temperature, is constant over the event horizon of a stationary black hole.

### 1st law

The first law of thermodynamics states that for a process that only involves infinitesimal variations of the thermodynamic co-ordinates, it must be:

$$\delta E = T\delta S + P\delta V \tag{1.4.2}$$

Bardeen, Carter and Hawking [2] have found that for variations in the metric of a stationary black hole that do not alter its stationarity, it must be:

$$\delta M = \frac{1}{8\pi}\kappa_+\delta\mathcal{A} + \Omega_+\delta J \tag{1.4.3}$$

From equation (1.4.1) it follows that the two laws are analogous if a correspondence is established between  $E$  and  $M$ , between the entropy  $S$  and  $\frac{\mathcal{A}}{4}$ , and finally, between the “work term”  $P\delta V$  and  $\Omega_+\delta J$ .

### 2nd law

*Hawking’s area theorem* [44] requires the total event horizon area  $\mathcal{A}_T$  of black hole space-times to be non-decreasing, i.e.,  $d\mathcal{A}_T \geq 0$ , in all black hole processes for which the weak energy condition is satisfied. Since the entropy of the black

## 1.5. Physical phenomena associated with the ergosphere

---

hole is  $S = \frac{A}{4}$  from the first law, Hawking's area theorem is just a special case of the second law of thermodynamics:  $dS_T \geq 0$ . Black hole evaporation does not violate the 2nd law of thermodynamics since, even though the mass, and therefore also the event horizon area, decrease in time, account must be taken of the increase in entropy outside the black hole due to the Hawking radiation.

### 3rd law

The third law of thermodynamics states that it is not possible to reach the absolute zero of temperature through a finite series of processes. An analogue of this formulation of the third law exists in black hole physics. Israel [50] formulated it as: a non-extremal black hole ( $T_H > 0$ ) cannot become extremal ( $T_H = 0$ ) at a finite advanced time  $v$  in any continuous process in which the stress-energy tensor of accreted matter stays bounded and satisfies the weak energy condition in a neighbourhood of the outer horizon. The *cosmic censorship hypothesis* states that naked singularities cannot form from gravitational collapse. Injection of matter whose energy density is or becomes negative in a neighbourhood of the outer horizon of a non-extreme black hole can not only result in the formation of an extreme black hole but also violate cosmic censorship.

## 1.5 Physical phenomena associated with the ergosphere

The existence of the ergosphere has important physical consequences, both on a classical and on a quantum level.

Penrose [75] showed in 1969 that it is possible to extract energy from black holes that possess an ergosphere, in what is referred to as the *Penrose process*. The reason being that the change in the mass of a black hole when a test-particle falls into it is the energy of the particle as measured by a SO. This energy is equal to  $-p\xi$  for an uncharged particle. We know that the Killing vector  $\xi$  is timelike

## 1.5. Physical phenomena associated with the ergosphere

---

outside the ergosphere but spacelike inside it, and therefore for certain timelike orbits of the uncharged test-particle, its energy may be negative as viewed from radial infinity by a SO. These orbits of negative energy are, however, confined entirely within the ergosphere. Therefore, in order to send in a test-particle from outside the ergosphere that carries negative energy into the black hole, its orbit must be changed. Extraction of energy from the black hole can be achieved by dividing a geodesic particle that is coming in from radial infinity into two other particles, once inside the ergosphere. One of the particles falls into the black hole following a negative energy orbit as seen by a SO, and the other one is retrieved at radial infinity possessing an energy larger than that of the initially incoming particle.

If both the test-particle and the black hole are charged, then the region within which the energy of the particle may be negative as viewed from infinity by a SO is not exactly the ergosphere, but a region called the *effective ergosphere* [66]. Indeed, if the charges of the particle and of the black hole have opposite sign then the energy of the particle as viewed from infinity by a SO will be more negative and therefore the effective ergosphere will be larger than the ergosphere. Analogously, if the charges have the same sign then the effective ergosphere will be smaller than the ergosphere.

The second law of black hole dynamics shows that there is a limit to the decrease in the mass of the black hole which may be achieved via the Penrose process. This limit was found by Christodoulou [23] and Christodoulou and Ruffini [24], independently of Hawking's result [44], and is the *irreducible mass* of the black hole:

$$M_{\text{irred}} = \frac{1}{2} \sqrt{r_+^2 + a^2} \quad (1.5.1)$$

There is a corresponding effect in classical waves to the Penrose process, which was discovered by Zel'dovich [94] and Starobinskiĭ [83] for spin-0 and shortly after by Starobinskiĭ and Churilov [84] for spin-1 and spin-2. We shall see in subsequent chapters that certain modes that are part of the Fourier mode



## 1.5. Physical phenomena associated with the ergosphere

---

decomposition of field perturbations of black holes, may be reflected back by a black hole with an ergosphere with an amplitude larger than that of the incident wave mode. These modes are called *superradiant modes* and the amplification effect of these modes by the rotating black hole is called *superradiance*. As for the Penrose process, the part of the incident superradiant wave mode that has been transmitted through to the future horizon carries negative energy into the black hole. Similarly, certain field wave modes that emerge from the past horizon may be reflected by the black hole back to the future horizon with an increased amplitude. These modes are also superradiant modes. The phenomenon of superradiance occurs for the spin-0, spin-1 and spin-2 fields but it does not for the neutrino case.

Finally, there is a quantum counterpart to classical superradiance, which was discovered by Unruh [89] in 1974. He showed that a black hole possessing an ergosphere emits out to  $\mathcal{I}^+$  positive fluxes of energy and angular momentum when the field is in a quantum state which is empty at both  $\mathcal{H}^-$  and  $\mathcal{I}^-$ . The only contribution to these fluxes is from superradiant field modes. As a consequence of the emission of these positive fluxes, the mass and the angular momentum of the rotating black hole decrease. This process is called the *Starobinskiĭ-Unruh effect*. In Chapter 6 we will describe this effect further and calculate its radial flux for the spin-1 case.

# Chapter 2

## Field equations

### 2.1 Introduction

We consider the field equations satisfied by the electromagnetic field in a general Type D background. The background is considered fixed and the electromagnetic field appearing in the field equations is the total electromagnetic field, regardless of its origin, whether background or perturbation. In the case of an uncharged background, however, the electromagnetic field appearing in the field equations may alternatively be interpreted as the one corresponding to the first order of a linear perturbation only.

By making use of the NP formalism, Teukolsky ([86], [87]) showed that the equations describing linear electromagnetic, neutrino and gravitational perturbations of a general Type D background can be decoupled. He further showed that some of the decoupled equations can be solved by separation of variables in the Boyer-Lindquist co-ordinate system in the Kerr background. Carter [16] had previously shown the separability in the scalar case. Cohen and Kegeles [28] showed in 1974 that in a Type D background all the electromagnetic field components may be derived by double differentiation from one single, complex Maxwell scalar, thereby acting as a Debye potential. This scalar then carries

the two dynamical degrees of freedom of the perturbed field. Chrzanowski [25] was the first author to give, using Teukolsky's results, analytic expressions for the linear electromagnetic and gravitational perturbation potentials in the Kerr background in the homogeneous case. He showed that the electromagnetic potential may be derived from the Debye potential of Cohen and Kegeles's. He obtained the expressions for the potential from a conjecture about the form of the Green function for the uncoupled field equations, which he proved to be correct in the Kerr background for the particular case of spin-1 perturbations for high frequency and also for spin-0 perturbations. However, it was Wald [91] in 1978 who developed a very elegant and general formalism which was underlying Teukolsky's and Chrzanowski's results. Wald's formalism, which is valid in an arbitrary background, proved in a very simple manner that Chrzanowski's results (and also his conjecture about the Green function) were correct. This formalism also gives a much better understanding of the potential and field solutions and the relationships between the different quantities.

In this chapter we are going to develop Wald's formalism for the electromagnetic case and therefore derive Chrzanowski's expressions for the electromagnetic potential in the Kerr background. The clarity of this formalism will allow us to explain some features of the field equations, the origin of which remained so far unclear. This formalism will also enable us to produce the various expressions for the potential and the NP Maxwell scalars in a very compact and simple way. This derivation makes clear the origin of these expressions as well as the relationships between them. We will establish, when appropriate, the parallelism between our expressions and the analogous equations in the literature as we unravel Wald's formalism for the electromagnetic case. Our initial results are valid in an arbitrary background, are then specialized to a Type D background where  $\kappa = \sigma = \nu = \lambda = 0$  and finally to the Kerr-Newman background. In particular, we generalize Teukolsky's results to the Kerr-Newman background.

Finally, we derive formal and simple expressions for the potential in the ingoing

and upgoing gauges, both in terms of one single, complex Maxwell scalar. This means that quantum field theory could be constructed from these expressions as if it were a complex scalar field theory. This is indeed the case in the Reissner-Nordström background. Unfortunately, though, we shall show that this is not possible in the Kerr background since the uncoupled equation for this Maxwell scalar cannot be solved by separation of variables.

## 2.2 Wald's formalism

In this section we will describe Wald's [91] formalism for finding an analytic expression for the solution of a coupled equation in terms of a solution of a related decoupled equation. We will later use the latter solution to find the electromagnetic potential and field components. Everything in this section is valid in any smooth manifold with a smooth metric.

Let  $\mathcal{E}$  be a linear, partial differential operator and  $f$  a tensor field of the type on which  $\mathcal{E}$  acts. The general field equation we want to solve is given by

$$\mathcal{E}(f) = 0 \tag{2.2.1}$$

Suppose that we have been able to derive a decoupled equation for a new variable  $\phi \equiv \mathcal{T}(f)$  by applying the operator  $\mathcal{S}$  on (2.2.1):

$$\mathcal{S}\mathcal{E}(f) = \mathcal{O}\mathcal{T}(f) = \mathcal{O}(\phi) = 0 \tag{2.2.2}$$

where the operator  $\mathcal{O}$  is defined by the first equality in (2.2.2), and  $\mathcal{O}(\phi) = 0$  is a decoupled equation.

Throughout this chapter we shall use the following definition of the *adjoint* of a differential operator: if  $Q_{\mu_1 \dots \mu_m}^{\nu_1 \dots \nu_n}$  is a linear, partial differential operator mapping components  $f_{\nu_1 \dots \nu_n}$  of tensor fields of type  $(0, n)$  to components  $Q_{\mu_1 \dots \mu_m}^{\nu_1 \dots \nu_n} f_{\nu_1 \dots \nu_n}$  of tensor fields of type  $(0, m)$ , then the adjoint of  $Q_{\mu_1 \dots \mu_m}^{\nu_1 \dots \nu_n}$ , denoted by  $Q^{\dagger \nu_1 \dots \nu_n}_{\mu_1 \dots \mu_m}$ , is defined to be the (unique) linear, partial differential

## 2.3. Maxwell equations and gauge invariance

---

operator mapping components  $g^{\mu_1 \dots \mu_m}$  of tensor fields of type  $(m, 0)$  to components  $Q^{\dagger \nu_1 \dots \nu_n}_{\mu_1 \dots \mu_m} g^{\mu_1 \dots \mu_m}$  of tensor fields of type  $(n, 0)$  such that  $\forall f_{\nu_1 \dots \nu_n}, g^{\mu_1 \dots \mu_m}$ ,

$$g^{\mu_1 \dots \mu_m} (Q_{\mu_1 \dots \mu_m}^{\nu_1 \dots \nu_n} f_{\nu_1 \dots \nu_n}) - (Q^{\dagger \nu_1 \dots \nu_n}_{\mu_1 \dots \mu_m} g^{\mu_1 \dots \mu_m}) f_{\nu_1 \dots \nu_n} = t^\alpha{}_{;\alpha} \quad (2.2.3)$$

Wald showed in the following manner that by direct differentiation of a solution of the adjoint of the decoupled equation a solution of the initial field equation is obtained, if its operator is self-adjoint. Let  $\varphi$  be the solution of the adjoint of the decoupled equation, i.e.,

$$\mathcal{O}^\dagger(\varphi) = 0 \quad (2.2.4)$$

Then, if we apply the adjoint of (2.2.2) to  $\varphi$  we obtain

$$\mathcal{E}^\dagger \mathcal{S}^\dagger(\varphi) = \mathcal{T}^\dagger \mathcal{O}^\dagger(\varphi) = 0 \quad (2.2.5)$$

Therefore, if  $\mathcal{E} = \mathcal{E}^\dagger$ , then  $f = \mathcal{S}^\dagger(\varphi)$  is a solution of the field equation (2.2.1). The variable  $\phi$  satisfying (2.2.2) is then given by  $\phi = \mathcal{T} \mathcal{S}^\dagger(\varphi)$ .

## 2.3 Maxwell equations and gauge invariance

The Maxwell equations can be written in terms of the potential  $\mathbf{A}$  and the source terms  $\mathbf{J}$  as

$$D_\alpha{}^\beta A_\beta = J_\alpha \quad (2.3.1)$$

where

$$D_\alpha{}^\beta \equiv \delta_\alpha{}^\beta \nabla^\gamma \nabla_\gamma - \delta_\gamma{}^\beta \nabla^\gamma \nabla_\alpha \quad (2.3.2)$$

We are using rationalized units in the sense that Maxwell equations are written as in (2.3.1), whereas Teukolsky [87] uses unrationalized units which include a factor  $4\pi$  in these equations.

Alternatively, in terms of the field components

$$F_{\alpha\beta} = -F_{\beta\alpha} \equiv A_{\beta;\alpha} - A_{\alpha;\beta} \quad (2.3.3)$$

## 2.3. Maxwell equations and gauge invariance

---

the Maxwell equations become

$$g^{\alpha\gamma} F_{\alpha\beta;\gamma} = J_\beta \quad (2.3.4a)$$

$$F_{[\alpha\beta;\gamma]} = 0 \quad (2.3.4b)$$

The *law of current conservation*

$$\nabla_\alpha J^\alpha = 0 \quad (2.3.5)$$

follows directly from the field equation (2.3.4a) and the antisymmetry of the electromagnetic tensor  $F_{\alpha\beta}$ .

In terms of the NP Maxwell scalars (1.1.12) the Maxwell equations (2.3.4) take the form:

$$\phi_{0|(1)} - \phi_{-1|(4)} = \frac{1}{2} J_{(1)} \quad (2.3.6a)$$

$$\phi_{+1|(3)} - \phi_{0|(2)} = \frac{1}{2} J_{(2)} \quad (2.3.6b)$$

$$\phi_{0|(3)} - \phi_{-1|(2)} = \frac{1}{2} J_{(3)} \quad (2.3.6c)$$

$$\phi_{+1|(1)} - \phi_{0|(4)} = \frac{1}{2} J_{(4)} \quad (2.3.6d)$$

It is well known that there is a certain freedom in the choice of the potentials that satisfy the Maxwell equations (2.3.1) and yield the same electromagnetic field via equations (2.3.3). Indeed, if a certain potential satisfies equations (2.3.1) then it is always possible to apply the *gauge transformation*

$$A_\alpha \rightarrow A'_\alpha = A_\alpha + \frac{\partial \Phi}{\partial x_\alpha} \quad (2.3.7)$$

and the transformed potential  $A'_\alpha$  will also satisfy the Maxwell equations and it will yield the same electromagnetic field as the potential  $A_\alpha$ . The invariance of the field under these transformations is called *gauge invariance*.

The homogeneous Maxwell equations (2.3.1) in the Lorentz gauge  $\nabla_\alpha A^\alpha = 0$  become, in a vacuum space-time,

$$\nabla^\gamma \nabla_\gamma A_\alpha = 0 \quad (2.3.8)$$

## 2.3. Maxwell equations and gauge invariance

---

A plane-wave solution is of the form

$$A_\alpha = e_\alpha e^{ik_\beta x^\beta} + e_\alpha^* e^{-ik_\beta x^\beta} \quad (2.3.9)$$

where the following conditions

$$k_\alpha k^\alpha = 0 \quad (2.3.10a)$$

$$k_\alpha e^\alpha = 0 \quad (2.3.10b)$$

must be satisfied as a consequence of (2.3.8) and the Lorentz condition respectively. The tensor  $\mathbf{e}$  is called the *polarization* tensor and  $\mathbf{k}$  is the direction of propagation. The Lorentz gauge describes a transverse wave via (2.3.10b). Because of the condition (2.3.10b) out of the four components of  $\mathbf{e}$  only three are independent. Lorentz gauge still leaves a certain freedom in the choice of the electromagnetic potential: we can perform the gauge transformation (2.3.7) with

$$\Phi(x) = i\epsilon e^{ik_\beta x^\beta} - i\epsilon^* e^{-ik_\beta x^\beta} \quad (2.3.11)$$

The transformed potential is then given by

$$A'_\alpha = e'_\alpha e^{ik_\beta x^\beta} + e'^*_\alpha e^{-ik_\beta x^\beta} \quad (2.3.12)$$

with

$$e'_\alpha = e_\alpha - \epsilon k_\alpha \quad (2.3.13)$$

and  $\epsilon$  an arbitrary parameter. The transformed potential  $A'_\alpha$  will also satisfy the homogeneous Maxwell equations as well as the Lorenz gauge condition. This means that of the three independent components of  $\mathbf{e}$  only two of them are physically significant.

In an asymptotically flat space-time, like Kerr-Newman, the above discussion about the plane wave (2.3.9) is valid at radial infinity for a wave travelling in the direction of  $\mathbf{l}$ , i.e., such that  $\mathbf{k} = \mathbf{l}$ . In particular, the condition (2.3.10b) implies that  $e^n = 0 = e_l$  at radial infinity. The gauge transformation (2.3.13) then means that, asymptotically,  $e_m$  is left invariant as well as  $e'_l = e_l = 0$

## 2.4. Wald's formalism for spin-1

---

whereas  $e'_n = e_n - \epsilon$ . We can therefore make  $e'_n$  equal to zero by choosing  $\epsilon = e_n$  so that it is only  $e_m$  and  $e_{m^*}$  that carry physical significance at radial infinity.

Any plane wave  $\psi$ , which is transformed by a rotation of an angle  $\vartheta$  about the direction of propagation into

$$\psi' = e^{ih\vartheta}\psi \tag{2.3.14}$$

is said to have *helicity*  $h$ . When subjecting the null vector  $\boldsymbol{l}$  to a rotation of an angle  $\vartheta$ , then  $\boldsymbol{l}$  and  $\boldsymbol{n}$  are left unchanged whereas  $m^\mu \rightarrow e^{i\vartheta}m^\mu$ . Thus, an electromagnetic wave propagating in the direction of  $\boldsymbol{l}$  in an asymptotically flat background can be decomposed into parts which, at radial infinity, have helicity  $-1$ ,  $0$  and  $+1$ . However, the physically significant helicities at radial infinity are  $\pm 1$ , not  $0$ .

The conclusions we have reached for an electromagnetic wave travelling in the direction of  $\boldsymbol{l}$  in an asymptotically flat background are equally valid for an electromagnetic wave travelling in the direction of  $\boldsymbol{n}$  in the same background.

## 2.4 Wald's formalism for spin-1

In this section we will unfold for the spin-1 case Wald's formalism described in Section 2.2. The following are the correspondences between the general operators and other objects used in that section and the ones we are going to use for the spin-1 case:

$$\begin{aligned} f &\leftrightarrow \boldsymbol{A}; & \phi &\leftrightarrow \phi; & \varphi &\leftrightarrow \varphi \\ \mathcal{E} &\leftrightarrow D = 2K^\dagger K; & \mathcal{T} &\leftrightarrow K; & \mathcal{S} &\leftrightarrow 2\Pi; & \mathcal{O} &\leftrightarrow P \end{aligned} \tag{2.4.1}$$

Clearly, since  $D = 2K^\dagger K$ , the spin-1 field equations are self-adjoint.

The gravitational quantities (i.e., spin coefficients and null tetrad) appearing in the Maxwell equations in NP form are the ones of the background that we are considering. However, as mentioned in the introduction, the interpretation of the



## 2.4. Wald's formalism for spin-1

---

electromagnetic quantities in the Maxwell equations can differ if the background considered is uncharged. If the background is charged, then it is considered fixed and the NP Maxwell scalars include the electromagnetic field associated to the background (e.g., (1.3.12b) for Kerr-Newman) as well as an electromagnetic perturbation. On the other hand, if the background is uncharged, like Kerr, we may alternatively consider the Maxwell scalars in the Maxwell equations to correspond only to the first order of a linear electromagnetic perturbation. Since the electromagnetic stress-energy tensor is second order in the electromagnetic field, the change in an uncharged background caused by the first order perturbation will be of second order. The change in the gravitational quantities can then be neglected to first order in the Maxwell equations and we still consider the gravitational quantities in the equations to be background quantities. Unfortunately, this second interpretation is not possible in the case of the Kerr-Newman background (although it is in Reissner-Nordström's): all efforts in the literature to decouple the equations for the coupled electromagnetic-gravitational perturbations in this background have been unsuccessful so far. See Chandrasekhar [20] for a description of this treatment.

We thus choose to follow, even in uncharged backgrounds, the first interpretation out of the two described above. This reflects on the fact that we will always use the same symbol,  $\phi_h$ , to refer to the Maxwell scalars both in charged and uncharged backgrounds. That is, the symbol  $\phi_h$  will always represent an electromagnetic perturbation together with the electromagnetic field, if there is one, associated to the background. The symbols for the gravitational quantities always represent background quantities. Ipser [48] has proven that the only time-independent electromagnetic perturbation of the Kerr metric that is physically acceptable, is axisymmetric and is given by (1.3.12b), which corresponds to the addition of charge to the black hole, that is, to the passage from the Kerr metric to the Kerr-Newman metric.

We now define the operator  $K_h^{(a)}$  which maps the potential onto the NP scalars,

## 2.4. Wald's formalism for spin-1

---

i.e.,

$$\phi_h = K_h^{(a)} A_{(a)} \quad (2.4.2)$$

We can easily calculate  $K_h^{(a)}$  from (1.1.12) by expanding out the intrinsic derivatives in (2.3.3) after writing this equation in tetrad form. In this manner we obtain:

$$K_{-1}^{(a)} = -\delta_{(1)}^{(a)} \delta + \delta_{(2)}^{(a)} \kappa + \delta_{(3)}^{(a)} (D + \epsilon^* - \epsilon - \rho^*) - \delta_{(4)}^{(a)} \sigma \quad (2.4.3a)$$

$$K_0^{(a)} = \frac{1}{2} \left[ -\delta_{(1)}^{(a)} (\Delta - \gamma - \gamma^* + \mu^* - \mu) + \delta_{(2)}^{(a)} (D + \epsilon + \epsilon^* + \rho - \rho^*) + \right. \\ \left. + \delta_{(3)}^{(a)} (\delta^* - \pi - \tau^* + \beta^* - \alpha) - \delta_{(4)}^{(a)} (\delta + \pi^* + \tau + \beta - \alpha) \right] \quad (2.4.3b)$$

$$K_{+1}^{(a)} = \delta_{(1)}^{(a)} \nu + \delta_{(2)}^{(a)} (\delta^* + \alpha + \beta^* - \tau^*) - \delta_{(3)}^{(a)} \lambda - \delta_{(4)}^{(a)} (\Delta + \mu^* + \gamma - \gamma^*) \quad (2.4.3c)$$

Similarly, expanding out the intrinsic derivatives in (2.3.6) we can express the Maxwell equations in operator form as

$$2K^{\dagger h}_{(a)} \phi_h = J_{(a)} \quad (2.4.4)$$

where we raise and lower the Maxwell scalar index by applying

$$(\epsilon^{ij}) = \begin{pmatrix} 0 & 0 & -1 \\ 0 & 2 & 0 \\ -1 & 0 & 0 \end{pmatrix} \quad (\epsilon_{ij}) = \begin{pmatrix} 0 & 0 & -1 \\ 0 & 1/2 & 0 \\ -1 & 0 & 0 \end{pmatrix} \quad (2.4.5)$$

respectively.

The adjoint of  $K_h^{(a)}$  can be easily calculated from the definition (2.2.3) of adjoint to give

$$K_{-1}^{\dagger(a)} = \delta_{(1)}^{(a)} (\delta + 2\beta - \tau) + \delta_{(2)}^{(a)} \kappa - \delta_{(3)}^{(a)} (D + 2\epsilon - \rho) - \delta_{(4)}^{(a)} \sigma \quad (2.4.6a)$$

$$K_0^{\dagger(a)} = \frac{1}{2} \left[ +\delta_{(1)}^{(a)} (\Delta + 2\mu) - \delta_{(2)}^{(a)} (D - 2\rho) - \right. \\ \left. - \delta_{(3)}^{(a)} (\delta^* + 2\pi) + \delta_{(4)}^{(a)} (\delta - 2\tau) \right] \quad (2.4.6b)$$

$$K_{+1}^{\dagger(a)} = \delta_{(1)}^{(a)} \nu - \delta_{(2)}^{(a)} (\delta^* - 2\alpha + \pi) - \delta_{(3)}^{(a)} \lambda + \delta_{(4)}^{(a)} (\Delta + \mu - 2\gamma) \quad (2.4.6c)$$

## 2.4. Wald's formalism for spin-1

---

Combining equations (2.4.4) and (2.4.2) together and comparing with (2.3.1) it follows that

$$D_{(a)}^{(b)} = 2K^{\dagger h}_{(a)} K_h^{(b)} \quad (2.4.7)$$

as indicated at the beginning of the section.

All equations given so far in this section are valid for an arbitrary background. We now specialize to a Type D background such that  $\kappa = \sigma = \nu = \lambda = 0$  and a tetrad for which  $\mathbf{l}$  and  $\mathbf{n}$  correspond to the two principal null-directions. From the corollary of the Goldberg-Sachs theorem, we have that  $\kappa = \sigma = \nu = \lambda = 0$  for an empty Type D background. Even though the Goldberg-Sachs theorem only applies to empty space-times, its generalization by Kundt and Trümper means that what follows also applies to the Kerr-Newman background.

We will now proceed to decouple the NP equations (2.4.4) by applying a new operator  $\Pi_j^{(a)}$  onto them in the manner of (2.2.2) for the general case. We therefore need to find an operator  $\Pi_j^{(a)}$  such that  $\Pi_j^{(a)} K^{\dagger h}_{(a)}$  vanishes unless  $h = j$ . We make the ansatz  $\Pi_j^{(a)} = K_j^{(a)} + \xi_j^{(a)}$ , then it can be easily checked that the operators

$$\Pi_{-1}^{(a)} = \delta_{(1)}^{(a)} (K_{-1}^{(1)} + 2\tau) + \delta_{(3)}^{(a)} (K_{-1}^{(3)} - 2\rho) \quad (2.4.8a)$$

$$\begin{aligned} \Pi_0^{(a)} = & \delta_{(1)}^{(a)} (2K_0^{(1)} - 2\mu) + \delta_{(3)}^{(a)} (2K_0^{(3)} + 2\pi) \quad \text{or} \\ & \delta_{(2)}^{(a)} (2K_0^{(2)} - 2\rho) + \delta_{(4)}^{(a)} (2K_0^{(4)} + 2\tau) \end{aligned} \quad (2.4.8b)$$

$$\Pi_{+1}^{(a)} = \delta_{(2)}^{(a)} (K_{+1}^{(2)} + 2\pi) + \delta_{(4)}^{(a)} (K_{+1}^{(4)} - 2\mu) \quad (2.4.8c)$$

which take the explicit form

$$\Pi_{-1}^{(a)} = -\delta_{(1)}^{(a)} (\delta + \pi^* - \alpha^* - \beta - 2\tau) + \delta_{(3)}^{(a)} (D + \epsilon^* - \epsilon - \rho^* - 2\rho) \quad (2.4.9a)$$

$$\begin{aligned} \Pi_0^{(a)} = & -\delta_{(1)}^{(a)} (\Delta - \gamma - \gamma^* + \mu^* + \mu) + \delta_{(3)}^{(a)} (\delta^* + \pi - \tau^* + \beta^* - \alpha) \quad \text{or} \\ & + \delta_{(2)}^{(a)} (D + \epsilon + \epsilon^* - \rho - \rho^*) - \delta_{(4)}^{(a)} (\delta + \pi^* - \tau + \beta - \alpha^*) \end{aligned} \quad (2.4.9b)$$

$$\Pi_{+1}^{(a)} = \delta_{(2)}^{(a)} (\delta^* + \alpha + \beta^* - \tau^* + 2\pi) - \delta_{(4)}^{(a)} (\Delta + \mu^* + \gamma - \gamma^* + 2\mu) \quad (2.4.9c)$$

## 2.4. Wald's formalism for spin-1

---

are the ones we are looking for. Note that the two expressions for  $\Pi_0^{(a)}$  are not equal but they both achieve the desired decoupling and they are physically equivalent. The decoupling operators satisfy

$$2\Pi_j^{(a)} K^{\dagger h}_{(a)} = \delta_j^h P_j \quad (2.4.10)$$

where the operators  $P_j$  are given by

$$P_{-1} = -2[(D - 2\rho - \rho^* - \epsilon + \epsilon^*)(\Delta - 2\gamma + \mu) - (\delta - 2\tau - \alpha^* - \beta + \pi^*)(\delta^* - 2\alpha + \pi)] \quad (2.4.11a)$$

$$P_0 = -2[(\Delta - \gamma - \gamma^* + \mu + \mu^*)(D - 2\rho) - (\delta^* + \pi - \tau^* + \beta^* - \alpha)(\delta - 2\tau)] \quad \text{or} \\ -2[(D - \rho - \rho^* + \epsilon + \epsilon^*)(\Delta + 2\mu) - (\delta - \tau + \beta - \alpha^* + \pi^*)(\delta^* + 2\pi)] \quad (2.4.11b)$$

$$P_{+1} = -2[(\Delta + 2\mu + \mu^* - \gamma^* + \gamma)(D - \rho + 2\epsilon) - (\delta^* + 2\pi - \tau^* + \alpha + \beta^*)(\delta - \tau + 2\beta)] \quad (2.4.11c)$$

Thus, applying  $\Pi_j^{(a)}$  onto the coupled NP Maxwell equations (2.4.4) will decouple them to

$$P_j \phi_j = \Pi_j^{(a)} J_{(a)} \quad (2.4.12)$$

which, in the absence of sources, is the equivalent of  $\mathcal{O}(\phi) = 0$  of Section 2.2 for the spin-1 case in a Type D background. There is no summation over the index  $j$  in equation (2.4.12).

Note that operators  $P_{+1}$  and  $P_{-1}$  are obtainable one from the other under the interchange  $\{\mathbf{l} \leftrightarrow \mathbf{n}, \mathbf{m} \leftrightarrow \mathbf{m}^*\}$ , which results in (1.1.17). Likewise for the operators  $\Pi_{+1}^{(a)} J_{(a)}$  and  $-\Pi_{-1}^{(a)} J_{(a)}$ . This means that equations (2.4.12) for  $\phi_{+1}$  and  $\phi_{-1}$  can be obtained one from the other under the interchange  $\{\mathbf{l} \leftrightarrow \mathbf{n}, \mathbf{m} \leftrightarrow \mathbf{m}^*\}$ , as expected.

The two expressions for the operator  $P_0$  in (2.4.11b), formed from either of the two expressions for  $\Pi_0^{(a)}$ , are identical, as can be checked by using the commutation relations (1.1.14). Not only the left hand side of (2.4.12) remains the same whichever expression for  $\Pi_0^{(a)}$  we use, but so also does the right hand side

## 2.4. Wald's formalism for spin-1

---

when we make use of the law (2.3.5) of current conservation. The NP scalar  $\phi_0$  resulting from the use of either expression for  $\Pi_0^{(a)}$  will be the same. Indeed, the two expressions correspond to different gauge choices, as we see specifically below.

By substituting  $\phi_j$  from (2.4.2) and  $J_{(a)}$  from the tetrad form of (2.3.1) into the decoupled NP equations (2.4.12), we obtain the operator relation

$$P_j K_j^{(b)} = \Pi_j^{(a)} D_{(a)}^{(b)} \quad (2.4.13)$$

The adjoint of this equation results in (2.2.5) for the electromagnetic case in a Type D background:

$$K_j^\dagger P_j^\dagger = D_{(a)}^{(b)} \Pi_j^{\dagger(a)} \quad (2.4.14)$$

where

$$P_{-1}^\dagger = -2 [(\Delta + \gamma - \gamma^* + \mu^*)(D + \rho + 2\epsilon) - (\delta^* - \tau^* + \alpha + \beta^*)(\delta + \tau + 2\beta)] \quad (2.4.15a)$$

$$\begin{aligned} P_0^\dagger &= -2 [(D + \rho - \rho^* + \epsilon + \epsilon^*)\Delta - (\delta + \tau + \beta - \alpha^* + \pi^*)\delta^*] \text{ or} \\ &= -2 [(\Delta - \gamma - \gamma^* - \mu + \mu^*)D - (\delta^* - \pi - \tau^* + \beta^* - \alpha)\delta] \end{aligned} \quad (2.4.15b)$$

$$P_{+1}^\dagger = -2 [(D - \rho^* - \epsilon + \epsilon^*)(\Delta - 2\gamma - \mu) - (\delta - \beta - \alpha^* + \pi^*)(\delta^* - \pi - 2\alpha)] \quad (2.4.15c)$$

and

$$\Pi_{-1}^{\dagger(a)} = \delta_{(1)}^{(a)} (\delta + 2\beta + \tau) - \delta_{(3)}^{(a)} (D + 2\epsilon + \rho) \quad (2.4.16a)$$

$$\Pi_0^{\dagger(a)} = \delta_{(1)}^{(a)} \Delta - \delta_{(3)}^{(a)} \delta^* \quad \text{or} \quad -\delta_{(2)}^{(a)} D + \delta_{(4)}^{(a)} \delta \quad (2.4.16b)$$

$$\Pi_{+1}^{\dagger(a)} = -\delta_{(2)}^{(a)} (\delta^* - 2\alpha - \pi) + \delta_{(4)}^{(a)} (\Delta - 2\gamma - \mu) \quad (2.4.16c)$$

As a consequence of (2.4.14), if  $\varphi_j$  is a solution of the adjoint of the decoupled NP equation (2.4.12) for the the Maxwell scalars with  $J_{(a)}=0$ , i.e.,

$$P_j^\dagger \varphi_j = 0 \quad (2.4.17)$$

## 2.4. Wald's formalism for spin-1

---

then we can obtain a potential, which is a solution of the sourceless Maxwell equations (2.3.1), by direct differentiation of  $\varphi_j$ :

$$A_j^{(a)} = \Pi_j^{\dagger(a)} \varphi_j \quad (2.4.18)$$

This equation is the one corresponding to  $f = \mathcal{S}^\dagger(\varphi)$  for the spin-1 case in a Type D background. There is a complication, which is that this expression for the potential turns out to be pure gauge:

$$K^h{}_{(a)} A_j^{(a)} = K^h{}_{(a)} \Pi_j^{\dagger(a)} \varphi_j = \frac{1}{2} \delta_j^h P^\dagger_j \varphi_j = 0 \quad (2.4.19)$$

However, if we impose that the potential components  $A_j^\alpha$  must be real, we can express them as

$$A_j^\alpha = \left( \Pi_j^{\dagger\alpha} \varphi_j \right)^* \pm \Pi_j^{\dagger\alpha} \varphi_j \quad (2.4.20)$$

As we have just seen in (2.4.19) the second term is pure gauge so it does not contribute to  $\phi_j$ , but the first term is non-trivial, i.e.,  $K^h{}_\alpha \left( \Pi_j^{\dagger\alpha} \varphi_j \right)^* \neq 0$ . In what follows we are only going to include the non-trivial term in the potential components  $A_j^\alpha$ . We can therefore obtain four different expressions for the potential depending on what scalar  $\varphi_j$  and what expression for  $\Pi_0^{\dagger(a)}$  we choose to use:

$$A_{-1}^\alpha = \left( \Pi_{-1}^{\dagger\alpha} \varphi_{-1} \right)^* = [l^\alpha(\delta^* + 2\beta^* + \tau^*) - m^{*\alpha}(D + 2\epsilon^* + \rho^*)] \varphi_{-1}^* \quad (2.4.21a)$$

$$A_0^\alpha = \left( \Pi_0^{\dagger\alpha} \varphi_0 \right)^* = [l^\alpha \Delta - m^{*\alpha} \delta] \varphi_0^* \quad \text{or} \quad [-n^\alpha D + m^\alpha \delta^*] \varphi_0^* \quad (2.4.21b)$$

$$A_{+1}^\alpha = \left( \Pi_{+1}^{\dagger\alpha} \varphi_{+1} \right)^* = [-n^\alpha(\delta - 2\alpha^* - \pi^*) + m^\alpha(\Delta - 2\gamma^* - \mu^*)] \varphi_{+1}^* \quad (2.4.21c)$$

All different expressions are gauge-related. In particular, the two expressions for  $A_0^\alpha$  are related by

$$[l^\alpha \Delta - m^{*\alpha} \delta] \varphi_0^* + \varphi_0^{*;\alpha} = [-n^\alpha D + m^\alpha \delta^*] \varphi_0^* \quad (2.4.22)$$

We can finally calculate the NP Maxwell scalars using (2.4.2) and choose for each  $\phi_j$  any one of the expressions (2.4.21) for the potential that we wish. In

## 2.4. Wald's formalism for spin-1

---

particular, if we choose either of the two expressions we have for  $A_0^\alpha$  we obtain

$$\phi_{-1} = K_{-1\alpha} A_0^\alpha = -(D + \epsilon^* - \epsilon - \rho^*) \delta \varphi_0^* \quad (2.4.23a)$$

$$\phi_0 = K_{0\alpha} A_0^\alpha = (\rho^* - \rho) \Delta \varphi_0^* - (\delta^* + \beta^* - \alpha) \delta \varphi_0^* \quad (2.4.23b)$$

$$\phi_{+1} = K_{+1\alpha} A_0^\alpha = -(\Delta + \mu^* + \gamma - \gamma^*) \delta^* \varphi_0^* \quad (2.4.23c)$$

If instead, we choose to use  $A_{-1}^\alpha$  or  $A_{+1}^\alpha$ , we obtain

$$\phi_{-1} = K_{-1\alpha} A_{-1}^\alpha = -(D - \epsilon + \epsilon^* - \rho^*) (D + 2\epsilon^* + \rho^*) \varphi_{-1}^* \quad (2.4.24a)$$

$$\phi_0 = K_{0\alpha} A_{-1}^\alpha = [-(D + \epsilon^* + \epsilon)(\delta^* + 2\beta^* + \tau^*) + (\pi + \tau^*)(D + 2\epsilon^* + \rho^*)] \varphi_{-1}^* \quad (2.4.24b)$$

$$\phi_{+1} = K_{+1\alpha} A_{-1}^\alpha = -(\delta^* + \alpha + \beta^* - \tau^*)(\delta^* + 2\beta^* + \tau^*) \varphi_{-1}^* \quad (2.4.24c)$$

or

$$\phi_{-1} = K_{-1\alpha} A_{+1}^\alpha = -\delta(\delta - 2\alpha^* - \pi^*) \varphi_{+1}^* \quad (2.4.25a)$$

$$\begin{aligned} \phi_0 &= K_{0\alpha} A_{+1}^\alpha = \\ &= \frac{1}{2} [-(\Delta - \gamma - \gamma^* + \mu^* - \mu)(\delta - \alpha^* - \pi^*) - (\Delta + \mu^* + \gamma - \gamma^*)(\Delta - 2\gamma - \mu^*)] \varphi_{+1}^* \end{aligned} \quad (2.4.25b)$$

$$\phi_{+1} = K_{+1\alpha} A_{+1}^\alpha = -(\Delta + \mu^* + \gamma - \gamma^*)(\Delta - 2\gamma^* - \mu^*) \varphi_{+1}^* \quad (2.4.25c)$$

respectively. Expressions (2.4.23), (2.4.24) and (2.4.25) were originally obtained by Cohen and Kegeles [28].

Finally, consider the equations

$$2\tilde{\Pi}^{\dagger-i}{}_{(a)} \varphi_h = \tilde{J}_{(a)} \quad (2.4.26)$$

where  $\tilde{\Pi}_{\pm 1}^{(a)} \equiv \Pi_{\pm 1}^{(a)}$  and  $\tilde{\Pi}_0^{(a)}$  is the arithmetic average of the two expressions for  $\Pi_0^{(a)}$  given in (2.4.9b). The tetrad components  $\tilde{J}_{(a)}$  correspond to new ‘source terms’ which are so far arbitrary. Analogously to (2.4.4) these new equations can be decoupled by applying the operator  $K_{-j}^{(a)}$  to give

$$P_j^\dagger \varphi_j = K_{-j}^{(a)} \tilde{J}_{(a)} \quad (2.4.27)$$

## 2.5. Wald's formalism for spin-1 in the Kerr-Newman background

---

That is, the solutions of equations (2.4.26) with  $\tilde{J}_{(a)} = 0$  are also solutions of equations (2.4.17). We will see in the next section that, in the Kerr-Newman space-time, equations (2.4.26) are satisfied for some new source terms  $\tilde{J}_{(a)}$  proportional to  $J_{(a)}$ . From equations (2.4.26) when  $\tilde{J}_{(a)} = 0$ , we can express the different terms with  $\varphi_{\pm 1}^*$  appearing in (2.4.21a) and (2.4.21c) as operators on  $\varphi_0^*$  to yield the simple expressions

$$A_{-1}{}^\alpha = [l^\alpha \Delta - m^{*\alpha} \delta] \varphi_0^* \quad (2.4.28a)$$

$$A_{+1}{}^\alpha = [-n^\alpha D + m^\alpha \delta^*] \varphi_0^* \quad (2.4.28b)$$

which coincide precisely with the two expressions we had obtained for  $A_0{}^\alpha$  in (2.4.21b).

## 2.5 Wald's formalism for spin-1 in the Kerr-Newman background

In order to separate the differential equations for the Maxwell scalars in the Kinnersley tetrad (1.3.10) in Boyer-Lindquist coordinates in the Kerr background, Teukolsky [87] started off from the decoupled equations (2.4.12) for  $\phi_{\pm 1}$ . However, the final expressions he gave were in terms of operators acting on  $\phi_{-1}$  and on  $\rho^{-2}\phi_{+1}$ , instead of  $\phi_{+1}$ . As Wald [91] remarked, in the Kerr background the quantity  $(\psi_0)^{-2/3}\phi_{+1} \propto \rho^{-2}\phi_{+1}$  satisfies the adjoint of the decoupled field equation for  $\phi_{-1}$ , i.e., (2.4.17) for  $j = -1$ . In other words,  $\varphi_{-1} = \rho^{-2}\phi_{+1}$  in the Kerr background. We are next going to show why this is so by finding a simple relationship between the solutions  $\phi_h$  of the decoupled equations and the solutions  $\varphi_h$  of the adjoint of the decoupled equations in a general Type D background.

Suppose there is a scalar function  $v$  such that

$$K_j^{(a)} = v^{-1} \tilde{\Pi}_j^{(a)} v \quad (2.5.1)$$



## 2.5. Wald's formalism for spin-1 in the Kerr-Newman background

---

By using its adjoint

$$K_j^{\dagger(a)} = v \tilde{\Pi}_j^{\dagger(a)} v^{-1} \quad (2.5.2)$$

together with the adjoint of equation (2.4.10), it follows that

$$P_j = v P_{-j}^{\dagger} v^{-1} \quad (2.5.3)$$

where we used the fact that, because the two expressions for  $P_0$  in (2.4.11b) are identical, then  $\delta_j^h P_j = 2 \tilde{\Pi}_j^{(a)} K^{\dagger h}_{(a)}$ . When substituting the form (2.5.3) of  $P_j$  into the decoupled equations (2.4.12) we obtain

$$P_{-j}^{\dagger} (v^{-1} \phi_j) = v^{-1} \tilde{\Pi}_j^{(a)} J_{(a)} \quad (2.5.4)$$

where we have used the property mentioned earlier that  $\tilde{\Pi}_j^{(a)} J_{(a)} = \Pi_j^{(a)} J_{(a)}$ . Comparing equations (2.5.4) with (2.4.17), we then have a simple relationship between the solutions of the decoupled equations and the solutions of the adjoint of the decoupled equations:

$$\varphi_j = v^{-1} \phi_{-j} \quad (2.5.5)$$

up to a factor of proportionality, which we choose to be one. This relationship does not involve operators, unlike equations (2.4.23), (2.4.24) or (2.4.25). Condition (2.5.1) for the scalar function  $v$  is equivalent to it satisfying the relations

$$v^{-1} D v = D + 2\rho \quad (2.5.6a)$$

$$v^{-1} \Delta v = \Delta - 2\mu \quad (2.5.6b)$$

$$v^{-1} \delta v = \delta + 2\tau \quad (2.5.6c)$$

$$v^{-1} \delta^* v = \delta^* - 2\pi \quad (2.5.6d)$$

as can be seen by comparing (2.4.3) and (2.4.9).

It is easy that if the property (2.5.5) is satisfied by a certain background, then the relations (2.4.26) are satisfied with  $\tilde{J}_{(a)} = v^{-1} J_{(a)}$ . Indeed, we first replace  $\varphi_j$  with  $v^{-1} \phi_{-j}$  in the coupled NP equations (2.4.4), which relate  $\phi_0$  to  $\phi_{\pm 1}$ . We then make use of (2.5.2) and we immediately find that equations (2.4.26), which

## 2.6. Equation for $\phi_0$

---

relate  $\varphi_0$  to  $\varphi_{\pm 1}$ , are satisfied with  $\tilde{J}_{(a)} = v^{-1}J_{(a)}$ . Equations (2.4.28) would then be valid in the sourceless case  $J_{(a)} = 0$ .

In the Kerr-Newman background, the scalar function that satisfies condition (2.5.1) exists and it can be easily checked that it is  $v = \rho^2$ . We therefore have that

$$\varphi_j = \rho^{-2}\phi_{-j} \quad (2.5.7)$$

in the Kerr-Newman background.

We can then make use of the simple relation (2.5.7) and then equations (2.4.21) yield

$$A_{-1}^\alpha = \left( \Pi_{-1}^{\dagger\alpha} \rho^{-2} \phi_{+1} \right)^* = [l^\alpha (\delta^* + 2\beta^* + \tau^*) - m^{*\alpha} (D + 2\epsilon^* + \rho^*)] \rho^{*-2} \phi_{+1}^* \quad (2.5.8a)$$

$$A_0^\alpha = \left( \Pi_0^{\dagger\alpha} \rho^{-2} \phi_0 \right)^* = [l^\alpha \Delta - m^{*\alpha} \delta] \rho^{*-2} \phi_0^* \text{ or } [-n^\alpha D + m^\alpha \delta^*] \rho^{*-2} \phi_0^* \quad (2.5.8b)$$

$$A_{+1}^\alpha = \left( \Pi_{+1}^{\dagger\alpha} \rho^{-2} \phi_{-1} \right)^* = [-n^\alpha (\delta - 2\alpha^* - \pi^*) + m^\alpha (\Delta - 2\gamma^* - \mu^*)] \rho^{*-2} \phi_{-1}^* \quad (2.5.8c)$$

where  $\phi_j$  are any solutions of sourceless (2.4.12).

We know from (2.4.28) and the discussion above that equations (2.5.8) reduce to the simple expressions

$$A_{-1}^\alpha = [l^\alpha \Delta - m^{*\alpha} \delta] \rho^{*-2} \phi_0^* \quad (2.5.9a)$$

$$A_{+1}^\alpha = [-n^\alpha D + m^\alpha \delta^*] \rho^{*-2} \phi_0^* \quad (2.5.9b)$$

in the sourceless case  $J_{(a)} = 0$  in the Kerr-Newman background.

## 2.6 Equation for $\phi_0$

It is clear from the relation (2.5.7) that by using one set of equations among (2.4.23), (2.4.24) and (2.4.24) the knowledge of any one NP Maxwell scalar of

our choice suffices to obtain all the components of the electromagnetic field tensor. This NP Maxwell scalar is therefore a Debye potential for electromagnetic perturbations. This complex Maxwell scalar carries all the information of the theory, that is, its real and imaginary parts represent the two dynamical degrees of freedom of the perturbed field. Furthermore, the potential can be readily derived from that same Maxwell scalar via the appropriate equation in (2.5.8).

When quantizing the theory in the Kerr-Newman space-time, we shall see that a complete set of mode solutions requires two sets of solutions with different boundary conditions. Two possible sets are solutions with ‘ingoing’ and ‘upgoing’ boundary conditions. We shall see in the next section that the potentials  $A_{-1}^\alpha$  and  $A_{+1}^\alpha$  adapt themselves in a natural way to the former and latter type of boundary conditions respectively. It would therefore be very useful to quantize the theory by using the simple expressions (2.5.9), which yield the potentials naturally adapted to a set of complete solutions from one single Maxwell scalar.

This is indeed the case in the Reissner-Nordström space-time where the equation for  $\phi_0$  can be separated. This is the procedure that ultimately underlies in the calculation in [51] of simple, elegant expressions for the NP Maxwell scalars and expectation values of the stress-energy tensor. Unfortunately, as we shall now see, we have not been able to separate the equation for  $\phi_0$  in the Kerr-Newman or, indeed, Kerr backgrounds.

Teukolsky showed that the differential equations for  $\phi_{-1}$  and for  $\rho^{-2}\phi_{+1}$  are separable in the Kinnersley tetrad in Boyer-Lindquist co-ordinates in the Kerr background. He indicated that these equations are actually separable in any co-ordinates related to Boyer-Lindquist’s by:  $t \rightarrow t + f_1(r) + f_2(\theta)$ ,  $\phi \rightarrow \phi + g_1(r) + g_2(\theta)$ ,  $r \rightarrow h(r)$  and  $\theta \rightarrow j(\theta)$ . However, he does not find a decoupled equation in relation to  $\phi_0$ .

Using the Kinnersley tetrad, we calculated  $P_0^\dagger(\varphi_0)$  explicitly in Boyer-Lindquist co-ordinates in the Kerr-Newman background where  $\varphi_0 = \rho^{-2}\phi_0$  and  $P_0^\dagger$  is given by (2.4.15b) (remember that both expressions for  $P_0^\dagger$  are identical). We

## 2.6. Equation for $\phi_0$

found that  $2\rho^{*-1}P_0^\dagger(\rho^{-2}\phi_0)$  differs only slightly from the equation that Teukolsky wrote down explicitly. We write it later in (2.7.2) with  $h = 0$ , and where the function  $\Omega_h$  to solve for is  $\rho^{-1}\phi_0$ . The only difference being an extra term  $2\rho^2(M/\rho^* + Q^2)\rho^{-1}\phi_0$ . That is, writing the equation  $P_0^\dagger(\varphi_0) = 0$  explicitly gives

$$\left\{ \left[ \frac{(r^2 + a^2)^2}{\Delta} - a^2 \sin^2 \theta \right] \frac{\partial^2}{\partial t^2} + \frac{4Mar}{\Delta} \frac{\partial^2}{\partial t \partial \phi} + \left[ \frac{a^2}{\Delta} - \frac{1}{\sin^2 \theta} \right] \frac{\partial^2}{\partial \phi^2} - \frac{\partial}{\partial r} \left( \Delta \frac{\partial}{\partial r} \right) - \frac{1}{\sin \theta} \frac{\partial}{\partial \theta} \left( \sin \theta \frac{\partial}{\partial \theta} \right) + 2\rho^2 \left( \frac{M}{\rho^*} + Q^2 \right) \right\} (\rho^{-1}\phi_0) = 0 \quad (2.6.1)$$

The differential equation for  $\rho^{-1}\phi_0$  is therefore surprisingly similar to the one for the scalar field, where the only difference is the extra term indicated. It is the form of this extra term:

$$\frac{2}{(r - ia \cos \theta)^2} [-M(r + ia \cos \theta) + Q^2] \quad (2.6.2)$$

that stops (2.6.1) from being separable, even in the Kerr background where  $Q = 0$ . This extra term does not vanish in the Reissner-Nordström background where  $a = 0$ , however it reduces to just  $2(-Mr + Q^2)/r^2$  so that (2.6.1) does indeed become separable in this background.

After seeing that the differential equation for  $\phi_0$  is not separable in the Kinnersley tetrad in Kerr one might wonder whether the inherent symmetry in the Carter null tetrad renders the differential equation for the Maxwell scalars separable.

We define  ${}_cP_0$  as either of the two identical expressions in (2.4.11) where the directional derivatives and the spin coefficients in the Carter null tetrad are given by (1.3.16) and (1.3.17) respectively. In the Kerr background, the equation  ${}_cP_0{}_c\phi_0 = 0$  can be explicitly expressed as an operator acting on  $\rho^{-1}{}_c\phi_0$ , where the subscript  $c$  in the NP Maxwell scalar indicates the use of the Carter null tetrad. This equation is

$$\left[ \Delta {}_c\mathcal{D}_{2c}^\dagger {}_c\mathcal{D}_0 - 2(r - M)\rho - 2\Delta\rho^2 + (a^2 - q^2){}_c\mathcal{L}_{2c}^\dagger {}_c\mathcal{L}_0 + 2i\rho(\sigma - q) + 2(a^2 - q^2)\rho^2 \right] (\rho^{-1}{}_c\phi_0) = 0 \quad (2.6.3)$$

where we have already written out the  $\tilde{t}$  and  $\tilde{\phi}$  dependence as  $e^{-i(\sigma\tilde{t} - \tilde{m}\tilde{\phi})}$  already.

## 2.7. The Teukolsky equation and the homogeneous potential solution

---

The operators in (2.6.3) are defined as

$${}_c\mathcal{D}_n^{\{\dagger\}} \equiv \partial_r \mp \frac{i(r^2\sigma - \tilde{m})}{\Delta} + n \frac{r - M}{\Delta} \quad (2.6.4a)$$

$${}_c\mathcal{L}_n^{\{\dagger\}} \equiv \partial_q \pm \frac{\tilde{m} + q^2\sigma}{a^2 - q^2} - n \frac{q}{a^2 - q^2} \quad (2.6.4b)$$

The equation (2.6.3) is clearly not separable in the variables  $r$  and  $q$  due to the various terms containing  $\rho$  or  $\rho^2$ .

## 2.7 The Teukolsky equation and the homogeneous potential solution

As mentioned earlier, Teukolsky ([86], [87]) wrote the differential equations for spin-1 perturbations in the Kerr background as operators acting on  $\phi_{-1}$  and  $\rho^{-2}\phi_{+1}$  (rather than  $\phi_{+1}$  itself). Since the latter turns out to be  $\varphi_{-1}$  in this background, the actual equations that Teukolsky wrote down explicitly correspond to

$$P_{-1}\phi_{-1} = -\Pi_{-1}^\alpha J_\alpha \quad (2.7.1a)$$

$$P_{-1}^\dagger\varphi_{-1} = P_{-1}^\dagger(\rho^{-2}\phi_{+1}) = -\rho^{-2}\Pi_{+1}^\alpha J_\alpha \quad (2.7.1b)$$

which are particular cases of (2.4.12) and (2.5.4) (with  $v = \rho^2$  and  $\tilde{\Pi}_{+1}^\alpha = \Pi_{+1}^\alpha$ ) respectively. The reason why these are the equations that he wrote out explicitly (rather than  $P_{+1}\phi_{+1} = 0$  instead of  $P_{-1}^\dagger\varphi_{-1} = 0$ , or  $P_{+1}^\dagger\varphi_{+1} = 0$  instead of  $P_{-1}\phi_{-1} = 0$ ) is that these are the equations that turn out to be separable. A similar situation holds for the NP Weyl scalars and the corresponding differential equations that Teukolsky gave.

Teukolsky wrote equations (2.7.1) using the Kinnersley tetrad in Boyer-Lindquist coordinates. Since Teukolsky's equations are the ones that we are going to solve, we will write them out explicitly. Teukolsky presented the results for the electromagnetic and gravitational perturbations in [86] and he proved them and

## 2.7. The Teukolsky equation and the homogeneous potential solution

---

extended them to the neutrino case in [87]. Carter [16] had previously shown the separability for the scalar case. Teukolsky wrote the field equations in the Kerr background in compact form for the various spin fields, as one single ‘master’ equation where the parameter  $h = 0, \pm 1/2, \pm 1, \pm 2$  refers to the helicity of the field. An analogous equation can be derived in the Kerr-Newman background. In this background, we derived the equation for spin-1 whereas for spin-1/2 and spin-2 it is given in [6]. We will still refer to the original Teukolsky equation with the inclusion of the modifications so that it is valid in the Kerr-Newman background as the Teukolsky equation. This equation, valid in Kerr-Newman background, is:

$$\begin{aligned}
& \left[ \frac{(r^2 + a^2)^2}{\Delta} - a^2 \sin^2 \theta \right] \frac{\partial^2 \Omega_h}{\partial t^2} + \frac{2(2Mr - Q^2)a}{\Delta} \frac{\partial^2 \Omega_h}{\partial t \partial \phi} + \left[ \frac{a^2}{\Delta} - \frac{1}{\sin^2 \theta} \right] \frac{\partial^2 \Omega_h}{\partial \phi^2} - \\
& - \Delta^{-h} \frac{\partial}{\partial r} \left( \Delta^{h+1} \frac{\partial \Omega_h}{\partial r} \right) - \frac{1}{\sin \theta} \frac{\partial}{\partial \theta} \left( \sin \theta \frac{\partial \Omega_h}{\partial \theta} \right) - 2h \left[ \frac{a(r - M)}{\Delta} + \frac{i \cos \theta}{\sin^2 \theta} \right] \frac{\partial \Omega_h}{\partial \phi} - \\
& - 2h \left[ \frac{(Mr - Q^2)r - Ma^2}{\Delta} - r - ia \cos \theta \right] \frac{\partial \Omega_h}{\partial t} + \\
& + \left( h^2 \cos^2 \theta - h - \frac{2Q^2}{\Sigma} \delta_{2,|h|} \right) \Omega_h = \Sigma T_h
\end{aligned} \tag{2.7.2}$$

where the field  $\Omega_h$  and the source term  $T_h$  denote different quantities depending on the value of the helicity  $h$  as indicated in Table 2.1. Clearly the Teukolsky equation (2.7.2) is separable for any value of the helicity  $h$ . Its solution can therefore be written as a sum over the Fourier modes

$$\begin{aligned}
\Omega_h(t, r, \theta, \phi) &= \int_{-\infty}^{+\infty} d\omega \sum_{l=|h|}^{+\infty} \sum_{m=-l}^{+l} {}_{lm\omega} \Omega_h(t, r, \theta, \phi) \\
{}_{lm\omega} \Omega_h(t, r, \theta, \phi) &= \frac{1}{\sqrt{2\pi}} {}_h R_{lm\omega}(r) {}_h S_{lm\omega}(\theta) e^{-i\omega t} e^{+im\phi} = \\
&= {}_h R_{lm\omega}(r) {}_h Z_{lm\omega}(\theta, \phi) e^{-i\omega t}
\end{aligned} \tag{2.7.3}$$

where we have made the obvious definition

$${}_h Z_{lm\omega}(\theta, \phi) \equiv \frac{(-1)^{m+1}}{\sqrt{2\pi}} {}_h S_{lm\omega}(\theta) e^{+im\phi} \tag{2.7.4}$$

We impose that the angular function  ${}_h S_{lm\omega}$  is normalized to one:

$$\int_0^\pi d\theta \sin \theta {}_h S_{lm\omega}^2 = 1 \tag{2.7.5}$$

## 2.7. The Teukolsky equation and the homogeneous potential solution

---

$h$	$\Omega_h$	$T_h$
0	$\Phi$	$4\pi T^\alpha{}_\alpha$
$+\frac{1}{2}$	$\chi_{-1/2}$	$X_{-1/2}$
$-\frac{1}{2}$	$\rho^{-1}\chi_{1/2}$	$X_{+1/2}$
+1	$\phi_{-1}$	$J_{-1} = -\Pi_{-1}{}^\alpha J_\alpha$
-1	$\rho^{-2}\phi_{+1}$	$\rho^{-2}J_{+1} = -\rho^{-2}\Pi_{+1}{}^\alpha J_\alpha$
+2	$\psi_{-2}$	$8\pi T_{-2}$
-2	$\rho^{-4}\psi_{+2}$	$8\pi\rho^{-4}T_{+2}$

Table 2.1: Field quantities  $\Omega_h$  and source terms  $T_h$  in the Teukolsky equation (2.7.2). The quantities  $T_{\pm 2}$  and  $X_{\pm 1/2}$  are the result of the decoupling operators acting on the sources for the gravitational and neutrino cases respectively (see [6], [87]).

## 2.7. The Teukolsky equation and the homogeneous potential solution

---

The  $t$ - and  $\phi$ - dependences of the modes  ${}_{lm\omega}\Omega_h$  are a consequence of the fact that the Kerr-Newman background is stationary and axially symmetric. The parameter  $l$  labels the eigenvalues of the angular differential equation for  ${}_hS_{lm\omega}$ . The sign factor  $(-1)^{m+1}$  appearing in the definition of  ${}_hZ_{lm\omega}$  differs from that of Chrzanowski [25] because of a difference in the normalization of the angular function  ${}_hS_{lm\omega}$ . The inclusion of this sign factor simplifies the equations for the field and the potential that we derive later, given our normalization of the spherical functions.

Specifically for the electromagnetic case:

$${}_{lm\omega}\phi_h(t, r, \theta, \phi) = \rho^{h+1} {}_{-h}R_{lm\omega}(r) {}_{-h}Z_{lm\omega}(\theta, \phi) e^{-i\omega t} \quad (2.7.6)$$

i.e.,

$${}_{lm\omega}\Omega_{-1} = {}_{lm\omega}\varphi_{-1}(t, r, \theta, \phi) = \rho^{-2} {}_{lm\omega}\phi_{+1}(t, r, \theta, \phi) = {}_{-1}R_{lm\omega}(r) {}_{-1}Z_{lm\omega}(\theta, \phi) e^{-i\omega t} \quad (2.7.7a)$$

$${}_{lm\omega}\Omega_{+1} = {}_{lm\omega}\phi_{-1}(t, r, \theta, \phi) = {}_{+1}R_{lm\omega}(r) {}_{+1}Z_{lm\omega}(\theta, \phi) e^{-i\omega t} \quad (2.7.7b)$$

The radial and angular Teukolsky equations into which the sourceless Teukolsky equation (2.7.2) separates for the electromagnetic case can be written in a compact manner as follows:

$$\left( \Delta \mathcal{D}_1 \mathcal{D}_1^\dagger + 2i\omega r \right) {}_{+1}R_{lm\omega} = {}_{-1}\lambda_{lm\omega+1} R_{lm\omega} \quad (2.7.8a)$$

$$\left( \Delta \mathcal{D}_0^\dagger \mathcal{D}_0 - 2i\omega r \right) {}_{-1}R_{lm\omega} = {}_{-1}\lambda_{lm\omega-1} R_{lm\omega} \quad (2.7.8b)$$

and

$$\left( \mathcal{L}_0^\dagger \mathcal{L}_1 - 2a\omega \cos \theta \right) {}_{+1}S_{lm\omega} = -{}_{-1}\lambda_{lm\omega+1} S_{lm\omega} \quad (2.7.9a)$$

$$\left( \mathcal{L}_0 \mathcal{L}_1^\dagger + 2a\omega \cos \theta \right) {}_{-1}S_{lm\omega} = -{}_{-1}\lambda_{lm\omega-1} S_{lm\omega} \quad (2.7.9b)$$

where the constant of separation  ${}_h\lambda_{lm\omega}$  is an eigenvalue of the angular equation.



## 2.7. The Teukolsky equation and the homogeneous potential solution

---

We are using the definitions of the operators

$$\mathcal{L}_n^{\{\dagger\}} \equiv \partial_\theta \pm \mathcal{Q} + n \cot \theta \quad (2.7.10a)$$

$$\mathcal{D}_n^{\{\dagger\}} \equiv \partial_r \mp \frac{iK}{\Delta} + 2n \frac{r-M}{\Delta} \quad (2.7.10b)$$

where

$$\mathcal{Q} \equiv -a\omega \sin \theta + \frac{m}{\sin \theta} \quad (2.7.11a)$$

$$K \equiv (r^2 + a^2)\omega - am \quad (2.7.11b)$$

Throughout this thesis, we use the convention that the upper and lower symbols inside braces go with the upper and lower signs in the equation. We will analyze the radial and angular equations in the following chapters.

We can now substitute expressions (2.7.6) for  ${}_{lm\omega}\phi_{\pm 1}$  into (2.5.8) and use the symmetries (3.1.3b) and (4.2.1c) of the radial and angular functions:

$${}_h R_{lm\omega}(r) = {}_h R_{l-m-\omega}^*(r) \quad \text{and} \quad {}_h S_{lm\omega}(\theta) = (-1)^{h+m} {}_{-h} S_{l-m-\omega}(\theta) \quad (2.7.12)$$

which we shall show in the next two chapters. We then obtain for the homogeneous potential:

$$\begin{aligned} {}_{lm\omega} A_{-1}^\alpha &= \left( \Pi_{-1}^\dagger \alpha \rho^{-2} {}_{lm\omega} \phi_{+1} \right)^* = \\ &= [l^\alpha (\delta^* + 2\beta^* + \tau^*) - m^{*\alpha} (D + 2\epsilon^* + \rho^*)] \end{aligned} \quad (2.7.13a)$$

$$\begin{aligned} {}_{lm\omega} A_{+1}^\alpha &= \left( \Pi_{+1}^\dagger \alpha \rho^{-2} {}_{lm\omega} \phi_{-1} \right)^* = \\ &= [-n^\alpha (\delta - 2\alpha^* - \pi^*) + m^\alpha (\Delta - 2\gamma^* - \mu^*)] \\ &\quad \rho^{*-2} {}_{+1} R_{l-m-\omega}(r) {}_{-1} Z_{l-m-\omega}(\theta, \phi) e^{+i\omega t} = \\ &= \rho^{*-2} [-n^\alpha (\delta - 2\alpha^* + \pi^*) + m^\alpha (\Delta - 2\gamma^* + \mu^*)] \\ &\quad {}_{+1} R_{l-m-\omega}(r) {}_{-1} Z_{l-m-\omega}(\theta, \phi) e^{+i\omega t} \end{aligned} \quad (2.7.13b)$$

## 2.7. The Teukolsky equation and the homogeneous potential solution

---

The real potential (2.4.20) can be expressed as a Fourier mode sum as

$$A_j^\alpha = \int_{-\infty}^{+\infty} d\omega \sum_{l=|h|}^{+\infty} \sum_{m=-l}^{+l} \sum_{P=\pm 1} {}_{lm\omega P} a {}_{lm\omega P} A_j^\alpha \quad (2.7.14a)$$

$${}_{lm\omega P} A_j^\alpha \equiv {}_{lm\omega} A_j^\alpha + P(-1)^{l+m} {}_{l-m-\omega} A_j^{*\alpha} \quad (2.7.14b)$$

where the potential modes are obtained from (2.7.13):

$$\begin{aligned} {}_{l-m-\omega P} A_{-1}^\alpha &= \\ &= \left\{ [l^\alpha(\delta^* + 2\beta^* + \tau^*) - m^{*\alpha}(D + 2\epsilon^* + \rho^*)] {}_{-1} R_{lm\omega}(r) {}_{+1} Z_{lm\omega}(\theta, \phi) e^{-i\omega t} + \right. \\ &\quad \left. + P[l^\alpha(\delta + 2\beta + \tau) - m^\alpha(D + 2\epsilon + \rho)] {}_{-1} R_{lm\omega}(r) {}_{-1} Z_{lm\omega}(\theta, \phi) e^{-i\omega t} \right\} \end{aligned} \quad (2.7.15a)$$

$$\begin{aligned} {}_{l-m-\omega P} A_{+1}^\alpha &= \\ &= \left\{ \rho^{*-2} [-n^\alpha(\delta - 2\alpha^* + \pi^*) + m^\alpha(\Delta - 2\gamma^* + \mu^*)] {}_{+1} R_{lm\omega}(r) {}_{-1} Z_{lm\omega}(\theta, \phi) e^{-i\omega t} + \right. \\ &\quad \left. + P\rho^{*-2} [-n^\alpha(\delta^* - 2\alpha + \pi) + m^{*\alpha}(\Delta - 2\gamma + \mu)] {}_{+1} R_{lm\omega}(r) {}_{+1} Z_{lm\omega}(\theta, \phi) e^{-i\omega t} \right\} \end{aligned} \quad (2.7.15b)$$

Expressions (2.7.15), valid in the Kerr-Newman background, were originally obtained by Chrzanowski [25] in the Kerr background. The only difference with his expressions is an overall change in the sign of  $m$  and  $\omega$ , justified because of the sum over  $m$  and integration over  $\omega$ . The parameter  $P$  is summed in (2.7.14a) over the values  $+1$  and  $-1$ , corresponding to two linearly independent polarization states for the potential, as we shall see in the last chapter. This was indeed Chrzanowski's justification for the inclusion of this sum. The two linearly independent solutions are actually related via the parity operation  $\mathcal{P}$ , as we shall also see in the last chapter. Chrzanowski made use of this relationship to calculate one linearly independent solution from the other. We have chosen the sign factor and the change in the signs of  $m$  and  $\omega$  in equation (2.7.14b) so that this relationship between the two independent solutions holds like in Chrzanowski's. The Fourier coefficients must satisfy the following condition so that the potential remains real:

$${}_{lm\omega P} a^* = (-1)^{l+m} P {}_{l-m-\omega P} a \quad (2.7.16)$$

## 2.7. The Teukolsky equation and the homogeneous potential solution

---

This condition becomes immediately clear by making use of the symmetries of the radial and angular functions and the normalization we have chosen for them, which we shall give in the following chapters.

We will label the electromagnetic potential with the superscript ‘in’, ‘up’, ‘out’ or ‘down’ to indicate that the radial function used has the corresponding boundary conditions, which are made explicit in the next chapter.

For completeness and so that we can establish the appropriate comparison with his results, we will next briefly outline the method that Chrzanowski [25] uses to calculate the homogeneous electromagnetic potential prior to adaptation to our operator notation.

Chrzanowski’s starting point is a conjecture made previously by Chrzanowski and Misner [27]. Knowing what the retarded Green function for the radial Teukolsky equation looks like for the scalar case in Kerr, they conjecture that the form of the retarded Green function for the spin-1 case in Kerr is

$$G_{\mu\alpha}(x, x') = \begin{cases} \int_{-\infty}^{+\infty} d\omega \sum_{lmP} \frac{i\omega}{|\omega|} g^{PP'}_{lm\omega P} A_{\mu}^{\text{up}}(x)_{lm\omega P'} A_{\alpha}^{\text{out}*}(x'), & r > r' \\ \int_{-\infty}^{+\infty} d\omega \sum_{lmP} \frac{i\omega}{|\omega|} g^{PP'}_{lm\omega P} A_{\mu}^{\text{in}}(x)_{lm\omega P'} A_{\alpha}^{\text{dn}*}(x'), & r < r' \end{cases} \quad (2.7.17)$$

which Chrzanowski proves to be valid for high frequency. As a corollary of Wald’s results in Section 2.2, this form of the Green function is valid for all frequency, not just high frequency. The quantity  $g^{PP'}$  is the reciprocal of  $g_{PP'}$ , which is a 2-dimensional metric for the polarization states; it is  $g_{PP'} = -\delta_{PP'}$  if the states are orthogonal. It immediately follows that

$$A_{\alpha} = \int_{-\infty}^{+\infty} d\omega \sum_{lmP} \frac{i\omega}{|\omega|} g^{PP'}_{lm\omega P} A_{\alpha}^{\text{up}} \langle_{lm\omega P'} A_{\beta}^{\text{out}}, J^{\beta} \rangle \quad (2.7.18)$$

where the inner product is defined as  $\langle A, B \rangle \equiv \int d^4x \sqrt{-g} A^* B$  and the modes have been normalized so that

$$\langle_{lm\omega P} A_{\alpha}^{\text{up}}, l'm'\omega'P' A^{\text{out}\alpha} \rangle_{\mathcal{I}^+} = \langle_{lm\omega P} A_{\alpha}^{\text{in}}, l'm'\omega'P' A^{\text{dn}\alpha} \rangle_{\mathcal{H}^+} = \frac{\omega}{|\omega|} g_{PP'} \delta_{ll'} \delta_{mm'} \delta(\omega - \omega') \quad (2.7.19)$$

## 2.7. The Teukolsky equation and the homogeneous potential solution

---

When applying the operators  $K_{-1}^\alpha$  and  $\rho^{-2}K_{+1}^\alpha$  on (2.7.18) we obtain

$$\Omega_{\pm 1} = \int_{-\infty}^{+\infty} d\omega \sum_{lmP} \frac{i\omega}{|\omega|} {}_{lm\omega}\Omega_{\pm 1}^{\text{up}} \langle {}_{lm\omega}A_\beta^{\text{out}}, J^\beta \rangle \quad (2.7.20)$$

where

$${}_{lm\omega}A_\beta^{\text{out}} \equiv \sum_{P,P'} g^{PP'} {}_{lm\omega P}A_\beta^{\text{out}} \quad (2.7.21)$$

On the other hand, the radial Teukolsky equation can be solved by the method of radial Green's functions, so that the solution of the Teukolsky equation can be expressed as

$$\begin{aligned} \Omega_h &= \int_{-\infty}^{+\infty} d\omega \sum_{lmP} {}_hR_{lm\omega} Z_{lm\omega} e^{-i\omega t} = \\ &= \int_{-\infty}^{+\infty} d\omega \sum_{lmP} \frac{i\omega}{|\omega|} {}_{lm\omega}\Omega_h^{\text{up}} \langle -{}_hR_{lm\omega}^{\text{out}} {}_hZ_{lm\omega} e^{-i\omega t}, T_h \rangle \end{aligned} \quad (2.7.22)$$

where use has been made of the symmetry (3.1.3a) of the radial equation. Since, from Table 2.1, it is  $T_h = -\rho^{h-1}\Pi_{-h\beta}J^\beta$  for  $h = \pm 1$ , integrating by parts gives

$$\Omega_{\pm 1} = \int_{-\infty}^{+\infty} d\omega \sum_{lmP} \frac{i\omega}{|\omega|} {}_{lm\omega}\Omega_{\pm 1}^{\text{up}} \langle -\Pi_{\mp 1\beta}^{\dagger*} \rho^{*(\pm 1-1)} {}_{\mp 1}R_{lm\omega}^{\text{out}} {}_{\pm 1}Z_{lm\omega} e^{-i\omega t}, J^\beta \rangle \quad (2.7.23)$$

The complex conjugation of  $\Pi^\dagger$  is due to the slightly different definitions of adjoint used in (2.2.3) and implicit in Chrzanowski's inner product. Comparing (2.7.20) with (2.7.23) we have

$${}_{lm\omega}A_\beta = -\Pi_{\mp 1\beta}^{\dagger*} \rho^{*(h-1)} {}_{\mp 1}R_{lm\omega} {}_{\pm 1}Z_{lm\omega} e^{-i\omega t} \quad (2.7.24)$$

where the label 'out' has been dropped since the same argument could have carried through with the advanced Green function rather than the retarded one, and the result obtained is thus independent of the boundary condition. Chrzanowski also obtained equivalent results for the spin-2 case. The expression (2.7.24) coincides with our result (2.7.13) except for having the opposite sign for  $m$  and  $\omega$ .

As mentioned earlier,  $A_{+1}^\alpha$  and  $A_{-1}^\alpha$  correspond to two different gauge choices, neither of which is the Lorentz gauge. Clearly from (2.7.13), the potential with

## 2.7. The Teukolsky equation and the homogeneous potential solution

---

helicity  $-1$  corresponds to the ‘ingoing gauge’, i.e.,

$$l^\alpha A_{-1\alpha} = A_{-1l} = 0 \quad (2.7.25)$$

is the gauge condition. This potential is transverse at the future horizon and at past infinity and will thus be used in calculations in these asymptotic regions. The potential with helicity  $+1$  corresponds to the ‘upgoing gauge’:

$$n^\alpha A_{+1\alpha} = A_{+1n} = 0 \quad (2.7.26)$$

This potential is transverse at the past horizon and at future infinity and will be used in calculations in these regions.

Since Chrzanowski obtains the NP scalar  $\phi_{-1}$  from the ingoing gauge potential via equation (2.7.23) he calls  $\phi_{-1}$  the ‘ingoing’ field component. This is a consequence of the fact that  $T_{+1}$ , which contains  $\Pi^{-1\alpha}$  and thus does not involve  $J_n$ , is the source term in the differential equation for  $\phi_{-1}$ . The ‘ingoing’ potential  $A_{-1\alpha}$  was calculated by integrating  $T_{+1}$  by parts. Equivalently, he calls  $\phi_{+1}$  the ‘upgoing’ field component. This notation is in agreement with the asymptotics for large  $r$ . Indeed, as we shall see in the next chapter, the asymptotic behaviour of the solution of the Teukolsky equation separately for outgoing and ingoing waves in the limit  $r \rightarrow +\infty$  is

$$\begin{aligned} \Omega_h &\sim r^{-(2h+1)} e^{+i\omega r}, & r^{-1} e^{-i\omega r} & \quad (r \rightarrow +\infty) \\ \phi_{+1} &\sim r^{-1} e^{+i\omega r}, & r^{-3} e^{-i\omega r} & \quad (r \rightarrow +\infty) \\ \phi_0 &\sim r^{-2} e^{+i\omega r}, & r^{-2} e^{-i\omega r} & \quad (r \rightarrow +\infty) \\ \phi_{-1} &\sim r^{-3} e^{+i\omega r}, & r^{-1} e^{-i\omega r} & \quad (r \rightarrow +\infty) \end{aligned} \quad (2.7.27)$$

It is therefore the ‘upgoing’[‘ingoing’] scalar  $\phi_{+1[-1]}$  the one with the asymptotically dominant behaviour for the upgoing[ingoing] waves. The above asymptotic behaviour (2.7.27) was originally obtained by Newman and Penrose [69] and is commonly referred to as the *peeling off theorem*.

## 2.8. Field components and Teukolsky-Starobinskiĭ identities

---

### 2.8 Field components and Teukolsky-Starobinskiĭ identities

In order to obtain an expression for the NP scalars  $\phi_h$  we substitute the quantities  $\phi_{-1}$  and  $\varphi_{-1}$  in their mode expressions (2.7.7) into equations (2.4.24) and use the symmetries (2.7.12) for the radial and angular functions. The result is

$${}_{l-m-w}\phi_{-1} = K_{-1\alpha l-m-w} A_{-1}^\alpha = -\mathcal{D}_0 \mathcal{D}_{0-1} R_{lm\omega}(r) {}_{+1}Z_{lm\omega}(\theta, \phi) e^{-i\omega t} \quad (2.8.1a)$$

$$\begin{aligned} {}_{l-m-w}\phi_0 &= K_{0\alpha l-m-w} A_{-1}^\alpha = \\ &= \frac{\rho^2}{\sqrt{2}} [(\rho^{-1} \mathcal{D}_0 + 1) \mathcal{L}_1 + ia \sin \theta \mathcal{D}_0] {}_{-1}R_{lm\omega}(r) {}_{+1}Z_{lm\omega}(\theta, \phi) e^{-i\omega t} \end{aligned} \quad (2.8.1b)$$

$${}_{l-m-w}\phi_{+1} = K_{0\alpha l-m-w} A_{-1}^\alpha = -\frac{\rho^2}{2} \mathcal{L}_0 \mathcal{L}_{1-1} R_{lm\omega}(r) {}_{+1}Z_{lm\omega}(\theta, \phi) e^{-i\omega t} \quad (2.8.1c)$$

Similarly, we can simplify (2.4.25) to

$${}_{l-m-w}\phi_{-1} = K_{-1\alpha l-m-w} A_{+1}^\alpha = -\frac{1}{2} \mathcal{L}_0^\dagger \mathcal{L}_{1+1}^\dagger R_{lm\omega}(r) {}_{-1}Z_{lm\omega}(\theta, \phi) e^{-i\omega t} \quad (2.8.2a)$$

$$\begin{aligned} {}_{l-m-w}\phi_0 &= K_{0\alpha l-m-w} A_{+1}^\alpha = \\ &= -\frac{\rho^2}{2\sqrt{2}} \left[ (\rho^{-1} \mathcal{D}_0^\dagger + 1) \mathcal{L}_1^\dagger + ia \sin \theta \mathcal{D}_0^\dagger \right] \Delta_{+1} R_{lm\omega}(r) {}_{-1}Z_{lm\omega}(\theta, \phi) e^{-i\omega t} \end{aligned} \quad (2.8.2b)$$

$${}_{l-m-w}\phi_{+1} = K_{+1\alpha l-m-w} A_{+1}^\alpha = -\frac{\rho^2}{4} \Delta \mathcal{D}_0^\dagger \mathcal{D}_0^\dagger \Delta_{+1} R_{lm\omega}(r) {}_{-1}Z_{lm\omega}(\theta, \phi) e^{-i\omega t} \quad (2.8.2c)$$

The factor of proportionality in the relation (2.5.5) has arbitrarily been chosen to be one. This means that the scalars  ${}_{lm\omega}\phi_{\pm 1}$  derived from (2.5.5) and (2.7.7) will have an arbitrary normalization which will not necessarily have to coincide with the one of the scalars  ${}_{lm\omega}\phi_{\pm 1}$  obtained from (2.8.1) or (2.8.2), as we shall see. Of course, we could always change the normalization of the potentials in (2.7.13) so that expressions (2.7.6) held, but instead we will keep the potentials and the NP scalars resulting from (2.7.13) and (2.8.1) or (2.8.2).

The only difference in the calculation of expressions (2.8.1) and (2.8.2) is that the potentials used correspond to two different gauge choices and therefore the NP

## 2.8. Field components and Teukolsky-Starobinskiĭ identities

---

scalars  ${}_{lm\omega}\phi_h$  should be the same whichever set of expressions we choose to use. However, so far the solutions  ${}_hR_{lm\omega}$  and  ${}_hS_{lm\omega}$  of the radial and angular Teukolsky equations have arbitrary normalizations and boundary conditions (in the radial case). This means that the normalizations and boundary conditions of  ${}_{-1}R_{lm\omega}$  and  ${}_{+1}S_{lm\omega}$  used in (2.8.1) are independent of those of  ${}_{+1}R_{lm\omega}$  and  ${}_{-1}S_{lm\omega}$  used in (2.8.2). Therefore the normalization and boundary conditions of the scalars  ${}_{lm\omega}\phi_h$  which are derived from (2.8.1) do not necessarily coincide with those of the  ${}_{lm\omega}\phi_h$  which are derived from (2.8.2). Since expressions (2.8.1)[(2.8.2)] contain the potential in the ‘ingoing[upgoing] gauge’,  ${}_{lm\omega}A_{-[+]}{}^{\alpha}$ , it will be natural to use ingoing[upgoing] boundary conditions for the radial solution when using these expressions and name the resulting scalars  ${}_{lm\omega}\phi_h^{\text{in[up]}}$ .

Apart from a normalization factor, the expressions for each one of the NP scalars  ${}_{lm\omega}\phi_j$  in (2.8.1) and in (2.8.2) must be equal as long as the same boundary conditions are used for  ${}_{-1}R_{lm\omega}$  and  ${}_{+1}R_{lm\omega}$ . By equating them we find the *Teukolsky-Starobinskiĭ identities*:

$$\mathcal{D}_0\mathcal{D}_{0-1}R_{lm\omega} = C_{+1}R_{lm\omega} \quad \mathcal{L}_0\mathcal{L}_{1+1}S_{lm\omega} = D_{-1}S_{lm\omega} \quad (2.8.3a)$$

$$\Delta\mathcal{D}_0^\dagger\mathcal{D}_0^\dagger\Delta_{+1}R_{lm\omega} = C'_{-1}R_{lm\omega} \quad \mathcal{L}_0^\dagger\mathcal{L}_{1-1}^\dagger S_{lm\omega} = D'_{+1}S_{lm\omega} \quad (2.8.3b)$$

where, for clarity, we drop the subindices  $\{lm\omega\}$  in the constants of proportionality  $\{C, C', D, D'\}$ . There are three restrictions on these constants. Firstly, by applying the operator  $\Delta\mathcal{D}_0^\dagger\mathcal{D}_0^\dagger$  on the radial equation (2.8.3a) and using the radial relation (2.8.3b) and (2.7.8b) the condition

$$\Delta\mathcal{D}_0^\dagger\mathcal{D}_0^\dagger\Delta\mathcal{D}_0\mathcal{D}_0 = {}_1B_{lm\omega}^2 = CC' \quad (2.8.4)$$

follows. The first equality in (2.8.4) is only valid when operating on  ${}_{-1}R_{lm\omega}$ . We are using the definition

$${}_1B_{lm\omega}^2 \equiv {}_{-1}\lambda_{lm\omega}^2 + 4ma\omega - 4a^2\omega^2 \quad (2.8.5)$$

The subindex 1 in  ${}_1B_{lm\omega}$  indicates spin-1 case. Similarly, when applying the operator  $\mathcal{L}_0^\dagger\mathcal{L}_1^\dagger$  on the angular equation (2.8.3a) and using (2.7.9a) and the angular

## 2.8. Field components and Teukolsky-Starobinskiĭ identities

---

(2.8.3b), it follows that  $\mathcal{L}_0^\dagger \mathcal{L}_1^\dagger \mathcal{L}_0 \mathcal{L}_1 = {}_1B_{lm\omega}^2 = DD'$ , with the first equality being valid only when operating on  ${}_+1S_{lm\omega}$ .

The normalization (2.7.5) of the spherical functions immediately implies that  $D = D'$ . We therefore have  $D$  and  $D'$  determined:  $D = D' = {}_1B_{lm\omega}$ , and freedom in the choice of  $C$  and  $C'$  subject to the restriction  $CC' = {}_1B_{lm\omega}^2$ . Traditionally ([14], [26], [88]), the choice  $C = 1/2$  and  $C' = 2{}_1B_{lm\omega}^2$  has been made and we will be faithful to tradition by making the same choice. The Teukolsky-Starobinskiĭ identities (2.8.3) then become

$$\mathcal{D}_0 \mathcal{D}_{0-1} R_{lm\omega} = \frac{1}{2} {}_{+1}R_{lm\omega} \quad \mathcal{L}_0 \mathcal{L}_{1+1} S_{lm\omega} = {}_1B_{lm\omega-1} S_{lm\omega} \quad (2.8.6a)$$

$$\Delta \mathcal{D}_0^\dagger \mathcal{D}_0^\dagger \Delta_{+1} R_{lm\omega} = 2{}_1B_{lm\omega-1}^2 R_{lm\omega} \quad \mathcal{L}_0^\dagger \mathcal{L}_{1-1}^\dagger S_{lm\omega} = {}_1B_{lm\omega+1} S_{lm\omega} \quad (2.8.6b)$$

We will also include here the Teukolsky-Starobinskiĭ identities for the angular functions for the spin-2 case ([20]), since we will need them in Chapter 5. They are:

$$\begin{aligned} \mathcal{L}_{-1} \mathcal{L}_0 \mathcal{L}_1 \mathcal{L}_{2+2} S_{lm\omega} &= {}_2B_{lm\omega-2} S_{lm\omega} \\ \mathcal{L}_{-1}^\dagger \mathcal{L}_0^\dagger \mathcal{L}_1^\dagger \mathcal{L}_{2-2}^\dagger S_{lm\omega} &= {}_2B_{lm\omega+2} S_{lm\omega} \end{aligned} \quad (2.8.7)$$

where

$$\begin{aligned} {}_2B_{lm\omega}^2 &\equiv -2\lambda_{lm\omega}^2 (-2\lambda_{lm\omega} + 2)^2 - 8(a\omega)^2 {}_{-2}\lambda_{lm\omega} \left\{ \left(1 - \frac{m}{a\omega}\right) [5 {}_{-2}\lambda_{lm\omega} + 6] - 12 \right\} + \\ &\quad + 144(a\omega)^4 \left(1 - \frac{m}{a\omega}\right)^2 \end{aligned} \quad (2.8.8)$$

The signs of  ${}_sB_{lm\omega}$  for spin  $s = 1$  and  $2$  are arbitrary, but we will take them to be both positive. It can be shown that if they are taken to be positive, then (2.8.6) and (2.8.7) agree with the sign in the symmetry (4.2.1a) of the angular function.

We finally use the Teukolsky-Starobinskiĭ identities to simplify (2.8.1) and (2.8.2).



## 2.8. Field components and Teukolsky-Starobinskiĭ identities

---

The result is a set of very simple expressions for the NP scalar modes  ${}_{lm\omega}\phi_{\pm 1}^{\text{in/up}}$ :

$$\begin{aligned}
 {}_{l-m-\omega}\phi_{-1}^{\text{in}} &= -\frac{1}{2} {}_{+1}R_{lm\omega}^{\text{in}} Z_{lm\omega} e^{-i\omega t} \\
 {}_{l-m-\omega}\phi_{+1}^{\text{in}} &= -\frac{{}_1B_{lm\omega}}{2} \rho^2 {}_{-1}R_{lm\omega}^{\text{in}} Z_{lm\omega} e^{-i\omega t} \\
 {}_{l-m-\omega}\phi_{-1}^{\text{up}} &= -\frac{{}_1B_{lm\omega}}{2} {}_{+1}R_{lm\omega}^{\text{up}} Z_{lm\omega} e^{-i\omega t} \\
 {}_{l-m-\omega}\phi_{+1}^{\text{up}} &= -\frac{{}_1B_{lm\omega}^2}{2} \rho^2 {}_{-1}R_{lm\omega}^{\text{up}} Z_{lm\omega} e^{-i\omega t}
 \end{aligned} \tag{2.8.9}$$

Chandrasekhar [20] obtained an expression for the other NP scalar by comparing Maxwell equations (2.3.6a) and (2.3.6d) and using the Teukolsky-Starobinskiĭ identities. He also found another, equivalent expression for the same NP scalar using Maxwell equations (2.3.6b) and (2.3.6c) instead. These expressions are:

$$\begin{aligned}
 {}_{l-m-\omega}\phi_0^{\text{in}} &= -\frac{\rho^2}{2^{3/2} {}_1B_{lm\omega}} \left[ \left( \rho^{-1} \mathcal{D}_0^\dagger + 1 \right) \mathcal{L}_1^\dagger + ia \sin \theta \mathcal{D}_0^\dagger \right] \Delta_{+1} R_{lm\omega-1}^{\text{in}} Z_{lm\omega} e^{-i\omega t} = \\
 &= \frac{\rho^2}{\sqrt{2}} \left[ \left( \rho^{-1} \mathcal{D}_0 + 1 \right) \mathcal{L}_1 + ia \sin \theta \mathcal{D}_0 \right] {}_{-1}R_{lm\omega+1}^{\text{in}} Z_{lm\omega} e^{-i\omega t} \\
 {}_{l-m-\omega}\phi_0^{\text{up}} &= -\frac{\rho^2}{2^{3/2}} \left[ \left( \rho^{-1} \mathcal{D}_0^\dagger + 1 \right) \mathcal{L}_1^\dagger + ia \sin \theta \mathcal{D}_0^\dagger \right] \Delta_{+1} R_{lm\omega-1}^{\text{up}} Z_{lm\omega} e^{-i\omega t} = \\
 &= \frac{\rho^2 {}_1B_{lm\omega}}{\sqrt{2}} \left[ \left( \rho^{-1} \mathcal{D}_0 + 1 \right) \mathcal{L}_1 + ia \sin \theta \mathcal{D}_0 \right] {}_{-1}R_{lm\omega+1}^{\text{up}} Z_{lm\omega} e^{-i\omega t}
 \end{aligned} \tag{2.8.10}$$

Making use of the relations (3.2.54b) and (4.2.3b) it can be immediately checked that the two different expressions for  ${}_{lm\omega}\phi_0^{\text{in}}$  are indeed equivalent. Likewise for the two expressions for  ${}_{lm\omega}\phi_0^{\text{up}}$ .

In practise we are only going to numerically calculate one radial function ( ${}_{-1}R$ ) and its derivative with both ‘in’ and ‘up’ boundary conditions and one angular function ( ${}_{-1}S$ ) and its derivative. We will then calculate the other radial and angular functions and their derivatives from linear expressions derived from the Teukolsky-Starobinskiĭ identities. We will obtain the NP Maxwell scalars from the simple expressions (2.8.9) and (2.8.10).

# Chapter 3

## Radial solution

### 3.1 Introduction

The Teukolsky equation (2.7.2) for the field perturbation  $\Omega_h$  in the Kerr-Newman background is separable in Boyer-Lindquist coordinates. The resulting radial differential equation in the vacuum case is

$$\Delta^{-h} \frac{d}{dr} \left( \Delta^{h+1} \frac{d {}_h R_{lm\omega}}{dr} \right) - {}_h V {}_h R_{lm\omega} = 0 \quad (3.1.1)$$

where the potential is given by

$${}_h V = \frac{2ih(r-M)K - K^2}{\Delta} - 4ih\omega r + {}_h \lambda_{lm\omega} \quad (3.1.2)$$

where  ${}_h \lambda_{lm\omega}$  is the eigenvalue of the angular equation, which we deal with in the next chapter. It is immediate from the radial equation (3.1.1) that the following symmetries are satisfied:

$${}_h R_{lm\omega}(r) = \Delta^{-h} {}_{-h} R_{lm\omega}^*(r) \quad (3.1.3a)$$

$${}_h R_{lm\omega}(r) = {}_h R_{l-m-\omega}^*(r) \quad (3.1.3b)$$

These symmetries, however, is only satisfied subject to particular boundary conditions, which we will explore in the next section.

### 3.1. Introduction

---

Except for the case  $\omega = 0$ , the radial equation (3.1.1), has regular singular points at the two roots of  $\Delta$ , i.e., at the inner and outer horizons, and an irregular singular point at infinity. This equation is therefore not soluble in terms of standard functions and we do not know an integral representation of its solutions. We are forced to solve it numerically.

The radial potential (3.1.2) is a complex, long-range potential. In the next section we are going to see two possible transformations, one derived by Detweiler [29] and the other one by Sasaki and Nakamura [80], that convert the radial potential into a short-range one. Detweiler's main interest was in solving the homogeneous radial equation for spin-1 whereas Sasaki and Nakamura's was in solving the inhomogeneous radial equation for spin-2. The two approaches are, as a matter of fact, particular cases of a general-spin method that we present in the next section. This method is valid in the Kerr-Newman background whereas both Detweiler's and Sasaki and Nakamura's results were restricted to the Kerr background. In the same section we give the full set of transformations between the coefficients of the different radial solutions. We also study a particularly symmetric solution of the radial equation.

In the two subsequent sections we describe the numerical method we have used to integrate the homogeneous radial equation for spin-1. The numerical results are compared against the literature.

In Section 3.5 we calculate the asymptotic behaviour of the radial solution close to the horizon, which is needed in Chapter 6. We follow the method used by Candelas [13]. He, however, developed the method for spin-0 and we extend it to general-spin and specialize to spin-1 only at the very end.

In the last section, we find the asymptotic behaviour for small frequency of the radial function, based on a method used by Page [74], which we extend and generalize to the Kerr-Newman background.

## 3.2 Short-range potentials

A second-order differential equation

$$\frac{d^2 Y(x)}{dx^2} + A(x) \frac{dY(x)}{dx} + B(x)Y(x) = 0 \quad (3.2.1)$$

is said to be *short-range* if, and only if,  $A(x) = O(x^{-n})$  and  $B(x) = b_{\pm}^2 + O(x^{-n})$  when  $x \rightarrow \pm\infty$  with  $n \geq 2$  and where  $b_{\pm}$  are constants. If this condition is guaranteed, then the asymptotic form of the solution is

$$Y(x) \sim \begin{cases} e^{\pm ib_+ x} & (x \rightarrow +\infty) \\ e^{\pm ib_- x} & (x \rightarrow -\infty) \end{cases} \quad (3.2.2)$$

The potential (3.1.2) in the radial Teukolsky equation is a long-range potential. We will therefore not solve numerically this equation but we will instead solve one derived from it, which is short-range. Detweiler [29] on the one hand and Sasaki and Nakamura [80] on the other have independently derived from the radial Teukolsky equation two different differential equations which are short-range and valid in the Kerr background.

Both derivations impose for the resulting differential equations to be short-range, but there are two main differences between the two derivations. One difference is that Detweiler requires the potential to be real and the differential equation to have the same form as the radial Teukolsky equation, whereas Sasaki and Nakamura require the differential equation to become the Regge-Wheeler equation in the limit  $a \rightarrow 0$  for  $h = -2$ . The Regge-Wheeler equation is the differential equation that governs the odd parity gravitational perturbations of the Schwarzschild space-time. The other key difference between the two derivations is that Detweiler's main interest was in solving the homogeneous differential equation whereas Sasaki and Nakamura's was in solving the inhomogeneous one. Detweiler's new source term behaves actually worse than the original source for  $r \rightarrow +\infty$  whereas Sasaki and Nakamura's new source term is short-range.

In [29], Detweiler derived for general spin the set of equations that the new,

### 3.2. Short-range potentials

---

real potential and the new radial function should satisfy in order to meet his requirements. However, he only solved them and showed the explicit form of the new potential and radial function for the case of  $h = -1$ . In [30], he further wrote the required general form for any spin for the new potential and radial function in terms of the potential  ${}_hV$  and the variables that define the new radial function. These variables were left undetermined satisfying certain general-spin equations. Sasaki and Nakamura [80] were mainly interested in gravitational perturbations and their whole derivation was restricted to  $h = -2$ .

Both derivations are, in fact, particular cases of a more general derivation which we have calculated for the homogeneous case and will present next. This derivation is valid in the Kerr-Newman background. We also show when and how the two approaches differ and justify why we chose to pursue Detweiler's approach rather than Sasaki and Nakamura's.

First note that the solution  ${}_{-h}R_{lm\omega}$  can be expressed in terms of the solution  ${}_hR_{lm\omega}$  and its derivative. We only need to use one of the radial Teukolsky-Starobinskiĭ identities (2.8.6) and express the second derivative of the function appearing in the identity in terms of the function and its first derivative by using the radial Teukolsky equation. The result is

$${}_{-h}R_{lm\omega} = a_D {}_hR_{lm\omega} + b_D \Delta^{h+1} \frac{d {}_hR_{lm\omega}}{dr} \quad (3.2.3)$$

where, for  $h = -1$ ,

$$\begin{aligned} a_D &= -\frac{2}{\Delta} [2K^2 + \Delta(iK' - {}_{-1}\lambda_{lm\omega})] \\ b_D &= \frac{4iK}{\Delta} \end{aligned} \quad (3.2.4)$$

where a primed function denotes differentiation with respect to its only argument,  $r$  in this case. The general transformation of the radial function  ${}_hR_{lm\omega}$  which preserves the form of the linear wave equation (3.1.1) is

$$\chi_{lm\omega} = \alpha(r) {}_hR_{lm\omega} + \beta(r) \Delta^{h+1} \frac{d {}_hR_{lm\omega}}{dr} \quad (3.2.5)$$

or equivalently, using (3.2.3),

$$\chi_{lm\omega} = p(r) {}_hR_{lm\omega} + q(r) {}_{-h}R_{lm\omega} \quad (3.2.6)$$

### 3.2. Short-range potentials

with

$$\alpha = p + a_D q \quad (3.2.7)$$

$$\beta = b_D q$$

Detweiler's and Sasaki and Nakamura's derivations differ in the choices of the conditions on  $\alpha$  and  $\beta$  (or equivalently,  $p$  and  $q$ ). Transformation (3.2.5) can be inverted to give

$$\begin{aligned} \gamma {}_h R_{lm\omega} &= (\alpha + \beta' \Delta^{h+1}) \chi_{lm\omega} - \beta \Delta^{h+1} \frac{d\chi_{lm\omega}}{dr} \\ \gamma \frac{d {}_h R_{lm\omega}}{dr} &= -(\alpha' + \beta \Delta^h {}_h V) \chi_{lm\omega} + \alpha \frac{d\chi_{lm\omega}}{dr} \end{aligned} \quad (3.2.8)$$

where

$$\gamma = \alpha (\alpha + \beta' \Delta^{h+1}) - \beta \Delta^{h+1} (\alpha' + \beta \Delta^h {}_h V) \quad (3.2.9)$$

If we take the first and second derivatives of  $\chi_{lm\omega}$  in (3.2.5) with respect to  $r$  and use (3.1.1), we find that the differential equation satisfied by  $\chi_{lm\omega}$  is

$$\Delta^{-h} \frac{d}{dr} \left( \Delta^{h+1} \frac{d\chi_{lm\omega}}{dr} \right) - \Delta F \frac{d\chi_{lm\omega}}{dr} - {}_h U(r) \chi_{lm\omega} = 0 \quad (3.2.10)$$

with

$$F \equiv \frac{\gamma'}{\gamma} \quad (3.2.11a)$$

$${}_h U \equiv {}_h V + \frac{\Delta^{-h}}{\beta} \left[ (2\alpha + \beta' \Delta^{h+1})' - F (\alpha + \beta' \Delta^{h+1}) \right] \quad (3.2.11b)$$

It is then useful to define a new dependent variable

$$X_{lm\omega} \equiv (r^2 + a^2)^{1/2} \Delta^{h/2} \chi_{lm\omega} \quad (3.2.12)$$

From the differential equation (3.2.10) for  $\chi_{lm\omega}$  we then find that  $X_{lm\omega}$  satisfies

$$\frac{d^2 X_{lm\omega}}{dr_*^2} - \mathcal{F} \frac{dX_{lm\omega}}{dr_*} - {}_h \mathcal{U} X_{lm\omega} = 0 \quad (3.2.13)$$

with

$$\mathcal{F} \equiv \frac{\Delta F}{(r^2 + a^2)} \quad (3.2.14a)$$

$$G \equiv \frac{s\Delta'}{2(r^2 + a^2)} + \frac{r\Delta}{(r^2 + a^2)^2} \quad (3.2.14b)$$

$${}_h \mathcal{U} \equiv \frac{\Delta {}_h U}{(r^2 + a^2)^2} + G^2 + \frac{dG}{dr_*} - \frac{\Delta F G}{(r^2 + a^2)} \quad (3.2.14c)$$

## 3.2. Short-range potentials

---

In order to obtain now Detweiler's derivation as a particular case of the above, we impose that the differential equation (3.2.10) satisfied by  $\chi_{lm\omega}$  is of the same form as the radial Teukolsky equation (3.1.1). Detweiler makes this requirement as a starting point. That is, we require that  $F = 0$ , and therefore, from (3.2.11a), that  $\gamma = \text{const} \equiv \kappa$ . The other requirement Detweiler makes is for the potential  ${}_hU$  to be real. This requirement implies, using equations (3.1.1), (3.2.6) and (3.2.10), that the constant  $\kappa$  and the functions  $\alpha$  and  $\beta$  (or equivalently  $p$  and  $q$  via (3.2.7) where  $a_D$  and  $b_D$  are assumed to be known, as we do for the spin-1 case) must satisfy the equations

$$\Delta^{2h} \kappa \kappa^* = a_D^2 - a'_D b_D \Delta^{h+1} + a_D b'_D \Delta^{h+1} - b_D^2 \Delta^{2h+1} {}_hV \quad (3.2.15a)$$

$$\kappa^* q = \Delta^{-h} p^* \quad (3.2.15b)$$

$$\kappa \kappa^* = \kappa^* p^2 + \kappa p^{*2} + (a_D + a_D^*) \Delta^{-h} p p^* + b_D \Delta (p p^{*'} - p' p^*) \quad (3.2.15c)$$

The simplest choices for  $\kappa$  and  $p$  are made by assuming that they are real. From equations (3.2.15), where we now specialise to the  $h = -1$  case and therefore have  $a_D$  and  $b_D$  given by (3.2.4), it follows that

$$\kappa = \kappa^* = (4 {}_{-1}\lambda_{lm\omega}^2 - 16a^2\omega^2 + 16a\omega m)^{1/2} = 2 {}_1B_{lm\omega} \quad (3.2.16a)$$

$$p = \frac{\kappa}{\sqrt{2}} \left( \frac{4K^2}{\Delta} - 2 {}_{-1}\lambda_{lm\omega} + \kappa \right)^{-1/2} \quad (3.2.16b)$$

$$q = \frac{p\Delta}{\kappa} \quad (3.2.16c)$$

Detweiler [29] shows that the term inside the square root in (3.2.16b) is strictly positive as long as

$${}_{-1}\lambda_{lm\omega} - a^2\omega^2 + 2a\omega m < \frac{\sqrt{5}}{4} \quad \text{for} \quad a\omega > -\frac{1}{4} \quad (3.2.17)$$

The numerical results in [88] show that this condition necessarily holds.

The transformation of the radial function from  ${}_{-1}R_{lm\omega}$  to  $X_{lm\omega}$  is now fully determined via equations (3.2.5) and (3.2.12), since we know  $\alpha$  and  $\beta$  from (3.2.7) and  $p$  and  $q$  from (3.2.16b) and (3.2.16c) respectively.

### 3.2. Short-range potentials

From equations (3.1.2), (3.2.7), (3.2.15b) and (3.2.11b) where now  $F = 0$ , we can obtain the potential in the differential equation for  $\chi_{lm\omega}$ :

$${}_{-1}U(r) = -\frac{K^2}{\Delta} + {}_{-1}\lambda_{lm\omega} + \frac{\Delta(Kp')'}{Kp} \quad (3.2.18)$$

Finally, with (3.2.18) and  $F = 0$  the differential equation (3.2.13) for the dependent variable  $X_{lm\omega}$  becomes

$$\frac{d^2 X_{lm\omega}}{dr_*^2} - {}_{-1}\mathcal{U}(r)X_{lm\omega} = 0 \quad (3.2.19)$$

with

$$\begin{aligned} {}_{-1}\mathcal{U} &= \frac{\Delta {}_{-1}\lambda_{lm\omega} - K^2}{(r^2 + a^2)^2} + \frac{\Delta^2(Kp')'}{(r^2 + a^2)^2 Kp} - \left( \frac{\Delta}{r^2 + a^2} \right)^{3/2} \left[ \frac{\Delta^{1/2}}{(r^2 + a^2)^{1/2}} \right]'' = \\ &= \frac{[-\omega(r^2 + a^2) + am]^2}{(r^2 + a^2)^2} + \frac{\Delta {}_{-1}\lambda_{lm\omega}}{(r^2 + a^2)^2} - \frac{\Delta(\Delta r^2 + 4Ma^2r - Q^2(a^2 - r^2))}{(r^2 + a^2)^4} - \\ &- \frac{\Delta [\Delta(10r^2 + 2\nu^2) - (r^2 + \nu^2)(11r^2 - 10rM + \nu^2)]}{(r^2 + a^2)^2 [(r^2 + \nu^2)^2 + \eta\Delta]} + \\ &+ \frac{12\Delta r(r^2 + \nu^2)^2 [\Delta r - (r^2 + \nu^2)(r - M)]}{(r^2 + a^2)^2 [(r^2 + \nu^2)^2 + \eta\Delta]^2} - \frac{\Delta(r - M)^2\eta [2(r^2 + \nu^2)^2 - \eta\Delta]}{(r^2 + a^2)^2 [(r^2 + \nu^2)^2 + \eta\Delta]^2} \end{aligned} \quad (3.2.20)$$

where

$$\begin{aligned} \nu^2 &\equiv a^2 - am/\omega \\ \eta &\equiv \frac{\kappa - 2 {}_{-1}\lambda_{lm\omega}}{4\omega^2} \end{aligned} \quad (3.2.21)$$

Sasaki and Nakamura [80] derive the differential equation (3.2.13) for  $X_{lm\omega}$  but only for the case  $h = -2$ . They require (3.2.13) for  $h = -2$  to be short-range and to reduce to the Regge-Wheeler equation in the limit  $a \rightarrow 0$ . They show that the transformation

$$\chi_{lm\omega} = \frac{f\Delta(r^2 + a^2)}{gj} \mathcal{D}_0 \left[ j \mathcal{D}_0 \left( \frac{g_h R_{lm\omega}}{r^2 + a^2} \right) \right] \quad (3.2.22)$$

where  $f$ ,  $g$  and  $j$  are undetermined functions of  $r$  guarantees a short-range potential as long as  $f$ ,  $g$  and  $j$  are regular functions with no zero-points and (1)  $f = \text{const} + O(r^{-1})$ , (2)  $g = \text{const} + O(r^{-2})$ , (3)  $h = \text{const} + O(r^{-2})$  for  $r \rightarrow +\infty$  and (4) they all are  $O(1)$  for  $r \rightarrow r_+$ . The differential equation (3.2.13)



### 3.2. Short-range potentials

for  $h = -2$  becomes the Regge-Wheeler equation for  $a = 0$  if  $f$ ,  $g$  and  $j$  are constant in that case.

Even though Sasaki and Nakamura's derivation is purely limited to the case of gravitational perturbations, a similar transformation for the spin-1 case could be found. Such a transformation would possibly deliver a short-range source in the inhomogeneous case, but in the homogeneous case in principle it would not have any advantage over Detweiler's derivation. Nevertheless, we still tried to obtain a similar transformation to (3.2.22) such that for  $h = -1$  the new, radial differential equation is short-range, in case it turned out to be simpler than the one, (3.2.19), given by Detweiler. The generalized version of (3.2.22) we used is

$$\chi_{lm\omega} = \frac{f\Delta^n(r^2 + a^2)^p}{gj} \mathcal{D}_0 \left[ j \mathcal{D}_0 \left( \frac{g_h R_{lm\omega}}{(r^2 + a^2)^q} \right) \right] \quad (3.2.23)$$

but there was no set of values  $\{n, p, q\}$  and set of functions  $\{f, g, j\}$  such that the resulting equation (3.2.13) for  $X_{lm\omega}$  in the case  $h = -1$  is short-range.

We therefore decided to follow Detweiler's derivation and solve numerically the differential equation (3.2.19). We thus find the radial function  $_{-1}R_{lm\omega}$  and its derivative from the solution  $X_{lm\omega}$  and its derivative with (3.2.8). The radial function  $_{+1}R_{lm\omega}$  can then be obtained with (3.2.3). The first term in the potential (3.2.20) tends to  $-\omega^2$  at infinity ( $r \rightarrow +\infty$ ) and to  $-\tilde{\omega}^2$  at the horizon ( $r \rightarrow r_+$ ), whereas all the other terms go as  $O(r^{-2})$  at infinity and vanish at the horizon. We can therefore define two sets of solutions with the following asymptotic behaviours:

$$X_{lm\omega}^{\text{in}} \sim \begin{cases} B_{lm\omega}^{\text{in}} e^{-i\tilde{\omega}r_*} & (r \rightarrow r_+) \\ e^{-i\omega r_*} + A_{lm\omega}^{\text{in}} e^{+i\omega r_*} & (r \rightarrow +\infty) \end{cases} \quad (3.2.24a)$$

$$X_{lm\omega}^{\text{up}} \sim \begin{cases} e^{+i\tilde{\omega}r_*} + A_{lm\omega}^{\text{up}} e^{-i\tilde{\omega}r_*} & (r \rightarrow r_+) \\ B_{lm\omega}^{\text{up}} e^{+i\omega r_*} & (r \rightarrow +\infty) \end{cases} \quad (3.2.24b)$$

When the behaviour of the solution modes in terms of the time  $t$  and the angle  $\phi$  is included, we can find the asymptotic behaviour of the solution modes in terms

### 3.2. Short-range potentials

of the advanced and retarded time co-ordinates:

$$X_{lm\omega}^{\text{in}} e^{+im\phi - i\omega t} \sim \begin{cases} e^{-i\omega v + im\phi} & \text{at } \mathcal{I}^- \\ A_{lm\omega}^{\text{in}} e^{-i\omega u + im\phi} & \text{at } \mathcal{I}^+ \\ 0 & \text{at } \mathcal{H}^- \\ B_{lm\omega}^{\text{in}} e^{-i\tilde{\omega} v + im\phi_+} & \text{at } \mathcal{H}^+ \end{cases} \quad (3.2.25a)$$

$$X_{lm\omega}^{\text{up}} e^{+im\phi - i\omega t} \sim \begin{cases} 0 & \text{at } \mathcal{I}^- \\ B_{lm\omega}^{\text{up}} e^{-i\omega u + im\phi} & \text{at } \mathcal{I}^+ \\ e^{-i\tilde{\omega} u + im\phi_+} & \text{at } \mathcal{H}^- \\ A_{lm\omega}^{\text{up}} e^{-i\tilde{\omega} v + im\phi_+} & \text{at } \mathcal{H}^+ \end{cases} \quad (3.2.25b)$$

Equation (3.2.25a) represents a wave emerging from  $\mathcal{I}^-$ , being partially scattered back to  $\mathcal{I}^+$  and partially transmitted through to  $\mathcal{H}^+$ . Similarly, (3.2.25b) represents a wave emerging from  $\mathcal{H}^-$ , being partially scattered back to  $\mathcal{H}^+$  and partially transmitted through to  $\mathcal{I}^+$ .

Both sets of modes are eigenfunctions of the hamiltonians  $\hat{H}_{\xi}$  and  $\hat{H}_{\chi}$  with eigenvalues  $\omega$  and  $\tilde{\omega}$  respectively:

$$\begin{aligned} \hat{H}_{\xi} X_{lm\omega}^{\bullet} e^{+im\phi - i\omega t} &= \omega X_{lm\omega}^{\bullet} e^{+im\phi - i\omega t} \\ \hat{H}_{\chi} X_{lm\omega}^{\bullet} e^{+im\phi - i\omega t} &= \tilde{\omega} X_{lm\omega}^{\bullet} e^{+im\phi - i\omega t} \end{aligned} \quad (3.2.26)$$

where the symbol  $\bullet$  indicates either ‘in’ or ‘up’. We will restrict the definition of the ‘in’ and ‘up’ modes to those modes with positive  $\omega$  and positive  $\tilde{\omega}$  respectively. It then follows that the ‘in’ and ‘up’ modes are positive frequency with respect to the Killing vectors  $\xi$  and  $\chi$  respectively.

Analogously, it is possible to find the asymptotic behaviour of solutions  ${}_h R_{lm\omega}^{\text{in/up}}$

### 3.2. Short-range potentials

$\forall h = 0, \pm 1/2, \pm 1, \pm 3/2, \pm 2$  of the radial Teukolsky equation:

$${}_h R_{lm\omega}^{\text{in}} \sim \begin{cases} {}_h R_{lm\omega}^{\text{in,tra}} \Delta^{-h} e^{-i\tilde{\omega} r_*} & (r \rightarrow r_+) \\ {}_h R_{lm\omega}^{\text{in,inc}} r^{-1} e^{-i\omega r_*} + {}_h R_{lm\omega}^{\text{in,ref}} r^{-1-2h} e^{+i\omega r_*} & (r \rightarrow +\infty) \end{cases} \quad (3.2.27a)$$

$${}_h R_{lm\omega}^{\text{up}} \sim \begin{cases} {}_h R_{lm\omega}^{\text{up,inc}} e^{+i\tilde{\omega} r_*} + {}_h R_{lm\omega}^{\text{up,ref}} \Delta^{-h} e^{-i\tilde{\omega} r_*} & (r \rightarrow r_+) \\ {}_h R_{lm\omega}^{\text{up,tra}} r^{-1-2h} e^{+i\omega r_*} & (r \rightarrow +\infty) \end{cases} \quad (3.2.27b)$$

From equations (3.2.8), (3.2.12), (3.2.24a) and (3.2.24b) we can find the asymptotic coefficients of  ${}_{-1}R_{lm\omega}^\bullet$  from those of  $X_{lm\omega}^\bullet$ :

$$\begin{aligned} \frac{{}_{-1}R_{lm\omega}^{\text{in,ref}}}{{}_{-1}R_{lm\omega}^{\text{in,inc}} A_{lm\omega}^{\text{in}}} &= \frac{4\omega^2}{{}_1B_{lm\omega}} & \frac{{}_{-1}R_{lm\omega}^{\text{in,tra}}}{{}_{-1}R_{lm\omega}^{\text{in,inc}} B_{lm\omega}^{\text{in}}} &= \frac{-\text{sgn}(\tilde{\omega})|\omega|i}{(r_+^2 + a^2)^{1/2}\mathfrak{N}^*} \\ \frac{{}_{-1}R_{lm\omega}^{\text{up,ref}}}{{}_{-1}R_{lm\omega}^{\text{up,inc}} A_{lm\omega}^{\text{up}}} &= \frac{-i{}_1B_{lm\omega}}{4K_+ \mathfrak{N}^*} & \frac{{}_{-1}R_{lm\omega}^{\text{up,tra}}}{{}_{-1}R_{lm\omega}^{\text{up,inc}} B_{lm\omega}^{\text{up}}} &= \frac{|\omega|(r_+^2 + a^2)^{1/2}}{|K_+|} \\ {}_{-1}R_{lm\omega}^{\text{in,inc}} &= \frac{1}{2^{3/2}|\omega|} & {}_{-1}R_{lm\omega}^{\text{up,inc}} &= \frac{-2^{1/2}(r_+^2 + a^2)^{1/2}\tilde{\omega}}{{}_1B_{lm\omega}} \end{aligned} \quad (3.2.28)$$

where  $K_+ \equiv K(r_+)$  and we have also defined the new variable

$$\mathfrak{N} \equiv iK_+ + \frac{(r_+ - r_-)}{2} \quad (3.2.29)$$

In the calculation of  ${}_{-1}R_{lm\omega}^{\text{in,tra}} / {}_{-1}R_{lm\omega}^{\text{in,inc}}$  in (3.2.28) we needed an extra term in the asymptotic expansion of the ingoing part (the outgoing part is simply obtained by complex conjugation since the potential  ${}_{-1}\mathcal{U}$  is real) of  $X_{lm\omega}$  close to the horizon. By introducing the asymptotic expansion

$$\frac{X_{lm\omega}^{\text{in}}}{B_{lm\omega}^{\text{in}}} = [1 + \alpha_1(r - r_+) + O((r - r_+)^2)] e^{-i\tilde{\omega} r_*} \quad (3.2.30)$$

in the differential equation (3.2.19) and performing a Taylor series expansion around  $r_+$  of the potential (3.2.20), we find from the second order term that

$$\begin{aligned} \alpha_1 &= \\ &= \frac{-1}{2\mathfrak{N}^*} \left[ {}_{-1}\lambda_{lm\omega} - \frac{4Ma^2r_+ - Q^2(a^2 - r_+^2)}{(r_+^2 + a^2)^2} + \frac{a^2 + Q^2}{r_+^2 + \nu^2} - \frac{4amr_+\tilde{\omega}}{r_+ - r_-} - \frac{2(r_+ - M)^2\eta}{(r_+^2 + \nu^2)^2} \right] \end{aligned} \quad (3.2.31)$$

### 3.2. Short-range potentials

In the calculation of  $_{-1}R_{lm\omega}^{\text{in,inc}}$ , an extra term is also needed in the asymptotic expansion of the ingoing part of  $X_{lm\omega}$  for large  $r$ :

$$X_{lm\omega} = \left[ 1 + \frac{\beta_1}{r} + O(r^{-2}) \right] e^{-i\omega r_*} \quad (3.2.32)$$

with

$$\beta_1 = -\frac{(-1)\lambda_{lm\omega} + 2a\omega m}{2\omega}i \quad (3.2.33)$$

After obtaining the asymptotic coefficients of  $_{-1}R_{lm\omega}^\bullet$  from those of  $X_{lm\omega}^\bullet$ , we just need to derive those of  $_{+1}R_{lm\omega}^\bullet$  to complete the asymptotic picture of the solutions to the radial Teukolsky equation for spin-1. This is achieved by using the transformation (3.2.3) together with the asymptotic behaviour in (3.2.27):

$$\begin{aligned} \frac{_{+1}R_{lm\omega}^{\text{in,inc}}}{_{-1}R_{lm\omega}^{\text{in,inc}}} &= -2^3\omega^2; & \frac{_{+1}R_{lm\omega}^{\text{in,ref}}}{_{-1}R_{lm\omega}^{\text{in,ref}}} &= \frac{_{+1}R_{lm\omega}^{\text{up,tra}}}{_{-1}R_{lm\omega}^{\text{up,tra}}} = -\frac{B_{lm\omega}^2}{2\omega^2} \\ \frac{_{+1}R_{lm\omega}^{\text{in,tra}}}{_{-1}R_{lm\omega}^{\text{in,tra}}} &= \frac{_{+1}R_{lm\omega}^{\text{up,ref}}}{_{-1}R_{lm\omega}^{\text{up,ref}}} = -2^3K_+\mathfrak{N}^*i; & \frac{_{+1}R_{lm\omega}^{\text{up,inc}}}{_{-1}R_{lm\omega}^{\text{up,inc}}} &= \frac{-i_1B_{lm\omega}^2}{2K_+\mathfrak{N}} \end{aligned} \quad (3.2.34)$$

As mentioned in Section 2.6, the differential equation (2.6.1) for  $\rho^{-1}\phi_0$  is separable when  $a = 0$ . We can therefore write

$$r_{lm\omega}\phi_0 = {}_0R_{lm\omega}(r){}_0S_{lm\omega}(\theta)e^{-i\omega t}e^{+im\phi} \quad (3.2.35)$$

in the Reissner-Nordström background where  ${}_0R_{lm\omega}(r)$  and  ${}_0S_{lm\omega}(\theta)$  are, respectively, solutions of the radial and angular differential equations resulting from such separation. The differential equation for  $r{}_0R_{lm\omega}$  coincides with the differential equation (3.2.19) for  $X_{lm\omega}$  with  $a = 0$ . That is,  $r{}_0R_{lm\omega} = X_{lm\omega}$  when  $a = 0$ . In the Reissner-Nordström background not only  ${}_{lm\omega}\phi_0$  has the neat radial functionality of (3.2.35), but also the expressions for  $_{\pm 1}R_{lm\omega}$  in terms of  $r{}_0R_{lm\omega}$  and its derivative are very simple ones. It therefore seems reasonable to hope that in the Kerr-Newman background the expressions for  $_{\pm 1}R_{lm\omega}$  in terms of  $X_{lm\omega}$  and its derivative are also simple ones. More importantly, one would also hope that the expression for  ${}_{lm\omega}\phi_0$  in terms of  $X_{lm\omega}$  and its derivative is simpler than in terms of  $_{\pm 1}R_{lm\omega}$  and its derivative (see (2.8.10)). Unfortunately, the expressions

### 3.2. Short-range potentials

we obtained for  ${}_{\pm 1}R_{lm\omega}$  and  ${}_{lm\omega}\phi_0$  in terms of  $X_{lm\omega}$  and its derivative are actually much more complicated than the ones we already have for  ${}_{+1}R_{lm\omega}$  and  ${}_{lm\omega}\phi_0$  in terms of  ${}_{-1}R_{lm\omega}$  and its derivative.

It is clear from their asymptotic behaviour that neither  ${}_hR_{lm\omega}^{\text{in}}$  nor  ${}_hR_{lm\omega}^{\text{up}}$  satisfy the symmetry (3.1.3a). As a matter of fact, we shall now show that, under this symmetry, the functions  ${}_hR_{lm\omega}^{\bullet}$  transform to the radial functions that are derived from the solution  $X_{lm\omega}^{\bullet*}$  and its derivative. We construct a new radial function  ${}_{-1}\bar{R}_{lm\omega}^{\bullet}$  derived from  $X_{lm\omega}^{\bullet*}$  in the same manner that  ${}_{-1}R_{lm\omega}^{\bullet}$  is derived from  $X_{lm\omega}^{\bullet}$ :

$$\kappa_{-1}\bar{R}_{lm\omega} = (\alpha + \beta') [\Delta^{1/2}(r^2 + a^2)^{-1/2} X_{lm\omega}^*] - \beta \frac{d}{dr} [\Delta^{1/2}(r^2 + a^2)^{-1/2} X_{lm\omega}^*] \quad (3.2.36)$$

It can then be checked using equations (3.2.28) and (3.2.34) that the symmetries

$$\begin{aligned} {}_{+1}R_{lm\omega}^{\bullet} &= 2_1B_{lm\omega}\Delta^{-1}{}_{-1}\bar{R}_{lm\omega}^{\bullet*} \\ {}_{+1}\bar{R}_{lm\omega}^{\bullet} &= 2_1B_{lm\omega}\Delta^{-1}{}_{-1}R_{lm\omega}^{\bullet*} \end{aligned} \quad (3.2.37)$$

are satisfied, where  ${}_{+1}\bar{R}_{lm\omega}^{\bullet}$  is calculated by applying the operator in the radial equation (2.8.6a) to  ${}_{-1}\bar{R}_{lm\omega}^{\bullet}$ . Renaming  ${}_{\pm 1}\bar{R}_{lm\omega}^{\text{in}}$  and  ${}_{\pm 1}\bar{R}_{lm\omega}^{\text{up}}$  by  ${}_{\pm 1}R_{lm\omega}^{\text{out}}$  and  ${}_{\pm 1}R_{lm\omega}^{\text{down}}$  respectively, we have the following two sets of modes:

$${}_{\pm 1}R_{lm\omega}^{\text{out}} \equiv (2_1B_{lm\omega})^{\pm 1}\Delta^{\mp 1}{}_{\mp 1}R_{lm\omega}^{\text{in}*} \sim \quad (3.2.38a)$$

$$\sim \begin{cases} {}_{\pm 1}R_{lm\omega}^{\text{out,tra}} e^{+i\tilde{\omega}r_*} & (r \rightarrow r_+) \\ {}_{\pm 1}R_{lm\omega}^{\text{out,inc}} r^{-1\mp 2} e^{+i\tilde{\omega}r_*} + {}_{\pm 1}R_{lm\omega}^{\text{out,ref}} r^{-1} e^{-i\tilde{\omega}r_*} & (r \rightarrow +\infty) \end{cases} \quad (3.2.38b)$$

$${}_{\pm 1}R_{lm\omega}^{\text{down}} \equiv (2_1B_{lm\omega})^{\pm 1}\Delta^{\mp 1}{}_{\mp 1}R_{lm\omega}^{\text{up}*} \sim \quad (3.2.38c)$$

$$\sim \begin{cases} {}_{\pm 1}R_{lm\omega}^{\text{down,inc}} \Delta^{\mp 1} e^{-i\tilde{\omega}r_*} + {}_{\pm 1}R_{lm\omega}^{\text{down,ref}} e^{+i\tilde{\omega}r_*} & (r \rightarrow r_+) \\ {}_{\pm 1}R_{lm\omega}^{\text{down,tra}} r^{-1} e^{-i\tilde{\omega}r_*} & (r \rightarrow +\infty) \end{cases} \quad (3.2.38d)$$

where

$$\begin{aligned} {}_{\pm 1}R_{lm\omega}^{\text{out,inc}} &\equiv (2_1B_{lm\omega})^{\pm 1}{}_{\mp 1}R_{lm\omega}^{\text{in,inc}*}, & {}_{\pm 1}R_{lm\omega}^{\text{down,inc}} &\equiv (2_1B_{lm\omega})^{\pm 1}{}_{\mp 1}R_{lm\omega}^{\text{up,inc}*} \\ {}_{\pm 1}R_{lm\omega}^{\text{out,ref}} &\equiv (2_1B_{lm\omega})^{\pm 1}{}_{\mp 1}R_{lm\omega}^{\text{in,ref}*}, & {}_{\pm 1}R_{lm\omega}^{\text{down,ref}} &\equiv (2_1B_{lm\omega})^{\pm 1}{}_{\mp 1}R_{lm\omega}^{\text{up,ref}*} \\ {}_{\pm 1}R_{lm\omega}^{\text{out,tra}} &\equiv (2_1B_{lm\omega})^{\pm 1}{}_{\mp 1}R_{lm\omega}^{\text{in,tra}*}, & {}_{\pm 1}R_{lm\omega}^{\text{down,tra}} &\equiv (2_1B_{lm\omega})^{\pm 1}{}_{\mp 1}R_{lm\omega}^{\text{up,tra}*} \end{aligned} \quad (3.2.39)$$

### 3.2. Short-range potentials

Note that the factor  $(2_1 B_{lm\omega})^{\pm 1}$  is needed so that the Teukolsky-Starobinskiĭ identities are satisfied. Similarly, since the radial modes  ${}_{\pm 1} R_{lm\omega}^{\text{out}}$  and  ${}_{\pm 1} R_{lm\omega}^{\text{down}}$  are obtained from  $X_{lm\omega}^{\text{in}*}$  and  $X_{lm\omega}^{\text{up}*}$  respectively, we rename the latter as

$$X_{lm\omega}^{\text{out}} \equiv X_{lm\omega}^{\text{in}*} \sim \begin{cases} B_{lm\omega}^{\text{out}} e^{+i\tilde{\omega} r_*} & (r \rightarrow r_+) \\ e^{+i\omega r_*} + A_{lm\omega}^{\text{out}} e^{-i\omega r_*} & (r \rightarrow +\infty) \end{cases} \quad (3.2.40a)$$

$$X_{lm\omega}^{\text{down}} \equiv X_{lm\omega}^{\text{up}*} \sim \begin{cases} e^{-i\tilde{\omega} r_*} + A_{lm\omega}^{\text{down}} e^{+i\tilde{\omega} r_*} & (r \rightarrow r_+) \\ B_{lm\omega}^{\text{down}} e^{-i\omega r_*} & (r \rightarrow +\infty) \end{cases} \quad (3.2.40b)$$

with

$$\begin{aligned} A_{lm\omega}^{\text{out}} &\equiv A_{lm\omega}^{\text{in}*}, & A_{lm\omega}^{\text{down}} &\equiv A_{lm\omega}^{\text{up}*} \\ B_{lm\omega}^{\text{out}} &\equiv B_{lm\omega}^{\text{in}*}, & B_{lm\omega}^{\text{down}} &\equiv B_{lm\omega}^{\text{up}*} \end{aligned} \quad (3.2.41)$$

We follow the same positive-frequency convention for the ‘out’ and ‘down’ modes as that for the ‘in’ and ‘up’ modes respectively, namely, their definition is restricted to modes with positive  $\omega$  and positive  $\tilde{\omega}$  respectively. The asymptotic behaviour in terms of the advanced and retarded time co-ordinates of these two new sets of functions is

$$X_{lm\omega}^{\text{out}} e^{+im\phi - i\omega t} \sim \begin{cases} A_{lm\omega}^{\text{out}} e^{-i\omega v + im\phi} & \text{at } \mathcal{I}^- \\ e^{-i\omega u + im\phi} & \text{at } \mathcal{I}^+ \\ B_{lm\omega}^{\text{out}} e^{-i\tilde{\omega} u + im\phi_+} & \text{at } \mathcal{H}^- \\ 0 & \text{at } \mathcal{H}^+ \end{cases} \quad (3.2.42a)$$

$$X_{lm\omega}^{\text{down}} e^{+im\phi - i\omega t} \sim \begin{cases} B_{lm\omega}^{\text{down}} e^{-i\omega v + im\phi} & \text{at } \mathcal{I}^- \\ 0 & \text{at } \mathcal{I}^+ \\ A_{lm\omega}^{\text{down}} e^{-i\tilde{\omega} u + im\phi_+} & \text{at } \mathcal{H}^- \\ e^{-i\tilde{\omega} v + im\phi_+} & \text{at } \mathcal{H}^+ \end{cases} \quad (3.2.42b)$$

Modes (3.2.42a) describe a wave going out to  $\mathcal{I}^+$  whereas modes (3.2.42b) describe a wave going down  $\mathcal{H}^+$ .

It is easy to check that the ‘out’ NP scalars are precisely the ones that relate to the ‘in’ NP scalars under the symmetry transformation  $(t, \phi) \rightarrow (-t, -\phi)$  as in

### 3.2. Short-range potentials

(1.3.15b). Likewise for the ‘down’ NP scalars with respect to the ‘up’ NP scalars. Indeed, using the radial symmetry (3.1.3b) and the angular symmetry (4.2.1c), which we shall see in the next chapter, it immediately follows that

$$\left. \begin{aligned} {}_{lm\omega}\phi_{-1}^{\text{in/up}} &\rightarrow (-1)^{m+1}\Delta^{-1}\rho^{-2}{}_{l-m-\omega}\phi_{+1}^{\text{out/down}} \\ {}_{lm\omega}\phi_0^{\text{in/up}} &\rightarrow -(-1)^{m+1}{}_{l-m-\omega}\phi_0^{\text{out/down}} \\ {}_{lm\omega}\phi_{+1}^{\text{in/up}} &\rightarrow (-1)^{m+1}\Delta\rho^2{}_{l-m-\omega}\phi_{-1}^{\text{out/down}} \end{aligned} \right\} \text{under } (t, \phi) \rightarrow (-t, -\phi) \quad (3.2.43)$$

We can also find the pair of radial functions  ${}_{\pm 1}R_{lm\omega}^{\text{sym}}$  that satisfies the symmetry (3.1.3a). Imposing the condition

$$C\Delta^{-1}{}_{-1}R_{lm\omega}^{\text{sym}*} = {}_{+1}R_{lm\omega}^{\text{sym}} (= 2\mathcal{D}_0\mathcal{D}_{0-1}R_{lm\omega}^{\text{sym}}) \quad (3.2.44)$$

where  $C$  is a factor of proportionality, we find that this new, symmetric radial function can be expressed in terms of  ${}_{-1}R_{lm\omega}^{\text{in}}$  and  ${}_{-1}R_{lm\omega}^{\text{up}}$  as

$$\begin{aligned} {}_{-1}R_{lm\omega}^{\text{sym}} &= \alpha [A^{\text{sym}}{}_{-1}R_{lm\omega}^{\text{in}} + {}_{-1}R_{lm\omega}^{\text{up}}] \\ A^{\text{sym}} &\equiv \frac{1}{{}_{-1}R_{lm\omega}^{\text{in,tra}}} \left[ \frac{iC}{8K_+\mathfrak{N}^*} \left( \frac{\alpha^*}{\alpha} \right) - {}_{-1}R_{lm\omega}^{\text{up,ref}} \right] \end{aligned} \quad (3.2.45)$$

with  $|C| = 2_1B_{lm\omega}$  and where  $\alpha$  is an arbitrary complex number. Another consequence of imposing the symmetry (3.2.44) are the following new relations:

$${}_{+1}R_{lm\omega}^{\text{in}} = \frac{8iK_+\mathfrak{N}^*{}_{-1}R_{lm\omega}^{\text{in,tra}}}{\Delta} \left[ \frac{{}_{-1}R_{lm\omega}^{\text{up,ref}*}}{{}_{-1}R_{lm\omega}^{\text{in,tra}*}} {}_{-1}R_{lm\omega}^{\text{in}*} - {}_{-1}R_{lm\omega}^{\text{up}*} \right] \quad (3.2.46a)$$

$$\begin{aligned} {}_{+1}R_{lm\omega}^{\text{up}} &= \\ &= \frac{8iK_+\mathfrak{N}^*{}_{-1}R_{lm\omega}^{\text{up,ref}}}{\Delta} \left[ \left( 1 - \frac{2^4\omega^4}{{}_1B_{lm\omega}^2 |{}_{-1}R_{lm\omega}^{\text{in,ref}}|^2} \right) \frac{{}_{-1}R_{lm\omega}^{\text{up,ref}*}}{{}_{-1}R_{lm\omega}^{\text{in,tra}*}} {}_{-1}R_{lm\omega}^{\text{in}*} - {}_{-1}R_{lm\omega}^{\text{up}*} \right] \end{aligned} \quad (3.2.46b)$$

It immediately follows from (3.2.45) that the asymptotic form for  ${}_{-1}R_{lm\omega}^{\text{sym}}$  is

$$\frac{{}_{-1}R_{lm\omega}^{\text{sym}}}{\alpha} = \begin{cases} e^{+i\tilde{\omega}r_*} + \frac{iC}{8K_+\mathfrak{N}^*} \left( \frac{\alpha^*}{\alpha} \right) \Delta e^{-i\tilde{\omega}r_*} & (r \rightarrow r_+) \\ -\frac{4\omega^2}{{}_1B_{lm\omega}} \left( \frac{\alpha^*}{\alpha} \right) A^{\text{sym}*} r e^{+i\omega r_*} + A^{\text{sym}} \frac{1}{r} e^{-i\omega r_*} & (r \rightarrow +\infty) \end{cases} \quad (3.2.47)$$

### 3.2. Short-range potentials

An alternative transformation of the radial equation is given by Teukolsky and Press [88]. They perform the change of variable  ${}_hY_{lm\omega} \equiv \Delta^{h/2}(r^2 + a^2)^{1/2}{}_hR_{lm\omega}$ , and the radial equation transforms to

$$\frac{d^2{}_hY_{lm\omega}}{dr_*^2} + V_{TP}{}_hY_{lm\omega} = 0 \quad (3.2.48)$$

where the potential is

$$V_{TP} = \frac{K^2 - 2ihK(r - M) + \Delta(4ir\omega h - {}_{-1}\lambda_{lm\omega}) - h^2(M^2 - a^2)}{(r^2 + a^2)^2} - \frac{\Delta(2Mr^3 + a^2r^2 - 4Mra^2 + a^4)}{(r^2 + a^2)^4} \quad (3.2.49)$$

The potential is invariant under a change in the sign of the helicity parameter  $h$  together with complex conjugation. In consequence, the wronskian formed with two solutions  ${}_hY_{lm\omega}$  and  ${}_{-h}Y_{lm\omega}^*$  is constant, where we are using the following definition of wronskian

$$W[f(r), g(r)] \equiv \frac{df(r)}{dr_*}g(r) - f(r)\frac{dg(r)}{dr_*} \quad (3.2.50)$$

As Detweiler's radial potential  ${}_{-1}\mathcal{U}$  in (3.2.20) is real, the wronskian of a solution  $X_{lm\omega}$  and its complex conjugate is also constant. The various possible wronskians for spin-1 constructed with the 'in' and 'up' solutions are shown in Table 3.1. Each one of the wronskians for the solutions  ${}_hY_{lm\omega}$  can be derived from a particular one of the wronskians for the solutions  $X_{lm\omega}$ , and viceversa. The correspondence between the wronskians of the different types of solutions is indicated by the same letter on the right margin of the table. It can be easily shown that the wronskians for the solution  ${}_hY_{lm\omega}$  can be expressed in terms of the solutions  ${}_hR_{lm\omega}$  as

$$W[{}_{+1}Y_{lm\omega}, {}_{-1}Y_{lm\omega}^*] = {}_{-1}R_{lm\omega}^* \mathcal{D}_0^\dagger (\Delta_{+1}R_{lm\omega}) - \Delta_{+1}R_{lm\omega} \mathcal{D}_{0-1}^\dagger R_{lm\omega}^* = Ci \quad (3.2.51)$$

where  $C$  is a real constant, and in particular,

$$W[{}_{+1}Y_{lm\omega}^{\text{sym}}, {}_{-1}Y_{lm\omega}^{\text{sym}*}] = 0 \quad (3.2.52)$$



### 3.2. Short-range potentials

$r \rightarrow r_+$	$r \rightarrow +\infty$
$2i\tilde{\omega} (1 -  A^{\text{up}} ^2)$	$= W[X^{\text{up}}, X^{\text{up}*}] = 2i\omega  B^{\text{up}} ^2$ (a)
$-2i\tilde{\omega} A^{\text{up}*} B^{\text{in}}$	$= W[X^{\text{in}}, X^{\text{up}*}] = 2i\omega A^{\text{in}} B^{\text{up}*}$ (b)
$2i\tilde{\omega} B^{\text{in}}$	$= W[X^{\text{in}}, X^{\text{up}}] = 2i\omega B^{\text{up}}$ (c)
$-2i\tilde{\omega}  B^{\text{in}} ^2$	$= W[X^{\text{in}}, X^{\text{in}*}] = -2i\omega (1 -  A^{\text{in}} ^2)$ (d)
$\frac{-i_1 B^2}{K_+} + 2^4 K_+  \mathfrak{N} ^2 i  _{-1} R^{\text{up}, \text{ref}} ^2$	$= W[{}_{+1}Y^{\text{up}}, {}_{-1}Y^{\text{up}*}] = \frac{-i_1 B^2}{\omega}  _{-1} R^{\text{up}, \text{tra}} ^2$ (a)
$2^4 i K_+  \mathfrak{N} ^2 {}_{-1} R^{\text{in}, \text{tra}} {}_{-1} R^{\text{up}, \text{ref}*}$	$= W[{}_{+1}Y^{\text{in}}, {}_{-1}Y^{\text{up}*}] = \frac{-i_1 B^2}{\omega} {}_{-1} R^{\text{up}, \text{tra}} {}_{-1} R^{\text{in}, \text{ref}}$ (b)
$2\mathfrak{N}^* {}_{-1} R^{\text{in}, \text{tra}}$	$= W[{}_{-1}Y^{\text{in}}, {}_{-1}Y^{\text{up}}] = -2i\omega {}_{-1} R^{\text{up}, \text{tra}}$ (c)
$2^4 i K_+  \mathfrak{N} ^2  _{-1} R^{\text{in}, \text{tra}} ^2$	$= W[{}_{+1}Y^{\text{in}}, {}_{-1}Y^{\text{in}*}] = 2^4 i \omega^3 - \frac{i_1 B^2}{\omega}  _{-1} R^{\text{in}, \text{ref}} ^2$ (d)

Table 3.1: Wronskians for the radial solutions. For clarity purposes, the subindices  $\{lm\omega\}$  have been dropped. The values of the constants at the left and right columns have been obtained with the asymptotics for the radial solutions at the horizon and at infinity respectively.

It is also useful to note the following two relations between the wronskians of the ‘in’ and ‘up’ solutions once the normalization constants, which are determined later in (6.2.13), have been included:

$$\begin{aligned}
W[{}_{+1}Y_{lm\omega}^{\text{up}}, {}_{-1}Y_{lm\omega}^{\text{up}*}] &= -W[{}_{+1}Y_{lm\omega}^{\text{in}}, {}_{-1}Y_{lm\omega}^{\text{in}*}] \\
W[{}_{+1}Y_{lm\omega}^{\bullet}, {}_{-1}Y_{lm\omega}^{\bullet*}] &= +W[{}_{+1}Y_{l-m-\omega}^{\bullet}, {}_{-1}Y_{l-m-\omega}^{\bullet*}]
\end{aligned} \tag{3.2.53}$$

We give two well-known, useful expressions which are valid for any spin-1 radial solutions satisfying the Teukolsky-Starobinskiĭ identities as given in (2.8.6):

$$\Delta_{+1} R_{lm\omega} = 2 [(-1\lambda_{lm\omega} + 2i\omega r) - 2iK\mathcal{D}_0] {}_{-1} R_{lm\omega} \tag{3.2.54a}$$

$$2_1 B_{lm\omega}^2 \mathcal{D}_0^\dagger (\Delta_{+1} R_{lm\omega}) = [(-1\lambda_{lm\omega} - 2ir\omega) \mathcal{D}_0 + 2i\omega] {}_{-1} R_{lm\omega} \tag{3.2.54b}$$

We will finalize this section by referring to the phenomenon of superradiance which we described in Section 1.5. This phenomenon is manifest in the wronskian relations in Table 3.1. We shall see in Chapter 6 that the squared modulus of the reflection coefficient  $A_{lm\omega}^{\text{in}}$  is equal to the fractional gain or loss of energy in a scattered wave mode  ${}_{lm\omega}\phi_h^{\text{in}}$ . Wronskian relation (d) in Table 3.1 shows that for

the modes such that  $\tilde{\omega}\omega < 0$  the squared modulus of this reflection coefficient must be greater than one, and thus the wave mode is reflected back with a gain of energy. Since the ‘in’ modes are only defined for positive  $\omega$ , superradiance occurs for these modes for negative  $\tilde{\omega}$  only. The transmitted part of the superradiant wave falls into the rotating black hole carrying in negative energy. Similarly, from wronskian relation (a), when  $\tilde{\omega}\omega < 0$  the squared modulus of the reflection coefficient  $A_{lm\omega}^{\text{up}}$  for the ‘up’ modes must be greater than one. Therefore, the ‘up’ modes, which are defined for positive  $\tilde{\omega}$ , that experience superradiance are those for which  $\omega < 0$ . The condition  $\tilde{\omega}\omega < 0$  for superradiance, which is the same for scalar and gravitational perturbations, clearly shows that this phenomenon is only possible if  $a \neq 0$  and therefore it only occurs if the black hole possesses an ergosphere.

### 3.3 Numerical method

We wrote the Fortran90 program RADDRV2KN.F that solves the short-range differential equation (3.2.19) with the real potential (3.2.20). The program then uses equation (3.2.8) to find  ${}_{-1}R_{lm\omega}^\bullet$  and its derivative. The variable of numerical integration is  $r_*$ . In this section we will describe the various methods used by this program as well as its structure.

We cannot set the initial condition for the radial function in the program at  $r_* = -\infty$  ( $r = r_+$ ) and therefore we set it instead slightly away from the horizon, at  $r_* = r_{*0}$  ( $r = r_0 \gtrsim r_+$ ). The value of the function  $X_{lm\omega}^{\text{in}}$  (3.2.24a) at  $r_{*0}$  is accurately given by the first order expansion (3.2.30). The differential equation (3.2.19) is solved with the driver routine *odeint* described below so that  $G \equiv X_{lm\omega}^{\text{in}}(r)/B_{lm\omega}^{\text{in}}$  and its derivative with respect to  $r_*$  are obtained at a finite series of values of  $r_*$  ranging from  $r_{*0}$  to a final value  $r_{*f} \gg r_+$ .

The reflection and transmission coefficients  $A_{lm\omega}^\bullet$  and  $B_{lm\omega}^\bullet$  are obtained by using the wronskian relations in Table 3.1 where the wronskians are evaluated at the

### 3.3. Numerical method

last point  $r_{*f}$  of the integration. The value of  $X_{lm\omega}^{\text{up}}$  at  $r_{*f}$  used to calculate the coefficients is obtained by inserting the asymptotic expansion

$$S \equiv \frac{X_{lm\omega}^{\text{up}*}}{B_{lm\omega}^{\text{up}*}} \rightarrow \exp \left( -i\omega r_* + \sum_{i=1}^6 \frac{{}_i C_{lm\omega}}{r^i} \right) \quad (r_* \rightarrow +\infty) \quad (3.3.1)$$

into the differential equation and finding the values  ${}_i C_{lm\omega}$ , which we include in Appendix A. We initially calculated all the various wronskian relations numerically. However, we found a numerical problem when calculating  $W[G, G^*]$  for large  $r_*$  for modes for which  $\tilde{\omega}/\omega |B_{lm\omega}^{\text{in}}|^2$  is of the order of the precision of the calculations,  $10^{-32}$  in our case. Since  $(1 - |A_{lm\omega}^{\text{in}}|^2) = \tilde{\omega}/\omega |B_{lm\omega}^{\text{in}}|^2$ , for those modes  $|A_{lm\omega}^{\text{in}}|$  must be equal to 1 within the first 32 digits. But since that is the precision of the calculations, the next digits are round-off error and therefore the value of  $W[G, G^*] = -2i\omega (1 - |A_{lm\omega}^{\text{in}}|^2) / |B_{lm\omega}^{\text{in}}|^2$  is all round-off error. We avoid this problem by setting  $W[G, G^*]$  and  $W[S, S^*]$  directly in the program equal to  $-2i\tilde{\omega}$  and  $2i\omega$  respectively. All four coefficients can then be found from these analytical values of the wronskians together with the numerical calculations of  $W[G, S]$  and  $W[G, S^*]$  at  $r_{*f}$ , which do not pose any numerical problem. However, any subsequent evaluations of  $(1 - |A_{lm\omega}^{\text{in}}|^2)$  for the mentioned modes will obviously carry along large round-off error. We found those modes to be the ones with either large  $l$ , small  $m$  or small  $\omega$ . For example, (1) for  $l = 8$ ,  $\omega = 0.3$ : when  $m = 3$  the error in is in the 2nd digit already while for smaller  $m$  all digits are wrong, (2) for  $l = 8$ ,  $m = 1$ : when  $\omega < 0.6$  all digits are wrong, and (3) for  $m = 1$ ,  $\omega = 0.3$ : when  $l \geq 7$  all digits are wrong.

Once the reflection and transmission coefficients are calculated we can obtain the ‘up’ solution at all points in the interval  $[r_{*0}, r_{*f}]$  where  $X_{lm\omega}^{\text{in}}$  has been calculated. For this purpose we may use the expression

$$X_{lm\omega}^{\text{up}} = \frac{1}{B_{lm\omega}^{\text{in}*}} (X_{lm\omega}^{\text{in}*} - A_{lm\omega}^{\text{in}} X_{lm\omega}^{\text{in}}) \quad (3.3.2)$$

which follows from the wronskian relations in Table 3.1. The radial functions  ${}_{-1}R_{lm\omega}^\bullet$  and their derivative can then be obtained via (3.2.8) with  $h = -1$  and their coefficients via (3.2.28). We wish to normalize  ${}_{-1}R_{lm\omega}^\bullet$  with  ${}_{-1}R_{lm\omega}^{\bullet, \text{inc}}$  set equal

### 3.3. Numerical method

---

to 1. We thus divide both coefficients and radial functions across by  ${}_{-1}R_{lm\omega}^{\bullet,\text{inc}}$ , which is given in (3.2.28).

The second-order differential equation is rewritten as two coupled first-order differential equations in the usual way with a change of variable  $z \equiv dX/dr_*$ . That is, equation (3.2.19) is solved as

$$\begin{aligned} \frac{d\Re X}{dr_*} &= \Re z & \frac{d\Im X}{dr_*} &= \Im z \\ \frac{d\Re z}{dr_*} &= {}_{-1}\mathcal{U}\Re X & \frac{d\Im z}{dr_*} &= {}_{-1}\mathcal{U}\Im X \end{aligned} \tag{3.3.3}$$

The notation we will use within the routines described below is the following. The independent variable  $r_*$  is going to be called  $x$ . The two dependent complex variables  $X$  and  $dX/dr_*$  evaluated at a given point  $x_n$  are going to be represented by  $Y_n$ . For clarity of notation the index that refers to one particular differential equation out of the set of four has been eliminated, as all the following equations and descriptions are straight-forwardly generalizable to a set of equations. The subindices  $lm\omega$  have also been dropped in the radial functions for clarity. Finally, the functions on the right hand side of equations (3.3.3) are going to be denoted by  $f$ .

The actual integration of the differential equation (3.3.3) is done with the routines  $odeint(\text{driver}) \rightarrow bsstep(\text{stepper}) \rightarrow \left\{ \begin{smallmatrix} mmid(\text{algorithm}) \\ pzextr(\text{extrapolation}) \end{smallmatrix} \right\}$ , where the arrow indicates a routine call to another one.

The driver routine sets up the quantities that determine the desired accuracy for the numerical solution. It then calls the stepper routine with the present values of  $x$ ,  $Y$ ,  $f$  and a suggested stepsize and receives back and stores the values of the actual stepsize  $\Delta x$  used and the calculated value  $y(x + \Delta x)$ . It then starts again at the new point  $x + \Delta x$  until it reaches the final point  $r_{*f}$ . The stepper routine sets up the number of subintervals to divide  $[x, x + \Delta x]$  in and calls the algorithm routine to perform the integration from  $x$  to  $x + \Delta x$  with this number of subintervals. It then extrapolates the results obtained with different numbers of subintervals in order to improve on the accuracy of the final result. It

### 3.3. Numerical method

---

changes the present stepsize if needed and performs again the above steps until the result  $y(x + \Delta x)$  is found within the desired accuracy. It finally estimates the most efficient stepsize to be taken in the next integration. The algorithm routine integrates the solution from  $x$  to  $x + \Delta x$  for a certain stepsize and a certain number of subintervals of  $[x, x + \Delta x]$ . Finally, the extrapolation routine, called by the stepper, extrapolates various values of  $y(x + \Delta x)$  obtained with increasing number of subintervals to the value that would be obtained if an infinite number of subintervals were used. It also gives an estimate for the error of the method.

We have used the forms of these routines as given in [77] and have adapted them to solve the particular problem (3.3.3). We give below a description of these routines in order to show how the integration of the differential equation is performed.

#### ***odeint driver routine***

*odeint* contains a loop that calculates the value  $Y_n$  of the solution at the point  $x_n$  whose value is increased at each iteration of the loop by a stepsize  $\Delta x$  from an initial value  $x_0$  until a final point  $x_f$ . The stepsize  $\Delta x$  may vary from one iteration to the next. Within each iteration, *odeint* first calculates the value  $f$  of the derivatives (3.3.3) at the present point  $x_n$ . It then sets the quantity whose fractional error will be compared against the error of the method to decide whether the method has converged or not. Since the value of the solution may change a lot in magnitude from one point  $x_n$  to the other, the error may be determined by  $\epsilon Y_n$  where  $\epsilon$  is the desired fractional error, i.e., the solution will be good to one part in  $\epsilon$ . However, if the solution goes through a zero value this quantity would not be a good indicator of the error there. Another situation we must look out for is the accumulation of round-off error: the smaller the stepsize  $\Delta x$  is, the higher the number of times we will have to evaluate the derivatives in (3.3.3) and therefore the larger the accumulated error might become. If the fractional error were given in terms of  $\Delta x dY_n/dx$ , both of the mentioned situations would be taken care of. A good method for assessing whether the desired accuracy is

### 3.3. Numerical method

---

met or not is therefore achieved by comparing the absolute error of the solution against  $\epsilon Y_n^{\text{scal}}$  where

$$Y_n^{\text{scal}} = |Y_n| + \left| \Delta x \frac{dY_n}{dx} \right| + \delta \quad (3.3.4)$$

and  $\delta$  is of the order of the precision of the machine as a safeguard in case the other two terms in  $Y_n^{\text{scal}}$  are effectively zero. *odeint* then stores the values of  $x_n$  and  $Y_n$  calculated in the previous iteration and calls the stepper routine. The iteration finishes and *odeint* stops whenever the final point  $x_f$  is reached or else when a certain maximum number of iterations has been performed.

#### ***bsstep* stepper routine**

This routine makes use of the modified midpoint method included in the routine *mmid* to find the value of the solution of the differential equation at the point  $x + \Delta x$  from the knowledge of the value of the solution and the derivatives in (3.3.3) at the point  $x$ . This method requires splitting the interval  $[x, x + \Delta x]$  into a certain number  $N$  of substeps. By calling *mmid* the stepper routine *bsstep* obtains the value of  $Y(x + \Delta x)$  using a series of values of  $N$  and then uses the extrapolation routine *pzextr* to find the value of  $Y(x + \Delta x)$  for  $\Delta x/N \rightarrow 0$ . This idea for obtaining the value of the solution as though an infinite number of substeps were used is known as Richardson's deferred approach to the limit. The most efficient series of values of  $N$  that is known is the one given by  $N_l = 2l$ . In practise, the number of terms in the series is limited to  $l_{\max} = 8$ . The reason is that for  $N > N_8$  little more efficiency is gained whereas roundoff error can become a problem.

We will denote by  ${}_N Y_{n+1}$  the value of the solution at the point  $x = x_{n+1}$  calculated by *mmid* using  $N$  substeps and will denote by  $Y_{n+1}^{(k)}$  the result of the extrapolation for  $\Delta x/N \rightarrow 0$  when up to  $k$  terms in the series  ${}_N Y_{n+1}$  ( $l = 1 \dots k$ ) have been used. A loop will keep incrementing the number of terms in the series to do the extrapolation with, i.e., it will calculate  ${}_N Y_{n+1}$  ( $l = 1 \dots k$ ) and the corresponding  $Y_{n+1}^{(k)}$  for increasing  $k$ , and finish when either  $k = l_{\max}$  or convergence has been achieved. Convergence is achieved whenever the relative error  $\epsilon_k$  of the

### 3.3. Numerical method

---

method at this  $k$ th iteration is smaller than the desired tolerance  $\epsilon$ . We will denote this value of  $k$  by  $k_f$ . The relative error is calculated as

$$\epsilon_k = \frac{1}{S} \left| \frac{Y^{\text{err}}}{Y^{\text{scal}}} \right| \quad (3.3.5)$$

where  $Y^{\text{err}}$  is the absolute error of the extrapolation (given by *pzextr* as  $D_{k-1,1}$ , defined in (3.3.12)) and  $Y^{\text{scal}}$  is provided by *odeint* as (3.3.4).  $S$  is a safety factor that we set equal to 1/4 since the estimate of the error is not exact.

After calculating  $Y(x + \Delta x)$  up to the desired relative error and before returning to the driver routine in order to calculate the solution at a new point, *bsstep* estimates the number  $N_q$  of substeps such that the calculation of the series  $N_l Y_{n+1}$  ( $l = 1 \dots q$ ) is most efficient. It then calculates the corresponding stepsize  $\Delta x_q$  that would yield a value for the solution within the desired accuracy; this is the stepsize that should be attempted in the next step. In general, we denote by  $\Delta x_i$  the stepsize that provides convergence when series with a final number  $N_i$  of substeps is used. By ‘most efficient’ is meant the one that requires the smallest amount of work per unit step, where the amount of work is given by the number of times that we need to evaluate the right hand side of (3.3.3). It can be checked from (3.3.10) that for the series  $N_l Y_{n+1}$  ( $l = 1 \dots k$ ) this number of evaluations is given by the recursive relation

$$\begin{aligned} A_1 &= N_1 + 1 \\ A_k &= A_{k-1} + N_k \end{aligned} \quad (3.3.6)$$

On the other hand, the error in the extrapolation for the series  $N_l Y_{n+1}$  ( $l = 1 \dots k$ ) is calculated by the routine *pzextr* and is of order  $(\Delta x)^{2k-1}$ . Therefore, if  $\epsilon_k$  is the relative error in the extrapolation for this series using a stepsize of  $\Delta x$ , then the stepsize  $\Delta x_k$  required to obtain a relative error of order of the desired tolerance  $\epsilon$  when using the same series of substeps is estimated to be

$$\Delta x_k = \Delta x \left( \frac{\epsilon}{\epsilon_k} \right)^{1/(2k-1)} \quad (3.3.7)$$

The amount of work per unit step when using the series  $N_l$  ( $l = 1 \dots k$ ) and the

### 3.3. Numerical method

---

stepsize  $\Delta x_k$  is therefore equal to

$$W_k = \frac{A_k}{\Delta x_k} \Delta x = A_k \left( \frac{\epsilon_k}{\epsilon} \right)^{1/(2k-1)} \quad (3.3.8)$$

which has been nondimensionalized by multiplying by  $\Delta x$ . The optimal number  $N_q$  of substeps is then given by the term  $q$  in the series  $N_l$  ( $l = 1 \dots k$ ) such that  $W_q = \min_{k=1, \dots, k_f} W_k$  ) and the corresponding stepsize  $\Delta x_q$  that provides convergence is obtained from (3.3.7).

The following factor  $\alpha(i, j)$ , given in [77], is the factor by which  $\Delta x_i$  is to be multiplied so that the resulting stepsize  $\alpha(i, j)\Delta x_i$  provides convergence when series with a final number  $N_j$  of substeps is used:

$$\alpha(i, j) = \epsilon^{\frac{A_{i+2} - A_{j+2}}{(2i+3)(A_{j+2} - A_1 + 1)}} \quad \text{for } i < j \quad (3.3.9)$$

This factor helps to improve the routine in two particular circumstances. The first one is in the case that the current stepsize  $\Delta x$  being used is too small, which will be indicated by the fact that  $q = k_f$ . In that case, increasing the stepsize to  $\Delta x_{q+1}$  might be a better choice. We do not know the value  $\Delta x_{q+1}$  but it can be calculated from  $\Delta x_q$  with (3.3.9). If using  $\Delta x_{q+1}$  is more efficient than using  $\Delta x_q$  then we choose  $\Delta x_{q+1}$  over  $\Delta x_q$ . This check follows from the definition (3.3.8) of work per unit stepsize and turns out to be  $A_{q+1}\alpha(q, q+1) > A_{q+2}$ . The second circumstance in which  $\alpha(i, j)$  is useful is in the case that the current stepsize  $\Delta x$  is too large to achieve convergence with. This situation is detected by the condition  $\Delta x_k \alpha(k, q+1) < \Delta x$ . If this situation occurs then the current stepsize  $\Delta x$  is abandoned and the stepsize given by  $\Delta x_k \alpha(k, q)$  is attempted instead.

#### ***mmid* algorithm routine**

The routine *mmid* uses an algorithm called the modified midpoint method, which is based on a variation of Euler's method:  $Y_{n+1} = Y_n + \Delta x f(x_n, Y_n)$ . If instead of evaluating the derivative  $f$  at the point  $x_n$  it is evaluated at a middle point between  $x_n$  and  $x_{n+1}$  we then have the second-order Runge-Kutta method. The modified midpoint method splits the interval  $[x_n, x_{n+1}]$  into a sequence of  $N$



### 3.3. Numerical method

intervals equally spaced by  $\Delta x/N$  and then uses the second-order Runge-Kutta method at the end points of the intervals except at the very first and last points.

The result is

$$\begin{aligned}
 z_0 &\equiv Y_n \\
 z_1 &\equiv z_0 + \frac{\Delta x}{N} f(x_n, z_0) \\
 z_{m+1} &\equiv z_m + \frac{2\Delta x}{N} f\left(x_n + \frac{m\Delta x}{N}, z_m\right) \quad \text{for } m = 1, 2, \dots, N-1 \\
 {}_N Y_{n+1} &= \frac{1}{2} \left[ z_N + z_{N-1} + \frac{\Delta x}{N} f(x_n + \Delta x, z_N) \right]
 \end{aligned} \tag{3.3.10}$$

This algorithm is also second-order but it has the nice feature that its truncation error contains only even powers of  $\Delta x/N$ . As a consequence, if we combine the result  ${}_N Y_{n+1}$  obtained using a sequence of  $N$  intervals with the one  ${}_{N/2} Y_{n+1}$  obtained using half as many intervals in the manner  $Y_{n+1} = (4{}_N Y_{n+1} - {}_{N/2} Y_{n+1})/3$ , then the approximation  $Y_{n+1}$  is fourth-order accurate even though it uses approximately (for large  $N$ ) only 1.5 times as many derivative evaluations. The routine *mmid* directly implements the algorithm (3.3.10).

#### ***pzextr* extrapolation routine**

Given a set of sample values  $\{Z_1, Z_2, \dots, Z_k\}$  of a function at the sample points  $\{w_1, w_2, \dots, w_k\}$ , polynomial inter- or extrapolation consists in approximating the value of the function at a certain point  $w$  by evaluating at  $w$  the unique  $(k-1)$ -degree polynomial such that its value at each one of the points  $w_l$  coincides with the sample values  $Z_l$ . This polynomial is given by Lagrange's formula:

$$\begin{aligned}
 P(w) &= \frac{(w-w_2)(w-w_3)\dots(w-w_k)}{(w_1-w_2)(w_1-w_3)\dots(w_1-w_k)} Z_1 + \\
 &\quad + \frac{(w-w_1)(w-w_3)\dots(w-w_k)}{(w_2-w_1)(w_2-w_3)\dots(w_2-w_k)} Z_2 + \\
 &\quad + \dots + \frac{(w-w_1)(w-w_2)\dots(w-w_{k-1})}{(w_k-w_1)(w_k-w_2)\dots(w_k-w_{k-1})} Z_k
 \end{aligned} \tag{3.3.11}$$

Neville's algorithm implements (3.3.11) in a way that not only gives an error estimate but it also makes it easy to calculate the polynomial when an extra point  $w_{k+1}$  is added instead of having to evaluate the awkward formula (3.3.11)

### 3.3. Numerical method

back from scratch. If we define  $P_{l(l+1)\dots(l+m)}$  as the unique  $m$ -degree polynomial passing through the points  $\{w_l, w_{l+1}, \dots, w_{l+m}\}$  and define the differences

$$C_{m,l} \equiv P_{l\dots(l+m)} - P_{l\dots(l+m-1)} \quad (3.3.12a)$$

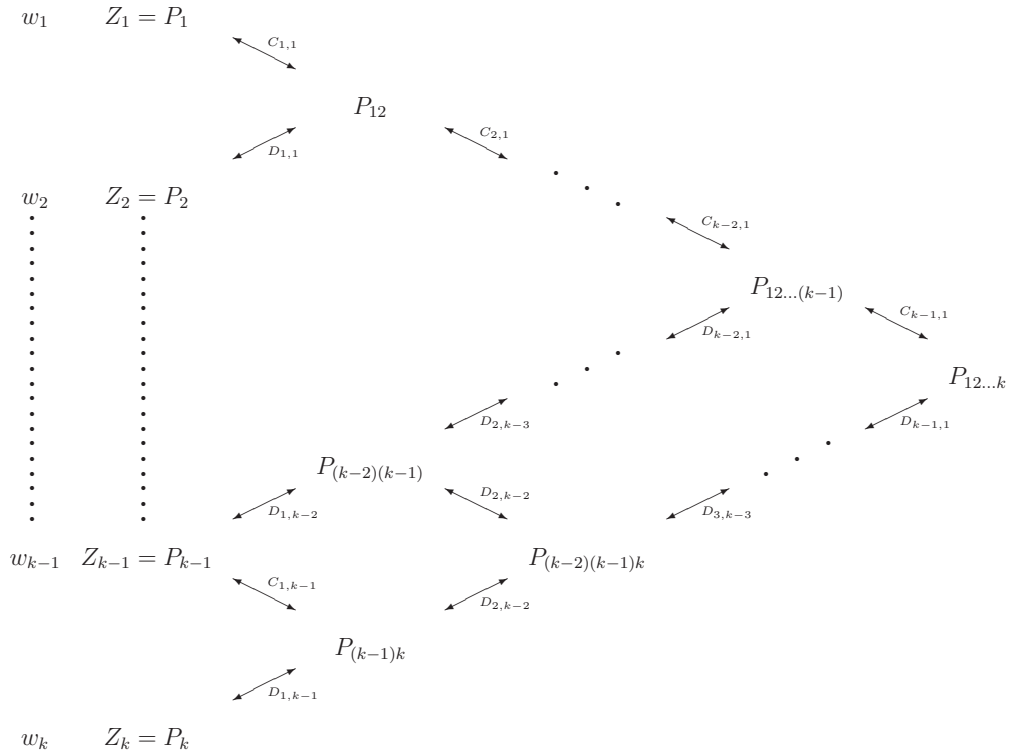
$$D_{m,l} \equiv P_{l\dots(l+m)} - P_{(l+1)\dots(l+m)} \quad (3.3.12b)$$

we then have from (3.3.11) the recursive relations

$$C_{m+1,l} = \frac{(w_{l+m+1} - w)(C_{m,l+1} - D_{m,l})}{w_l - w_{l+m+1}} \quad (3.3.13a)$$

$$D_{m+1,l} = \frac{(w_l - w)(C_{m,l+1} - D_{m,l})}{w_l - w_{l+m+1}} \quad (3.3.13b)$$

The Tableau below schematizes how a polynomial  $P_{l\dots(l+m)}$  of degree  $m$  can be obtained from a polynomial (either  $P_{(l+1)\dots(l+m)}$  or  $P_{l\dots(l+m-1)}$ ) of degree  $(m-1)$  that interpolates the same points except for one of the two ends (either  $w_l$  or  $w_{l+m}$ ) with the knowledge of either  $D_{m,l}$  or  $C_{m,l}$  which can be obtained using the recursive relations (3.3.13).



Apart from the values of  $w_l$  and  $Z_l$  ( $l = 1, \dots, k$ ), the routine *mmid* assumes initial knowledge of the values  $D_{l,k-1-l}$  ( $l = 1, \dots, k-2$ ), which have in practise

### 3.4. Numerical results

$\omega$	Chandrasekhar's	numerical result
-0.35	1.01565	1.015649
-0.455593	0.11332	0.11332896

Table 3.2: The coefficient  $|A_{lm\omega}^{\text{in}}|^2$  for  $M = 1$ ,  $Q = 0$ ,  $a = 0.95$ ,  $l = 1$ ,  $m = -1$  as given by Chandrasekhar's ([20]) TableIX, Chapter 8 and numerically calculated with the program RADDRV2KN.F.

been obtained from the previous call to this routine with the first  $k - 1$  sample points. The routine *pzextr* calculates  $D_{l,k-l}$  ( $l = 1, \dots, k - 1$ ) via (3.3.13) with  $w = 0$  and stores these values for the next time it is called. It finally evaluates at  $w = 0$  the polynomial of degree  $k$  by adding these values to the initial starting point  $P_k$ , i.e.,

$$P_{1\dots k} = P_k + \sum_{l=1}^{k-1} D_{l,k-l} \quad (3.3.14)$$

It finally returns  $D_{k-1,1}$  as an estimate of the error of the extrapolation.

The correspondence of notation with the routines *bsstep* and *odeint* is established by letting  $w_l = h/N_l$  and  $Z_l = {}_{N_l}Y_{n+1}$  where the subindex  $n+1$  has been dropped as all the values of  $Z_l$  refer to the same point  $x_{n+1}$ .

## 3.4 Numerical results

The numerical reflection coefficients  $|A_{lm\omega}^{\text{in}}|^2$  we obtained agree with Chandrasekhar's [20] TableIX, Chapter 8 as shown in Table 3.2.

In Table A.1, which we include in Appendix A because of its large size, we check the results for the radial solution for the particular case  $h = -1$ ,  $Q = 0$ ,  $a = 0.95$ ,  $l = 2$ ,  $m = -2$ ,  $\omega = -0.5$  against the ones given by Chandrasekhar [20] in Table V of his Appendix. The radius of the event horizon corresponding to these values is:  $r_+/M \simeq 1.3122$ . The normalization taken by Chandrasekhar is the same as that of  ${}_{-1}R_{lm\omega}^{\text{sym}}$  and is thus related to the numerical 'in'/'up' solutions that we

### 3.5. Asymptotics close to the horizon

---

obtained via the relation (3.2.45). Since we do not know the value of  $\alpha$  that Chandrasekhar used, we matched at the point  $r/M = 4$  Chandrasekhar's value  ${}_{-1}R_{lm\omega}^{\text{chandr}}$  with the value of  ${}_{-1}R_{lm\omega}^{\text{sym,num}}$ , which is calculated from the numerical values  ${}_{-1}R_{lm\omega}^{\text{in/up,num}}$  via (3.2.45). The resulting value for  $\alpha$  is  $-0.68514 + 1.6271i$  and the values of  ${}_{-1}R_{lm\omega}^{\text{sym,num}}$  at other points  $r$  were calculated with it. Since  $\alpha$  is actually obtained with Chandrasekhar's values, only its first 5 digits are actually valid, and similarly for  ${}_{-1}R_{lm\omega}^{\text{sym,num}}$ . These values are plotted in Figure 3.1, where an erroneous glitch is observed for the real part of  $d{}_{-1}R_{lm\omega}^{\text{chandr}}/dr$  but not in our numerical results.

## 3.5 Asymptotics close to the horizon

In this section we are interested in finding the asymptotic behaviour of the radial function close to the horizon. The main objective for this study is its particular application in Section 6.8 in the last chapter. We calculate in that section the behaviour close to the horizon of the renormalized expectation value of the stress-energy tensor when the field is in the past Boulware state. As we shall show in that section, only the 'up' modes are of interest for that calculation. That calculation involves a factor in front of the 'up' radial functions that decreases exponentially with  $\tilde{\omega}$ . We will therefore not consider the case of large  $\tilde{\omega}$ .

This study is based on the one performed by Candelas [13]. Even though Candelas started the calculation for general spin, he soon confined it to the scalar case. It is our intention to complete his asymptotic calculation for general spin and only specialize to the spin-1 case at the very end.

We perform a Taylor series expansion around  $r = r_+$  of the coefficients of  ${}_hR_{lm\omega}$  and its derivatives appearing in the radial Teukolsky equation (3.1.1). We only keep the first order terms in the expansion and also terms that involve parameters

### 3.5. Asymptotics close to the horizon

---

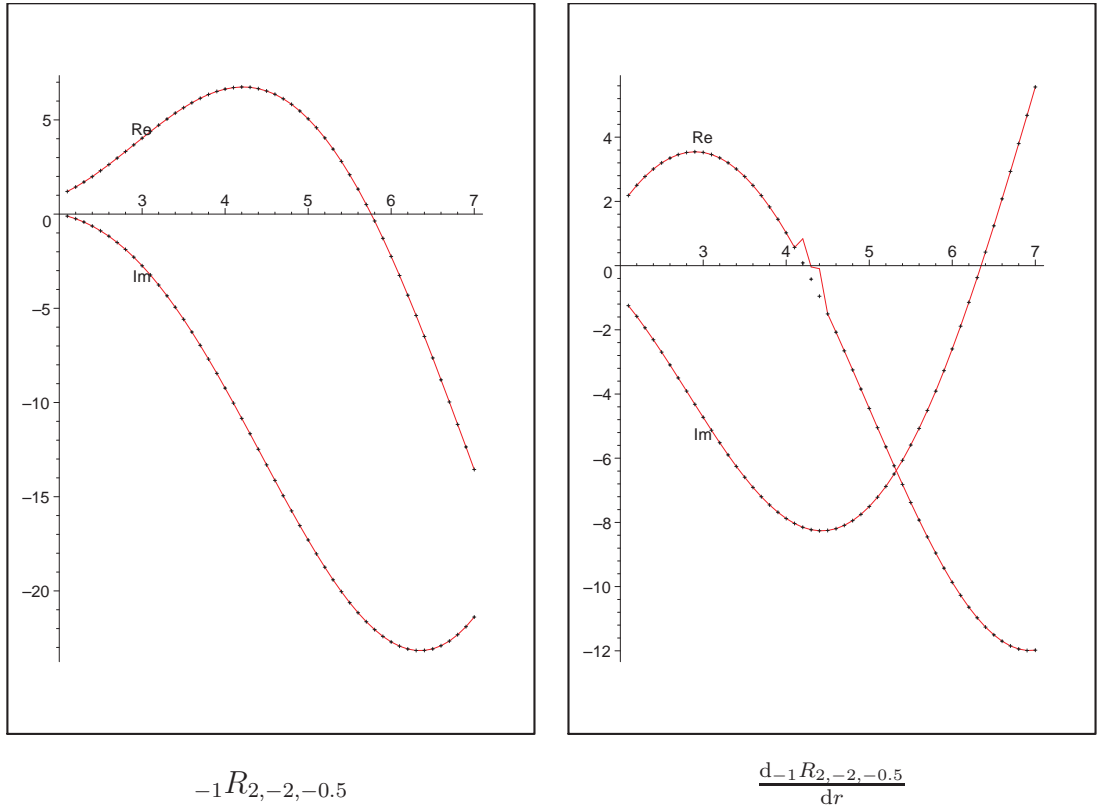


Figure 3.1: Real and Imaginary parts of  ${}_hR_{lm\omega}^{\text{chandr}}$  (in bold red line),  $-1R_{lm\omega}^{\text{sym,num}}$  (in black crosses) and their derivatives for  $h = -1$ ,  $Q = 0$ ,  $a = 0.95$ ,  $l = 2$ ,  $m = -2$ ,  $\omega = -0.5$ .

### 3.5. Asymptotics close to the horizon

---

which might become very large. We obtain:

$$(r - r_+) \frac{d^2 {}_h R_{lm\omega}}{dr^2} + (h + 1) \frac{d {}_h R_{lm\omega}}{dr} - \left[ \frac{{}_h \lambda_{lm\omega} - 4i\omega hr}{r_+ - r_-} - \frac{q(q - 2ih)}{4(r - r_+)} \right] {}_h R_{lm\omega} = 0 \quad (3.5.1)$$

where  $q$  is defined as

$$q \equiv \frac{2K_+}{r_+ - r_-} \quad (3.5.2)$$

The parameters in (3.5.1) that might become very large independently of the limit  $r \rightarrow r_+$  are  ${}_h \lambda_{lm\omega}$ ,  $\omega$  and  $\tilde{\omega}$ . As mentioned, we are going to discard the possibility  $\tilde{\omega} \rightarrow \infty$ . Keeping  $\tilde{\omega}$  bounded means that either both  $m$  and  $\omega$  are bounded or else that  $\omega \rightarrow \infty$  and  $m \sim \omega/\Omega_+$ . We are going to restrict ourselves to the first possibility (i.e.,  $m$  and  $\omega$  bounded) since it is only for this case that we are able to find the behaviour of the angular solutions, needed in the calculation in Section 6.8. This is a crucial point, as we will see later. We thus have that the only term in (3.5.1) that might become very large independently of  $r \rightarrow r_+$  is the one with  ${}_h \lambda_{lm\omega}$ . Since we are keeping  $m$  and  $\omega$  bounded,  ${}_h \lambda_{lm\omega}$  can only become large if we let  $l \rightarrow +\infty$ . Because of factors possessing positive powers of  $l$  for large  $l$  multiplying the ‘up’ radial functions in the calculations that we will perform in Section 6.8, we are only interested in the asymptotics close to the horizon in the modes with  $l \rightarrow +\infty$ .

Even though we only show the angular equation resulting from the separation of variables in the Teukolsky equation valid  $\forall h$  in the next chapter, we will give here a straight-forward result regarding this equation that we need in order to pursue the present calculations. When letting  $l \rightarrow +\infty$  and keeping  $\omega$  and  $m$  bounded in the Teukolsky angular equation (4.1.1), all the terms in the coefficient of the angular function  ${}_h S_{lm\omega}(\theta)$  can be ignored except for  ${}_h \lambda_{lm\omega}$  and those with a  $1/\sin\theta$  in them. This is equivalent to setting  $a\omega = 0$  in the angular equation. This means that in the limit  $l \rightarrow +\infty$  (with  $m$  and  $\omega$  bounded) the angular solution reduces to the spin-weighted spheroidal harmonics:  ${}_h S_{lm} \rightarrow {}_h Y_{lm}$  and that  ${}_h \lambda_{lm\omega} \rightarrow (l-h)(l+h+1) \rightarrow l^2$ . The latter expression implies that  ${}_1 B_{lm\omega} \rightarrow l^2$  in the same limit. We refer the reader to the next chapter for a description of

### 3.5. Asymptotics close to the horizon

---

the different angular solutions and eigenvalues.

We can now approximate equation (3.5.1) in the limit  $l \rightarrow +\infty$  (with  $\omega$  and  $m$  bounded):

$$(r - r_+) \frac{d^2 {}_h R_{lm\omega}}{dr^2} + (h + 1) \frac{d {}_h R_{lm\omega}}{dr} - \left[ \frac{l^2}{r_+ - r_-} - \frac{q(q - 2ih)}{4(r - r_+)} \right] {}_h R_{lm\omega} = 0 \quad (3.5.3)$$

Note that  $m$  and  $\omega$  do not appear explicitly anymore in the differential equation in this limit. This differential equation can be rewritten as

$$z^2 \frac{d^2 {}_h W_{lm\omega}}{dz^2} + z \frac{d {}_h W_{lm\omega}}{dz} - [z^2 + h^2 - q(q - 2ih)] {}_h W_{lm\omega} = 0 \quad (3.5.4)$$

after the change of variables

$$x \equiv \frac{r - r_+}{2(r_+ - M)} \quad (3.5.5a)$$

$$z \equiv 2lx^{1/2} \quad (3.5.5b)$$

$${}_h W_{lm\omega} \equiv x^{h/2} {}_h R_{lm\omega} \quad (3.5.5c)$$

The solutions of the differential equation (3.5.4) are the modified Bessel functions:

$${}_h W_{lm\omega} = I_{\pm(h+iq)}(2lx^{1/2}), K_{h+iq}(2lx^{1/2}) \quad (3.5.6)$$

It is at this point that Candelas' analysis specializes to the scalar case. We pursue it for general spin. The asymptotic behaviour close to the horizon of the 'up' radial functions with  $l \rightarrow +\infty$  is given by

$${}_h R_{lm\omega}^{\text{up}} \rightarrow {}_h a_l x^{-h/2} K_{h+iq}(2lx^{1/2}) + {}_h b_l x^{-h/2} I_{-(h+iq)}(2lx^{1/2}) \quad (l \rightarrow +\infty, r \rightarrow r_+) \quad (3.5.7)$$

which is uniformly valid in  $l$ . The factors  ${}_h a_l$  and  ${}_h b_l$  are the coefficients of the two independent solutions.

The following asymptotic formulae for the modified Bessel functions are well known ([1]):

$$\begin{aligned} I_\nu(z) &\rightarrow \frac{e^z}{\sqrt{2\pi z}} & (|z| \rightarrow +\infty, \nu \text{ fixed}) & \text{ if } |\arg z| < \pi/2 \\ K_\nu(z) &\rightarrow \sqrt{\frac{\pi}{2z}} e^{-z} & (|z| \rightarrow +\infty, \nu \text{ fixed}) & \text{ if } |\arg z| < 3\pi/2 \end{aligned} \quad (3.5.8)$$

### 3.5. Asymptotics close to the horizon

---

and

$$\begin{aligned}
 I_\nu(z) &\rightarrow \frac{1}{\Gamma(\nu+1)} \left(\frac{z}{2}\right)^\nu & (z \rightarrow 0, \nu \text{ fixed}) \quad \text{if } \nu \neq -1, -2, \dots \\
 K_\nu(z) &\rightarrow \begin{cases} \frac{\Gamma(\nu)}{2} \left(\frac{z}{2}\right)^{-\nu} & \text{if } \Re \nu > 0 \\ \frac{\Gamma(-\nu)}{2} \left(\frac{z}{2}\right)^\nu & \text{if } \Re \nu < 0 \end{cases} & (z \rightarrow 0, \nu \text{ fixed})
 \end{aligned} \tag{3.5.9}$$

If we fix  $r$  close to the horizon in (3.5.7) and let  $l \rightarrow +\infty$ , the value of the radial potential at that fixed value of  $r$  will go to infinity and thus it must be  ${}_h R_{lm\omega}^{\text{up}} \rightarrow 0$ . From the formulae (3.5.8), it is only possible that  ${}_h R_{lm\omega}^{\text{up}} \rightarrow 0$  in the limit  $l \rightarrow +\infty$  with  $r$  fixed in (3.5.7) if the coefficient  ${}_h b_l$  decreases exponentially with  $l$ . It follows from this result together with the formulae (3.5.9) that in the limits  $r \rightarrow r_+$  and  $l \rightarrow +\infty$ , while keeping  $lx^{1/2}$  finite, the second term in the asymptotic expression (3.5.7) can be neglected with respect to the first one. In this last statement we have made the implicit assumption that if the coefficient  ${}_h a_l$  decreases for large  $l$ , then it does slower than the coefficient  ${}_h b_l$ . This assumption is proved to be correct in what follows. We have from the above discussion that

$${}_h R_{lm\omega}^{\text{up}} \rightarrow {}_h a_l x^{-h/2} K_{h+iq}(2lx^{1/2}) \quad (l \rightarrow +\infty, r \rightarrow r_+, lx^{1/2} \text{ finite}) \tag{3.5.10}$$

We can determine the coefficient  ${}_h a_l$  by comparison with the WKB approximation (3.2.27b). By taking the limit  $lx^{1/2} \rightarrow 0$  on the solution (3.5.10) we obtain

$$\begin{aligned}
 {}_h R_{lm\omega}^{\text{up}} &\rightarrow \frac{{}_h a_l \pi (r_+ - r_-)^{2h} l^{-h-iq} I_{\tilde{\omega}}^*}{2 \sin[(h+iq)\pi] \Gamma(1-h-iq)} \Delta^{-h} e^{-i\tilde{\omega}r_* -} \\
 &\quad - \frac{{}_h a_l \pi l^{h+iq} I_{\tilde{\omega}}}{2 \sin[(h+iq)\pi] \Gamma(1+h+iq)} e^{+i\tilde{\omega}r_*} \quad (l \rightarrow \infty, r \rightarrow r_+, lx^{1/2} \rightarrow 0)
 \end{aligned} \tag{3.5.11}$$

where

$$I_{\tilde{\omega}} \equiv e^{-\tilde{\omega}r_+} (4M\kappa_+)^{-\frac{i\tilde{\omega}}{2\kappa_+}} (-4M\kappa_-)^{-\frac{-i\tilde{\omega}}{2\kappa_-}} \tag{3.5.12}$$

Comparing this asymptotic expression with the WKB approximation (3.2.27b)



### 3.5. Asymptotics close to the horizon

it follows that

$$\begin{aligned} {}_h a_l &= -\frac{2 \sin[(h+iq)\pi] \Gamma(1+h+iq) I_{\tilde{\omega}}^* l^{-h-iq}}{\pi} {}_h R_{lm\omega}^{\text{up,inc}} \\ {}_h R_{lm\omega}^{\text{up,ref}} &= -\frac{\Gamma(1+h+iq)}{\Gamma(1-h-iq)} (r_+ - r_-)^{2h} I_{\tilde{\omega}}^{*2} l^{-2(h+iq)} {}_h R_{lm\omega}^{\text{up,inc}} \end{aligned} \quad (3.5.13)$$

We now specialize to the spin-1 case. Combining equations (3.5.10) and (3.5.13), and using the same normalization as the one used in the numerical results of the preceding section (i.e., setting  ${}_{-1}R_{lm\omega}^{\text{up,inc}} = 1$  and  ${}_{+1}R_{lm\omega}^{\text{up,inc}} = -iB^2/(2\Re K_+)$ ), we have

$$\begin{aligned} {}_{+1}R_{lm\omega}^{\text{up}} &\rightarrow \frac{-2I_{\tilde{\omega}}^* l^{3-iq}}{(r_+ - r_-)K_+ \Gamma(-iq)} x^{-1/2} K_{1+iq}(2lx^{1/2}) \\ &\quad (l \rightarrow +\infty, r \rightarrow r_+, lx^{1/2} \text{ finite}) \\ {}_{-1}R_{lm\omega}^{\text{up}} &\rightarrow \frac{i(r_+ - r_-)I_{\tilde{\omega}}^* l^{+1-iq}}{K_+ \Gamma(-iq)} x^{1/2} K_{-1+iq}(2lx^{1/2}) \\ &\quad (l \rightarrow +\infty, r \rightarrow r_+, lx^{1/2} \text{ finite}) \end{aligned} \quad (3.5.14)$$

It is also useful to give the expressions that the ‘up’ radial functions (3.5.14) adopt in this limit whenever the constants of normalization (6.2.13) that we shall give in the last chapter are included. These expressions are, in compact form:

$$|N^{\text{up}}| {}_h R_{lm\omega}^{\text{up}} \rightarrow A_h N x^{-1/2} K_{h+iq}(2lx^{1/2}) \quad (l \rightarrow +\infty, r \rightarrow r_+, lx^{1/2} \text{ finite}) \quad (3.5.15)$$

for  $h = \pm 1$ , where

$$A_h \equiv \left\{ \begin{array}{ll} -4 & , h = +1 \\ \frac{2i}{l^4} & , h = -1 \end{array} \right\} [l(r_+ - r_-)]^{-h} \quad (3.5.16)$$

and

$$N \equiv \frac{I_{\tilde{\omega}}^* l^{-iq}}{\sqrt{2^3 \pi K_+} \Gamma(-iq)} \quad (3.5.17)$$

We therefore have finally found the asymptotic behaviour of the ‘up’ radial modes with  $l \rightarrow +\infty$  close to the horizon with  $\tilde{\omega}$ , and both  $m$  and  $\omega$ , bounded. We believe that this is the method behind the approximation given by Candelas,

### 3.5. Asymptotics close to the horizon

---

Chrzanowski and Howard [14] in their TableII. Their result, however, does not exactly coincide with either (3.5.14) or (3.5.15) (as a matter of fact, in their table there is a quantity  $\rho$  that they have not defined and it cannot be the spin coefficient as it cannot have a  $\theta$ -dependency).

Note that there is no reason why the ‘up’ radial modes in (3.5.14), or including the normalization constant in (3.5.15) should diverge in the stated limits. In fact, they clearly do not in the case of helicity  $-1$ . It is only when other factors (as in (2.8.9)) are included that the resulting expressions we will deal with in Section 6.8 diverge in this limit.

We are also interested in finding the result of applying the operator  $\mathcal{D}_0^\dagger \Delta$  on the asymptotic solution (3.5.15), as we will need this result in later calculations. It immediately follows from (3.5.15) and (3.5.16) that

$$\begin{aligned} \frac{1}{A_h N} \mathcal{D}_0^\dagger (\Delta_h R_{lm\omega}^{\text{up}}) &\rightarrow \\ &\rightarrow (r_+ - r_-) x^{-h/2} \left[ \left( -\frac{h}{2} + 1 + i\frac{q}{2} \right) K_{h+iq}(2lx^{1/2}) + lx^{1/2} K'_{h+iq}(2lx^{1/2}) \right] \\ &\quad (l \rightarrow +\infty, r \rightarrow r_+, lx^{1/2} \text{ finite}) \end{aligned} \quad (3.5.18)$$

An important simplification for  $h = +1$  happens when using the recurrence relation ([1])

$$K'_\nu(z) = -K_{\nu-1}(z) - \frac{\nu}{z} K_\nu(z) \quad (3.5.19)$$

for the modified Bessel function. Expression (3.5.18) then reduces to

$$\frac{1}{A_h N} \mathcal{D}_0^\dagger (\Delta_{+1} R_{lm\omega}^{\text{up}}) \rightarrow -\frac{(r_+ - r_-)}{2x^{1/2}} K_{iq} \quad (l \rightarrow +\infty, r \rightarrow r_+) \quad (3.5.20)$$

We used the program RADDRV2KN.F described in Section 3.3 to compare the numerical solution with the analytic asymptotic approximation (3.5.14) we have found. Graphs 3.2–3.5 show that this approximation indeed tends to the non-approximated (numerical) solution and that as  $r \rightarrow r_+$  the approximation is better for the higher values of  $l$ , as predicted.

### 3.5. Asymptotics close to the horizon

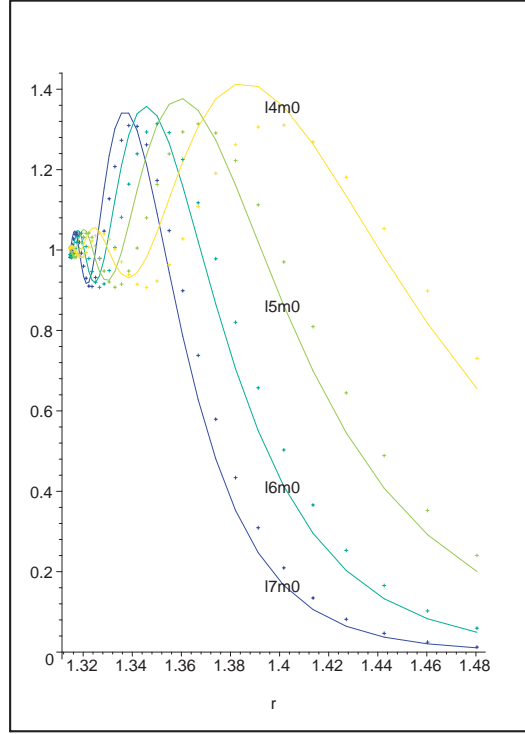


Figure 3.2:  $|_{-1}R_{lm\omega}^{up}|^2$ ,  $l = 4 \dots 7$ ,  $m = 0$ ,  $\omega = 0.5$  (dots are the numerical solution and straight lines are the approximation from (3.5.14)).

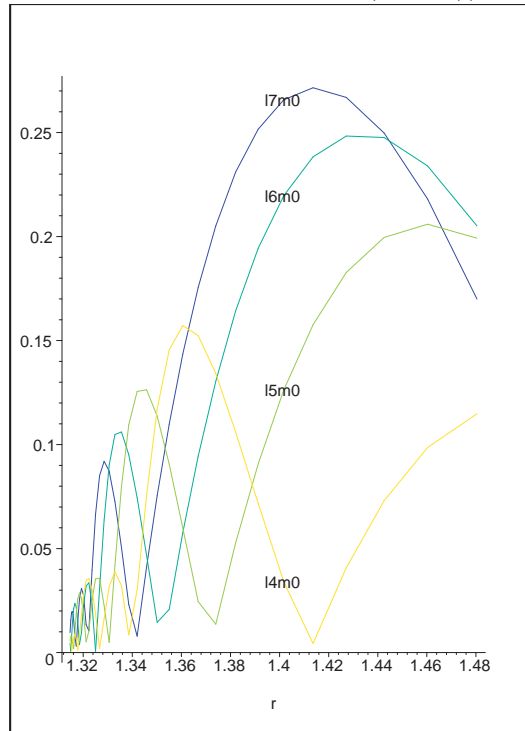


Figure 3.3: Relative error  $\frac{||_{-1}R_{lm\omega}^{up,num}|^2 - |_{-1}R_{lm\omega}^{up,approx}|^2|}{|_{-1}R_{lm\omega}^{up,num}|^2}$ ,  $l = 4 \dots 7$ ,  $m = 0$ ,  $\omega = 0.5$ .

### 3.5. Asymptotics close to the horizon

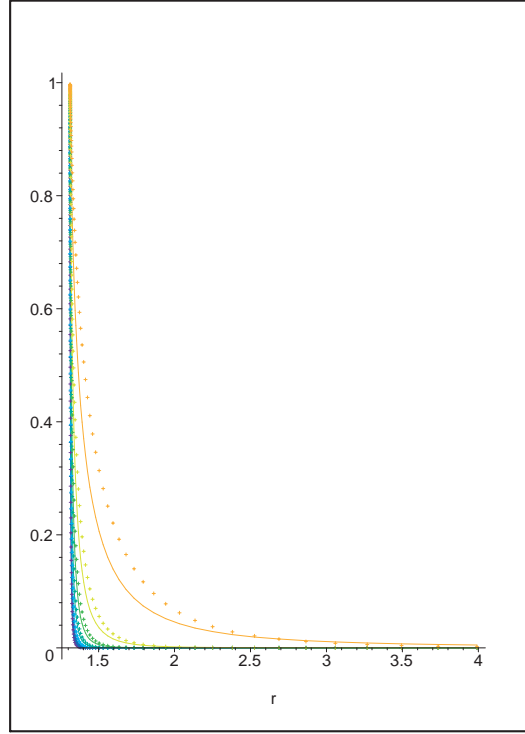


Figure 3.4:  $|_{-1}R_{lm\omega}^{\text{up}}|^2$ ,  $l = 4 \dots 7$ ,  $m = 0$ ,  $\omega = 0.01$ . Correspondence between colours and modes is the same as in Figure 3.2. (dots are the numerical solution and straight lines are the approximation from (3.5.14)).

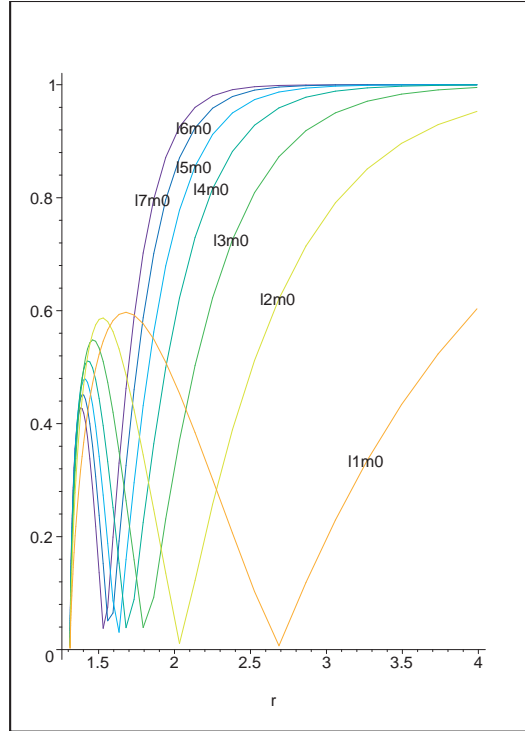


Figure 3.5: Relative error  $\frac{|_{-1}R_{lm\omega}^{\text{up,num}}|^2 - |_{-1}R_{lm\omega}^{\text{up,approx}}|^2}{|_{-1}R_{lm\omega}^{\text{up,num}}|^2}$ ,  $l = 1 \dots 7$ ,  $m = 0$ ,  $\omega = 0.01$ .

### 3.6 Asymptotics for small frequency

We conclude this chapter with an asymptotic analysis of the radial functions for  $M\omega \ll 1$ . This analysis follows that of Page [74] for general spin ‘in’ perturbations in the Kerr background. We complete it by generalizing it to the Kerr-Newman space-time and obtaining the asymptotics for the ‘up’ solutions as well. This analysis is useful for studying what are the contributions to the Fourier sum of modes with  $\omega \sim 0$ .

The radial Teukolsky equation can be rewritten as

$$\begin{aligned} & x^2(x+1)^2 \frac{d^2 {}_h R_{lm\omega}}{dx^2} + (h+1)x(x+1)(2x+1) \frac{d {}_h R_{lm\omega}}{dx} + \\ & + \left\{ k_p^2 x^4 + 2k_p x^3 [\alpha_p k_p + ih] + x^2 [-{}_h \lambda_{lm\omega} + (3ih + q)k_p + \alpha_p^2 k_p^2] + \right. \\ & \left. + x [-{}_h \lambda_{lm\omega} - ihq + (ih\alpha_p + q\alpha_p)k_p] - ih\frac{q}{2} + \frac{q^2}{4} \right\} {}_h R_{lm\omega} = 0 \end{aligned} \quad (3.6.1)$$

where we have defined

$$k_p \equiv \omega(r_+ - r_-) \quad (3.6.2a)$$

$$\alpha_p \equiv \frac{2r_+}{r_+ - r_-} \quad (3.6.2b)$$

Approximating this equation for  $k_p \ll 1$  by keeping the term with the lowest order in  $k_p$  in the coefficient of each power of  $x$  we obtain

$$\begin{aligned} & x^2(x+1)^2 \frac{d^2 {}_h R_{lm\omega}}{dx^2} + (h+1)x(x+1)(2x+1) \frac{d {}_h R_{lm\omega}}{dx} + \\ & + \left[ k_p^2 x^4 + 2ihk_p x^3 - {}_h \lambda_{lm\omega} x(x+1) - \frac{ihq}{2}(2x+1) + \frac{q^2}{4} \right] {}_h R_{lm\omega} = 0 \end{aligned} \quad (3.6.3)$$

In what follows we take  ${}_h \lambda_{lm\omega} = (l-h)(l+h+1)$ , which is exact for  $a\omega = 0$  and it is an approximation for  $a\omega \ll 1$ . Alternatively, we will consider it to be exact for  $a\omega \ll 1$  and use it as the redefinition of the parameter  $l$ . This implies that now  $l$  is nearly, but not an exactly, an integer. This will avoid possible singularities in the  $\Gamma$ -functions appearing in the solutions obtained below.

### 3.6. Asymptotics for small frequency

We find now approximations to the solution of the differential equation (3.6.3) in two different limits, which have an overlapping region. We will then proceed to match the two approximations in this common region of validity.

- Approximation for  $k_px \ll l + 1$

The approximation for  $k_px \ll l + 1$  is obtained by keeping only the lowest term in  $k_px$  in equation (3.6.3) and re-writing it as

$$\begin{aligned} \frac{d^2 {}_h R_{lm\omega}}{dz^2} + (h+1) \left[ \frac{h}{z} + \frac{1}{z-1} \right] \frac{d {}_h R_{lm\omega}}{dz} - \\ - \frac{{}_h R_{lm\omega}}{z(z-1)} \left[ {}_h \lambda_{lm\omega} - \frac{q^2 - 2ihq}{4z} + \frac{q^2 + 2ihq}{4(z-1)} \right] = 0 \end{aligned} \quad (3.6.4)$$

where  $z \equiv -x$ . The general solution of the differential equation (3.6.4), which we denote by  $R_1$ , is given in terms of the hypergeometric functions as

$$\begin{aligned} R_1 = C_1 x^{-h-iq/2} (x+1)^{-h+iq/2} {}_2F_1(-l-h, l-h+1; 1-h-iq; -x) + \\ + C_2 (-1)^h x^{+iq/2} (x+1)^{-h+iq/2} {}_2F_1(-l+iq, 1+l+iq; 1+h+iq; -x) \end{aligned} \quad (3.6.5)$$

where  $C_1$  and  $C_2$  are constants of integration. The asymptotic behaviour of this solution close to the horizon and for large  $r$  is

$$R_1 \sim C_1 (r_+ - r_-)^{2h} I_{\tilde{\omega}}^* \Delta^{-h} e^{-i\tilde{\omega}r_*} + C_2 I_{\tilde{\omega}} e^{+i\tilde{\omega}r_*}, \quad (x \rightarrow 0) \quad (3.6.6a)$$

$$R_1 \sim$$

$$\begin{aligned} \sim C_1 \left[ \frac{\Gamma(1-h-iq)\Gamma(1+2l)}{\Gamma(1-h+l)\Gamma(1+l-iq)} x^{l-h} + \right. \\ \left. + \frac{\Gamma(1-h-iq)\Gamma(-1-2l)}{\Gamma(-h-l)\Gamma(-l-iq)} x^{-l-h-1} \right] + \\ + (-1)^h C_2 \left[ \frac{\Gamma(1+h+iq)\Gamma(1+2l)}{\Gamma(1+l+iq)\Gamma(1+l+h)} x^{l-h} + \right. \\ \left. + \frac{\Gamma(1+h+iq)\Gamma(-1-2l)}{\Gamma(-l+iq)\Gamma(h-l)} x^{-l-h-1} \right], \quad (x \gg |q|/2 + 1) \end{aligned} \quad (3.6.6b)$$

### 3.6. Asymptotics for small frequency

- Approximation for  $x \gg |q|/2 + 1$

In order to obtain a solution of the differential equation (3.6.3) which is valid in the region  $x \gg |q|/2 + 1$  we only keep the terms in the equation with higher powers in  $x$ :

$$\frac{d^2 {}_h R_{lm\omega}}{dx^2} + \frac{2(h+1)}{x} \frac{d {}_h R_{lm\omega}}{dx} + \left[ k_p^2 + \frac{2ihk_p}{x} - \frac{h\lambda_{lm\omega}}{x^2} \right] {}_h R_{lm\omega} = 0 \quad (3.6.7)$$

Its general solution, which we denote by  $R_2$  is given in terms of the confluent hypergeometric functions as

$$R_2 = D_1 x^{-h+l} e^{-ik_p x} {}_1F_1(1-h+l, 2l+2; 2ik_p x) + \\ + D_2 x^{-1-h-l} e^{-ik_p x} {}_1F_1(-l-h, -2l; 2ik_p x) \quad (3.6.8)$$

where  $D_1$  and  $D_2$  are constants of integration. The behaviour of this solution in the region of overlap with  $R_1$  and for large  $r$  is

$$R_2 \sim D_1 x^{l-h} + D_2 x^{-1-h-l}, (k_p x \ll l+1) \quad (3.6.9a)$$

$$R_2 \sim$$

$$\sim x^{-1} e^{-ik_p x} \left[ \frac{\Gamma(2l+2)}{\Gamma(1+h+l)} D_1 (-2ik_p)^{-1+h-l} + \frac{\Gamma(-2l)}{\Gamma(+h-l)} D_2 (-2ik_p)^{h+l} \right] + \\ + x^{-2h-1} e^{+ik_p x} \left[ \frac{\Gamma(2l+2)}{\Gamma(1-h+l)} D_1 (2ik_p)^{-1-h-l} + \frac{\Gamma(-2l)}{\Gamma(-h-l)} D_2 (2ik_p)^{-h+l} \right], \\ (x \rightarrow +\infty) \quad (3.6.9b)$$

We can now match the two solutions  $R_1$  and  $R_2$  in the region of overlap, which is given by  $|q|/2 + 1 \ll x \ll (l+1)/k_p$ . We obtain:

$$D_1 = C_1 \frac{\Gamma(1-h-iq)\Gamma(1+2l)}{\Gamma(1-h+l)\Gamma(1+l-iq)} + (-1)^h C_2 \frac{\Gamma(1+h+iq)\Gamma(1+2l)}{\Gamma(1+l+iq)\Gamma(1+l+h)} \\ D_2 = C_1 \frac{\Gamma(1-h-iq)\Gamma(-1-2l)}{\Gamma(-h-l)\Gamma(-l-iq)} + (-1)^h C_2 \frac{\Gamma(1+h+iq)\Gamma(-1-2l)}{\Gamma(-l+iq)\Gamma(h-l)} \quad (3.6.10)$$

Relations (3.6.10) coincide with the equivalent ones in [53] in the limit  $Q = a = 0$  and with the equivalent ones in [32] in the limit  $Q = h = 0$ .

### 3.6. Asymptotics for small frequency

We finally proceed to obtain the behaviour for small frequency of the ‘in’ and ‘up’ radial functions and coefficients:

- ‘in’ solution:

Comparing the behaviour of  $R_1$  for  $r \rightarrow r_+$  in equation (3.6.6a) with the ‘in’ WKB approximation (3.2.27a) in the same region we find

$$\begin{aligned} C_1^{\text{in}} &= \frac{{}_h R_{lm\omega}^{\text{in,tra}} I_{\tilde{\omega}}}{(r_+ - r_-)^{2h}} \\ C_2^{\text{in}} &= 0 \end{aligned} \quad (3.6.11)$$

Similarly, comparing  $R_2$  and the ‘in’ WKB approximation solution for  $r \rightarrow +\infty$  we find

$$\begin{aligned} \frac{\Gamma(2l+2)}{\Gamma(1+h+l)} D_1^{\text{in}} (-2ik_p)^{-1+h-l} + \frac{\Gamma(-2l)}{\Gamma(+h-l)} D_2^{\text{in}} (-2ik_p)^{h+l} &= \\ &= \frac{{}_h R_{lm\omega}^{\text{in,inc}}}{(r_+ - r_-)} \\ \frac{\Gamma(2l+2)}{\Gamma(1-h+l)} D_1^{\text{in}} (2ik_p)^{-1-h-l} + \frac{\Gamma(-2l)}{\Gamma(-h-l)} D_2^{\text{in}} (2ik_p)^{-h+l} &= \\ &= \frac{{}_h R_{lm\omega}^{\text{in,ref}}}{(r_+ - r_-)(1+2h)} \end{aligned} \quad (3.6.12)$$

Combining together equations (3.6.10), (3.6.11) and (3.6.12) we can find asymptotic expressions for small frequency for the coefficients of the ‘in’ radial solutions:

$$\begin{aligned} \frac{{}_h R_{lm\omega}^{\text{in,tra}}}{{}_h R_{lm\omega}^{\text{in,inc}}} &\sim \\ &\sim (r_+ - r_-)^{2h-1} I_{\tilde{\omega}}^* \frac{\Gamma(1-h+l)\Gamma(1+h+l)\Gamma(1+l-iq)}{\Gamma(1+2l)\Gamma(2+2l)\Gamma(1-h-iq)} (-2ik_p)^{1-h+l} \\ &\quad (k_p \rightarrow 0) \\ \frac{{}_h R_{lm\omega}^{\text{in,ref}}}{{}_h R_{lm\omega}^{\text{in,inc}}} &\sim (-1)^{1+h+l} (r_+ - r_-)^{2h} \frac{\Gamma(1+h+l)}{\Gamma(1-h+l)} (2ik_p)^{-2h} \\ &\quad (k_p \rightarrow 0) \end{aligned} \quad (3.6.13)$$



### 3.6. Asymptotics for small frequency

In particular, for helicity  $-1$ ,

$$\begin{aligned} \frac{-1R_{lm\omega}^{\text{in,tra}}}{-1R_{lm\omega}^{\text{in,inc}}} &\sim \frac{I_{\tilde{\omega}}^*}{(r_+ - r_-)^3} \frac{\Gamma(2+l)\Gamma(l)\Gamma(1+l-iq)}{\Gamma(1+2l)\Gamma(2+2l)\Gamma(2-iq)} (-2ik_p)^{2+l} \propto \omega^{2+l} \\ &\quad (k_p \rightarrow 0) \\ \frac{-1R_{lm\omega}^{\text{in,ref}}}{-1R_{lm\omega}^{\text{in,inc}}} &\sim (-1)^l \frac{1}{(r_+ - r_-)^2} \frac{\Gamma(l)}{\Gamma(2+l)} (2ik_p)^2 \propto \omega^2 \\ &\quad (k_p \rightarrow 0) \end{aligned} \tag{3.6.14}$$

The asymptotic behaviour for small frequency of the ‘in’ radial solution is obtained from equations (3.6.5), (3.6.11) and (3.6.13):

$$\begin{aligned} \frac{{}_hR_{lm\omega}^{\text{in}}}{{}_hR_{lm\omega}^{\text{in,inc}}} &\sim \\ &\sim (r_+ - r_-)^{l+iq/2} (r - r_+)^{-h-iq/2} \frac{\Gamma(1-h+l)\Gamma(1+h+l)\Gamma(1+l-iq)}{\Gamma(1+2l)\Gamma(2+2l)\Gamma(1-h-iq)} \times \\ &\times {}_2F_1 \left( -l-h, l-h+1; 1-h-iq; -\left( \frac{r-r_+}{r_+-r_-} \right) \right) (-2i\omega)^{1-h+l} \\ &\quad (k_px \ll l+1) \end{aligned} \tag{3.6.15}$$

In particular, for helicity  $\pm 1$ ,

$$\begin{aligned} \frac{-1R_{lm\omega}^{\text{in}}}{-1R_{lm\omega}^{\text{in,inc}}} &\sim \\ &\sim (r_+ - r_-)^{l+iq/2} (r - r_+)^{1-iq/2} \frac{\Gamma(2+l)\Gamma(l)\Gamma(1+l-iq)}{\Gamma(1+2l)\Gamma(2+2l)\Gamma(2-iq)} \times \\ &\times {}_2F_1 \left( 1-l, 2+l; 2-iq; -\left( \frac{r-r_+}{r_+-r_-} \right) \right) (-2i\omega)^{2+l}, \quad (k_px \ll l+1) \\ \frac{+1R_{lm\omega}^{\text{in}}}{+1R_{lm\omega}^{\text{in,inc}}} &\sim \\ &\sim (r_+ - r_-)^{l+iq/2} (r - r_+)^{-1-iq/2} \frac{\Gamma(l)\Gamma(2+l)\Gamma(1+l-iq)}{\Gamma(1+2l)\Gamma(2+2l)\Gamma(-iq)} \times \\ &\times {}_2F_1 \left( -1-l, l; -i; -\left( \frac{r-r_+}{r_+-r_-} \right) \right) (-2i\omega)^l, \quad (k_px \ll l+1) \end{aligned} \tag{3.6.16}$$

- ‘up’ solution:

Proceeding likewise for the ‘up’ radial solution with WKB approximation

### 3.6. Asymptotics for small frequency

(3.2.27b), we find

$$\begin{aligned} C_1^{\text{up}} &= \frac{{}_h R_{lm\omega}^{\text{up,ref}} I_{\tilde{\omega}}}{(r_+ - r_-)^{2h}} \\ C_2^{\text{up}} &= {}_h R_{lm\omega}^{\text{up,inc}} I_{\tilde{\omega}}^* \end{aligned} \quad (3.6.17)$$

and

$$\frac{\Gamma(2l+2)}{\Gamma(1+h+l)} D_1^{\text{up}} (-2ik_p)^{-1+h-l} + \frac{\Gamma(-2l)}{\Gamma(+h-l)} D_2^{\text{up}} (-2ik_p)^{h+l} = 0 \quad (3.6.18)$$

$$\begin{aligned} \frac{\Gamma(2l+2)}{\Gamma(1-h+l)} D_1^{\text{up}} (2ik_p)^{-1-h-l} + \frac{\Gamma(-2l)}{\Gamma(-h-l)} D_2^{\text{up}} (2ik_p)^{-h+l} = \\ = \frac{{}_h R_{lm\omega}^{\text{up,tra}}}{(r_+ - r_-)(1+2h)} \end{aligned} \quad (3.6.19)$$

Proceeding as for the ‘in’ case, from equations (3.6.17), (3.6.10) and (3.6.18)

we find

$$\begin{aligned} \frac{{}_h R_{lm\omega}^{\text{up,ref}}}{{}_h R_{lm\omega}^{\text{up,inc}}} &\sim \\ &\sim (-1)^{h+1} I_{\tilde{\omega}}^{*2} \frac{\Gamma(1+h+iq)\Gamma(1-h+l)\Gamma(1+l-iq)}{\Gamma(1+l+iq)\Gamma(1+h+l)\Gamma(1-h-iq)} (r_+ - r_-)^{2h}, \quad (k_p \rightarrow 0) \end{aligned} \quad (3.6.20)$$

which agrees with [53] in the limit  $Q = 0 = 0$  and  $h = +2$ .

Proceeding the same way we are not able to find the asymptotic behaviour for  ${}_h R_{lm\omega}^{\text{up,tra}}$ . It follows from (3.6.17) and (3.6.10), that in the expressions for  $D_1^{\text{up}}$  and  $D_2^{\text{up}}$  in terms of  ${}_h R_{lm\omega}^{\text{up,inc}}$  and  ${}_h R_{lm\omega}^{\text{up,ref}}$  there appears no explicit  $k_p$ . This means that, when these expressions are inserted in (3.6.18), then  ${}_h R_{lm\omega}^{\text{up,ref}}$  will be such that, to its lowest order in  $k_p$ , makes  $D_1^{\text{up}}$  zero. This implies that, when the expressions are inserted in (3.6.19), to the lowest order in the calculations,  ${}_h R_{lm\omega}^{\text{up,tra}}$  will be zero. We can, however, find the asymptotic behaviour of  ${}_h R_{lm\omega}^{\text{up,tra}} / {}_h R_{lm\omega}^{\text{up,inc}}$  by using the wronskian relations. From (c) in Table 3.1 and equation (3.6.14) we obtain

$$\frac{{}_{-1} R_{lm\omega}^{\text{up,tra}}}{{}_{-1} R_{lm\omega}^{\text{up,inc}}} \rightarrow -I_{\tilde{\omega}}^* \frac{\Gamma(2+l)\Gamma(l)\Gamma(1+l-iq)}{\Gamma(2+2l)\Gamma(1+2l)\Gamma(1-iq)} \frac{(-2ik_p)^{l+1}}{(r_+ - r_-)} \quad (k_p \rightarrow 0) \quad (3.6.21)$$

It is easy to check that all the coefficients with  $h = -1$ , given by (3.6.14), (3.6.20) and (3.6.21), do satisfy the wronskian relations in Table 3.1. For the coefficients

### 3.6. Asymptotics for small frequency

---

with  $h = +1$ , it can also be checked that  ${}_{+1}R_{lm\omega}^{\text{in,ref}} / {}_{-1}R_{lm\omega}^{\text{in,ref}}$ ,  ${}_{+1}R_{lm\omega}^{\text{in,tra}} / {}_{-1}R_{lm\omega}^{\text{in,tra}}$  and  ${}_{+1}R_{lm\omega}^{\text{up,ref}} / {}_{-1}R_{lm\omega}^{\text{up,ref}}$  satisfy the relations (3.2.34).

# Chapter 4

## Spin-weighted spheroidal harmonics

### 4.1 Introduction

The angular Teukolsky equation resulting from the separation of the Teukolsky equation and its solution are important for several reasons. For one, the angular equation determines the eigenvalue which appears in the radial equation. The angular solution is of particular interest to us due to its central role in the parity transformation  $\{\theta \leftrightarrow \pi - \theta, \phi \leftrightarrow \phi + \pi\}$ , an issue that we deal with in Chapter 6. Finally, the asymptotic behaviour of the eigenvalues and the angular solution for large frequency is important in its own right and is the subject of Chapter 5.

In the remainder of this section we present a summary of the main results in the literature relating to the angular Teukolsky equation and its solution in the various limits of values of its parameters. In the next section, we present the asymptotic behaviour close to the boundary points of the angular solutions as well as other basic properties that we have obtained, all of which are needed for later calculations. In Section 4.3 we describe the numerical method, algorithms and their implementation in different Fortran90 programs that we have used in

order to numerically solve the angular differential equation. In the last section of this chapter we display and analyze the numerical results that we have obtained and we compare them against previous results in the literature.

When expanding the field  $\Omega_h$  in terms of the Fourier modes (2.7.3), the Teukolsky equation (2.7.2) becomes separable. The corresponding angular ordinary differential equation is

$$\left[ \frac{d}{dx} \left( (1-x^2) \frac{d}{dx} \right) + c^2 x^2 - 2hc x - \frac{(m+hx)^2}{1-x^2} + {}_h\mathcal{A}_{lm\omega} + h \right] {}_hS_{lm\omega}(x) = 0 \quad (4.1.1)$$

where the new variables  $x \equiv \cos \theta$  and  $c \equiv a\omega$  have been defined. The constant of separation between the angular and radial equations is

$${}_h\mathcal{A}_{lm\omega} \equiv {}_hE_{lm\omega} - h(h+1) \equiv {}_h\lambda_{lm\omega} - c^2 + 2mc \quad (4.1.2)$$

It might be more logical to label the angular solutions and the eigenvalues by  $c$  rather than  $\omega$ , but following the convention of literature on the Teukolsky equation we label them by  $\omega$ .

The differential equation (4.1.1) has two regular singular points at  $x = \pm 1$  and one essential singularity at  $x = \infty$ . We are only interested, however, in solutions for real values of the independent variable  $x$  that lie in the interval  $x \in [-1, +1]$ . We henceforth restrict  $x$  to this range of validity and therefore we have only to consider the two regular singular points at  $x = \pm 1$ . The differential equation (4.1.1), together with the boundary condition that its solution  ${}_hS_{lm\omega}(x)$  is regular for  $x \in [-1, +1]$ , is a parametric eigenvalue problem, the parameters being  $c$ ,  $m$  and  $h$ . This differential equation is called the *spin-weighted spheroidal differential equation*; it reduces to the *spin-weighted spherical differential equation* when  $c = 0$  (but  $h \neq 0$ ), it reduces to the *spheroidal differential equation* when  $h = 0$  (but  $c \neq 0$ ) and to the *spherical differential equation* when  $c = 0$  as well as  $h = 0$ . All four equations possess the same singularity structure described above. The spheroidal differential equation also follows from the scalar wave equation in flat space-time separated in oblate spheroidal co-ordinates (see [61]).

## 4.1. Introduction

Values of parameters	Name of solution of corresponding equation
$c = 0, h = 0$	Spherical harmonics $Y_{lm}(\theta, \phi)$
$c \neq 0, h = 0$	Spheroidal harmonics $S_{lm\omega}(\theta), Z_{lm\omega}(\theta, \phi)$
$c = 0, h \neq 0$	Spin-weighted spherical harmonics ${}_hY_{lm}(\theta, \phi)$
$c \neq 0, h \neq 0$	Spin-weighted spheroidal harmonics ${}_hS_{lm\omega}(\theta), {}_hZ_{lm\omega}(\theta, \phi)$

Table 4.1: Names and symbols of the regular solutions of the various differential equations that are derived from (4.1.1) by making zero none, one or two of the parameters  $c = a\omega$  and  $h$ .

The physical requirements of single-valuedness and of regularity at  $x = \pm 1$  requires that  $l$  and  $m$  are integers with  $|m| \leq l$ . In the particular case of integral  $l$  and  $m$ , the spherical differential equation and its regular solution are respectively called the *associated Legendre equation* and *associated Legendre functions of the first kind*  $P_l^m(\theta)$ . Similarly, for integral  $l$  and  $m$ , the spheroidal differential equation and its regular solution are respectively called the *oblate angular differential equation* and *oblate angle functions of the first kind*  $S_{lm\omega}(\theta)$  (the other independent solutions of this equation have logarithmic singularities at  $x = \pm 1$  and are called *oblate angle functions of the second kind*).

When the regular solution of the spherical equation, the spin-weighted spherical equation, the spheroidal equation or the spin-weighted spheroidal equation is multiplied by  $e^{im\phi}$ , we then obtain the *spherical harmonics*  $Y_{lm}(\theta, \phi)$ , the *spin-weighted spherical harmonics*  ${}_hY_{lm}(\theta, \phi)$ , the *spheroidal harmonics*  $Z_{lm\omega}(\theta)$  or the *spin-weighted spheroidal harmonics (SWSH)*  ${}_hZ_{lm\omega}(\theta)$  respectively. With a slight abuse of terminology, common throughout the literature, we will also refer to the solutions  $S_{lm\omega}(\theta)$  and  ${}_hS_{lm\omega}(\theta)$  as spheroidal harmonics and spin-weighted spheroidal harmonics (SWSH) respectively. It will be clear from the context which of the two possible functions we are referring to. See Table 4.1 for a summary of the notation of the different angular functions we have introduced.

## 4.1. Introduction

---

There exists in the literature much analytic and numerical work on the spheroidal harmonics and substantial analytic, but not so much numerical, work on the spin-weighted spherical harmonics. There exists little work, either analytic or numerical, on the spin-weighted spheroidal harmonics. We will now present the main known properties of these various angular functions.

Flammer [35] together with Abramowitz and Stegun [1] are the most comprehensive works on the different properties, expansions and approximations for different limits of the parameters of the solutions and eigenvalues of the spheroidal differential equation. In addition, they both tabulate numerical results obtained for certain values of the parameters.

Newman and Penrose [70] introduced the spin-weighted spherical harmonics. They first define *spin weight*  $s$  in the same manner as helicity  $h$  is defined in (2.3.14) for a wave travelling in the direction of  $\mathbf{l}$  or  $\mathbf{n}$ . That is, they say that a quantity  $\eta$  has helicity (spin-weight)  $h$  if it transforms as  $\eta \rightarrow e^{hi\vartheta}\eta$  under the transformation  $m^\mu \rightarrow e^{i\vartheta}m^\mu$ . Since it was later proven by Campbell [12] that the spin weight defined by Newman and Penrose actually corresponds to a helicity, as we shall see later, we will use the term helicity even where Newman and Penrose used the term spin weight. They define the operator  $\eth$  (called *edth* or *thop*) and  $\bar{\eth}$  acting on a quantity  $\eta$  of helicity  $h$  defined on the  $(\theta, \phi)$ -sphere as

$$\begin{aligned}\eth\eta &= -\sin^h\theta \left[ \frac{\partial}{\partial\theta} + \frac{i}{\sin\theta} \frac{\partial}{\partial\phi} \right] ((\sin^{-h}\theta)\eta) \\ \bar{\eth}\eta &= -\sin^{-h}\theta \left[ \frac{\partial}{\partial\theta} - \frac{i}{\sin\theta} \frac{\partial}{\partial\phi} \right] ((\sin^h\theta)\eta)\end{aligned}\tag{4.1.3}$$

If the  $\phi$ -dependence of  $\eta$  is  $e^{im\phi}$ , then  $\eth$  and  $\bar{\eth}$  are related to the operator defined in (2.7.10a) in the manner:

$$\mathcal{L}_{\mp h}^{\{\dagger\}}\eta = \left[ -\left\{ \begin{array}{c} \eth \\ \bar{\eth} \end{array} \right\} \pm a\omega \sin\theta \right] \eta\tag{4.1.4}$$

It can be proven that  $\eth\eta$  is then a quantity of helicity  $h+1$ , i.e.,  $\eta \rightarrow e^{(h+1)i\vartheta}\eth\eta$  under  $m^\mu \rightarrow e^{i\vartheta}m^\mu$ , so that  $\eth$  is effectively a quantity of helicity unity. It is in this sense that we can say that  $\eth$  raises the helicity by one unit. Similarly,  $\bar{\eth}$

## 4.1. Introduction

---

lowers the helicity by one unit. The spin-weighted spherical harmonics satisfy equation (4.1.1) with  $c = 0$ , which can be re-written as

$$\bar{\partial}\partial_h Y_{lm} = -(l-h)(l+h+1)_h Y_{lm} \quad (4.1.5)$$

since in that case

$$_h E_{lm} \equiv _h E_{lm\omega=0} = l(l+1) - h(h+1). \quad (4.1.6)$$

Newman and Penrose proved that

$$_{h+1} Y_{lm} = [(l-h)(l+h+1)]^{-1/2} \bar{\partial} _h Y_{lm} \quad (4.1.7a)$$

$$_{h-1} Y_{lm} = -[(l+h)(l-h+1)]^{-1/2} \bar{\partial} _h Y_{lm} \quad (4.1.7b)$$

so that by repeated application of (4.1.7) the spin-weighted spherical harmonics can be expressed in terms of the spherical harmonics

$$_{h=0} Y_{lm} \equiv Y_{lm} = \left[ \frac{2l+1}{4\pi} \frac{(l-m)!}{(l+m)!} \right]^{1/2} P_l^m(\cos \theta) e^{im\phi} \quad (4.1.8)$$

where the associated Legendre polynomials are given by

$$P_l^m(x) = \frac{(-1)^m}{2^l l!} (1-x^2)^{m/2} \frac{d^{l+m}}{dx^{l+m}} (x^2-1)^l = (-1)^m \frac{(l+m)!}{(l-m)!} P_l^{-m}(x) \quad (4.1.9)$$

It is clear from (4.1.7) that the  $_h Y_{lm}$  vanish for  $|h| > l$ . It is easy to prove by induction on (4.1.7) that the  $_h Y_{lm}$  form a set of orthonormal functions of helicity  $h$  on the  $(\theta, \phi)$ -sphere:

$$\int d\Omega \, _h Y_{lm} \, _h Y_{l'm'}^* = \delta_{ll'} \delta_{mm'} \quad (4.1.10)$$

and that they are complete for helicity  $h$  quantities on the sphere, so that apart from (4.1.10) they also satisfy:

$$\sum_{l=h}^{\infty} \sum_{m=-l}^l _h Y_{lm}(\theta, \phi) _h Y_{lm}^*(\theta', \phi') = \delta(\phi - \phi') \delta(\cos \theta - \cos \theta') \quad (4.1.11)$$

Other properties satisfied by the spin-weighted spherical harmonics are ([51])

$$\sum_{m=-l}^l {}_{-1} Y_{lm}(\theta, \phi) {}_1 Y_{lm}^*(\theta, \phi) = 0 \quad (4.1.12)$$



and the “addition theorem” ([64])

$$\sum_{m=-l}^l {}_h Y_{lm}(\theta, \phi) {}_h Y_{lm}^*(\theta', \phi') = \frac{2l+1}{4\pi} P_l(\cos \gamma) \quad (4.1.13)$$

where  $\gamma$  is defined by  $\cos \gamma \equiv \cos \theta \cos \theta' + \sin \theta \sin \theta' \cos(\phi - \phi')$ . The “addition theorem” is a consequence of the group multiplication law.

The following results by Goldberg et al. [39] and by Campbell [12] that we briefly present below were obtained in those papers in flat space-time, and they are therefore valid asymptotically in the Kerr-Newman space-time. In particular, a tetrad can be written in the limit  $r \rightarrow +\infty$  in terms of the usual unit polar vectors  $\{\hat{e}_t, \hat{e}_r, \hat{e}_\theta, \hat{e}_\phi\}$  in flat space-time. In this limit, the Kinnersley tetrad becomes:

$$\begin{aligned} \boldsymbol{l} &\rightarrow -\hat{e}_t + \hat{e}_r & (r \rightarrow +\infty) \\ \boldsymbol{n} &\rightarrow -\frac{1}{2}(\hat{e}_t + \hat{e}_r) & (r \rightarrow +\infty) \\ \boldsymbol{m} &\rightarrow +\frac{1}{\sqrt{2}}(\hat{e}_\theta + i\hat{e}_\phi) & (r \rightarrow +\infty) \end{aligned} \quad (4.1.14)$$

and the vector  $\boldsymbol{m}$  defined in those papers coincides with the Kinnersley tetrad vector  $\boldsymbol{m}$ .

In a subsequent paper to Newman and Penrose’s, Goldberg et al. [39] further identify the spin-weighted spherical harmonics with the elements of the matrices of the representation  $D^l$  of the ordinary rotation group  $R_3$  associated with total angular momentum  $l$ . If a spatial rotation  $R(\phi, \theta, \gamma)$  of Euler angles  $\phi, \theta, \gamma$  is composed of  $\gamma$  about the OZ axis followed by  $\theta$  about OY and then  $\phi$  about OZ and it transforms  $x^i$  to  $x'^i = R^{ij}x^j$ , then the matrix  $D^l$  may be defined by its action on spherical harmonics:  $Y_{lm}(\boldsymbol{x}') = \sum_{m'} Y_{lm'}(\boldsymbol{x}) D_{m'm}^l(R^{-1})$ . Goldberg et al. prove that

$${}_h Y_{lm}(\theta, \phi) e^{-ih\gamma} = \left[ \frac{(2l+1)}{4\pi} \right]^{1/2} D_{-hm}^l(\phi, \theta, \gamma) \quad (4.1.15)$$

and therefore

$${}_h Y_{lm}(\theta, \phi) = \left[ \frac{(2l+1)}{4\pi} \right]^{1/2} D_{-hm}^l(\phi, \theta, 0) \quad (4.1.16)$$

## 4.1. Introduction

---

The orthogonality and completeness relations for the spin-weighted spherical harmonics then follow directly from the fact that the functions  $D_{m'm}^l(\phi, \theta, \gamma)$  form a complete orthonormal basis for functions defined on  $R_3$ .

Goldberg et al. also relate  $\eth$  to an ordinary angular-momentum raising operator. The well-known *angular momentum commutation relations* are

$$\begin{aligned} [J_z, J_{\pm}] &= \pm J_{\pm} \\ [J_+, J_-] &= 2J_z \end{aligned} \tag{4.1.17}$$

where  $J_{\pm} \equiv J_x \pm iJ_y$ . If  $|j, m_j\rangle$  is a simultaneous eigenvector of  $\mathbf{J}^2$  and  $J_z$  with

$$\begin{aligned} \mathbf{J}^2 |j, m_j\rangle &= j(j+1) |j, m_j\rangle \\ J_z |j, m_j\rangle &= m_j |j, m_j\rangle \end{aligned} \tag{4.1.18}$$

then it is also an eigenvector of  $J_{\pm}$  with

$$J_{\pm} |j, m_j\rangle = [(j(j+1) - m_j(m_j \pm 1))]^{1/2} |j, m_j \pm 1\rangle \tag{4.1.19}$$

which is why  $J_+$  and  $J_-$  are respectively called angular-momentum *raising* and *lowering* operators.

It is well-known that the spherical harmonics  $Y_{lm}$  are eigenvectors of the orbital angular momentum operator  $\mathbf{L} = -i\mathbf{r} \times \nabla$  satisfying equations (4.1.18) and (4.1.19) with  $\mathbf{J} \rightarrow \mathbf{L}$ ,  $|j, m_j\rangle \rightarrow Y_{lm}$ ,  $j \rightarrow l$  and  $m_j \rightarrow m$ .

We next give the relationship between the orbital angular momentum and the edth operators, which will be of use later on:

$$\begin{Bmatrix} \eth \\ \bar{\eth} \end{Bmatrix} \eta = \mp \sin^{\pm h} \theta [(\mathbf{e}_{\theta} \pm i\mathbf{e}_{\phi}) \mathbf{L}] (\sin^{\mp h} \theta) \eta \tag{4.1.20}$$

where  $\hat{\mathbf{e}}_{\theta}$  and  $\hat{\mathbf{e}}_{\phi}$  are the usual unit polar angular vectors in flat space and  $\eta$  is a quantity of helicity  $h$ .

It is also known that the operator  $\mathbf{L}$  defined as

$$\begin{aligned} L_z &\equiv -i \frac{\partial}{\partial \phi} \\ L_{\pm} &\equiv \pm e^{\pm i\phi} \left( \frac{\partial}{\partial \theta} \pm i \cot \theta \frac{\partial}{\partial \phi} \pm i \csc \theta \frac{\partial}{\partial \gamma} \right) \end{aligned} \tag{4.1.21}$$

## 4.1. Introduction

---

obeys the angular momentum commutation relations (4.1.17) and that  $D_{-hm}^l$  are its eigenvectors, i.e., equations (4.1.18) and (4.1.19) are satisfied with  $\mathbf{J} \rightarrow \mathbf{L}$ ,  $|j, m_j\rangle \rightarrow D_{-hm}^l$ ,  $j \rightarrow l$  and  $m_j \rightarrow m$ . It is therefore immediate to show that the operator  $\mathbf{\Lambda}$  such that  $\Lambda_z \equiv L_z$  and  $\Lambda_{\pm} \equiv L_{\pm} - h \csc \theta e^{\pm i\phi}$ , satisfies (4.1.17) and that the spin-weighted spherical harmonics  ${}_h Y_{lm}$  are its eigenvectors with  $\mathbf{J} \rightarrow \mathbf{\Lambda}$ ,  $|j, m_j\rangle \rightarrow {}_h Y_{lm}$ ,  $j \rightarrow l$  and  $m_j \rightarrow m$ .

Based on the symmetry of  $D_{-hm}^l(\phi, \theta, \gamma)$  with respect to  $(m, \phi)$  on the one hand and  $(h, -\gamma)$  on the other, Goldberg et al. define an angular-momentum operator  $\mathbf{K}$ , which commutes with  $\mathbf{L}$ , as:

$$\begin{aligned} K_z &\equiv i \frac{\partial}{\partial \gamma} \\ K_{\pm} &\equiv \pm e^{\pm i\gamma} \left( \frac{\partial}{\partial \theta} \pm i \cot \theta \frac{\partial}{\partial \gamma} \pm i \csc \theta \frac{\partial}{\partial \phi} \right) \end{aligned} \quad (4.1.22)$$

It is then easy to see that it does indeed satisfy (4.1.17) as well as equations (4.1.18) and (4.1.19) with  $\mathbf{J} \rightarrow \mathbf{K}$ ,  $|j, m_j\rangle \rightarrow D_{-hm}^l$ ,  $j \rightarrow l$  and now with  $m_j \rightarrow s$  (rather than  $m$ ). The relationship between the operator  $\mathfrak{D}$  and the angular-momentum raising differential operator  $K_+$  is thus established as

$$[K_+ D_{-hm}^l]_{\gamma=0} = \mathfrak{D} D_{-hm}^l(\phi, \theta, 0) \quad (4.1.23)$$

from which equations (4.1.7) immediately follow given (4.1.19). Table 4.2 summarizes the different angular momentum operators and corresponding eigenvectors and eigenvalues we have looked at.

By using vector harmonics, Campbell [12] shows that  $h$  can be interpreted as a helicity. The *vector harmonics* are defined as

$$\begin{aligned} T_i(+1, l, m; \hat{\mathbf{r}}) &\equiv m_i [{}_{-1}Y_{lm}(\theta, \phi)] \\ T_i(0, l, m; \hat{\mathbf{r}}) &\equiv r_i [{}_0Y_{lm}(\theta, \phi)] \\ T_i(-1, l, m; \hat{\mathbf{r}}) &\equiv -m_i^* [{}_{+1}Y_{lm}(\theta, \phi)] \end{aligned} \quad (4.1.24)$$

where  $m_i$  are the co-ordinates of the vector  $\mathbf{m}$  in the limit of large  $r$  in equation (4.1.14). It is easy to see that the vector harmonics form a complete set for

<b><math>\mathbf{J}</math></b>	$ j, m_j\rangle$	$(j, m_j)$
<b><math>\mathbf{L}</math></b>	$Y_{lm}$	$(l, m)$
<b>L</b>	$D_{-hm}^l$	$(l, m)$
<b><math>\Lambda</math></b>	${}_h Y_{lm}$	$(l, m)$
<b><math>\mathbf{K}</math></b>	$D_{-hm}^l$	$(l, h)$

Table 4.2: Different angular momentum operators  $\mathbf{J}$  and their corresponding eigenvectors  $|j, m_j\rangle$  and parameters  $(j, m_j)$  that make up the eigenvalues in (4.1.18) and (4.1.19).

## 4.1. Introduction

---

vector functions of  $\theta$  and  $\phi$ . The total angular momentum operator for these harmonics, which is the generator of rotations for vector functions, is given by

$$\begin{aligned} (\mathcal{J}_k)_{ij} &= \delta_{ij} L_k + (S_k)_{ij} \\ (S_k)_{ij} &\equiv -i\epsilon_{ijk} \end{aligned} \tag{4.1.25}$$

where  $S_k$  is the *spin operator* for cartesian 3-vectors. Campbell then proves that

$$\begin{aligned} (\mathcal{J}^2)_i^j T_j(h, l, m; \hat{\mathbf{r}}) &= l(l+1) T_i(h, l, m; \hat{\mathbf{r}}) \\ (\mathcal{J}_z)_i^j T_j(h, l, m; \hat{\mathbf{r}}) &= m T_i(h, l, m; \hat{\mathbf{r}}) \\ (\mathcal{J}_\pm)_i^j T_j(h, l, m; \hat{\mathbf{r}}) &= [l(l+1) - m(m \pm 1)]^{1/2} T_i(h, l, m \pm 1; \hat{\mathbf{r}}) \\ (S^2)_i^j T_j(h, l, m; \hat{\mathbf{r}}) &= 2 T_i(h, l, m; \hat{\mathbf{r}}) \\ (\hat{\mathbf{r}} \mathbf{S})_i^j T_j(h, l, m; \hat{\mathbf{r}}) &= (\hat{\mathbf{r}} \mathcal{J})_i^j T_j(h, l, m; \hat{\mathbf{r}}) = h T_i(h, l, m; \hat{\mathbf{r}}) \end{aligned} \tag{4.1.26}$$

We are therefore able to relate  $l$  to a total angular momentum,  $m$  to its  $z$ -projection, and  $h$  to the radial component of the spin. If we think in terms of outgoing radiation,  $h$  can be thought of as a *helicity*. Note that the value of the helicity of a vector harmonic is minus the value of the parameter  $h$  of the spin-weighted spherical harmonic used to construct the vector harmonic with.

As mentioned above, despite the large amount of research on both spheroidal harmonics and spin-weighted spherical harmonics, little has been done on the angular functions that concern us, the spin-weighted spheroidal harmonics. These functions were first introduced in 1973 by Teukolsky [87] as a result of the separation of the Teukolsky equation for general spin, as we have seen. Shortly after, Press and Teukolsky [76] used ordinary perturbation theory to obtain an expansion to second order in  $c$  for the eigenvalue  ${}_h E_{lm\omega}$  and used a continuation technique for small, real  $c$  to obtain solutions of (4.1.1) in the form  ${}_h S_{lm\omega}(\theta) = \sum_{l'} {}_h A_{l'}^m(\theta, c) {}_h Y_{lm}(\theta)$ . They ([76] and [88]) tabulated their results for  ${}_h E_{lm\omega}$  for certain sets of  $\{s, l, m\}$  and range of  $c$ , which we discuss later. Fackerell and Grossman [34] expressed  ${}_h S_{lm\omega}$  as a series involving Jacobi polynomials to find a certain transcendental equation involving a continued fraction for the determination of  ${}_h E_{lm\omega}$  as a power series in  $c$  (particularly useful in the case of

complex frequencies), which they evaluated (later corrected by Seidel [82]) up to order 7. A similar geometrical interpretation of the SWSH to the one for spin-weighted spherical harmonics as eigenfunctions of the Laplace operator on the unit sphere has not been found. As a matter of fact, the SWSH are not eigenfunctions of the Laplace operator on a spheroid. They do, however, form a complete and orthonormal set of functions on a prolate spheroid ([8]). Stewart [85] showed that the SWSH form a strongly complete set if  $c$  is real and he could only prove weak completeness if  $c$  is complex. Finally, some attempts ([8], [9]) have been made at finding the behaviour of  ${}_hE_{lm\omega}$  and  ${}_hS_{lm\omega}$  for large frequency, which we will discuss at length in Chapter 5.

## 4.2 General properties

In this section we wish to establish some basic, useful properties of the solutions of the angular Teukolsky equation (4.1.1).

The symmetries of the equation are immediate: the equation remains invariant under the change in sign of two quantities among  $[h, (m, \omega), x]$ , where we are considering that  $(m, \omega)$  constitutes one single quantity. As a consequence, the SWSH satisfy the following symmetries, where the choice of signs will be justified later on:

$${}_hS_{lm\omega}(\theta) = (-1)^{l+m} {}_{-h}S_{lm\omega}(\pi - \theta) \quad (4.2.1a)$$

$${}_hS_{lm\omega}(\theta) = (-1)^{l+h} {}_hS_{l-m-\omega}(\pi - \theta) \quad (4.2.1b)$$

$${}_hS_{lm\omega}(\theta) = (-1)^{h+m} {}_{-h}S_{l-m-\omega}(\theta) \quad (4.2.1c)$$

where any one symmetry follows from the other two. The eigenvalues must consequently also satisfy the symmetries:

$${}_hE_{lm\omega} = -{}_{-h}E_{lm\omega} \quad (4.2.2a)$$

$${}_hE_{lm\omega} = {}_hE_{l-m-\omega} \quad (4.2.2b)$$

## 4.2. General properties

---

We give here some useful expressions for  $h = \pm 1$ , which may be easily obtained using the angular differential equation and the Teukolsky-Starobinskiĭ identities (2.8.6):

$${}_1B_{lm\omega\pm 1}S_{lm\omega} = \left[ \mp 2\mathcal{Q}\mathcal{L}_1^{\{\dagger\}} - (\pm 2a\omega \cos \theta + {}_{-1}\lambda_{lm\omega}) \right] {}_{\mp 1}S_{lm\omega} \quad (4.2.3a)$$

$${}_1B_{lm\omega}\mathcal{L}_1^{\{\dagger\}} {}_{\pm 1}S_{lm\omega} = \left[ (\pm 2a\omega \cos \theta - {}_{-1}\lambda_{lm\omega})\mathcal{L}_1^{\{\dagger\}} \pm 2a\omega \sin \theta \right] {}_{\mp 1}S_{lm\omega} \quad (4.2.3b)$$

$$\pm 2\mathcal{Q}\mathcal{L}_1^{\{\dagger\}} {}_{\pm 1}S_{lm\omega} = (\mp 2a\omega \cos \theta + {}_{-1}\lambda_{lm\omega}) {}_{\pm 1}S_{lm\omega} + {}_1B_{lm\omega\mp 1}S_{lm\omega} \quad (4.2.3c)$$

Combining the symmetry (4.2.1a) with the relation (4.2.3b) evaluated at  $\theta = \pi/2$ , the following relation at the equator can be immediately obtained:

$$\left. \frac{d_{{}_{-1}}S_{lm\omega}}{d\theta} \right|_{\pi/2} = \left[ \frac{2a\omega}{({}_{-1}\lambda_{lm\omega} - (-1)^{l+m}{}_1B_{lm\omega})} - a\omega + m \right] {}_{-1}S_{lm\omega}(\pi/2) \quad (4.2.4)$$

which we have verified to be satisfied by our numerical results for modes for several sets of  $\{l, m, \omega\}$ .

The differential equation (4.1.1) has singular points at  $x = \pm 1$ . By using the Frobenius method it can be found that the solution that is regular at both boundary points  $x = +1$  and  $-1$  is given by

$${}_hS_{lm\omega}(x) = (1-x)^\alpha (1+x)^\beta {}_hy_{lm\omega}(x) \quad (4.2.5)$$

where

$$\alpha = \frac{|m+h|}{2}, \quad \beta = \frac{|m-h|}{2} \quad (4.2.6)$$

and the function  ${}_hy_{lm\omega}(x)$  behaves close to the boundary points as

$${}_hy_{lm\omega}(x) = \sum_{n=0}^{\infty} {}_h\left\{ \begin{matrix} a \\ b \end{matrix} \right\}_{n,lm\omega} (1 \mp x)^n \quad \text{for } x \rightarrow \pm 1 \quad (4.2.7)$$

On the other hand, the irregular solution at  $x = \pm 1$  is given by

$${}_hS_{lm\omega}^{\text{irreg}} = (1-x)^\alpha (1+x)^\beta {}_hy_{lm\omega}^{\text{irreg}} \quad (4.2.8a)$$

$${}_hy_{lm\omega}^{\text{irreg}} = \sum_{n=0}^{\infty} {}_h\left\{ \begin{matrix} a \\ b \end{matrix} \right\}_n^{\text{irreg}} (1 \mp x)^{-2\left\{ \begin{matrix} \alpha \\ \beta \end{matrix} \right\} + n} \quad \text{for } x \rightarrow \pm 1 \quad (4.2.8b)$$

## 4.2. General properties

---

It immediately follows from the above equations that

$$\frac{d {}_h y_{lm\omega}^{\text{irreg}}}{dx} = \frac{\pm |m \pm h|}{(1 \mp x)} {}_h y_{lm\omega}^{\text{irreg}}, \quad x \rightarrow \pm 1 \quad (4.2.9)$$

for  $m \neq \mp h$ , which will be useful for the numerical integration.

The function  ${}_h y_{lm\omega}(x)$  satisfies the differential equation

$$\left\{ (1-x^2) \frac{d^2}{dx^2} - 2[\alpha - \beta + (\alpha + \beta + 1)x] \frac{d}{dx} + \right. \\ \left. + {}_h E_{lm\omega} - (\alpha + \beta)(\alpha + \beta + 1) + c^2 x^2 - 2hc x \right\} {}_h y_{lm\omega}(x) = 0 \quad (4.2.10)$$

We are interested in finding the behaviour of the regular solution  ${}_h y_{lm\omega}$  at the boundary points. We therefore substitute the expansion (4.2.7) for  ${}_h y_{lm\omega}$  into the differential equation (4.2.10) and obtain the recursive relation

$${}_h \left\{ \begin{matrix} a \\ b \end{matrix} \right\}_{n+1, lm\omega} = \frac{1}{2(n+1) \left( n+1 + 2 \left\{ \begin{matrix} \alpha \\ \beta \end{matrix} \right\} \right)} \left\{ \left[ 2n(\alpha + \beta + 1) - \right. \right. \\ \left. \left. - ({}_h E_{lm\omega} - (\alpha + \beta)(\alpha + \beta + 1) + c^2 \mp 2ch) + n(n+1) \right] {}_h \left\{ \begin{matrix} a \\ b \end{matrix} \right\}_{n, lm\omega} + \right. \\ \left. + 2c(c \mp h) {}_h \left\{ \begin{matrix} a \\ b \end{matrix} \right\}_{n-1, lm\omega} - c^2 {}_h \left\{ \begin{matrix} a \\ b \end{matrix} \right\}_{n-2, lm\omega} \right\}, \quad \forall n \in \mathbb{N} \quad (4.2.11)$$

where it is understood that  ${}_h \left\{ \begin{matrix} a \\ b \end{matrix} \right\}_{n, lm\omega} \equiv 0$  for  $n < 0$ .

It is also useful to find the relationship between the asymptotic behaviours of  ${}_h S_{lm\omega}$  and  $-{}_h S_{lm\omega}$  at the boundaries. By inserting the asymptotic behaviour (4.2.5) and (4.2.7) for  ${}_h S_{lm\omega}$  into the Teukolsky-Starobinskiĭ identities and making use of the relations (4.2.11), we obtain



$$\frac{{}_{+1}S_{lm\omega}(x)}{{}_{-1}S_{lm\omega}(x)} \rightarrow \left\{ \begin{array}{ll} {}_1B_{lm\omega} \frac{(1-x)}{2} \frac{1}{m(m+1)} = \frac{(1-x)}{(1+x)} \frac{{}_{+1}a_{0,lm\omega}}{{}_{-1}a_{0,lm\omega}}, & m \geq 1 \\ - \left( \frac{{}_{-1}\lambda_{l,m=0,\omega} - 2c}{{}_{-1}\lambda_{l,m=0,\omega} + 2c} \right)^{1/2} = \frac{{}_{+1}a_{0,l,m=0,\omega}}{{}_{-1}a_{0,l,m=0,\omega}}, & m = 0 \\ \frac{1}{{}_1B_{lm\omega}} \frac{2}{(1-x)} m(m-1) = \frac{(1+x)}{(1-x)} \frac{{}_{+1}a_{0,lm\omega}}{{}_{-1}a_{0,lm\omega}}, & m \leq -1 \end{array} \right\},$$

(x → +1)  
(4.2.12)

Analogous relations for  $x \rightarrow -1$  immediately follow from the ones above when the symmetry (4.2.1a) is used. It is clear from (4.2.12) that  ${}_{+1}S_{lm\omega}(x)$  and  ${}_{-1}S_{lm\omega}(x)$ , where one is calculated from the other with the Teukolsky-Starobinskiĭ identities (2.8.6), have the same sign for  $x \rightarrow +1$  and for  $x \rightarrow -1$  except when  $m = 0$ . This fact combined with the knowledge of the number of zeros that the SWSH have, given in Chapter 5, means that the sign taken in the symmetry relation (4.2.1a) is indeed the one that corresponds to the Teukolsky-Starobinskiĭ identities (2.8.6) that we are using. The sign in (4.2.1a) also agrees with the corresponding sign for the associated Legendre polynomials in the case  $c = 0$  via equations (4.1.7). The sign in the symmetry (4.2.1c) has been chosen to coincide, in the case  $c = 0$ , with the corresponding sign for the associated Legendre polynomials given by (4.1.9).

## 4.3 Numerical method

The solution to the eigenvalue problem given by the second order differential equation (4.2.10) that we wish to solve involves three unknowns: two constants of integration plus the eigenvalue. These three unknowns become determined by imposing one boundary condition at each one of the end-points and one normalization condition. The boundary conditions we need to impose are for the solution  ${}_h y_{lm\omega}$  to be regular at  $x = \pm 1$ . The normalization condition is the one in equation (2.7.5).

### 4.3. Numerical method

---

By means of the change of variables  $y_1 \equiv {}_h y_{lm\omega}$ ,  $y_2 \equiv {}_h y'_{lm\omega}$ ,  $y_3 \equiv {}_h E_{lm\omega}$ , the differential equation (4.2.10) can be reduced to the following system of first order differential equations

$$\begin{aligned} y_1' &= y_2 \\ y_2' &= \frac{1}{(1-x^2)} \left\{ 2(\alpha - \beta + (\alpha + \beta + 1)x) y_2 - \right. \\ &\quad \left. - [y_3 - (\alpha + \beta)(\alpha + \beta + 1) + c^2 x^2 - 2hc x] y_1 \right\} \\ y_3' &= 0 \end{aligned} \tag{4.3.1}$$

The shooting method requires two initial, arbitrary values which, added to the boundary condition at one of the end-points, determine all three unknowns. The equation is then integrated from that end-point  $x_1$  until the other one  $x_2$  as an initial value problem. It is then assessed how well the values at  $x_2$  of the solution obtained agree with a condition resulting from the boundary condition at that point. If the condition is not satisfied within the desired accuracy, one of the two initial, arbitrary values is modified and the integration starts again with the new value. The steps of modifying this value and integrating the differential equation are iterated until the condition at the final end-point  $x_2$  is met within the desired accuracy. The other initial, arbitrary value is finally determined by imposing the normalization condition on the solution.

It is clear from (4.3.1) that we cannot impose boundary conditions at exactly the end-points  $x = \pm 1$ . Instead, we impose them slightly away from the end-points, at  $x_{\{2\}} = \mp 1 \pm dx$ , where  $dx \ll 1$ , and we therefore use the asymptotic expansion (4.2.5) to find the value of the solution at  $x_{\{1\}}$ . We set  $dx = 10^{-2}$  in the code. We take initial, arbitrary values for  ${}_1 a_{0,lm\omega}$  and for the eigenvalue, which we denote by  ${}_h \hat{E}_{lm\omega}$  to distinguish it from the actual eigenvalue  ${}_h E_{lm\omega}$ . The initial value  ${}_h \hat{E}_{lm\omega}$  is not entirely arbitrary but is chosen to be close to the eigenvalue obtained for a value of  $\omega$  slightly smaller than the one in the present calculation. The initial value for  ${}_1 a_{0,lm\omega}$  plus the boundary condition (4.2.5) of regularity at  $x_1$  provide the initial values of  $y_1(x_1)$  and  $y_2(x_1)$  whereas the initial values  ${}_h \hat{E}_{lm\omega}$  provides the initial value  $y_3(x_1) = {}_h \hat{E}_{lm\omega}$ . The arbitrary

### 4.3. Numerical method

value  ${}_h\hat{E}_{lm\omega}$  will be modified appropriately so that  $y_1(x_2)$  and  $y_2(x_2)$  satisfy the boundary condition of regularity at  $x_2$  within the desired accuracy. Once the correct eigenvalue  ${}_hE_{lm\omega}$  and solution  ${}_hy_{lm\omega}(x)$  and  ${}_hy'_{lm\omega}(x)$  are obtained, the initially arbitrary value  ${}_h a_{0,lm\omega}$  is rescaled so that the normalization condition (2.7.5) is satisfied.

In general, for a value of  ${}_h\hat{E}_{lm\omega}$  different from the actual eigenvalue, the numerically integrated solution is a combination of both the regular and the irregular solutions, i.e.,

$${}_hy_{lm\omega}^{\text{num}} = A({}_h\hat{E}_{lm\omega}){}_hy_{lm\omega} + A({}_h\hat{E}_{lm\omega}){}_hy_{lm\omega}^{\text{irreg}} \quad (4.3.2)$$

where  ${}_hy_{lm\omega}^{\text{num}}$  is the numerically obtained value and  ${}_hy_{lm\omega}$  is the analytic, regular value.  $A$  and  $B$  are unknown functions of  ${}_h\hat{E}_{lm\omega}$ . We need to modify the value of  ${}_h\hat{E}_{lm\omega}$  so that only the regular term  $A{}_hy_{lm\omega}$  is retained. In the scalar case, the boundary condition at  $x_2$  may be imposed by requiring that  ${}_{h=0}\hat{E}_{lm\omega}$  is a zero of the function  $g({}_{h=0}\hat{E}_{lm\omega}) \equiv {}_{h=0}y_{lm\omega}'^{\text{num}}(x_2) - {}_{h=0}y_{lm\omega}'(x_2)$ , where the analytic value  ${}_hy_{lm\omega}'(x_2)$  is known for the scalar case because  ${}_{h=0}y_{lm\omega}'(x) \propto {}_{h=0}y_{lm\omega}'(-x)$ . The function  $g({}_{h=0}\hat{E}_{lm\omega})$  should tend to zero as  ${}_{h=0}\hat{E}_{lm\omega}$  approaches the correct eigenvalue and should tend to infinity when it is far from it because of the behaviour (4.2.9) of the irregular solution. However, in general we have  ${}_hy_{lm\omega}'(x) \propto -{}_hy_{lm\omega}'(-x)$ , relating solutions of equations with different helicity when  $h \neq 0$ , and therefore we do not know the analytic value  ${}_hy_{lm\omega}'(x_2)$  for a particular value  $h \neq 0$  of the helicity. Instead, we can look for a zero of the function

$$g({}_h\hat{E}_{lm\omega}) \equiv \frac{{}_hy_{lm\omega}'^{\text{num}}(x_2)}{{}_hy_{lm\omega}^{\text{num}}(x_2)} - \frac{{}_hy_{lm\omega}'(x_2)}{{}_hy_{lm\omega}(x_2)} \quad (4.3.3)$$

which does not require the knowledge of  ${}_h a_{0,lm\omega}$ . The function  $g({}_h\hat{E}_{lm\omega})$  should also tend to zero as  ${}_h\hat{E}_{lm\omega}$  approaches the correct eigenvalue and to infinity when it is far from it. However, this function has the same sign whether  ${}_h\hat{E}_{lm\omega}$  is greater or smaller than the actual eigenvalue, and therefore the zero of this function is also a minimum or a maximum point. This is a considerable drawback because looking for an extreme point of a function generally requires many more

### 4.3. Numerical method

---

evaluations of the function than looking for a zero which is not an extreme point, and yet the accuracy is much smaller. Typically, an extreme point is only calculated up to the square root of the computer's floating-point precision. We therefore decided to find a zero of the function

$$g({}_h\hat{E}_{lm\omega}) \equiv {}_hy'_{lm\omega}{}^{\text{num}}(x_2) - {}_hy'_{lm\omega}{}^{\text{approx}}(x_2) \quad (4.3.4)$$

instead, where  ${}_hy'_{lm\omega}{}^{\text{approx}}(x_2)$  is not the actual analytic value, which we do not know, but an approximation to it:

$${}_hy'_{lm\omega}{}^{\text{approx}}(x_2) \simeq \frac{{}_hy'_{lm\omega}{}^{\text{num}}(x_2)}{{}_hy_{lm\omega}(x_2)} {}_hy'_{lm\omega}(x_2) \quad (4.3.5)$$

We see numerically that  $g({}_h\hat{E}_{lm\omega})$  changes sign at the eigenvalue so that it is not an extreme point.

As in the numerical integration of the radial equation in Section 3.3, we adapted the methods in [77] to the particular problem we wish to solve. In this section  $Y$  denotes any of the numerically-calculated dependent variables  $y_1$ ,  $y_2$  or  $y_3$ , where for clarity we omit the index that refers to a specific dependent variable. The actual integration from  $x_1$  until  $x_2$  of the system of differential equations (4.3.1) is done with the Runge-Kutta method. We will use a fifth-order Runge-Kutta formula to calculate the value of  $Y(x+h)$  by evaluating at six different points the right hand side of the differential equations (4.3.1), which we denote by  $f$ . The advantage of the method is that a fourth-order Runge-Kutta formula is obtained with a different combination of the evaluations of  $f$  at the same six points. By combining the fourth-order and the fifth-order formulae, not only do we obtain  $Y(x+h)$  but also an estimate of the error being made, both with only six evaluations of  $f$ . Having an actual estimate of the error allows us to adapt the stepsize (*adaptive stepsize*) to be taken at every step so that we can obtain the solution within the required accuracy without taking too many steps. The sole knowledge of the order of the method does not provide an actual estimate of the error being made. Efficient values of the constants involved in the two formulae were found by Cash and Karp and we give them in Table 4.3. The

### 4.3. Numerical method

$i$	$a_i$	$b_{ij}$					$c_i$	$\bar{c}_i$
1							$\frac{37}{378}$	$\frac{2825}{27648}$
2	$\frac{1}{5}$	$\frac{1}{5}$					0	0
3	$\frac{3}{10}$	$\frac{3}{40}$	$\frac{9}{40}$				$\frac{250}{621}$	$\frac{18575}{48384}$
4	$\frac{3}{5}$	$\frac{3}{10}$	$-\frac{9}{10}$	$\frac{6}{5}$			$\frac{125}{594}$	$\frac{13525}{55296}$
5	1	$-\frac{11}{54}$	$\frac{5}{2}$	$-\frac{70}{27}$	$\frac{35}{27}$		0	$\frac{277}{14336}$
6	$\frac{7}{8}$	$\frac{1631}{55296}$	$\frac{175}{512}$	$\frac{575}{13824}$	$\frac{44275}{110592}$	$\frac{253}{4096}$	$\frac{512}{1771}$	$\frac{1}{4}$
$j =$		1	2	3	4	5		

Table 4.3: Cash-Karp parameters for embedded Runge-Kutta method

formula that calculates the value of the solution  $Y_{n+1} \equiv Y(x+h)$  from the value  $Y_n \equiv Y(x)$  is the fifth-order Runge-Kutta expression

$$\begin{aligned}
k_1 &= hf(x_n, Y_n) \\
k_2 &= hf(x_n + a_2h, Y_n + b_{21}k_1) \\
&\vdots \\
k_6 &= hf(x_n + a_6h, Y_n + b_{61}k_1 + \cdots + b_{65}k_5) \\
Y_{n+1} &= Y_n + c_1k_1 + c_2k_2 + c_3k_3 + c_4k_4 + c_5k_5 + c_6k_6 + O(h^6)
\end{aligned} \tag{4.3.6}$$

The fourth-order Runge-Kutta formula that we use to find an estimate of the error is

$$\bar{Y}_{n+1} = Y_n + \bar{c}_1k_1 + \bar{c}_2k_2 + \bar{c}_3k_3 + \bar{c}_4k_4 + \bar{c}_5k_5 + \bar{c}_6k_6 + O(h^5) \tag{4.3.7}$$

An estimate of the error is thus given by

$$Y_{n+1}^{\text{err}} = Y_{n+1} - \bar{Y}_{n+1} \tag{4.3.8}$$

which is of order  $O(h^5)$ .

The driver routine *odeint* is the same routine as the one used in the integration of the radial equation in Section 3.3. The quantity  $Y_{n+1}^{\text{scal}}$ , used to compare the absolute error  $Y_{n+1}^{\text{err}}$  at the point  $x_{n+1}$  with, is correspondingly given by equation

---

### 4.3. Numerical method

(3.3.4). The stepper routine *rkqs* obtains the numerical value  $Y(x + h)$  of the solution and the error  $Y_{n+1}^{\text{err}}$  of the method at this step by calling the algorithm routine *rkck*. If the fractional error is too large, i.e.,  $\epsilon_{n+1} \equiv |Y_{n+1}^{\text{err}}/Y_{n+1}^{\text{scal}}| > \epsilon$ , the stepper routine then calls *rkck* to try the integration again with a new, reduced stepsize. Since the error of the method is of order  $O(h^5)$ , and the stepsize  $h$  has resulted in a relative error  $\epsilon_{n+1}$ , then an estimate for a new stepsize that would produce a relative error  $\epsilon$  is given by  $h (\epsilon_{n+1}/\epsilon)^{1/5}$ . The factor  $1/5$  in the exponent is not exact since  $Y_{n+1}^{\text{scal}}$  in (3.3.4) is in its turn also rescaled with the new stepsize. The new, reduced stepsize will thus be  $Sh (\epsilon_{n+1}/\epsilon)^{1/4}$ , where  $S = 0.9$  is a safety factor. If on the other hand, the error of the integration is smaller than the minimum required, then *rkqs* increases the stepsize to  $Sh (\epsilon_{n+1}/\epsilon)^{1/5}$ . The algorithm routine *rkck* straight-forwardly implements the fifth-order Cash-Karp Runge-Kutta method and returns the numerical value  $Y(x + h)$  obtained with (4.3.6) and an estimate of the error  $Y_{n+1}^{\text{err}}$  given by (4.3.8).

Because of the symmetry (4.2.1a) we only need to calculate the solution  ${}_h S_{lm\omega}(\theta)$   $\forall \theta \in [0, \pi]$  for one particular value  $h$  of the helicity, which we choose to be  $-1$  as that is the value of the helicity for which we have calculated the radial solution.

The Fortran90 program SPHDRVKN MPI.F90 calculates the eigenvalue to quadruple precision and the spherical function and its derivative to double precision.

#### Parallel Programming

To complete the explanation of the various methods and routines used for numerical calculations for this thesis, we shall briefly discuss a parallel algorithm which we used in the program SPHDRVKN MPI.F90 as well as in other programs used in Chapters 5 and 6. In particular, this algorithm could have been used in the radial program discussed in Chapter 3 or in any other program involving calculations which must be performed in the exact same manner for different values of certain parameters. In all the programs we developed, these parameters consisted in the pair  $(l, m)$ . This algorithm only requires minor modifications for it to adapt to different programs of the characteristics mentioned. Parallel

### 4.3. Numerical method

---

programming is used in order to make the most out of several CPUs that may be available. The parallel algorithm we implemented uses the Message-Passing Interface (MPI) [41] as the message-passing library.

The parallel algorithm we implemented is an instance of a ‘master’/‘slave’ application. It consists in the initialization of one ‘master’ process, which has knowledge of the various values of the parameters for which the calculations must be performed, and a number  $N$  of ‘slave’ processes, which will actually perform the calculations for particular values of the parameters. The ‘master’ process first reads the common data, if any, that is required by all the ‘slave’ processes (e.g., the eigenvalues and tabulated data for the function  $r_* = r_*(r)$  in the case of programs in Chapter 6), and it broadcasts this data to all the ‘slaves’. The ‘master’ process then reads the data that is necessary for the calculations to be performed for a pair of values of  $(l, m)$ . It then sends to a ‘slave’ the values of the parameters that it should perform the calculation with as well as the data that it requires. This is done for the first  $N$  number of pairs of values of  $(l, m)$ . Each one of the ‘slave’ processes receives the information from the ‘master’ and then proceeds to perform the calculations for a particular pair of values of  $(l, m)$  and range of values of  $\omega$ . Once finished with the calculations, the ‘slaves’ send the results back to the ‘master’. When the ‘master’ receives the results from one of the ‘slaves’ it then either sends to this ‘slave’ a new pair of values  $(l, m)$  to perform the calculations with or, if all pairs of values have been completed, it tells the ‘slave’ to finalize. The ‘master’ process then stores the results in a file. Since reading/writing data from/in a file is a very time-consuming process, it is an efficient procedure that the ‘master’ is in charge of these tasks and performs them while the ‘slaves’ are performing the calculations.

The result of the implementation of this parallel algorithm is that the amount of time required to perform the calculations a large number of times for various values of certain parameters is approximately reduced  $N$  times.

## 4.4 Numerical results

The results for the spherical function obtained with the program SPHDRVKN MPI.F90 are compared in Table 4.4 against Chandrasekhar's [20].

Chandrasekhar also displays results for the eigenvalue. Note that his eigenvalue, which we call  $\lambda_{lm\omega}^{\text{chandr}}$ , is actually  $_{-1}\lambda_{lm\omega}$  for the spin-1 case and  $_{+2}\lambda_{lm\omega} + 4$  for the spin-2 case. Note also that his frequency  $\sigma$  is equal to  $-\omega$ . Our numerical results for the eigenvalue do not coincide with his. We believe that Chandrasekhar calculated  $\lambda_{lm\omega}^{\text{chandr}}$  by using an approximation given previously by Teukolsky and Press, but Chandrasekhar used it for the wrong range of values for the frequency thus producing incorrect results. Teukolsky and Press ([76] and [88]) obtained polynomial (in  $\omega$ ) approximations of the eigenvalues for several sets of  $\{h, l, m\}$  by applying a continuation method to a representation of spin-weighted spheroidal harmonics in terms of spin-weighted spherical harmonics. Their approximations are valid only for  $0 \leq a\omega \leq 3$  and are accurate to five digits. The results in Chandrasekhar's table are given for negative  $\omega$  and coincide exactly with the ones produced by Teukolsky and Press's polynomials for that negative value of  $\omega$ , which is obviously not within the range of validity  $0 \leq a\omega \leq 3$ . For Teukolsky and Press's polynomials to produce results for a certain  $m$  and a certain negative  $\omega$ , the polynomial corresponding to  $-m$  must be evaluated at  $-\omega > 0$  and then the symmetry (4.2.2b) must be used. All results (except for three of them discussed below) produced in this way coincide with our numerical results up to the fifth digit. This is shown in Table 4.5.

In view of the fact that for  $a\omega = -0.2, -1.2, -1.4$  our numeric results for  ${}_1E_{2,-2,\omega}$  do not coincide with those produced by Teukolsky and Press's polynomial, we decided to check them by using two other methods. One is the relaxation method, which consists in replacing the ordinary differential equation by a finite-difference equation and iteratively improve an initial guess for the solution at all grid points so that it ends up satisfying the finite-difference equation and the required bound-



## 4.4. Numerical results

---

ary conditions. The other method we implemented is the one suggested by Sasaki and Nakamura [80], consisting in also replacing the differential equation by a finite-difference equation but then imposing for the determinant of the matrix that represents the finite-difference equation to be zero. This method will be described in detail in the next chapter since it was the main tool we used to obtain the eigenvalues for large frequency. Both the relaxation method and Sasaki and Nakamura's agree for the  $a\omega = -0.2, -1.2, -1.4$  cases in Table 4.5 with our numerical results rather than with Teukolsky and Press's. We therefore believe that the latter are not accurate to the fifth digit in these three instances.

#### 4.4. Numerical results

$\cos \theta$	$-1S_{2,-2,-0.25}^{\text{chandr}}$	$-1S_{2,-2,-0.25}^{\text{num}}$
0.	0.768015	0.768023791282718
0.04	0.734306	0.734314263501826
0.08	0.699739	0.699746529751899
0.12	0.664460	0.664467540117839
0.16	0.628612	0.628618596243942
0.20	0.592331	0.592336366304714
0.24	0.555748	0.555753833600832
0.28	0.518996	0.519001205617666
0.32	0.482202	0.482206809678456
0.36	0.445494	0.445498002401709
0.40	0.408999	0.409002123321547
0.44	0.372844	0.372847528852603
0.48	0.337162	0.337164752355464
0.52	0.302086	0.302087851246282
0.56	0.267754	0.267756026125980
0.60	0.234314	0.234315635527191
0.64	0.201921	0.201922793693838
0.68	0.170746	0.170746848326145
0.72	0.140974	0.140975232456899
0.76	0.112820	0.112820561950217
0.80	0.086531	0.086531629301585
0.84	0.062411	0.062411721362379
0.88	0.040852	0.040852325588169
0.92	0.022405	0.022405022463833
0.96	0.007979	0.007979518753337

Table 4.4:  ${}_hS_{lm\omega}$  for  $h = -1$ ,  $Q = 0$ ,  $a = 0.95$ ,  $l = 2$ ,  $m = -2$  and  $\omega = -0.25$ .  $-1S_{2,-2,-0.25}^{\text{chandr}}$  is taken from Table VI in Chandrasekhar's [20] Appendix and  $-1S_{2,-2,-0.25}^{\text{num}}$  has been calculated with Fortran90 program SPHDRVKN MPI.F90

## 4.4. Numerical results

---

$a\omega$	${}_1E_{2,-2,\omega}^{\text{chandr}}$	${}_1E_{2,-2,\omega}^{\text{TP}}$	${}_1E_{2,-2,\omega}^{\text{num}}$	${}_1E_{2,2, \omega }^{\text{TP}}$
0.	6.	6.	6.	6.
-0.2	5.8534	5.8534	5.8534429399013102317	5.8535
-0.4	5.6789	5.6789	5.6790807066777195764	5.6791
-0.6	5.4741	5.4741	5.4746409095537499953	5.4746
-0.8	5.2362	5.2362	5.2375343807523856300	5.2375
-1.0	4.9618	4.9618	4.9648622055126348357	4.9649
-1.2	4.6472	4.6472	4.6534383466611133856	4.6535
-1.4	4.2880	4.2880	4.2998313934573516407	4.2999
-1.6	3.8792	3.8792	3.9004271601816162329	3.9004
-1.8	3.4149	3.4149	3.4515108815270425522	3.4515
-2.0	2.8886	2.8886	2.9493639889615692063	2.9494
-2.2	2.2929	2.2929	2.3903668120214223888	2.3904
-2.4	1.6194	1.6194	1.7710962418980976975	1.7711
-2.6	0.8586	0.8586	1.0884074322264239240	1.0884
-2.8	-0.0002	-0.0002	0.3394912459602174195	0.3395
-3.0	-0.9688	-0.9688	-0.4780963537474403940	-0.4781

Table 4.5:  ${}_hE_{lm\omega}$  for  $h = \pm 1$ ,  $Q = 0$ ,  $l = 2$  and  $m = -2$ .  ${}_1E_{2,-2,\omega}^{\text{chandr}}$  is taken from Table VII in Chandrasekhar's [20] Appendix;  ${}_1E_{2,-2,\omega}^{\text{TP}}$  and  ${}_1E_{2,2,|\omega|}^{\text{TP}}$  are calculated with polynomial in Table 2 in Teukolsky and Press [88];  ${}_1E_{2,-2,\omega}^{\text{num}}$  has been calculated with Fortran90 program SPHDRVKN MPI.F90.

# Chapter 5

## High frequency asymptotics for the angular solution

### 5.1 Introduction

Following standard conventions, in this thesis we refer to ‘high frequency’ in relation to the angular function and eigenvalues when in fact what it is meant is large  $c(= a\omega)$ . The high frequency approximation of the spin-weighted spheroidal equation is a particularly important subject that, nevertheless, has been left unresolved thus far, except for the spin-0 case, due to its difficulty. This asymptotic study is important when considering both classical and quantum perturbations. In the classical case it is important, for example, when calculating gravitational radiation emitted by a particle near the black hole since the typical time-scale of the motion is short compared to the scale set by the curvature of the black hole. In the quantum case its importance lies in the fact that the high frequency limit is at the root of the divergences that the expectation value of the stress-energy tensor possesses. The correct subtraction of the divergent terms from the expectation value of the stress-energy tensor is extremely troublesome in curved space-time, particularly in one that is not spherically symmetric. Because the

divergent terms arise from the high frequency behaviour of the field, knowledge of this behaviour is fundamental in such a subtraction. This limit has also been recently considered in the Kerr background in the context of quasinormal modes (see [5]). Quasinormal frequencies with large imaginary part have acquired great importance since Hod [47] established a correspondence between these frequencies and transitions in energy level of the quantum black hole.

The new results that we present in this chapter contribute towards making this problem more tractable. However, we should note that the asymptotic study in this paper is valid for fixed  $m$  as  $c$  tends to infinity, a fuller understanding of the asymptotic behaviour of the solution would require an analysis uniform in  $m$ . It is worthwhile remarking that the whole analysis in this chapter has been done for general integral spin, so that it applies to the scalar, electromagnetic and, in particular, gravitational perturbations, which are of great interest in astrophysics.

In the remainder of this introductory section we discuss the results for high frequency asymptotics of SWSH that have been obtained in the literature up until now, show their shortcomings and outline what our new results achieve. In the next section we lay down the basic theory that we use in the following sections. In Sections 5.3, 5.4, 5.5 and 5.6 we fully determine the asymptotic behaviour of the angular solution that is uniform in  $x$  and the asymptotic behaviour of the eigenvalue. In Section 5.7 we describe the numerical method and programs used to obtain the numerical results, which in the last section we show, analyze and compare to numerical results in the literature.

Different authors have obtained high-frequency approximations to the solution and eigenvalues of the spheroidal differential equation. Erdélyi et al. [33], Flammer [35] and Meixner and Schäfke [65] have all done so using the fact that this differential equation becomes the Laguerre differential equation in that limit.

Breuer [9] was the first author to study the high-frequency behaviour of the

spin-weighted spheroidal harmonics. Based on the work on the spin-0 case by the above authors he related the solution of a transformation of the spin-weighted spheroidal equation for large  $c$  and finite  $m$  to the generalized Laguerre polynomials. His work, however, was fundamentally erroneous as it assumed that the solution was either symmetric or antisymmetric under  $x \rightarrow -x$ , which is only true for  $h = 0$ .

Breuer, Ryan and Waller [8] (hereafter referred to as BRW) corrected this error and further developed this study by first relating the SWSH to the confluent hypergeometric functions and then reducing them to the generalized Laguerre polynomials by imposing regularity far from the boundary points  $x = \pm 1$ . Unfortunately, their study of the high-frequency behaviour was flawed and incomplete. The behaviour for high frequency of both the spherical functions and the eigenvalues obtained by BRW depend critically on a certain parameter  $\gamma$  which they left undetermined for the  $h \neq 0$  case. BRW did obtain the analytic value of  $\gamma$  for the  $h = 0$  case but for the  $h \neq 0$  case they could only calculate it numerically for a handful of sets of values of  $\{h, l, m\}$ . BRW achieved this numerical calculation for the  $h \neq 0$  case by matching the high-frequency asymptotic expression for the eigenvalue that they obtained with the expression for the eigenvalue given by Press and Teukolsky [76] valid for low frequency. Not only their analytic expressions for both the spherical solution and the eigenvalue for high frequency were thus left undetermined, but also their expressions for the spherical solution are only valid sufficiently close to the boundary points  $x = 1$  and  $x = -1$ , but not for the region in-between them. This results in the possibility that a zero of the solution near  $x = 0$ , away from  $x = \pm 1$ , be overlooked. Furthermore, and crucially, their assumption that the confluent hypergeometric functions should reduce to the generalized Laguerre polynomials by imposing regularity far from the boundary points is not correct. The reason why it is not correct is that in the cases for which the confluent hypergeometric function diverges far from one of the boundaries, the coefficient in front of it decreases exponentially with  $c$  so that the solution remains finite in the whole region  $x \in [-1, +1]$ . We believe

---

## 5.2. Boundary layer theory

that the reason why they were not able to analytically determine the value of the parameter  $\gamma$  is because they ignored the behaviour of the solution far from the boundaries, thus overlooking a possible zero, and wrongly imposed regularity.

The study of the behaviour of the solution and eigenvalues of the spin-weighted spheroidal equation for high, real frequency and finite  $m$  has not been developed any further by these or any other authors and therefore BRW's work is where this study stood until this thesis.

In this chapter we correct and complete BRW's study for high, real frequency and finite  $m$ . We thus obtain an asymptotic solution for large, real frequency to the spin-weighted spheroidal equation which is uniformly valid everywhere within the range  $x \in [-1, +1]$ , not just near the boundaries. We also analyze the existence and location of a possible zero of the solution near  $x = 0$ . We analytically determine the value of  $\gamma$  by matching the number of zeros that our asymptotic solution has with the number of zeros that the SWSH has. As a consequence, the asymptotics of the eigenvalue in the same limit also become fully determined. Finally, we have complemented all the analytic work with graphs produced with numerically-obtained data. The graphs show the behaviour of the eigenvalues for large frequency and how they match with Press and Teukolsky's approximation for low frequency. They also show the behaviour of the SWSH in this limit and the location of its zeros.

## 5.2 Boundary layer theory

In the rest of this chapter we follow the approach to boundary layer theory as presented by Bender and Orszag [4]. The asymptotic solution that is a valid approximation to the solution of the differential equation from the boundary point  $\pm 1$  until  $x \sim \pm 1 + O(c^\delta)$ , where  $-1 \leq \delta < 0$ , is called the *inner solution*. The region within which an inner solution is valid is a *boundary layer*. As we shall see, for the large frequency approximation of the spin-weighted spheroidal

## 5.2. Boundary layer theory

---

equation, there are two boundary layers within the region  $x \in [-1, 1]$ , one close to  $x = -1$  and one close to  $x = +1$ . Close to the boundary points the spin-weighted spheroidal function oscillates rather quickly in  $x$ , and indeed it is there where all (with the possible exception of one) the zeros of the function are located.

The asymptotic solution that is a valid approximation to the solution of the differential equation in the range  $-1 + O(c^{-1}) \ll x \ll +1 - O(c^{-1})$ , is called the *outer solution*. This range comprises not only the region in between the two boundary layers but also a certain region of both boundary layers. This region where both an inner solution and the outer solution are valid is called the *overlap region*, and it is there that the outer and inner solutions are matched.

We shall see that in between the two boundary layers the function behaves rather smoothly, like a  $\cosh x$  or a  $\sinh x$ , so that the SWSH may have at the most one zero close to  $x = 0$ . The behaviour of the outer solution is important despite its smoothness because when matching it with the inner solutions it will allow us to find an asymptotic solution which is uniformly valid throughout the whole range of  $x$ . The outer solution is also necessary in order to find out whether or not the uniform solution has a zero close to  $x = 0$  and, if it does, to calculate the analytic location of the zero.

This is a key feature that singles out the scalar case from the others: for the spin-0 case the differential equation (4.1.1) is clearly symmetric under  $\{x \leftrightarrow -x\}$  and therefore, depending on its parity, it will have a zero at  $x = 0$  or not. On the other hand, for the general spin case, the differential equation does not satisfy this symmetry but it does remain unchanged under the transformation  $\{x \leftrightarrow -x, h \leftrightarrow -h\}$  instead. There is therefore no apparent reason why it should have a zero near the origin. The outer solution is important for the general spin case and not for spin-0 since, as we shall see, the differential equation that the outer solution satisfies is symmetric under  $\{x \leftrightarrow -x, h \leftrightarrow -h\}$  to leading order in  $c$ .



### 5.3 Inner solutions

BRW obtained an expression for the inner solution for general spin in terms of an undetermined parameter  $\gamma$ . In this section we summarize and present their results in a compact way.

By making the variable substitution  $u = 2c(1 - x)$ , equation (4.2.10) becomes

$$\begin{aligned} u \frac{d^2 {}_h y_{lm\omega}}{du^2} + (2\alpha + 1) \frac{d {}_h y_{lm\omega}}{du} - \\ - \frac{1}{4} \left[ u + 2h - \frac{1}{c} (c^2 - (\alpha + \beta)(\alpha + \beta + 1) + {}_h E_{lm\omega}) \right] {}_h y_{lm\omega} - \\ - \frac{1}{4c} \left[ u^2 \frac{d^2 {}_h y_{lm\omega}}{du^2} + 2(\alpha + \beta + 1) \frac{d {}_h y_{lm\omega}}{du} - \left( \frac{1}{4} u^2 + hu \right) {}_h y_{lm\omega} \right] = 0 \end{aligned} \quad (5.3.1)$$

It is clear from this equation that the leading order behaviour of  ${}_h E_{lm\omega}$  for large  $c$  must be:

$${}_h E_{lm\omega} = -c^2 + \gamma c + O(1) \quad (5.3.2)$$

If its leading order were not  $-c^2$ , there would then be a leading order term  $+\frac{1}{4}c {}_h y_{lm\omega}$  in the equation that it could not be matched with any other term. Lower order terms for  ${}_h E_{lm\omega}$  are given in BRW. It is crucial to know the value of the parameter  $\gamma$ , as it will determine how the angular function behaves asymptotically to leading order in  $c$ . At this stage,  $\gamma$  is an undetermined real number; we will determine its value later on.

Using the asymptotic behaviour (5.3.2) and letting  $c \rightarrow \infty$ , the terms in (5.3.1) of order  $O(c^{-1})$  can be ignored with respect to the other ones and, to leading order in  $c$ , the function  ${}_h y_{lm\omega}$  satisfies

$$u \frac{d^2 {}_h y_{lm\omega}}{du^2} + (2\alpha + 1) \frac{d {}_h y_{lm\omega}}{du} - \frac{1}{4} (u + 2h - \gamma) {}_h y_{lm\omega} = 0 \quad (5.3.3)$$

The solution of this differential equation that satisfies the boundary condition of regularity at  $x = +1$  is related to the confluent hypergeometric function:

$${}_h y_{lm\omega}^{\text{inn},+1} = {}_h C_{lm\omega} e^{-u/2} {}_1F_1\left((|m + h| + h + 1)/2 - \gamma/4, |m + h| + 1, u\right) \quad (5.3.4)$$

where  ${}_h C_{lm\omega}$  is a constant of integration.

### 5.3. Inner solutions

Similarly, if we instead make a change of variable  $u^* = 2c(1 + x)$  in equation (4.2.10), due to the  $\{x \leftrightarrow -x, h \leftrightarrow -h\}$  symmetry we obtain

$${}_h y_{lm\omega}^{\text{inn},-1} = {}_h D_{lm\omega} e^{-u^*/2} {}_1 F_1\left((|m-h| - h + 1)/2 - \gamma/4, |m-h| + 1, u^*\right) \quad (5.3.5)$$

as the solution that is regular at  $x = -1$ .

We use the following obvious notation to refer to the solutions of the spin-weighted spheroidal equation that correspond to the inner solutions of (5.3.3):

$${}_h S_{lm\omega}^{\text{inn},\pm 1} = (1-x)^\alpha (1+x)^\beta {}_h y_{lm\omega}^{\text{inn},\pm 1} \quad (5.3.6)$$

The inner solution  ${}_h S_{lm\omega}^{\text{inn},\pm 1}$  is only a valid approximation in the region from the boundary point  $\pm 1$  until a point  $x \sim \pm 1 \mp O(c^\delta)$  with  $-1 \leq \delta < 0$ . The reason is that in the step from (5.3.1) to (5.3.3) we have ignored terms with  $u^{\{\ast\}}/c$  with respect to terms of order  $O(1)$ , and therefore the inner solution has been found for  $\pm 1 - x \sim u^{\{\ast\}}/c \ll O(1)$  and so we must have  $\delta < 0$ . On the other hand, we are not ignoring  $u$  with respect to the  $O(1)$  term  $2(h-q)$  in equation (5.3.3), so that it must be  $u \sim O(c^{\delta+1})$  with  $\delta + 1 \geq 0$ . From the fact that we are not ignoring  $2(h-q)$  with respect to  $u$  it does not follow that  $\delta + 1 \leq 0$ , since the inner solution is valid at the boundary point  $x = +1$ , where  $u = 0$ . That is, the term  $2(h-q)$  cannot be ignored with respect to  $u$  everywhere in the region from  $+1$  up to a point  $x \sim +1 - O(c^\delta)$  even if  $\delta + 1 \geq 0$ . A similar reasoning applies to  $u^*$ .

We therefore have one boundary layer comprising the region in  $x$  from  $-1$  to  $(-1-x) \sim O(c^\delta)$  and another boundary layer from  $(+1-x) \sim O(c^\delta)$  to  $+1$ .

To leading order in  $c$  the solution to the spin-weighted spheroidal equation which is valid within the two boundary layers is given by

$${}_h S_{lm\omega}^{\text{inn}} = (1-x)^\alpha (1+x)^\beta \begin{cases} {}_h C_{lm\omega} e^{-u/2} {}_1 F_1(-p, 2\alpha + 1, u) & x > 0 \\ {}_h D_{lm\omega} e^{-u^*/2} {}_1 F_1(-p', 2\beta + 1, u^*) & x < 0 \end{cases} \quad (5.3.7)$$

where we have defined

$$\begin{cases} p \equiv -(|m+h|+h+1)/2 + \gamma/4 \\ p' \equiv -(|m-h|-h+1)/2 + \gamma/4 \end{cases} \quad (5.3.8)$$

BRW then require that  $p, p' \in \mathbb{Z}^+$  in order that the inner solution  ${}_hS_{lm\omega}^{\text{inn}}$  is regular at  $x=0$ , where  $u, u^* \rightarrow \infty$ . Correspondingly, they replace the confluent hypergeometric functions  ${}_1F_1(a, b, x)$  by the generalized Laguerre polynomials  $L_{-a}^{(b-1)}(x)$ . As we shall see, this is erroneous:  $p, p' \in \mathbb{Z}^+$  is not a necessary condition for regularity since in the cases for which this condition is not satisfied, the coefficients  ${}_hC_{lm\omega}$  and  ${}_hD_{lm\omega}$  diminish exponentially for large  $c$  in such a way that  ${}_hS_{lm\omega}^{\text{inn}}$  remains regular.

## 5.4 Outer solution

We now proceed to find the outer solution of (4.1.1). The analysis in this section is new as the outer solution has been overlooked by previous authors. We first make the variable substitution

$$y(x) = g(x) \exp \int \frac{\alpha - \beta + (\alpha + \beta + 1)x}{1 - x^2} dx = g(x)(1-x)^{-\frac{(2\alpha+1)}{2}}(1+x)^{-\frac{(2\beta+1)}{2}} \quad (5.4.1)$$

which transforms equation (4.1.1) into

$$g''(x) + f(x, c)g(x) = 0 \quad (5.4.2)$$

where

$$\begin{aligned} f(x, c) = & \frac{G(x, c)}{1 - x^2} + \frac{(\alpha + \beta + 1)(1 - x^2) + 2x[\alpha - \beta + (\alpha + \beta + 1)x]}{(1 - x^2)^2} - \\ & - \frac{[\alpha - \beta + (\alpha + \beta + 1)x]^2}{(1 - x^2)^2} \end{aligned} \quad (5.4.3)$$

and  $G(x, c)$  is the coefficient of  ${}_hy_{lm\omega}$  in (4.2.10), i.e.,

$$G(x, c) = {}_hE_{lm\omega} - (\alpha + \beta)(\alpha + \beta + 1) + c^2x^2 - 2hcx \quad (5.4.4)$$

## 5.4. Outer solution

---

We now perform a WKB-type expansion:  $g(x) = e^{\mathcal{G}(x)}$ . This change of variable converts equation (5.4.2) into

$$\mathcal{G}''(x) + \mathcal{G}'(x)^2 + f(x, c) = 0 \quad (5.4.5)$$

Performing an asymptotic expansion of  $f(x, c)$  in  $c$ :

$$f(x, c) = f_0(x)c^2 + f_1(x)c + O(1), \quad (5.4.6)$$

with

$$f_0(x) = -1, \quad f_1(x) = \frac{2(q - hx)}{1 - x^2}, \quad (5.4.7)$$

where we have used the asymptotic expansion of  ${}_hE_{lm\omega}$  in  $c$  and we have also introduced the parameter  $q \equiv \gamma/2$ . We will prove in Section 5.6 that  $q$  must be an integer. It is clear that to leading order in  $c$  the outer solution is symmetric under  $\{x \leftrightarrow -x\}$ . We are avoiding any possible turning points by assuming that  $f(x, c) \neq 0$  for  $x$  values of interest. This condition is clearly satisfied if  $c$  is large enough.

Next we perform an asymptotic expansion of  $\mathcal{G}(x)$  in  $c$ . We do not know what the leading order is, and we will determine it with the method of dominant balance. Let the expansion of  $\mathcal{G}(x)$  for large  $c$  be  $\mathcal{G}(x) = h_0(c)\mathcal{G}_0(x) + o(h_0(c))$ . We use the small letter  $o$  to indicate lower order than the order of its argument. On substituting the asymptotic expansions for  $f(x, c)$  and  $\mathcal{G}(x)$  into (5.4.5) we obtain

$$h_0(c)\mathcal{G}_0''(x) + h_0(c)^2 [\mathcal{G}_0'(x)]^2 + c^2 f_0(x) + o(h_0(c)^2) + o(c^2) = 0 \quad (5.4.8)$$

We could try and cancel out the  $c^2 f_0(x)$  term with  $h_0(c)\mathcal{G}_0''(x)$ . That would give  $h_0 = c^2$ , but then  $h_0(c)\mathcal{G}_0''(x)$  would be subdominant to  $h_0^2(\mathcal{G}_0')^2$ . The other option is to cancel the  $c^2 f_0(x)$  term with  $h_0^2(\mathcal{G}_0')^2$  instead. This gives  $h_0 = c$ , which works. We therefore find  $\mathcal{G}(x) = c\mathcal{G}_0(x) + \mathcal{G}_1(x) + O(c^{-1})$ .

The resulting equation for the leading order term in  $\mathcal{G}$  is

$$[\mathcal{G}_0'(x)]^2 + f_0(x) = 0, \quad (5.4.9)$$

## 5.5. Matching the solutions

---

the solution of which is  $\mathcal{G}_0 = \pm(x - x_0)$ . The equation for the next order in  $c$  is

$$\mathcal{G}_0''(x) + 2\mathcal{G}_0'(x)\mathcal{G}_1'(x) + f_1(x) = 0, \quad (5.4.10)$$

which gives

$$\mathcal{G}_1 = \pm \left[ -\frac{h}{2} \log(1 - x^2) - \frac{q}{2} \log\left(\frac{1+x}{1-x}\right) \right]. \quad (5.4.11)$$

The physical optics approximation for the outer solution is therefore:

$$\begin{aligned} {}_hS_{lm\omega}^{\text{out}}(x) &= (1-x)^\alpha (1+x)^\beta {}_h y_{lm\omega}^{\text{out}}(x) \\ {}_h y_{lm\omega}^{\text{out}}(x) &= (1-x)^{-(2\alpha+1)/2} (1+x)^{-(2\beta+1)/2} \times \\ &\quad \times \left[ {}_h A_{lm\omega} (1-x)^{+(q-h)/2} (1+x)^{-(q+h)/2} e^{+cx} + \right. \\ &\quad \left. + {}_h B_{lm\omega} (1-x)^{-(q-h)/2} (1+x)^{+(q+h)/2} e^{-cx} \right] \end{aligned} \quad (5.4.12)$$

where the constant  $x_0$  has been absorbed within  ${}_h A_{lm\omega}$  and  ${}_h B_{lm\omega}$ .

This solution is valid in the region  $-1 + O(c^{-1}) \ll x \ll +1 - O(c^{-1})$ .

## 5.5 Matching the solutions

We have found three different solutions. One of the two inner solutions is valid in the region  $-1 \leq x \lesssim -1 + O(c^\delta)$  for any  $\delta$  such that  $-1 \leq \delta < 0$ , and the other one for  $+1 - O(c^\delta) \lesssim x \leq +1$ . The outer solution is valid for  $-1 + O(c^{-1}) \ll x \ll +1 - O(c^{-1})$ . Clearly all three solutions together span the whole physical region  $-1 \leq x \leq +1$ . There are also two regions of overlap, one close to  $-1$  and one close to  $+1$ , where both the outer solution and one of the inner solutions are valid. We can proceed to match the solutions in these regions and we will do so only to leading order in  $c$  as matching to lower orders would not bring any more insight into the behaviour of the SWSH. When the matching is completed to leading order, the two overlap regions are given one by the points  $x$  satisfying  $O(c^{-1}) \ll 1+x \lesssim O(c^\delta)$  and the other one by the points satisfying  $O(c^{-1}) \ll 1-x \lesssim O(c^\delta)$ . For the overlap regions to exist it is therefore required that we choose a  $\delta$  satisfying  $-1 < \delta < 0$ .

## 5.5. Matching the solutions

---

In order to obtain an expression for the inner solution in the overlap region, we expand the inner solution for  $u, u^* \sim \infty$ . For that, we need to know how the confluent hypergeometric functions behave when the independent variable is large. From [1] we have

$${}_1F_1(b, c, z) \rightarrow \frac{\Gamma(c)e^{+i\pi b}z^{-b}}{\Gamma(c-b)} + \frac{\Gamma(c)e^z z^{b-c}}{\Gamma(b)}, \quad (|z| \rightarrow +\infty) \quad (5.5.1)$$

when  $z = |z|e^{i\vartheta}$  with  $-\pi/2 < \vartheta < 3\pi/2$ , which includes the case we are considering:  $\vartheta = 0$ . This means that the inner solution valid close to  $x = +1$  behaves like

$$\begin{aligned} {}_h y_{lm\omega}^{\text{inn},+1} &\rightarrow \\ &\rightarrow {}_h C_{lm\omega} \left\{ \begin{array}{ll} \frac{\Gamma(|m+h|+1) [2c(1-x)]^{(-p-|m+h|-1)} e^{+c(1-x)}}{\Gamma(-p)}, & p \notin \mathbb{Z}^+ \cup \{0\} \\ \frac{\Gamma(|m+h|+1) e^{-i\pi p} [2c(1-x)]^p e^{-c(1-x)}}{\Gamma(|m+h|+1+p)}, & p \in \mathbb{Z}^+ \cup \{0\} \end{array} \right\} \\ &\quad , (|u| \rightarrow +\infty) \end{aligned} \quad (5.5.2)$$

The behaviour of the inner solution valid close to  $x = -1$  is similarly obtained by simultaneously replacing  $x$  with  $-x$ ,  $h$  with  $-h$  (which also implies replacing  $p$  by  $p'$ ) and  ${}_h C_{lm\omega}$  with  ${}_h D_{lm\omega}$  above.

On the other hand, in order to obtain an expression for  ${}_h y_{lm\omega}^{\text{out}}$  valid in the overlap region we perform a Taylor series expansion around  $x = +1$  or  $-1$  depending on where we are doing the matching, and keep only the first order in the series:

a) **Around**  $x = +1$ .

To first order in  $(1-x)$ :

$$\begin{aligned} {}_h y_{lm\omega}^{\text{out}}(x) &\sim {}_h A_{lm\omega} (1-x)^{[(q-h-1)/2-\alpha]} 2^{[-(q+h+1)/2-\beta]} e^{+cx} + \\ &\quad + {}_h B_{lm\omega} (1-x)^{[-(q-h+1)/2-\alpha]} 2^{[+(q+h-1)/2-\beta]} e^{-cx} \quad (x \rightarrow +1) \end{aligned} \quad (5.5.3)$$

By matching the inner and outer solution in the overlap region  $O(c^{-1}) \ll 1-x \lesssim O(c^\delta)$ , i.e., by matching equations (5.5.2) and (5.5.3), we obtain the following relations depending on the value of  $p$ :

## 5.5. Matching the solutions

---

a1) if  $p \notin \mathbb{Z}^+ \cup \{0\}$ :

$$\begin{cases} {}_hA_{lm\omega} = 0 \\ {}_hB_{lm\omega} = 2^{[-(q+h-1)/2+\beta]} \frac{\Gamma(|m+h|+1)}{\Gamma(-p)} (2c)^{[-p-|m+h|-1]} e^{+c} {}_hC_{lm\omega} \end{cases} \quad (5.5.4)$$

a2) if  $p \in \mathbb{Z}^+ \cup \{0\}$ :

$${}_hA_{lm\omega} = 2^{[+(q+h+1)/2+\beta]} \frac{\Gamma(|m+h|+1)}{\Gamma(|m+h|+1+p)} e^{-i\pi p} (2c)^p e^{-c} {}_hC_{lm\omega} \quad (5.5.5)$$

b) **Around**  $x = -1$  (similar to the  $x = +1$  case).

To first order in  $(1+x)$ :

$$\begin{aligned} {}_hy_{lm\omega}^{\text{out}}(x) &\sim {}_hA_{lm\omega}(1+x)^{[-(q+h+1)/2-\beta]} 2^{[+(q-h-1)/2-\alpha]} e^{+cx} + \\ &\quad + {}_hB_{lm\omega}(1+x)^{[+(q+h-1)/2-\beta]} 2^{[-(q-h+1)/2-\alpha]} e^{-cx} \quad (x \rightarrow -1) \end{aligned} \quad (5.5.6)$$

b1) if  $p' \notin \mathbb{Z}^+ \cup \{0\}$ :

$$\begin{cases} {}_hB_{lm\omega} = 0 \\ {}_hA_{lm\omega} = 2^{[-(q-h-1)/2+\alpha]} \frac{\Gamma(|m-h|+1)}{\Gamma(-p')} (2c)^{[-p'-|m-h|-1]} e^{+c} {}_hD_{lm\omega} \end{cases} \quad (5.5.7)$$

b2) if  $p' \in \mathbb{Z}^+ \cup \{0\}$ :

$${}_hB_{lm\omega} = 2^{[+(q-h+1)/2+\alpha]} \frac{\Gamma(|m-h|+1)}{\Gamma(|m-h|+1+p')} e^{-i\pi p'} (2c)^{p'} e^{-c} {}_hD_{lm\omega} \quad (5.5.8)$$

From the above matching equations we can obtain a uniform asymptotic approximation to  ${}_hS_{lm\omega}$  valid throughout the whole region  $x \in [-1, +1]$  and also find out where the zeros of the function are. Following [4], the uniform asymptotic approximation is obtained by adding the outer and the two inner solutions, and then subtracting the asymptotic approximations in the two overlap regions since

## 5.5. Matching the solutions

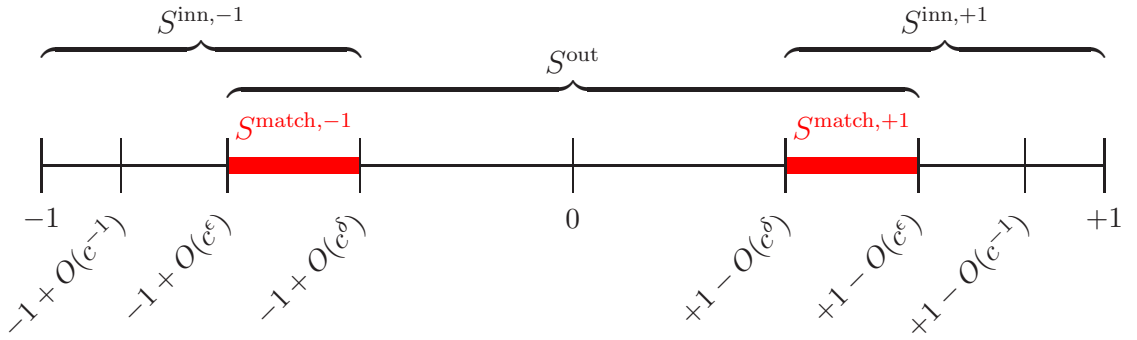


Figure 5.1: Regions of validity in the  $x$  axis of the various approximations to the SWSH for large  $c$ . It must be  $-1 < \epsilon < \delta < 0$ . For clarity, the mode labels have been dropped.  $S^{\text{match},\pm 1}$  refers to the asymptotic approximation valid in the overlap region (red) close to  $x = \pm 1$ . The uniform solution is constructed as  $S^{\text{unif}} = S^{\text{out}} + S^{\text{inn},+1} + S^{\text{inn},-1} - S^{\text{match},+1} - S^{\text{match},-1}$ .



## 5.5. Matching the solutions

---

these have been included twice. Figure 5.1 depicts the region of validity of the various asymptotic solutions for large  $c$  that we have obtained.

We can distinguish three cases:

$$p, p' \notin \mathbb{Z}^+ \cup \{0\}$$

From equations (5.5.4) and (5.5.7) it must be  ${}_hA_{lm\omega} = {}_hB_{lm\omega} = 0 = {}_hC_{lm\omega} = {}_hD_{lm\omega}$ , so this case is the trivial solution and we discard it.

$$p \in \mathbb{Z}^+ \cup \{0\} \text{ and } p' \notin \mathbb{Z}^+ \cup \{0\}, \text{ or vice-versa}$$

Either  ${}_hA_{lm\omega}$  or  ${}_hB_{lm\omega}$  is equal to zero (but not both), so that the function  ${}_hS_{lm\omega}$  cannot have a zero close to  $x = 0$ . All the zeros, if there are any, of  ${}_hS_{lm\omega}$  are zeros of the inner solutions and thus they are located inside the boundary layers, close to  $x = \pm 1$ .

In this case we can already directly obtain the uniform asymptotic approximation, up to an overall normalization constant  ${}_hC_{lm\omega}$ :

$$\begin{aligned} {}_hS_{lm\omega}^{\text{unif}} = & {}_hC_{lm\omega} (1-x)^\alpha (1+x)^\beta \left\{ e^{-c(1-x)} {}_1F_1\left(-p, 2\alpha+1, 2c(1-x)\right) + \right. \\ & + \frac{\Gamma(2\alpha+1)}{\Gamma(2\alpha+1+p)} \frac{\Gamma(-p')}{\Gamma(2\beta+1)} e^{-i\pi p} (2c)^{p+p'+2\beta+1} e^{-2c} 2^{(q+\beta-\alpha)} e^{-c(1+x)} \times \\ & \times {}_1F_1\left(-p', 2\beta+1, 2c(1+x)\right) + 2^{[(q+h+1)/2+\beta]} \frac{\Gamma(2\alpha+1)}{\Gamma(2\alpha+1+p)} e^{-i\pi p} (2c)^p e^{-c} e^{cx} \times \\ & \times \left[ (1-x)^{(q-h-1)/2-\alpha} (1+x)^{-(q+h+1)/2-\beta} - 2^{[-(q+h+1)/2-\beta]} (1-x)^{(q-h-1)/2-\alpha} - \right. \\ & \left. \left. - 2^{[(q-h-1)/2-\alpha]} (1+x)^{-(q+h+1)/2-\beta} \right] \right\} \quad \text{when } p \in \mathbb{Z}^+ \cup \{0\} \text{ and } p' \notin \mathbb{Z}^+ \cup \{0\} \end{aligned} \quad (5.5.9)$$

The uniform approximation when  $p \notin \mathbb{Z}^+ \cup \{0\}$  and  $p' \in \mathbb{Z}^+ \cup \{0\}$  may be obtained by making the substitutions  $x \leftrightarrow -x$  and  $h \leftrightarrow -h$  (which imply the substitutions  $\alpha \leftrightarrow \beta$  and  $p \leftrightarrow p'$ ) in (5.5.9).

## 5.5. Matching the solutions

---

The irregularity arising from  $e^{-c(1+x)} {}_1F_1(-p', 2\beta + 1, 2c(1+x)) \sim e^{2c}$  (ignoring factors independent of  $x$  and  $c$ ) in the limit  $x \rightarrow +1$  and  $c \rightarrow +\infty$  prompted BRW to discard the case  $p' \notin \mathbb{Z}^+ \cup \{0\}$ . It is clear from (5.5.9), however, that this irregularity is nullified by the factor  $e^{-2c}$  in front of it, brought in by the coefficient  ${}_hD_{lm\omega}$ . Note that despite the factor  $e^{-2c}$ , close to  $x = -1$  this term (which is part of the inner solution valid in the boundary layer there) is not dominated by the first term in (5.5.9) (which is the inner solution valid in the boundary layer near  $x = +1$ ). The reason is that  $e^{-c(1+x)} {}_1F_1(-p', 2\beta + 1, 2c(1+x)) \sim e^{-2c}$  and  $e^{-c(1-x)} {}_1F_1(-p, 2\alpha + 1, 2c(1-x)) \sim e^{-2c}$  where both limits are  $x \rightarrow -1$  and  $c \rightarrow +\infty$  and we have ignored factors independent of  $x$  and  $c$ . In the boundary layer around  $x = \pm 1$ , the asymptotic approximation valid in the overlap region close to  $x = \mp 1$  cancels out the inner solution  ${}_hS_{lm\omega}^{\text{inn}, \mp 1}$  in expression (5.5.9). Similarly, in the same boundary layer, the asymptotic approximation valid in the overlap region close to  $x = \pm 1$  cancels out the outer solution, so that only  ${}_hS_{lm\omega}^{\text{inn}, \pm 1}$  contributes to the uniform approximation in that boundary layer.

A similar reasoning can be applied to the case  $p \notin \mathbb{Z}^+ \cup \{0\}$ .

$$p, p' \in \mathbb{Z}^+ \cup \{0\}$$

In this case, apart from the overall normalization constant there is another unknown constant. We are going to determine this extra unknown by imposing the  $\{x \leftrightarrow -x, h \leftrightarrow -h\}$  symmetry. Using the Teukolsky-Starobinskiĭ identities (2.8.6) and (2.8.7) together with the symmetry (4.2.1a) in the inner solution

## 5.5. Matching the solutions

---

(5.3.7) we obtain

$$\begin{aligned} \frac{-1D_{lm\omega}}{-1C_{lm\omega}} &= \frac{+1C_{lm\omega}}{+1D_{lm\omega}} = (-1)^{(l+m)} \frac{+1C_{lm\omega}}{-1C_{lm\omega}} = \\ &= (-1)^{(l+m)} \begin{cases} \frac{2\sqrt{(m-q+1)(m-q-1)}}{m(m+1)}c & \text{when } m \geq +1 \\ -\frac{\sqrt{q-1}}{\sqrt{q+1}} & \text{when } m = 0 \\ \frac{m(m-1)}{2\sqrt{(m-q+1)(m-q-1)}}\frac{1}{c} & \text{when } m \leq -1 \end{cases} \end{aligned} \quad (5.5.10)$$

$$\begin{aligned} \frac{-2D_{lm\omega}}{-2C_{lm\omega}} &= \frac{+2C_{lm\omega}}{+2D_{lm\omega}} = (-1)^{(l+m)} \frac{+2C_{lm\omega}}{-2C_{lm\omega}} = (-1)^{(l+m)} \times \\ &\times \begin{cases} \frac{4\sqrt{(m-q+1)(m-q-1)(m-q+3)(m-q-3)}}{(m+2)(m+1)m(m-1)}c^2 & \text{when } m \geq +2 \\ -\frac{\sqrt{q(q-2)(q-4)}}{3\sqrt{q+2}}c & \text{when } m = +1 \\ \frac{\sqrt{(q-3)(q-1)}}{\sqrt{(q+3)(q+1)}} & \text{when } m = 0 \\ -\frac{3\sqrt{q-2}}{\sqrt{q(q+2)(q+4)}}\frac{1}{c} & \text{when } m = -1 \\ \frac{(m+1)m(m-1)(m-2)}{4\sqrt{(m-q+1)(m-q-1)(m-q+3)(m-q-3)}}\frac{1}{c^2} & \text{when } m \geq -2 \end{cases} \end{aligned} \quad (5.5.11)$$

Equations (5.5.10) and (5.5.11) have been obtained without imposing any restrictions on the values of  $p$  or  $p'$  and might therefore seem to contradict the result from (5.5.5) and (5.5.7) [or (5.5.4) and (5.5.8)] giving an exponential behaviour with  $c$  for the ratio  ${}_hD_{lm\omega}/{}_hC_{lm\omega}$  for the case  $p \in \mathbb{Z}^+ \cup \{0\}$  and  $p' \notin \mathbb{Z}^+ \cup \{0\}$  [or viceversa]. We shall see in the next section, however, that equations (5.5.10) and (5.5.11) can only actually be applied to the case  $p, p' \in \mathbb{Z}^+ \cup \{0\}$  so that there is no such contradiction.

We can already determine in what cases the outer solution has a zero. Clearly, from equations (5.5.5), (5.5.8), (5.5.10) and (5.5.11), the ratio between the coefficients  ${}_hA_{lm\omega}$  and  ${}_hB_{lm\omega}$  is proportional to a power of  $c$ , where the constant of proportionality does not depend on  $c$ . It then follows from the form (5.4.12) of the outer solution that one exponential term will dominate for positive  $x$  and the other exponential term will dominate for negative  $x$ , when  $c \rightarrow \infty$ . There-

## 5.5. Matching the solutions

---

fore the outer solution does not possess a zero far from  $x = 0$  for large  $c$ . The outer solution has a zero if  ${}_hA_{lm\omega}$  and  ${}_hB_{lm\omega}$  have different sign and it does not otherwise. From equations (5.3.8), (5.5.5), (5.5.8), (5.5.10) and (5.5.11) we have:

$$\text{sign}\left(\frac{{}_hA_{lm\omega}}{{}_hB_{lm\omega}}\right) = (-1)^{(p-p')} * \text{sign}\left(\frac{{}_hC_{lm\omega}}{{}_hD_{lm\omega}}\right) = (-1)^{(l+m)} \quad (5.5.12)$$

Furthermore, we can calculate what the location of the zero of the outer solution is to leading order in  $c$ : by setting the outer solution (5.4.12) equal to zero and using (5.5.5) and (5.5.8) (since we have already seen that if  $p$  and/or  $p' \notin \mathbb{Z}^+ \cup \{0\}$  the outer solution does not have a zero) we obtain that for large frequency the zero is located at the following value of  $x$ :

$$\begin{aligned} x_0 &= \frac{1}{2c} \log \left( -\frac{{}_hB_{lm\omega}}{{}_hA_{lm\omega}} \right) = \\ &= \frac{1}{2c} \log \left( -2^{(-h+\alpha-\beta)} \frac{\Gamma(|m-h|+1)\Gamma(|m+h|+1+p)}{\Gamma(|m+h|+1)\Gamma(|m-h|+1+p')} \times \right. \\ &\quad \left. \times e^{-i\pi(p'-p)} (2c)^{(p'-p)} \frac{{}_hD_{lm\omega}}{{}_hC_{lm\omega}} \right) \end{aligned} \quad (5.5.13)$$

Clearly there is one zero in the region between the two boundary layers tending to the location  $x = 0$  as  $c$  becomes large if  ${}_hB_{lm\omega}$  and  ${}_hA_{lm\omega}$  have different sign and there is not a zero if they have the same sign.

Finally, the uniform asymptotic approximation for this case is:

$$\begin{aligned} {}_hS_{lm\omega}^{\text{unif}} &= {}_hC_{lm\omega}(1-x)^\alpha(1+x)^\beta \left\{ e^{-c(1-x)} {}_1F_1\left(-p, 2\alpha+1, 2c(1-x)\right) + \right. \\ &\quad + \frac{{}_hD_{lm\omega}}{{}_hC_{lm\omega}} e^{-c(1+x)} {}_1F_1\left(-p', 2\beta+1, 2c(1+x)\right) + \\ &\quad + 2^{[(q+h+1)/2+\beta]} \frac{\Gamma(2\alpha+1)}{\Gamma(2\alpha+1+p)} e^{-i\pi p} (2c)^p e^{-c} e^{cx} \times \\ &\quad \times \left[ (1-x)^{+(q-h-1)/2-\alpha} (1+x)^{-(q+h+1)/2-\beta} - 2^{-[(q+h+1)/2+\beta]} (1-x)^{+(q-h-1)/2-\alpha} \right] + \\ &\quad + \frac{{}_hD_{lm\omega}}{{}_hC_{lm\omega}} 2^{[(q-h+1)/2+\alpha]} \frac{\Gamma(2\beta+1)}{\Gamma(2\beta+1+p')} e^{-i\pi p'} (2c)^{p'} e^{-c} e^{-cx} \\ &\quad \left. \left[ (1+x)^{+(q+h-1)/2-\beta} (1-x)^{-(q-h+1)/2-\alpha} - 2^{-[(q-h+1)/2+\alpha]} (1+x)^{+(q+h-1)/2-\beta} \right] \right\} \\ &\quad \text{when } p, p' \in \mathbb{Z}^+ \cup \{0\} \end{aligned} \quad (5.5.14)$$

where the ratio between  ${}_hD_{lm\omega}$  and  ${}_hC_{lm\omega}$  is given by (5.5.10) for  $h = \pm 1$  and by (5.5.11) for  $h = \pm 2$ .

Similar cancelations to the ones for the case  $p \in \mathbb{Z}^+ \cup \{0\}$  and  $p' \notin \mathbb{Z}^+ \cup \{0\}$  occur in the present case for the uniform solution (5.5.14). The only difference is that now, in the boundary layer around  $x = \pm 1$ , the asymptotic approximation valid in the overlap region close to  $x = \mp 1$  only cancels out part of the outer solution. The other part of the outer solution, however, is exponentially negligible with respect to the inner solution  ${}_hS_{lm\omega}^{\text{inn}, \pm 1}$ .

## 5.6 Calculation of $\gamma$

To finally determine the value of  $\gamma$  we only need to impose that our asymptotic solution must have the correct number of zeros. BRW give the number of zeros of the SWSH for non-negative  $m$  and  $h$ . Straightforwardly generalizing their result for all  $m$  and  $h$  using the symmetries of the differential equation we have:

**Theorem 1 Zeros of  $S$ :** *The number of zeros of  ${}_hS_{lm\omega}$  is independent of  $c$  and for  $x \in (-1, 1)$  is equal to*

$$\begin{cases} l - |m| & \text{for } |m| \geq |h| \\ l - |h| & \text{for } |m| < |h| \end{cases} \quad (5.6.1)$$

The number of zeros of the confluent hypergeometric function is also needed, and that is given by Buchholz [11]:

The number of positive, real zeros of  ${}_1F_1(-a, b, z)$  when  $b > 0$  is

$$\begin{cases} -[-a] & \text{for } +\infty > a \geq 0 \\ 0 & \text{for } 0 \geq a > -\infty \end{cases} \quad (5.6.2)$$

where  $[n]$  means the largest integer  $\leq n$ .

Since the confluent hypergeometric functions are part of the inner solutions and the region of validity of these solutions becomes tighter to the boundary points as

## 5.6. Calculation of $\gamma$

---

$c$  increases, the zeros of  ${}_1F_1(-p, 2\alpha + 1, u)$  are grouped together close to  $x = +1$ , and likewise for  ${}_1F_1(-p', 2\beta + 1, u^*)$  close to  $x = -1$ . Apart from these zeros, for large  $c$ , the function  ${}_hS_{lm\omega}$  may only have other zeros at  $x = \pm 1$  and/or at  $x = x_0$ . The possible one at  $x = x_0$  is not due to the confluent hypergeometric functions but to the outer solution. We define the variable  $z_0$  so that it has value  $+1$  if  ${}_hS_{lm\omega}$  has a zero at  $x = x_0$  and value  $0$  if it does not.

From equation (5.3.8) we see that  $p' = p + (|m + h| + 2h - |m - h|)/2$ , and therefore if either  $p$  or  $p'$  is integer then the other one must be integer as well. But, as we saw in Section 5.5, at least one of  $p$  and  $p'$  (if not both) must be a positive integer or zero. Therefore both  $p$  and  $p'$  must be integers and at least one of them is positive or zero. It also follows from (5.3.8) that

$$\gamma = 2(p + p') + 2 + |m + h| + |m - h| = 2q \quad (5.6.3)$$

where it is now clear that  $q \in \mathbb{Z}$ .

Requiring that the number of zeros of the asymptotic solution coincides with the number of zeros of the SWSH results in the condition

$$\begin{aligned} & \left\{ \begin{array}{ll} -(|m + h| + h + 1)/2 + q/2 & \text{for } q \geq |m + h| + h + 1 \\ 0 & \text{for } q < |m + h| + h + 1 \end{array} \right\} + \\ & + \left\{ \begin{array}{ll} -(|m - h| - h + 1)/2 + q/2 & \text{for } q \geq |m - h| - h + 1 \\ 0 & \text{for } q < |m - h| - h + 1 \end{array} \right\} + \quad (5.6.4) \\ & + z_0 = \left\{ \begin{array}{ll} l - |m| & \text{for } |m| \geq |h| \\ l - |h| & \text{for } |m| < |h| \end{array} \right\} \end{aligned}$$

From (5.6.4) and the fact that  $z_0 = 0$  when either  $p$  or  $p' \notin \mathbb{Z}^+ \cup \{0\}$  as seen in Section 5.5, we obtain the value of  $q$  in all different cases:

## 5.6. Calculation of $\gamma$

---

$$q = \begin{cases} l - |m| & \text{for } |m| \geq |h| \\ l - |h| & \text{for } |m| < |h| \end{cases} + \frac{(|m+h| + |m-h|)}{2} + 1 - z_0$$

if  $l \geq l_1, l_2$  (i.e.,  $p, p' \in \mathbb{Z}^+ \cup \{0\}$ )

(5.6.5a)

$$q = 2 \begin{cases} l - |m| & \text{for } |m| \geq |h| \\ l - |h| & \text{for } |m| < |h| \end{cases} + |m+h| + h + 1$$

if  $l < l_2$  (i.e.,  $p \in, p' \notin \mathbb{Z}^+ \cup \{0\}$ )

(5.6.5b)

$$q = 2 \begin{cases} l - |m| & \text{for } |m| \geq |h| \\ l - |h| & \text{for } |m| < |h| \end{cases} + |m-h| - h + 1$$

if  $l < l_1$  (i.e.,  $p \notin, p' \in \mathbb{Z}^+ \cup \{0\}$ )

(5.6.5c)

where

$$l_1 \equiv \begin{cases} |m| & \text{for } |m| \geq |h| \\ |h| & \text{for } |m| < |h| \end{cases} + (|m+h| - |m-h|)/2 + h$$

$$l_2 \equiv \begin{cases} |m| & \text{for } |m| \geq |h| \\ |h| & \text{for } |m| < |h| \end{cases} + (|m-h| - |m+h|)/2 - h$$

By requiring in (5.6.5a) that  $q$  must also satisfy (5.3.8) and bearing in mind that  $z_0$  can only have the values 0 or 1, it must be

$$z_0 = \begin{cases} 0 & \text{for } l - l_1 \text{ even} \\ 1 & \text{for } l - l_1 \text{ odd} \end{cases} \quad (5.6.6)$$

where  $l_2$  instead of  $l_1$  could have been used, since one is equal to the other one plus an even number.

It can be trivially seen that if  $l_1$  has an allowed value, i.e.,

$$l_1 \geq \begin{cases} |m| & \text{for } |m| \geq |h| \\ |h| & \text{for } |m| < |h| \end{cases}, \quad (5.6.7)$$

then  $l_2$  does not, and vice-versa, so that cases (5.6.5b) and (5.6.5c) are mutually exclusive.

Clearly, when  $l < l_1$  or  $l < l_2$ , for fixed  $h$  and  $m$ , as  $l$  is increased by 1 the corresponding value of  $q$  is also increased by 1, so that two different values of  $l$  correspond to two different values of  $q$ . However, once the threshold  $l \geq \max(l_1, l_2)$  is reached, every increase of 2 in  $l$  will involve the subtraction of an extra 1 in (5.6.5a) via  $z_0$ , so that its corresponding value of  $q$  will be the same as for the previous  $l$ . Therefore, in the region  $l \geq \max(l_1, l_2)$ , every value of  $q$  will correspond to two consecutive, different  $l$ 's: the two corresponding SWSH's will have the same number of zeros and behaviour close to the boundary points, but one will have a zero at  $x = x_0$  and the other one will not.

Another feature that can be seen is that, for  $h = \pm 1$ , the case  $l < \max(l_1, l_2)$  (i.e.,  $p_+$  and/or  $p_- \notin \mathbb{Z}^+ \cup \{0\}$ ) implies  $q - m = \pm 1$  or  $q = +1$  when  $m \geq 1$  and  $m = 0$  respectively, so that the leading order behaviour given by (5.5.10) vanishes for these cases. That is, in these cases we have not gone far enough in the asymptotic expansion (5.5.10). When  $m \leq -1$  it follows from (5.6.5b) and (5.6.5c) that  $l < l_1 (= l_2)$  requires  $l < |m|$ , which is not allowed. Therefore, expression (5.5.10) is not applicable to the case  $l < \max(l_1, l_2)$ , as already mentioned in the previous section.

Similarly, for  $h = \pm 2$ , the case  $l < \max(l_1, l_2)$  implies

$$\begin{cases} m - q = \pm 1, \pm 3 & \text{when } m \geq 2 \\ q = 0, 2, 4 & \text{when } m = 1 \\ q = 1, 3 & \text{when } m = 0 \\ q = 2 & \text{when } m = -1 \\ l < |m| & \text{when } m \leq -2 \end{cases}$$



## 5.7. Numerical method

---

so that the leading order behaviour given by (5.5.11) does then not apply.

Note that the scalar case is obtained from our formulae as a particular case. Setting  $h = 0$  in the equations above we have  $l_1 = l_2 = |m|$  and therefore  $l$  will always be greater or equal than both  $l_1$  and  $l_2$  so that (5.6.5a) will apply, and it gives  $q = l + 1 - z_0$  with

$$z_0 = \begin{cases} 0 & \text{for } l - |m| \text{ even} \\ 1 & \text{for } l - |m| \text{ odd} \end{cases}.$$

We also have  $p = p' \in \mathbb{Z}^+ \cup \{0\}$  and  $2\alpha = 2\beta = |m|$  and then the confluent hypergeometric functions are just the generalized Laguerre polynomials:  ${}_1F_1(-p, |m| + 1, z) \propto L_p^{(|m|)}(z)$ . Finally, because of the existence of the  $x \leftrightarrow -x$  symmetry in the scalar case, we have that  ${}_0B_{lm\omega} = \pm {}_0A_{lm\omega}$  in (5.4.12) and therefore the zero of the outer solution, if it exists, will be located exactly at  $x = 0$ . All these results for the scalar case coincide with [33], [35] and [65].

## 5.7 Numerical method

Two different methods have been used to obtain the numerical data. One method is the one used by Sasaki and Nakamura [80], consisting in approximating the differential equation (4.2.10) by a finite difference equation, and then finding the eigenvalue as the value of  ${}_hE_{lm\omega}$  that makes zero the determinant of the resulting (tri-diagonal) matricial equation. We have used this method to find the eigenvalues for several large values of the frequency. However, we used the shooting method described in the previous chapter to calculate the spin-weighted spheroidal function.

Sasaki and Nakamura's method, which they only develop explicitly for the case  $h = -2$  and  $m = 0$  solves the angular differential equation (4.2.10) re-written

## 5.7. Numerical method

---

with derivatives with respect to  $\theta$  rather than  $x$ :

$$\left\{ \frac{d^2}{d\theta^2} + \frac{1}{\sin \theta} [2(\alpha - \beta) + 2(\alpha + \beta) \cos \theta + \cos \theta] \frac{d}{d\theta} + \right. \\ \left. + {}_hE_{lm\omega} - (\alpha + \beta)(\alpha + \beta + 1) + c^2 \cos^2 \theta - 2hc \cos \theta \right\} {}_hy_{lm\omega}(\theta) = 0 \quad (5.7.1)$$

This equation is approximated by a finite-difference equation. Apart from at the boundaries, the derivatives are replaced with central differences. At the boundary points, the regularity condition (4.2.5) requires that  $d{}_hy_{lm\omega}/d\theta|_{x=\pm 1} = 0$  and the first order derivative (which has a factor  $1/\sin \theta$  in front) is approximated by a forward/backward difference at  $x = +1/-1$  respectively. The result is that equation (5.7.1) is approximated by

$$\begin{aligned} & \frac{{}_hy_{lm\omega}^{i+1} - 2{}_hy_{lm\omega}^i + {}_hy_{lm\omega}^{i-1}}{(\Delta\theta)^2} + \\ & + \frac{1}{\sin \theta_i} [2(\alpha - \beta) + 2(\alpha + \beta) \cos \theta_i + \cos \theta_i] \frac{{}_hy_{lm\omega}^{i+1} - {}_hy_{lm\omega}^{i-1}}{2\Delta\theta} + \\ & + [{}_hE_{lm\omega} - (\alpha + \beta)(\alpha + \beta + 1) + c^2 \cos^2 \theta_i - 2hc \cos \theta_i] {}_hy_{lm\omega}^i = 0, \\ & \text{for } i = 2, \dots, 2N \\ & 2(1 + 2\alpha) \frac{2{}_hy_{lm\omega}^{i+1} - 2{}_hy_{lm\omega}^i}{(\Delta\theta)^2} + \\ & + [{}_hE_{lm\omega} - (\alpha + \beta)(\alpha + \beta + 1) + c^2 - 2hc] {}_hy_{lm\omega}^i = 0, \text{ for } i = 1 (\theta = 0) \\ & - 4\beta \frac{2{}_hy_{lm\omega}^{i-1} - 2{}_hy_{lm\omega}^i}{(\Delta\theta)^2} + \\ & + [{}_hE_{lm\omega} - (\alpha + \beta)(\alpha + \beta + 1) + c^2 + 2hc] {}_hy_{lm\omega}^i = 0, \text{ for } i = 2N + 1 (\theta = \pi) \end{aligned} \quad (5.7.2)$$

where  $\theta_i = \pi(i - 1)/(2N) \equiv \Delta\theta(i - 1)$  and  $i = 1, 2, \dots, 2N + 1$ . Equation (5.7.2) can be represented as the product of a square, tridiagonal matrix  $A$  of dimension  $(2N + 1) \times (2N + 1)$  and the vector of elements  ${}_hy_{lm\omega}^i$  equal to zero. In order to find the eigenvalue we impose that the determinant of matrix  $A$  is zero.

We found that, already with  $N = 100$ , for most modes the values of  ${}_hE_{lm\omega}$  obtained to quadruple precision actually provided values of the determinant so large that were even greater than the machine's largest number. We therefore

## 5.7. Numerical method

---

decided to use this method (where the argument and the exponent of the value of the determinant must be passed on separately to the zero-finding routine *zbrent*) only to find eigenvalues and use the program `SPHDRVKN MPI.F90` (described in the previous chapter) when we wish to find both eigenvalues and spherical functions. In fact, Sasaki and Nakamura's method without finding the spherical function is so much faster than `SPHDRVKN MPI.F90`, that it is the preferable method to use if we want to find eigenvalues far from any known eigenvalue (as we analytically do for  $\omega = 0$  for example). This is why we used Sasaki and Nakamura's method to find the eigenvalues for large frequency and then used the resulting eigenvalue to find the corresponding spherical function with `SPHDRVKNLARGEW MPI.F90`, a variation of `SPHDRVKN MPI.F90`.

The Fortran90 program `SPHDRVDETZEROKN MPI.F90` implements Sasaki and Nakamura's method to find eigenvalues, particularly adapted to the case of large frequency. It calculates  ${}_h\lambda_{lm\omega}$  rather than  ${}_hE_{lm\omega}$  since  ${}_h\lambda_{lm\omega} \sim O(c)$  for large  $c$  whereas  ${}_hE_{lm\omega} \sim O(c^2)$ . It starts with the known value of  ${}_h\lambda_{l,m,\omega=0}$  (4.1.6) and finds the eigenvalue  ${}_h\lambda_{lm\omega}$  for increasing frequency by looking for a zero of the determinant of the matrix  $A$ . This procedure is smooth no matter how large the frequency is if  $l < l_1$  or  $l < l_2$ . However, if  $l \geq \max(l_1, l_2)$ , for some large value of the frequency, the eigenvalues for two consecutive values of  $l$  are so close (since they correspond to the same  $q$  and therefore their leading order term for large frequency is the same) that the initial bracketing of the eigenvalue includes both eigenvalues and therefore  $\det A$  calculated with the values of  ${}_h\lambda_{lm\omega}$  at the two ends of the bracket has the same sign. From this value of the frequency on, instead of looking for a zero of the determinant the program just looks for the value  ${}_h\lambda_{lm\omega}$  that is an extreme of the determinant. The reason is that this provides a point which is in between the two actual eigenvalues and it is therefore useful both as an approximation and as a bracket point for either of them. Instead of using minimization/maximization routines, which are very costly in terms of accuracy and time, in order to find an extreme of  $\det A$ , the program `SPHDRVDETZEROKN MPI.F90` looks for a zero of the derivative of

$\det A$ , which can be calculated to be

$$\frac{d(\det A)}{d_h \lambda_{lm\omega}} = \text{trace} [(\det A)A^{-1}] \quad (5.7.3)$$

and is very easy to evaluate. The program SPHDRVDETZEROKN MPI.F90 provided the graphs of  ${}_h\lambda_{lm\omega}$  as a function of  $\omega$  for large frequency and there is therefore no need for it to distinguish with accuracy between the two consecutive eigenvalues.

The extreme point of the determinant found by SPHDRVDETZEROKN MPI.F90 is used by the program SPHDRVKNLARGEW MPI.F90 to bracket and determine the two close eigenvalues and their corresponding angular functions. The program SPHDRVKNLARGEW MPI.F90 uses the shooting method and Runge-Kutta integration as used by SPHDRVKN MPI.F90 but the main part of the program is adapted to look for eigenvalues for large frequency. It initially looks for a zero of the function  $g({}_hE_{lm\omega})$  inside a bracket of the eigenvalue, and if it is not bracketed it then assumes that it is because the frequency is large enough so that there are two eigenvalues inside the bracket corresponding to two different, consecutive  $l$ 's. It then calls the routine *brent* to look for a minimum of  $g({}_hE_{lm\omega})$  (with a possible change of sign if there is a maximum instead) and uses that minimum to find a zero to its right or to its left depending on which one corresponds to the  $l$  we are interested in, according to (5.6.5). The program SPHDRVKNLARGEW MPI.F90 also finds the zero of the function  ${}_hS_{lm\omega}$  close to  $x = 0$  for large  $\omega$  if it has one as indicated by (5.6.6), uses a smaller stepsize in  $x$  close to  $x = \pm 1$  to cater for the rapid oscillations of the angular function there for large  $\omega$  and makes use of equations (5.6.5) and (5.3.2) to help bracket the eigenvalue. The program SPHDRVKNLARGEW MPI.F90 provided the graphs of  ${}_hS_{lm\omega}(\theta)$  for large frequency.

## 5.8 Numerical results

All the numerical results and graphs in this section have been obtained setting  $Q = 0$ ,  $a = 0.95$  and  $M = 1$ .

There is an obvious numerical problem when  $p, p' \in \mathbb{Z}^+ \cup \{0\}$ . In this case, as mentioned in Section 5.6, the eigenvalues for two different values of  $l$  (but same  $h, m$ ) become exponentially close as  $c$  increases ([8]). This means that for this case we are not able to find the functions for very large values of the frequency. For example, in the case below for  $h = -1$  and  $m = 1$ , when  $\omega = 25$  the eigenvalues for  $l = 3$  and  $l = 4$  only differ in their 14th digit.

BRW do give the analytical value for  $q$  for spin-0. For spin different from zero, however, they try to numerically match their large-frequency asymptotic expansion of the eigenvalue with the expansion for small frequency given by Press and Teukolsky ([76] and [88]). As can be seen in Figures 5.2 and 5.3, this matching at intermediate values of the frequency might be good for certain cases, especially for small  $l$ , but not for other ones. All eigenvalues start off for frequency zero at the value given by (4.1.6), as expected, and when  $l \geq l_1$  or  $l_2$  the pairs of curves that share the same value of  $q$  become exponentially closer and closer to each other as the frequency increases. When the frequency is as large as 100, the curves fully coincide in the expected pairs for large frequency (given by equation (5.3.2), and BRW for lower order terms) where  $q$  comes in as a parameter. From this, the corresponding value of  $q$  for a certain set of values of  $\{l, m, h\}$  can be inferred, and this coincides with the one given by equations (5.6.5a), (5.6.5b) and (5.6.5c).

We calculated and plotted in Figure 5.4 the SWSH for  $h = -1$ ,  $l = 3$  &  $4$ ,  $m = 1$ , where the value of  $q$ , given by (5.6.5b), is the same for both of them:  $q = 4$  (this is a case where  $p, p' \in \mathbb{Z}^+ \cup \{0\}$ ). Several features can be seen. Firstly, as the frequency increases from  $\omega = 5$  to 25, the functions become flattened out in the middle region of  $x$  and squeezed out towards the edges. Since the value of  $q$  is

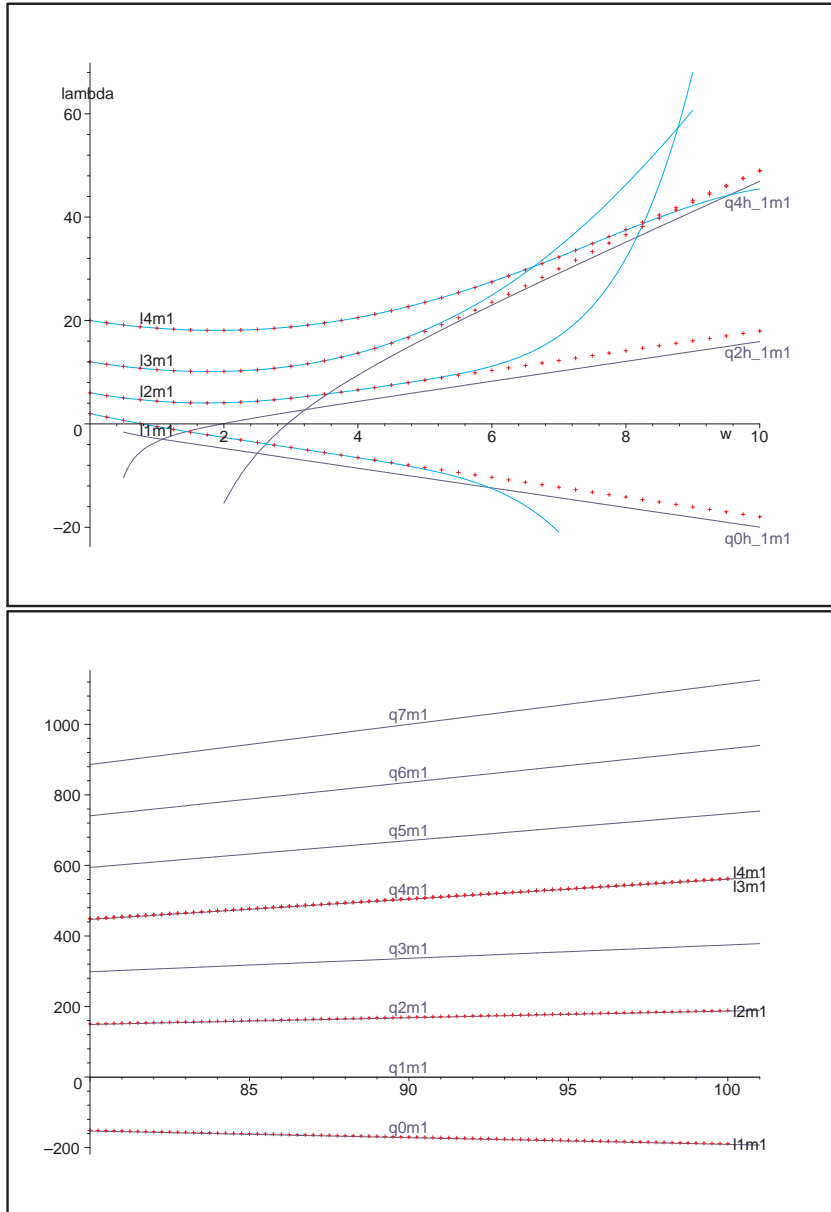


Figure 5.2:  $-1\lambda_{l,1,\omega}$  as a function of  $\omega$  for several  $l$  and  $q$ . The red crosses are the numerical data. The navy blue lines are using BRW's expansion for  ${}_h\lambda_{lm\omega}$  and the light blue lines are Press and Teukolsky's.

## 5.8. Numerical results

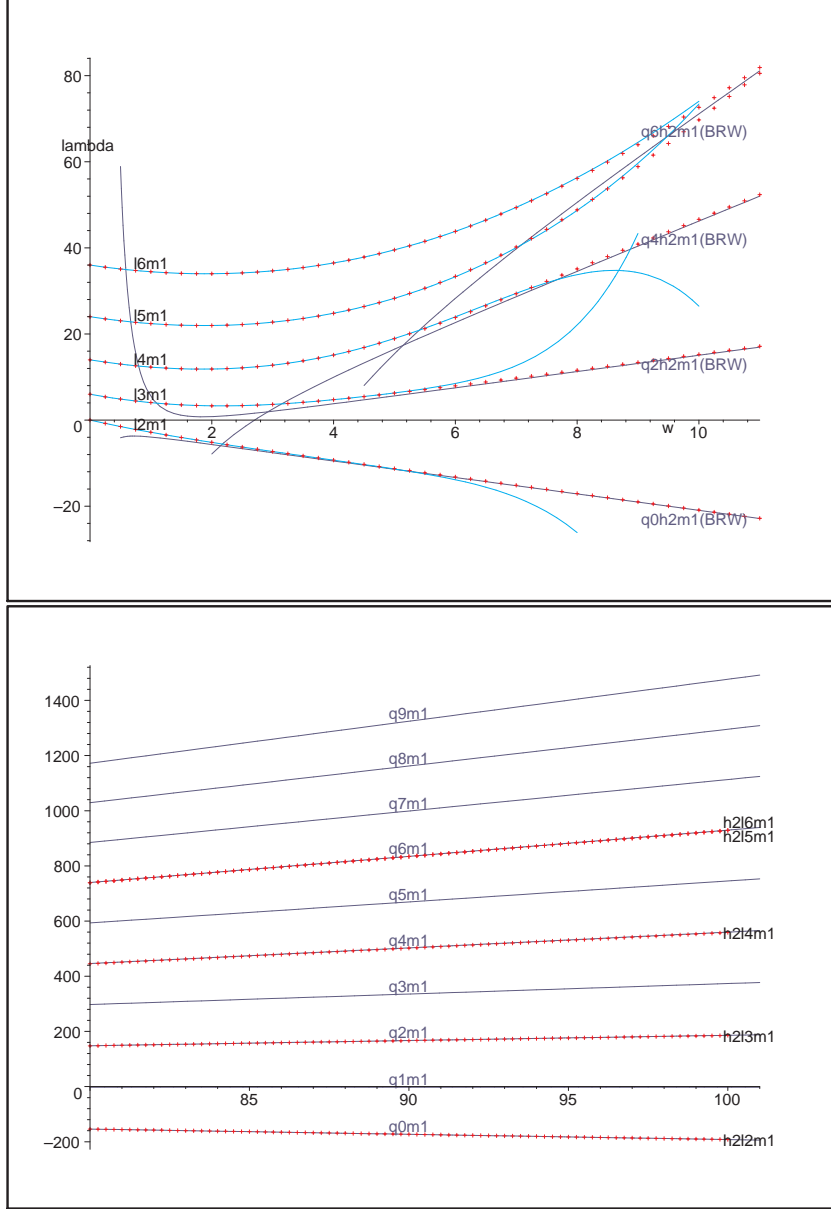


Figure 5.3:  $+2\lambda_{l,1,\omega}$  as a function of  $\omega$  for several  $l$  and  $q$ . The red crosses are the numerical data. The navy blue lines are using BRW's expansion for  ${}_h\lambda_{lm\omega}$  and the light blue lines are Press and Teukolsky's.

## 5.8. Numerical results

---

the same for both cases, the inner solution is the same for both of them, with the only exception of the relative sign between the inner solution for positive  $x$  and negative  $x$  (5.5.10). The function for  $l = 4$  has three zeros and the one for  $l = 3$  has two (see Theorem 1). The inner solution provides for the two zeros of  $l = 3$  and the corresponding two of  $l = 4$ , and these become closer to the boundary point  $x = +1$  as the frequency increases. The extra zero of  $l = 4$  comes from the outer solution and becomes closer to  $x = 0$  with increasing frequency.

In Figures 5.5–5.7 the lines labelled as ‘inner’ have been obtained with (5.3.7), the ones labelled ‘outer’ with (5.4.12), the ones labelled ‘uniform’ with (5.5.14) and the ones labelled ‘numerics’ with the programs described in Section 5.7. These figures show that the outer (normalized to agree with the numerical data at  $x = 0$ ), inner (normalized to agree with the numerical data at  $x = \pm 0.96$ ) and uniform (also normalized to agree with the numerical data at  $x = 0$ ) solutions approximate the numerical data for  $\omega = 25$  in the boundary layers and in the neighbourhood of  $x = 0$ . The outer solution is valid until the boundary point  $x = -1$  but not until  $x = +1$  since the function has two zeros close to it and the outer solution cannot cater for them, whereas the uniform solution is a valid approximation for all  $x$ . The inner solutions, on the other hand, prove to be a good approximation in the boundary layers but not close to  $x = 0$ .

Figures 5.8 and 5.9 prove equation (5.5.10) to be correct for the case  $m \geq 1$ : for the specific values  $h = -1$ ,  $l = 4$ ,  $m = 1$  and  $q = 4$  the inner solution (5.3.7) has been normalized to match the numerical data at the points  $x = \pm 0.998$  for different values of the frequency from 5 to 25, in order to be able to calculate  ${}_{-1}D_{4,1,\omega}$ ,  ${}_{-1}C_{4,1,\omega}$  and  ${}_{-1}D_{4,1,\omega}/{}_{-1}C_{4,1,\omega}$ . When plotting this numerical ratio together with the analytical result (5.5.10), the two lines are parallel and therefore agree to highest order, and the ratio between the numerical and the analytical data tends to 1.

Figures 5.10–5.15 correspond to modes with  $h = +2$ ,  $m = 1$ ,  $\omega = 35$  and  $l = 5$  or  $l = 6$ . The modes for both values of  $l$  yield  $q = 6$ . However, the mode with



## 5.8. Numerical results

---

$l = 5$  does not possess a zero at  $x_0$  whereas the mode with  $l = 6$  does. The behaviour for positive  $x$  is very similar for both values of  $l$  but for negative  $x$  the behaviours for the two modes differ by a sign.

For  $h = -1$ ,  $l = 2$ ,  $m = 1$  and  $\omega = 100$ , the corresponding value of  $q$  is 2. This is a case where  $p \in \mathbb{Z}^+ \cup \{0\}$  and  $p' \notin \mathbb{Z}^+ \cup \{0\}$ . The numerical solution together with the uniform expansion (5.5.9) is plotted over the whole range  $x \in [-1, 1]$  in Figures 5.18–5.20.

As we have seen, in this case the function has an exponential behaviour far from the boundary layers, so that a plot of the log of the function allows us to see the behaviour over the whole range of  $x$ . Both the uniform expansion and the outer solution have been normalized so that they coincide with the numerical value at  $x = 0$ , and the inner solution has been normalized once at  $x = 10^{-8}$  and once at  $x = -10^{-8}$ . The uniform expansion agrees with the numerical solution for all values of  $x$ . The outer solution agrees with the numerics everywhere except very close to  $x = \pm 1$ , where it veers off. The inner solutions are valid all the way from their respective boundary layers until, and past,  $x = 0$ , which is due to the exponential nature of the function in the region between the boundary layers. The inner solutions show a jump at  $x = 0$  due to the different orders in  $c$  of  ${}_h C_{lm\omega}$  and  ${}_h D_{lm\omega}$ .

The above features can be seen in detail for  $x$  close to 0 and  $\pm 1$  in Figures 5.21–5.23 where they have been rescaled by  $10^{40}$  for  $x$  close to 0 and  $-1$ .

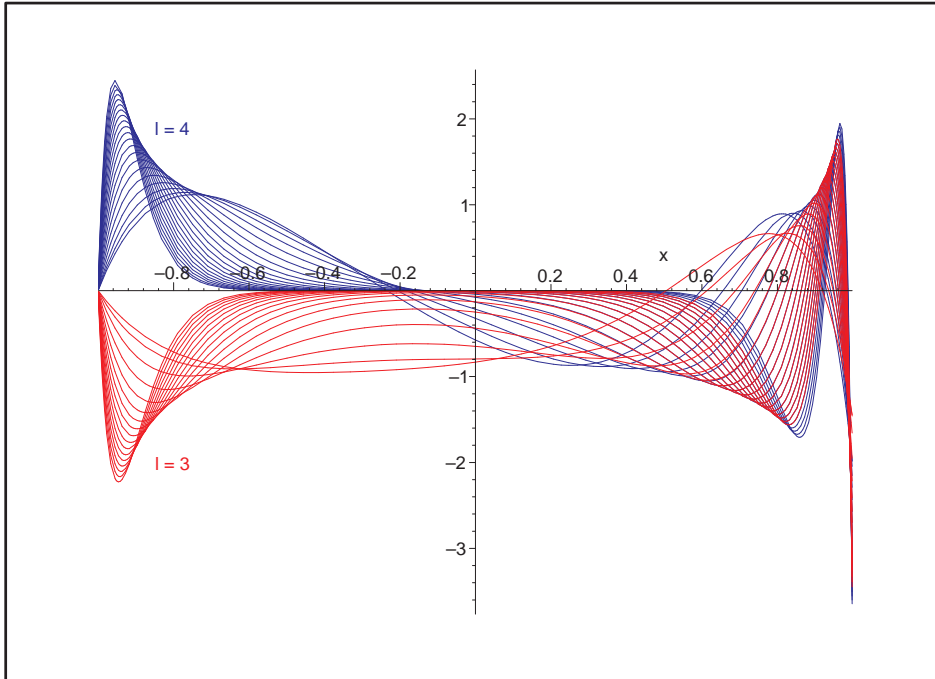


Figure 5.4:  $-1S_{l,1,\omega}$  for  $l = 3$  &  $4$ ,  $\omega = 5 \rightarrow 25$ . Blue lines correspond to  $l = 4$  and the red ones to  $l = 3$ . As  $\omega$  increases the curves become increasingly flattened out in the region close to the origin.

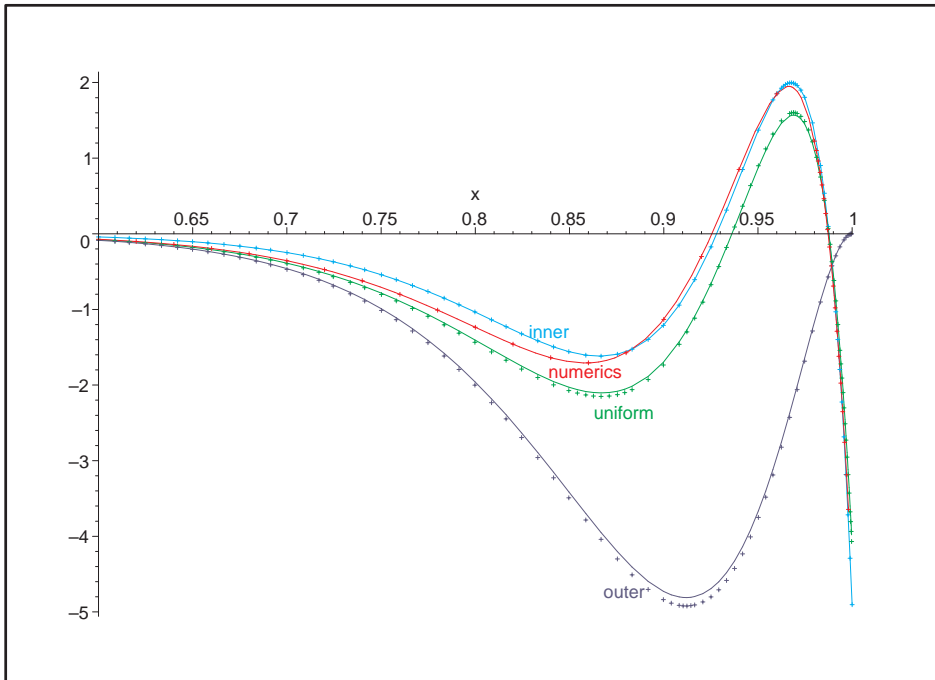


Figure 5.5:  $-1S_{l,1,25}$  for  $l = 3$  &  $4$ . Different solutions as labeled. The continuous lines correspond to  $l = 4$  and the dotted ones to  $l = 3$ .

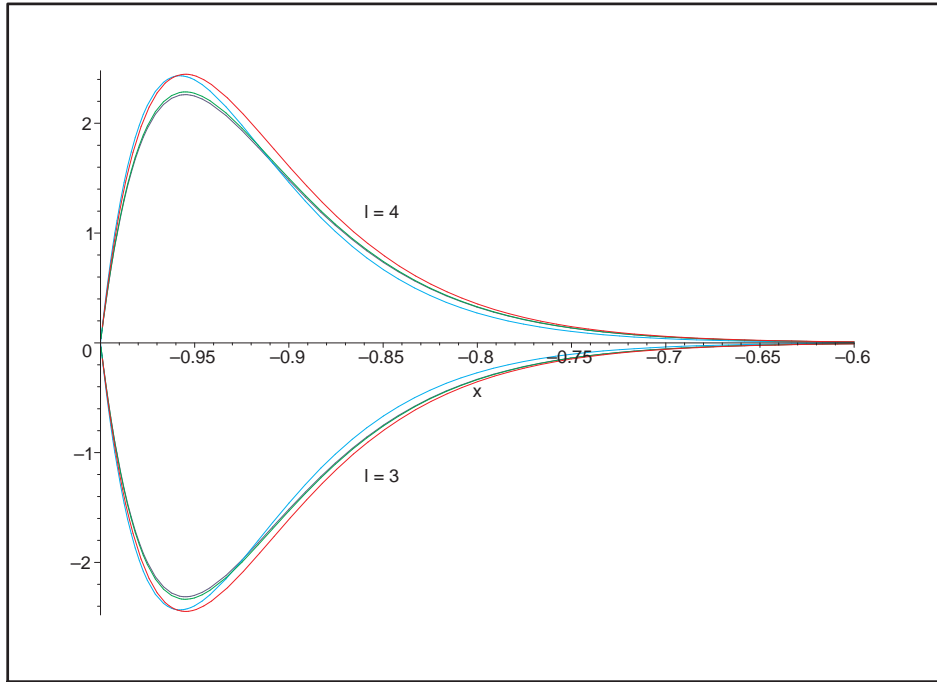


Figure 5.6:  $-1S_{l,1,25}$  for  $l = 3$  & 4. The curves above the  $x$ -axis correspond to  $l = 4$  and below the axis to  $l = 3$ . Correspondence between colours and solutions is the same as in Figure 5.5.

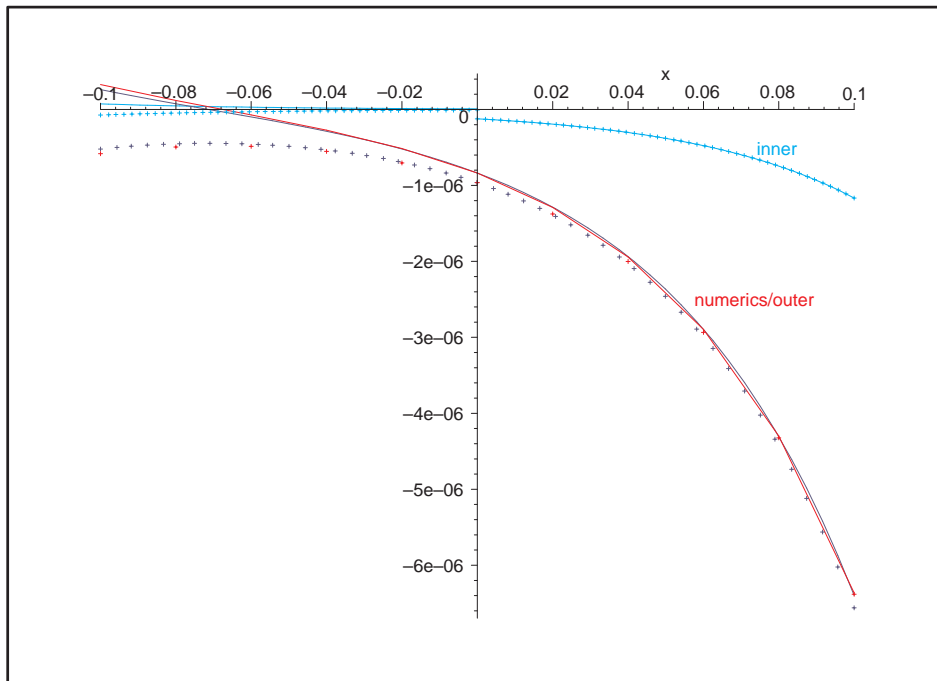


Figure 5.7:  $-1S_{l,1,25}$  for  $l = 3$  & 4. The continuous lines correspond to  $l = 4$  and the dotted ones to  $l = 3$ . Correspondence between colours and solutions is the same as in Figure 5.5.

## 5.8. Numerical results

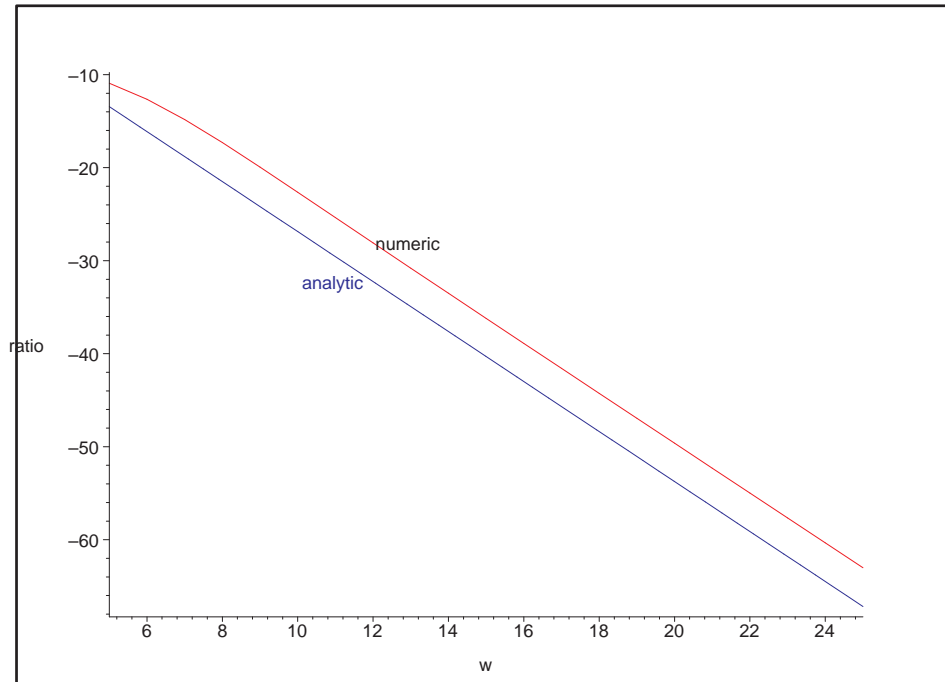


Figure 5.8:  $\frac{-1D_{4,1,\omega}}{-1C_{4,1,\omega}}$  for  $\omega = 5 \rightarrow 25$ . The slope of the analytic curve is given by the leading order behaviour (5.5.10). The shift between the two curves is due to lower order,  $O(1)$ , terms.

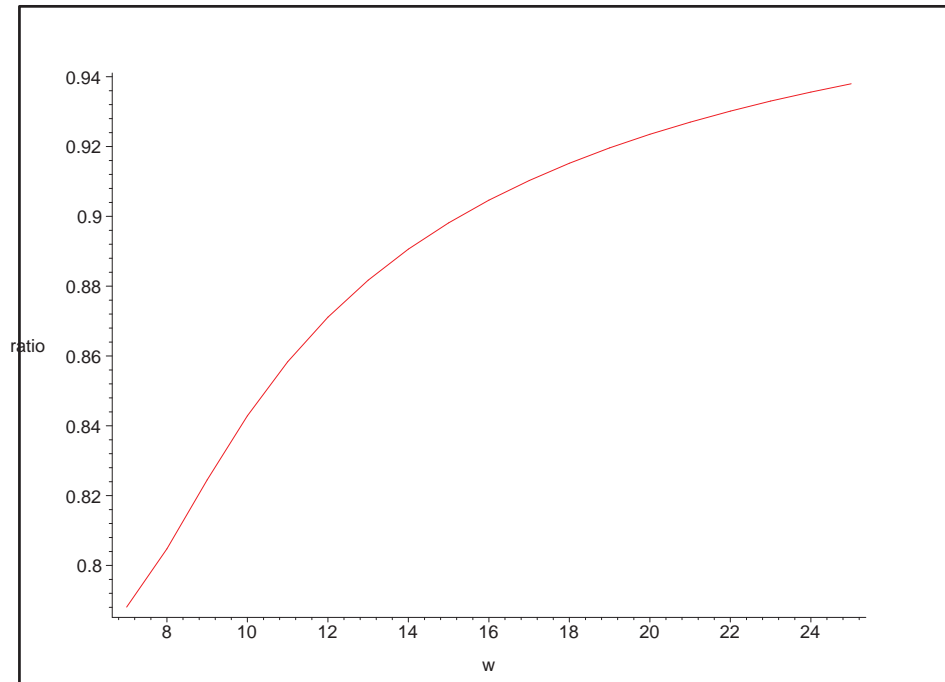


Figure 5.9: Ratio between numeric and analytic values of  $\frac{-1D_{4,1,\omega}}{-1C_{4,1,\omega}}$ . The analytic values have been obtained with (5.5.10).

## 5.8. Numerical results

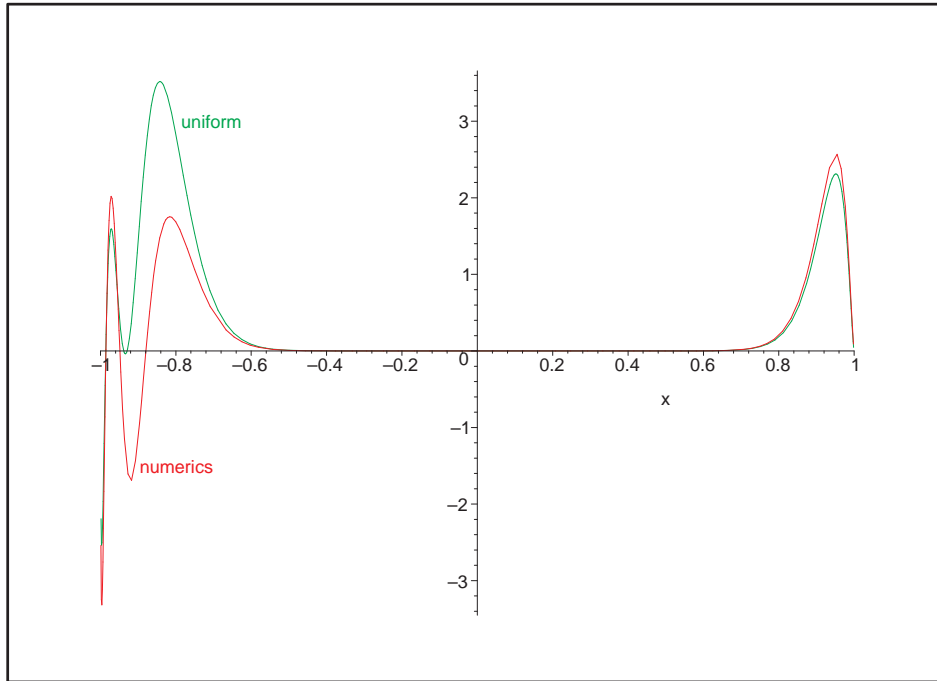


Figure 5.10:  $+2S_{5,1,35}$ . Green line corresponds to uniform solution (5.5.14) and red line to numerics.

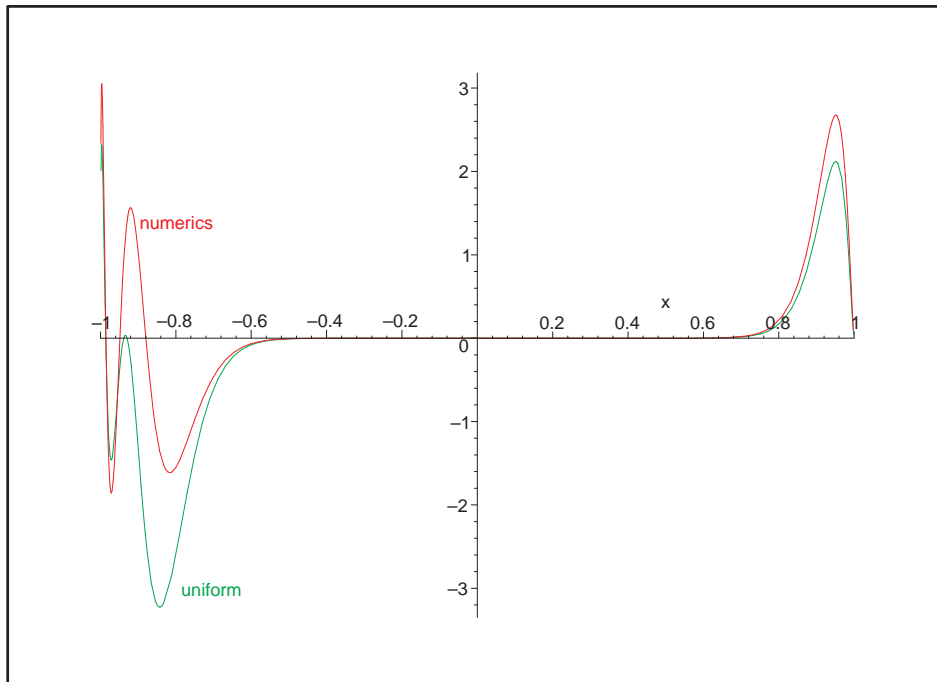


Figure 5.11:  $+2S_{6,1,35}$ . Green line corresponds to uniform solution (5.5.14) and red line to numerics.

## 5.8. Numerical results

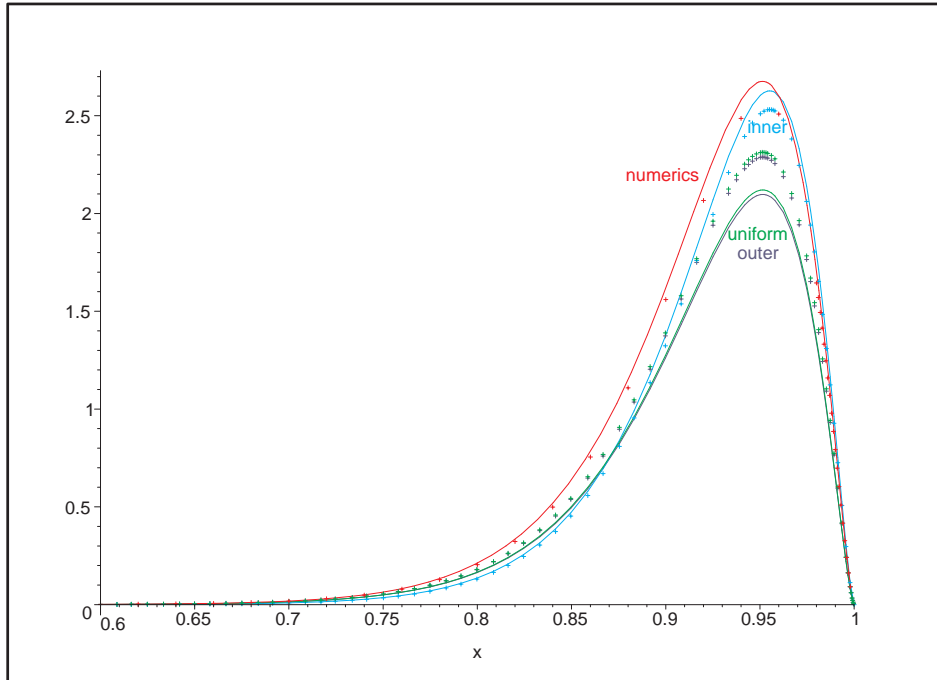


Figure 5.12:  $+_2S_{l,1,35}$  for  $l = 5$  &  $6$ . The continuous lines correspond to  $l = 6$  and the dotted ones to  $l = 5$ . Correspondence between colours and solutions is the same as in Figure 5.5.

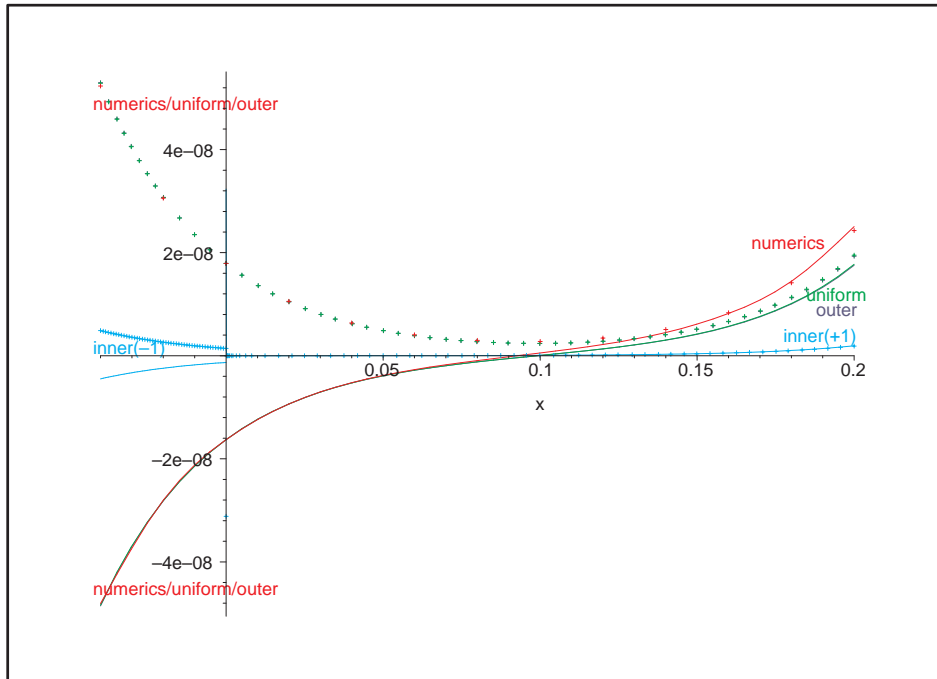


Figure 5.13:  $+_2S_{l,1,35}$  for  $l = 5$  &  $6$ . The continuous lines correspond to  $l = 6$  and the dotted ones to  $l = 5$ . Correspondence between colours and solutions is the same as in Figure 5.5.

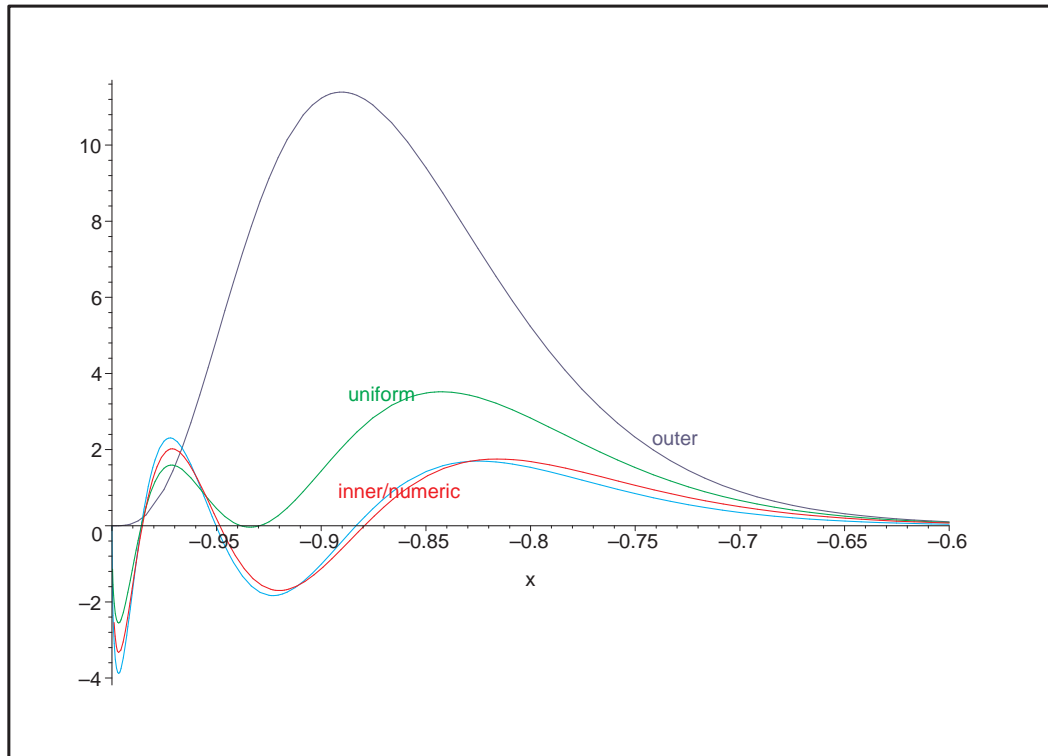


Figure 5.14:  $+2S_{5,1,35}$ . Correspondence between colours and solutions is the same as in Figure 5.5.

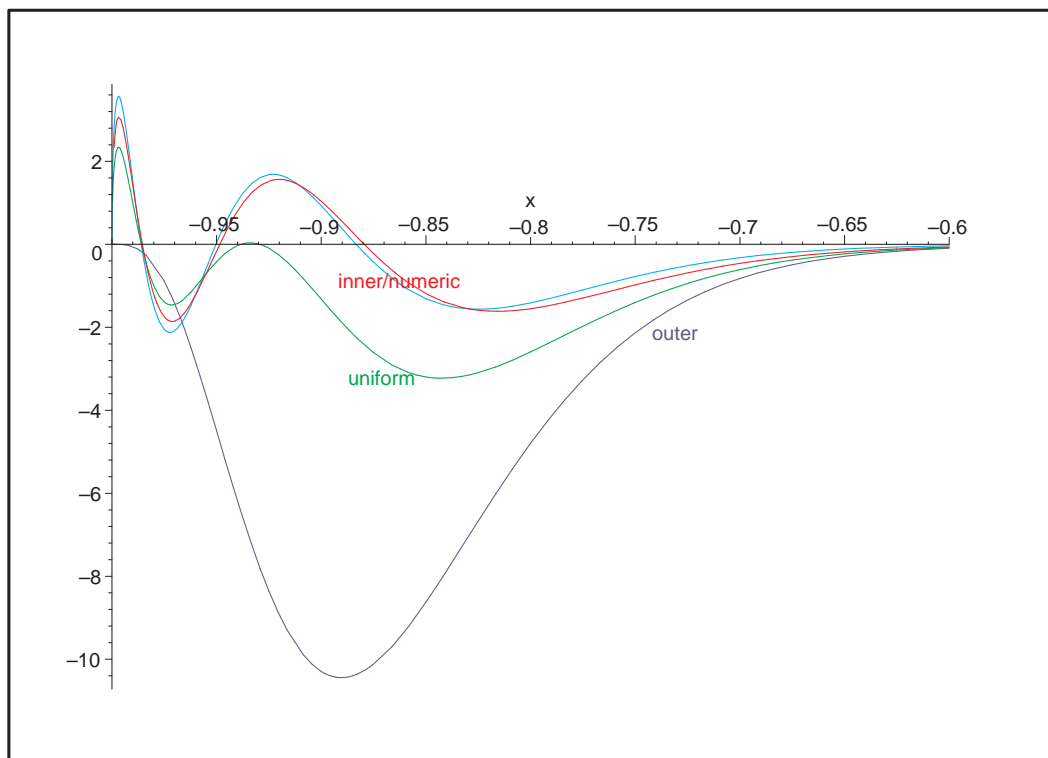


Figure 5.15:  $+2S_{6,1,35}$ . Correspondence between colours and solutions is the same as in Figure 5.5.

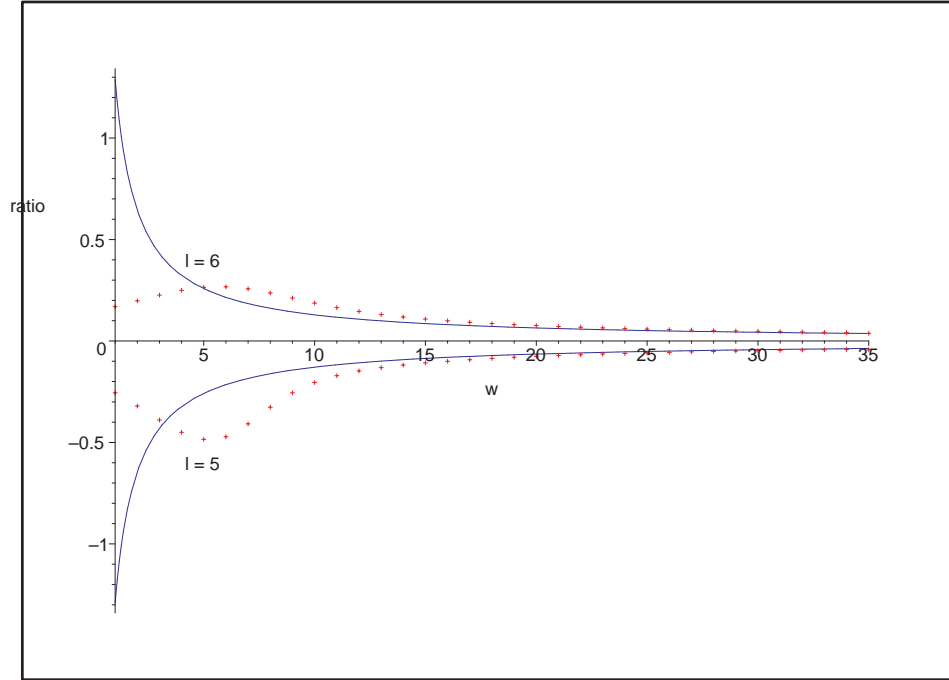


Figure 5.16:  $\frac{-1D_{4,1,\omega}}{-1C_{4,1,\omega}}$  for  $\omega = 1 \rightarrow 35$ . The curves above the x-axis correspond to  $l = 6$  and below to  $l = 5$ . The continuous lines correspond to the analytic expression (5.5.11) and the dotted ones to the numerical data.

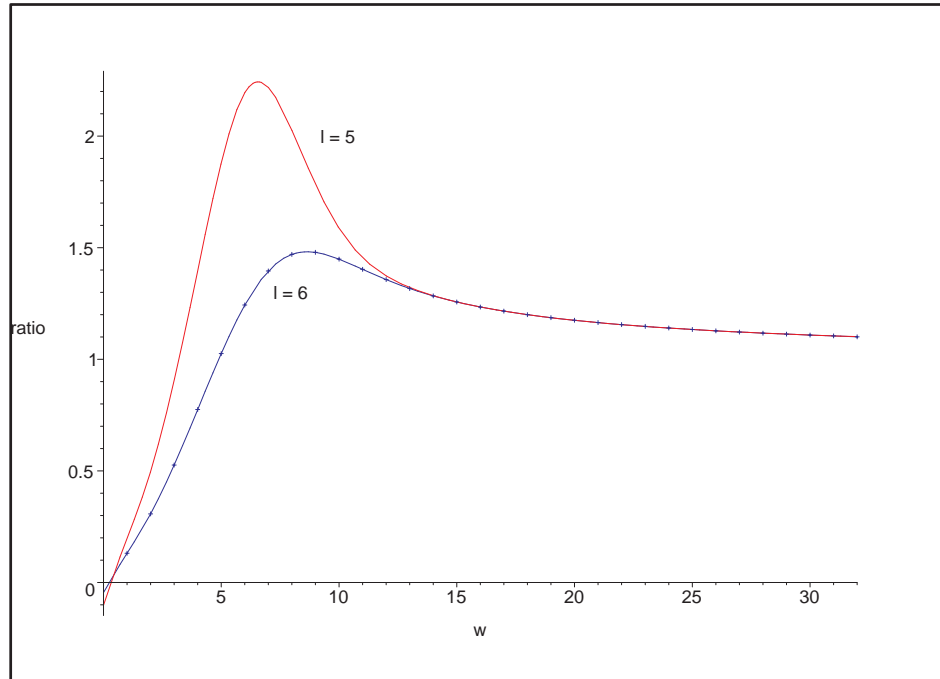


Figure 5.17: Ratio between numeric and analytic values of  $\frac{+2D_{l,1,\omega}}{+2C_{l,1,\omega}}$  for  $\omega = 1 \rightarrow 34$ . Blue lines (plotted both continuous and dotted to show agreement with red line for large  $\omega$ ) correspond to  $l = 6$  and red line to  $l = 5$ .



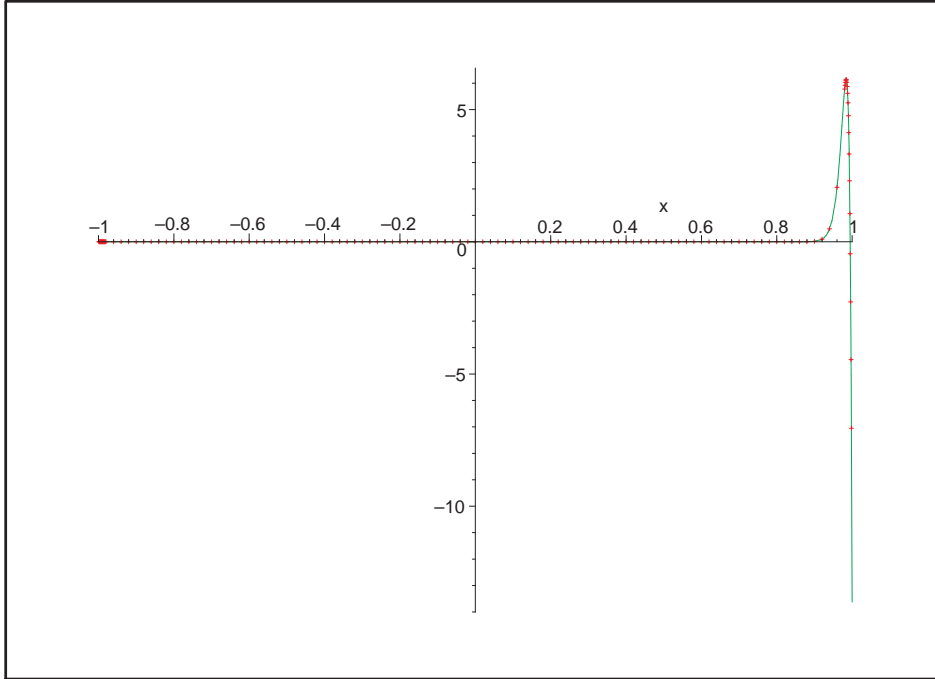


Figure 5.18:  $-_1S_{2,1,100}$ . The continuous, green line corresponds to the uniform solution (5.5.9) and the dotted, red one to the numerical data

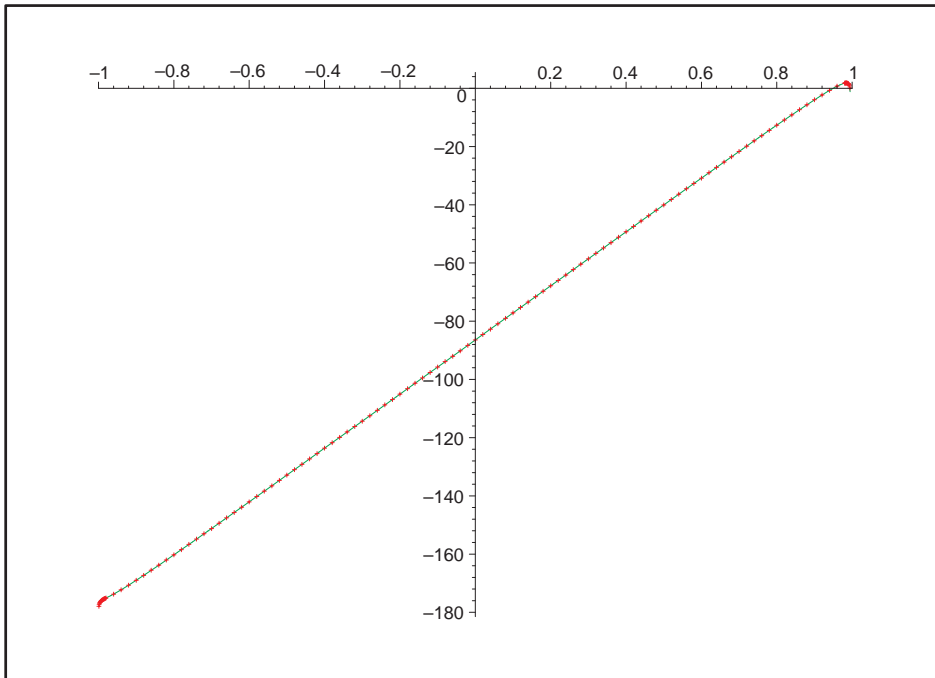


Figure 5.19:  $\log(-_1S_{2,1,100})$ . The continuous, green line corresponds to the uniform solution (5.5.9) and the dotted, red one to the numerical data

## 5.8. Numerical results

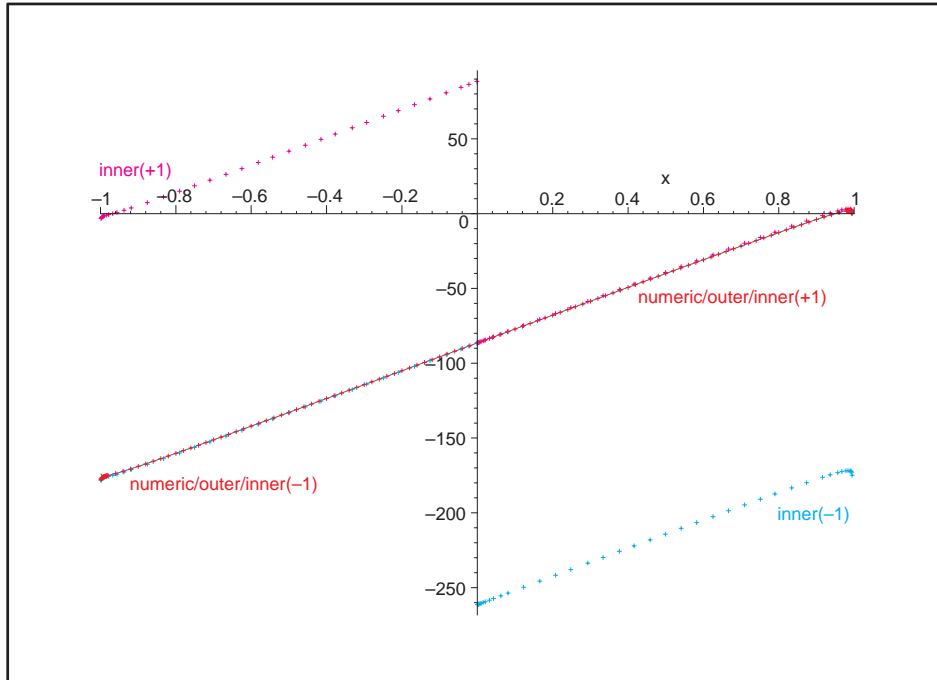


Figure 5.20:  $\log(-_1S_{2,1,100})$ . The red line (numerical data) overlaps with the navy line (outer solution). The light blue line (inner solution valid at  $x \sim -1$ ) and the magenta line (inner solution valid at  $x \sim +1$ ) overlap with the red/navy lines for negative and positive  $x$  respectively.

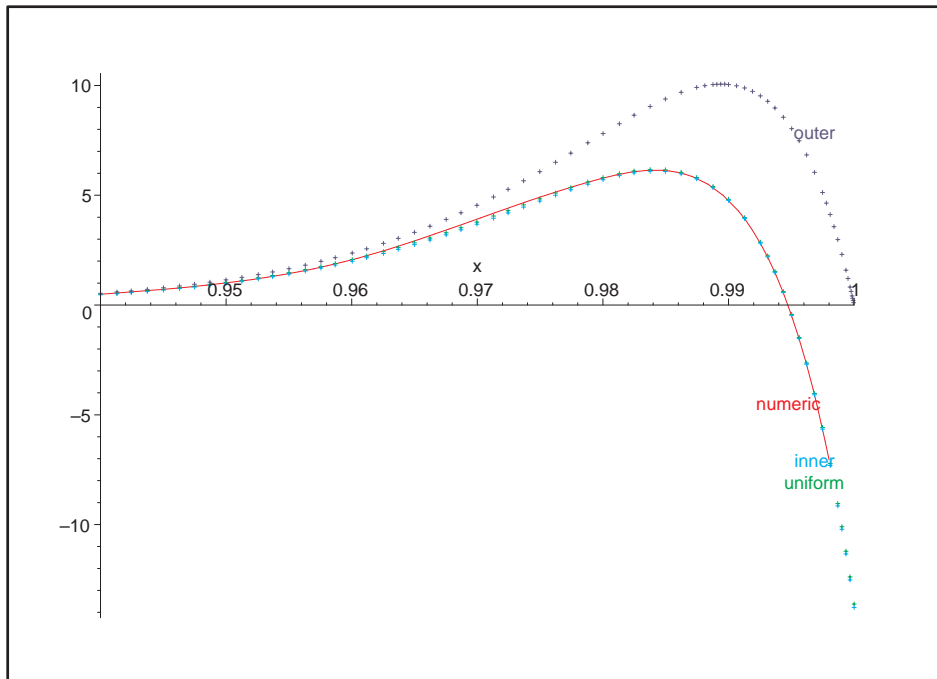


Figure 5.21:  $-_1S_{2,1,100}$ . The numeric (continuous, red), inner (light blue) and uniform (green) solutions overlap close to  $x = +1$ .

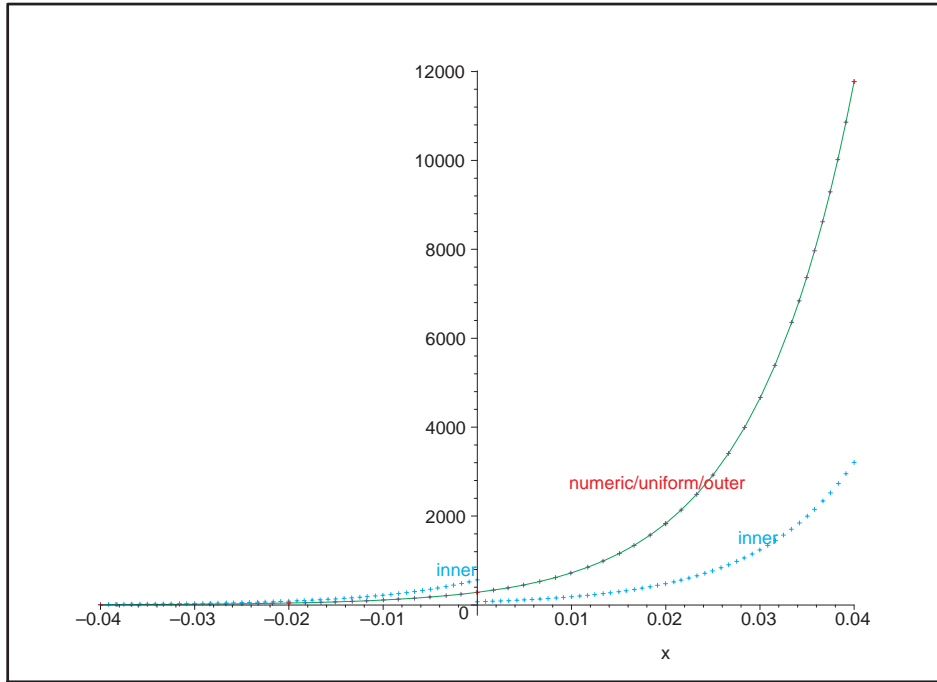


Figure 5.22:  $10^{40} {}_{-1}S_{2,1,100}$ . The numeric (red), outer (navy) and uniform (continuous, green) solutions overlap close to  $x = 0$ .

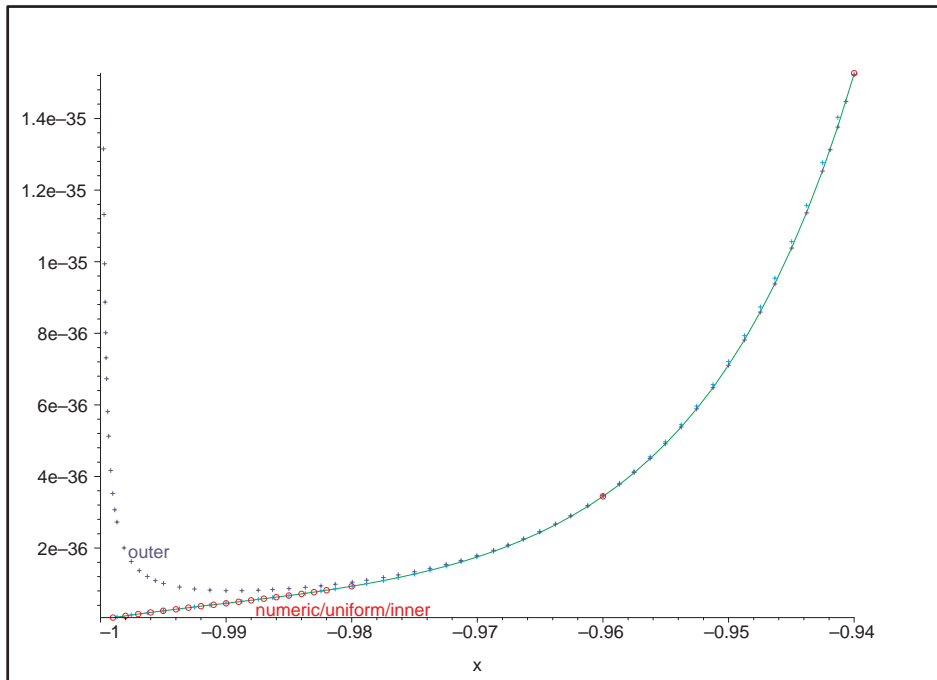


Figure 5.23:  $10^{40} {}_{-1}S_{2,1,100}$ . The numeric (red circles), inner (light blue crosses) and uniform (continuous, green) solutions overlap close to  $x = -1$ .

# Chapter 6

## Stress-energy tensor

### 6.1 Introduction

This chapter is restricted to the uncharged case  $Q = 0$  for definiteness. Most of the results presented in this chapter do also apply to the Kerr-Newman space-time, which we will on occasion point out, and the programs we have developed may perform the calculations in this space-time merely by setting  $Q \neq 0$ . However, all results in the literature that we refer to in this chapter focus on the Kerr (or Schwarzschild) space-time; most notably the construction of the various physical states as well as a paper that is central to this thesis, [14].

This chapter is organized as follows. In Section 6.2 we provide a canonical quantization of the electromagnetic potential and field.

In the following three sections we give a description of the main physical states on the Schwarzschild and Kerr space-times. Most of these descriptions relate to the scalar field. We particularly focus on the various attempts in the literature to construct states on the Kerr space-time with the same defining features as the Hartle-Hawking state on Schwarzschild.

In Section 6.6 we give expressions for the expectation value of the electromag-

netic field in the Kerr space-time, originally given in Candelas, Chrzanowski and Howard [14], hereafter referred to as CCH. We also present the results from numerical calculations of differences between two states of the renormalized expectation value of the stress-energy tensor (abbreviated as RSET).

In the subsequent section we endeavor to calculate the luminosity of the Kerr black hole in the past Boulware and past Unruh states for the spin-1 case. We discuss the difficulties in the calculation and the differences with respect to the scalar case.

In Section 6.8 we study the form of the RSET close to the horizon when the field is in the past Boulware state. CCH show a form of this RSET which is not exactly (minus) thermal. We rederive CCH's analytic result, show why it is incorrect and compare it against our numerical results. We also study the rate of rotation of this RSET, for which there is no unanimous consensus in the literature.

We initially used expressions given by CCH for the expectation value of the stress-energy tensor when the field is in various states in order to calculate differences between two states of the RSET. The results, both analytically and numerically were not symmetric under the parity operation  $\mathcal{P} : (\theta, \phi) \rightarrow (\pi - \theta, \phi + \pi)$ . This is the topic of the last section. It is split into three subsections. In the first one we show that this lack of symmetry is indeed present. In the second subsection we see that the reason for its presence are incorrect expressions given by CCH. We derive the correct expressions for the expectation value of the stress-energy tensor when the electromagnetic field is in the main physical states in the Kerr space-time. In the last subsection we give a physical interpretation of the various sets of terms appearing in the expectation value of the stress-energy tensor when the field is in different states.

All figures in this chapter have been obtained for the values:  $Q = 0$ ,  $a = 0.95M$  and  $M = 1$ . Note that the Boyer-Lindquist radius of the event horizon for such values of the black hole parameters is  $r_+ \simeq 1.3122$ .

## 6.1. Introduction

---

Before finishing this introductory section, we will derive the classical stress-energy tensor of the theory. Einstein's field equations, which describe the generation of space-time curvature by energy, are

$$R_{\mu\nu} - \frac{1}{2}Rg_{\mu\nu} + \Lambda g_{\mu\nu} = +8\pi T_{\mu\nu} \quad (6.1.1)$$

where  $\Lambda$  is the cosmological constant. We may construct the total action

$$S = S_g + S_m \quad (6.1.2)$$

where  $S_g$  refers to the gravitational action and  $S_m$  includes the contribution from the matter fields. If the gravitational action is given by

$$S_g = \frac{1}{16\pi} \int_{\mathcal{M}} (R - 2\Lambda) \sqrt{-g} d^4x \quad (6.1.3)$$

where  $\mathcal{M}$  is a fixed space-time, and the action  $S_m$  is related to the stress-energy tensor by

$$\frac{2}{\sqrt{-g}} \frac{\delta S_m}{\delta g^{\mu\nu}} = T_{\mu\nu} \quad (6.1.4)$$

then Einstein's field equations may be derived by imposing that the total action  $S$  satisfies the condition

$$\frac{2}{\sqrt{-g}} \frac{\delta S}{\delta g^{\mu\nu}} = 0 \quad (6.1.5)$$

It is clear that, except for a factor, the imposition of this condition to only the gravitational action  $S_g$  instead of  $S$  yields the left hand side of (6.1.1), whereas imposing it to only the action  $S_m$  yields the right hand side of the equation.

In this thesis we are interested in the case where the only matter field present is the electromagnetic field. Therefore, in this thesis, the action  $S_m$  is equal to the electromagnetic action  $S_{em}$ . The electromagnetic action must yield the Maxwell field equations (2.3.1) via the Euler-Lagrange equations, which result from requiring the electromagnetic action to be stationary under an infinitesimal variation of the fields:

$$\frac{\delta S_{em}}{\delta A_\mu(x)} = 0 \quad (6.1.6)$$

## 6.1. Introduction

---

The simplest electromagnetic action which leads to the Maxwell field equations via the Euler-Lagrange equations is

$$S_{em} = \int_{\mathcal{M}} \mathcal{L}_{em}(x) d^4x \quad (6.1.7)$$

with the electromagnetic Lagrangian

$$\mathcal{L}_{em}(x) = \left( -\frac{1}{4} F_{\alpha\beta} F^{\alpha\beta} - J_{\alpha} A^{\alpha} \right) \sqrt{-g} \quad (6.1.8)$$

Although in the absence of a charge current the Maxwell lagrangian  $\mathcal{L}_{em}$  is gauge-invariant, in the presence of a charge current it is not: under a gauge transformation (2.3.7) it acquires a new, pure-divergence term, which does not alter the field equations by virtue of the law of current conservation.

We will restrict ourselves to the case of absence of a charge current. The electromagnetic stress-energy tensor  $T^{\mu\nu}$  is calculated from the action (6.1.7) using (6.1.4), and the result is

$$T^{\mu\nu} = \frac{1}{4} g^{\mu\nu} F_{\alpha\beta} F^{\alpha\beta} - F^{\mu\alpha} F_{\alpha}^{\nu} \quad (6.1.9)$$

in the absence of sources. This form for the stress-energy tensor is gauge-invariant, conserved, symmetric and traceless.

By virtue of the Maxwell field equations, the stress-energy tensor (6.1.9) satisfies the following *conservation equation*

$$T^{\mu\nu}{}_{;\mu} = 0 \quad (6.1.10)$$

The classical, electromagnetic stress-energy tensor (6.1.9) can be expressed in terms of the NP Maxwell scalars as

$$\begin{aligned} T_{\mu\nu} = & \left\{ \phi_{-1} \phi_{-1}^* n_{\mu} n_{\nu} + 2\phi_0 \phi_0^* [l_{(\mu} n_{\nu)} + m_{(\mu} m_{\nu)}^*] + \phi_{+1} \phi_{+1}^* l_{\mu} l_{\nu} - \right. \\ & \left. - 4\phi_0 \phi_{-1}^* n_{(\mu} m_{\nu)} - 4\phi_{+1} \phi_0^* l_{(\mu} m_{\nu)} + 2\phi_{+1} \phi_{-1}^* m_{\mu} m_{\nu} \right\} + c.c. \end{aligned} \quad (6.1.11)$$

Note that it follows from (1.3.13) that all the pairs of null tetrad vectors appearing in the different terms in (6.1.11) remain invariant under the parity operation,

## 6.2. Quantization of the electromagnetic potential/field

---

except for the ones that have a factor containing  $\phi_0$  together with either  $\phi_{-1}$  or  $\phi_{+1}$ , which change sign. That is, a pair of null vectors  $e_{(a)}e_{(b)}$  appearing in (6.1.11) with a factor  $\phi_h\phi_{h'}^*$  changes under the parity operation as

$$\mathcal{P}(e_{(a)}e_{(b)}) = (-1)^{h+h'} e_{(a)}e_{(b)} \quad (6.1.12)$$

## 6.2 Quantization of the electromagnetic potential/field

The abundance in the literature of the quantization of the scalar field in a curved background is in sharp contrast with the scarce treatment of the quantization of the electromagnetic -or gravitational- field in such a background. In particular, the definitions of the various states that we shall give in the following three sections have all been done in relation to the scalar case. CCH did quantize both the electromagnetic and the gravitational fields in the Kerr background. They used a canonical quantization method, which is the one we have chosen to use in this thesis.

The terminology we will use is the following. As until now, a bullet (and a primed bullet) superscript indicates either ‘in’ or ‘up’ modes. Correspondingly, the symbol  $\omega^\bullet$  is defined as being equal to  $\omega$  when it is part of an expression containing ‘in’ modes and it is equal to  $\tilde{\omega}$  when the expression contains ‘up’ modes. We will refer to the ‘ingoing’ and ‘upgoing’ gauge potentials with the corresponding superscript, rather than with the notation in Chapter 2 of a  $\pm 1$  subindex. The variable  $\Gamma$  refers to either the potential components  $A_\mu$  or the NP scalars  $\phi_h$ .

Notice first that the symmetry property

$$\mathcal{P}_{lm\omega} A_\mu^\bullet = (-1)^{l+m} {}_{l-m-\omega} A_\mu^{\bullet*} \quad (6.2.1)$$

which is easily obtained from (3.1.3b), (4.2.1c) and (2.7.13), leads to the following



## 6.2. Quantization of the electromagnetic potential/field

---

expression for the potential modes (2.7.14b):

$${}_{lm\omega P}A_\mu^\bullet = {}_{lm\omega}A_\mu^\bullet + P\mathcal{P}{}_{lm\omega}A_\mu^\bullet \quad (6.2.2)$$

This was actually Chrzanowski's [25] starting point for the derivation of the potential modes, as referred to in Section 2.7. The decomposition of the potential into eigenstates of the parity operator  $\mathcal{P}$  is the natural choice because of the invariance of the Kerr metric under this operation. Note that this also applies to the Kerr-Newman solution, as both its metric and the Maxwell's equations are invariant under  $\mathcal{P}$ .

With the above definitions the Fourier series expansion for either the potential components or the NP Maxwell scalars may be expressed as

$$\Gamma^\bullet = \sum_{lmP} \int_{-\infty}^{+\infty} d\omega^\bullet {}_{lm\omega P}a^\bullet {}_{lm\omega P}\Gamma^\bullet \quad (6.2.3)$$

where  ${}_{lm\omega P}a^\bullet$  are the coefficients of the Fourier series. This Fourier series may be re-arranged as

$$\Gamma^\bullet = \sum_{lmP} \int_0^{+\infty} d\omega^\bullet \left( {}_{lm\omega P}a^\bullet {}_{lm\omega P}\Gamma^\bullet + (-1)^{l+m} P {}_{lm\omega P}a^{\bullet*} {}_{l-m-\omega P}\Gamma^\bullet \right) \quad (6.2.4)$$

We can now use the symmetry relations

$$\mathcal{P}{}_{lm\omega P}A_\mu^\bullet = (-1)^{l+m} {}_{l-m-\omega P}A_\mu^{\bullet*} = P {}_{lm\omega P}A_\mu^\bullet \quad (6.2.5a)$$

$$\mathcal{P}{}_{lm\omega}\phi_h^\bullet = (-1)^{l+m+1+h} {}_{l-m-\omega}\phi_h^{\bullet*} \quad (6.2.5b)$$

where the property that  $\mathcal{P}^2$  is the identity operator was used in (6.2.5a). The equations above for  $\Gamma$  are equally valid for  $A_\mu$  and  $\phi_h$ . In particular, we only need to apply the operator  $K_h^{(a)}e_{(a)}^\mu$  (which is explicitly given in (2.4.3)) to an equation for  $A_\mu$  in order to obtain the corresponding equation for  $\phi_h$ . However the last step in (6.2.5a) has no equivalent for  $\phi_h$  in (6.2.5b). The reason is that

$$\left( K_h^{(a)}e_{(a)}^\mu \right) \mathcal{P}{}_{lm\omega}A_\mu^\bullet \propto \left( K_h^{(a)}e_{(a)}^\mu \right) {}_{l-m-\omega}A_\mu^{\bullet*} \equiv 0 \quad (6.2.6)$$

as can be checked; that is, this term is pure gauge. Hence the fact that  ${}_{lm\omega}\phi_h^\bullet = \left( K_h^{(a)}e_{(a)}^\mu \right) {}_{lm\omega P}A_\mu^\bullet$  does not actually depend on  $P$  and that is why  $P$  is not

## 6.2. Quantization of the electromagnetic potential/field

---

a subindex of the NP scalar modes. The potential is real whereas the field components are not, as seen in equations (6.2.7) and (6.2.8) below. From (6.2.4) and using (6.2.5a) and (6.2.5b) for the potential and the field respectively, we have

$$\begin{aligned} A_\mu^\bullet &= \sum_{lmP} \int_0^{+\infty} d\omega^\bullet ({}_{lm\omega P}a^\bullet {}_{lm\omega P}A_\mu^\bullet + P {}_{lm\omega P}a^{\bullet*} \mathcal{P} {}_{lm\omega P}A_\mu^{\bullet*}) = \\ &= \sum_{lmP} \int_0^{+\infty} d\omega^\bullet ({}_{lm\omega P}a^\bullet {}_{lm\omega P}A_\mu^\bullet + {}_{lm\omega P}a^{\bullet*} {}_{lm\omega P}A_\mu^{\bullet*}) \end{aligned} \quad (6.2.7)$$

and

$$\phi_h^\bullet = \sum_{lmP} \int_0^{+\infty} d\omega^\bullet ({}_{lm\omega P}a^\bullet {}_{lm\omega P}\phi_h^\bullet + (-1)^{h+1} P {}_{lm\omega P}a^{\bullet*} \mathcal{P} {}_{lm\omega P}\phi_h^{\bullet*}) \quad (6.2.8)$$

We now quantize the field by promoting  ${}_{lm\omega P}a^\bullet$  and  ${}_{lm\omega P}a^{\bullet*}$  to operators  ${}_{lm\omega P}\hat{a}^\bullet$  and  ${}_{lm\omega P}\hat{a}^{\bullet\dagger}$  respectively. It became apparent in Chapter 2 that the whole theory may be expressed in terms of one single NP complex scalar, which represents the two radiative degrees of freedom of the electromagnetic perturbations. If we introduce expansion (6.2.8) for the NP scalars into  $T^{00}$  given by (6.1.11), we then obtain a hamiltonian which is a superposition of independent harmonic oscillator hamiltonians, one for each mode of the electromagnetic field. From the standard quantization of the harmonic oscillator, we know that the operators  ${}_{lm\omega P}\hat{a}^\bullet$  and  ${}_{lm\omega P}\hat{a}^{\bullet\dagger}$  must satisfy the commutation relations:

$$\begin{aligned} [\hat{a}_{lm\omega P}^\bullet, \hat{a}_{l'm'\omega'P'}^{\bullet\dagger}] &= \delta(\omega - \omega') \delta_{ll'} \delta_{mm'} \delta_{PP'} \\ [\hat{a}_{lm\omega P}^\bullet, \hat{a}_{l'm'\omega'P'}^\bullet] &= [\hat{a}_{lm\omega P}^{\bullet\dagger}, \hat{a}_{l'm'\omega'P'}^{\bullet\dagger}] = 0 \end{aligned} \quad (6.2.9)$$

These commutation relations are satisfied provided that the orthonormality conditions

$$\begin{aligned} \langle {}_{lm\omega P}A_\alpha^\bullet, {}_{l'm'\omega'P'}A_\alpha^{\bullet'} \rangle_{\mathcal{S}} &= \delta_{\bullet\bullet'} \delta_{ll'} \delta_{mm'} \delta(\omega - \omega') \delta_{PP'} \\ \langle {}_{lm\omega P}A_\alpha^{\bullet*}, {}_{l'm'\omega'P'}A_\alpha^{\bullet'} \rangle_{\mathcal{S}} &= 0 \end{aligned} \quad (6.2.10)$$

are satisfied, where  $\mathcal{S}$  is any complete Cauchy hypersurface for the outer region of the space-time and where the *Klein-Gordon inner product* is taken as

$$\langle \psi_\alpha, \varphi_\alpha \rangle_{\mathcal{S}} = i \int_{\mathcal{S}} d^3\Sigma^\mu (\psi^{\alpha*} \nabla_\mu \varphi_\alpha - \varphi^\alpha \nabla_\mu \psi_\alpha^* + \varphi_\mu \nabla_\alpha \psi^{\alpha*} - \psi_\mu^* \nabla_\alpha \varphi^\alpha) \quad (6.2.11)$$

## 6.2. Quantization of the electromagnetic potential/field

---

The inner product (6.2.11) has the same form as the one taken by CCH. However, CCH give an expression for the stress-energy tensor which includes a factor  $4\pi$  in (6.1.11), corresponding to unrationalized units. If unrationalized units are used, then a factor  $4\pi$  should also be included in the inner product (6.2.11). We believe that despite the fact that CCH give an expression of the stress-energy tensor in unrationalized units, they calculate it in rationalized units, as corresponds to (6.2.11).

Note that the electromagnetic inner product is gauge-independent

$$\left\langle {}_{lm\omega}P A_{\mu}^{\bullet} + \alpha_{,\mu}, {}_{l'm'\omega'}P' A_{\nu}^{\bullet'} \right\rangle_S = \left\langle {}_{lm\omega}P A_{\mu}^{\bullet}, {}_{l'm'\omega'}P' A_{\nu}^{\bullet'} \right\rangle_S \quad (6.2.12)$$

if the electromagnetic field is source-free.

Constants of normalization are to be included in front of the radial functions so that the potential modes (2.7.15) satisfy the orthonormality conditions (6.2.10) given the asymptotic behaviour of the radial functions in (3.2.27). In order to find the constants of normalization we use the potentials in (2.7.15):  $A_{-1\mu}$  is used when ‘in’ boundary conditions are taken and  $A_{+1\mu}$  when ‘up’ boundary conditions are taken. Using the ‘in’/‘up’ radial functions as determined by (3.2.27) we find that:

$$|N_{-1}^{\text{in}}|^2 = \frac{1}{2^5 \omega^3 \pi} \quad (6.2.13a)$$

$$|N_{+1}^{\text{up}}|^2 = \frac{1}{2^3 \pi |\mathfrak{N}|^2 \tilde{\omega} (r_+^2 + a^2)} \quad (6.2.13b)$$

$$|N_{-1}^{\text{up}}|^2 = |N_{+1}^{\text{up}}|^2 \left| \frac{{}_{-1}R_{lm\omega}^{\text{up,inc}}}{{}_{+1}R_{lm\omega}^{\text{up,inc}}} \right|^2 = \frac{\tilde{\omega} (r_+^2 + a^2)}{2\pi {}_1B_{lm\omega}^4} \quad (6.2.13c)$$

where  $\mathfrak{N}$  is given in (3.2.29). We have chosen  ${}_{-1}R_{lm\omega}^{\text{in,inc}} = 1$  and  ${}_{+1}R_{lm\omega}^{\text{up,inc}} = 1$  respectively for the first two equations. The constant of normalization  $|N_{-1}^{\text{up}}|$  is calculated as indicated with the use of (3.2.34). It is therefore the constant of normalization that corresponds to using the radial function (3.2.27b) when setting  ${}_{-1}R_{lm\omega}^{\text{up,inc}} = 1$ , which is the actual normalization we have used in the numerical calculation of the ‘up’ solutions. The NP scalars are therefore assumed

## 6.2. Quantization of the electromagnetic potential/field

---

to include the constants of normalization (6.2.13). That is, the NP scalar modes  ${}_{lm\omega}\phi_h^\bullet$  are to be calculated from expressions (2.8.9) and (2.8.10) with the inclusion of the appropriate constant of normalization (6.2.13), while the radial functions remain unaltered.

It can be checked that the set of modes  $\{{}_{lm\omega P}A_\mu^{\text{in}}, {}_{lm\omega P}A_\mu^{\text{up}}\}$  forms a complete set of orthonormal solutions to the Maxwell equations in the outer region of the Kerr space-time. Similarly, it can be checked that  $\{{}_{lm\omega P}A_\mu^{\text{out}}, {}_{lm\omega P}A_\mu^{\text{down}}\}$  also form a complete set. We may expand the electromagnetic potential by using the complete set of solutions  $\{{}_{lm\omega P}A_\mu^{\text{in}}, {}_{lm\omega P}A_\mu^{\text{up}}\}$  and then quantize it as:

$$\begin{aligned} \hat{A}_\mu = & \sum_{lmP} \int_0^{+\infty} d\omega \left( {}_{lm\omega P}\hat{a}^{\text{in}} {}_{lm\omega P}A_\mu^{\text{in}} + {}_{lm\omega P}\hat{a}^{\text{in}\dagger} {}_{lm\omega P}A_\mu^{\text{in}*} \right) + \\ & + \sum_{lmP} \int_0^{+\infty} d\tilde{\omega} \left( {}_{lm\omega P}\hat{a}^{\text{up}} {}_{lm\omega P}A_\mu^{\text{up}} + {}_{lm\omega P}\hat{a}^{\text{up}\dagger} {}_{lm\omega P}A_\mu^{\text{up}*} \right) \end{aligned} \quad (6.2.14)$$

Alternatively, we could proceed exactly in the same manner but using the complete set of solutions  $\{{}_{lm\omega P}A_\mu^{\text{out}}, {}_{lm\omega P}A_\mu^{\text{down}}\}$  instead. The result is then:

$$\begin{aligned} \hat{A}_\mu = & \sum_{lmP} \int_0^{+\infty} d\omega \left( {}_{lm\omega P}\hat{a}^{\text{out}} {}_{lm\omega P}A_\mu^{\text{out}} + {}_{lm\omega P}\hat{a}^{\text{out}\dagger} {}_{lm\omega P}A_\mu^{\text{out}*} \right) + \\ & + \sum_{lmP} \int_0^{+\infty} d\tilde{\omega} \left( {}_{lm\omega P}\hat{a}^{\text{down}} {}_{lm\omega P}A_\mu^{\text{down}} + {}_{lm\omega P}\hat{a}^{\text{down}\dagger} {}_{lm\omega P}A_\mu^{\text{down}*} \right) \end{aligned} \quad (6.2.15)$$

The asymptotic behaviour in terms of the advanced and retarded time co-ordinates of the electromagnetic potential and NP scalars for the ‘in’ and ‘up’ modes is the same as the one exhibited by the modes (3.2.25). The same applies to the asymptotic behaviour of the ‘out’ and ‘down’ modes exhibited in (3.2.42). Accordingly, the operators  ${}_{lm\omega P}\hat{a}^{\text{in}\dagger}$ ,  ${}_{lm\omega P}\hat{a}^{\text{up}\dagger}$ ,  ${}_{lm\omega P}\hat{a}^{\text{out}\dagger}$  and  ${}_{lm\omega P}\hat{a}^{\text{down}\dagger}$  are creation operators of particles incident from  $\mathcal{I}^-$ ,  $\mathcal{H}^-$ ,  $\mathcal{I}^+$  and  $\mathcal{H}^+$  respectively.

Since the ‘in’ and ‘out’ modes are only defined for  $\omega$  non-negative, they have non-negative energy as measured by an observer following the integral curve of  $\xi$ , by virtue of (3.2.26). Similarly, the ‘up’ and ‘down’ modes, defined for  $\tilde{\omega}$  non-negative, have non-negative energy with respect to observers following the integral curve of  $\chi$ .

## 6.2. Quantization of the electromagnetic potential/field

---

We may now construct the stress-energy tensor operator from either the potential operator (6.2.14) or (6.2.15). It is well-known that the stress-energy tensor as an operator does not have a well-defined meaning. It suffers from ultra-violet divergences and its expectation value when the field is in a certain state  $|\Psi\rangle$  must be renormalized. There are several techniques for renormalization. The *point-splitting technique* consists in temporarily displacing the point where one field in every quadratic term in the stress-energy tensor is evaluated, thus forming the object  $\langle \hat{T}_{\alpha\beta}(x, x') \rangle^\Psi$ . This object is finite. Specific divergent terms, gathered in the bitensor  $T_{\alpha\beta}^{\text{div}}(x, x')$ , which are purely geometric and thus independent of the quantum state, are then subtracted from  $\langle \hat{T}_{\alpha\beta}(x, x') \rangle^\Psi$ . The end result is obtained by finally bringing the separated points together:

$$\langle \hat{T}_{\alpha\beta}(x) \rangle_{\text{ren}}^\Psi = \lim_{x' \rightarrow x} \left( \langle \hat{T}_{\alpha\beta}(x, x') \rangle^\Psi - T_{\alpha\beta}^{\text{div}}(x, x') \right) \quad (6.2.16)$$

It is this renormalized expectation value of the stress-energy tensor (RSET) that is the source in Einstein's field equations (6.1.1) in the semiclassical theory. Christensen [21] has explicitly calculated the divergent terms  $T_{\alpha\beta}^{\text{div}}$  by using covariant geodesic point separation. Jensen, McLaughlin and Ottewill [54] calculated a linearly divergent term for the spin-1 case, which was not explicitly given by Christensen. The reason being that this term does not have to be included when an average is taken over the covariant derivative of the biscalar of geodesic interval  $\sigma^\mu$  and  $-\sigma^\mu$ , as performed by Christensen.

Before we start a description of the various physical states of the field, we give an important result found by Unruh [90] and further established by [10] and [42]. The result is that a 'particle detector' will react to states of the field which have positive frequency with respect to the detector's proper time. This means that a certain observer will see as a vacuum state the one that has been defined with positive frequency modes with respect to the 4-velocity of the observer. That is, if a certain observer  $\mathcal{A}$  makes measurements relative to a certain vacuum state  $|\Xi\rangle$ , then he or she will measure a stress tensor

$$\langle \hat{T}_{\alpha\beta} \rangle_{\mathcal{A}}^\Psi = \langle \hat{T}_{\alpha\beta} \rangle^\Psi - \langle \hat{T}_{\alpha\beta} \rangle^\Xi \quad (6.2.17)$$

when the field is in a certain state  $|\Psi\rangle$ . In flat space-time, this means that an inertial observer makes measurements relative to the Minkowski vacuum  $|M\rangle$  and a Rindler observer (RO) relative to the Fulling vacuum  $|F\rangle$ .

## 6.3 Boulware vacuum

### Schwarzschild space-time

The *Boulware vacuum state*, denoted by  $|B\rangle$ , is defined in the Schwarzschild space-time as the vacuum that corresponds to quantizing the field with normal modes that have all positive frequency with respect to the space-time's hypersurface-orthogonal timelike killing vector  $\xi$ . This state respects the isometries of the Schwarzschild space-time. Since it is the static observers SO the ones that move along integral curves of  $\xi$ , from Unruh's result stated in the previous section it follows that these observers will make measurements relative to the Boulware vacuum  $|B\rangle$ . That is, a SO will see the vacuum  $|B\rangle$  as empty. Candelas [13], based on conjectures made previously by Christensen and Fulling [22], has found that the RSET when the scalar field is in the Boulware vacuum is zero at both  $\mathcal{I}^-$  and  $\mathcal{I}^+$  in the Schwarzschild space-time. Candelas also found that the RSET, close to the horizon, when the field is in the Boulware vacuum diverges and corresponds to the absence from the vacuum of black-body radiation at the black hole temperature. The Boulware vacuum is therefore irregular at  $\mathcal{H}^-$  and  $\mathcal{H}^+$ . The Boulware vacuum models a cold star with a Boyer-Lindquist radius slightly larger than its Schwarzschild radius.

### Kerr space-time

In the Schwarzschild space-time the Boulware vacuum is associated to the field expansion in terms of either the 'in' and 'up' modes or the 'out' and 'down', both pairs of sets of complete modes defining the same vacuum  $|B\rangle$ . We can perform a similar expansion for the electromagnetic potential in the Kerr space-time. The

### 6.3. Boulware vacuum

*past Boulware state* is defined by

$$\begin{aligned} {}_{lm\omega P}\hat{a}^{\text{in}}|B^{-}\rangle &= 0 \\ {}_{lm\omega P}\hat{a}^{\text{up}}|B^{-}\rangle &= 0 \end{aligned} \tag{6.3.1}$$

corresponding to an absence of particles at  $\mathcal{H}^{-}$  and  $\mathcal{I}^{-}$ . This is the state mentioned in Section 1.5, which exhibits the Starobinskiĭ-Unruh effect. Due to this effect, the past Boulware state is not empty at  $\mathcal{I}^{+}$ .

We can also define the *future Boulware state*, as that state which is empty at  $\mathcal{I}^{+}$  and  $\mathcal{H}^{+}$ :

$$\begin{aligned} {}_{lm\omega P}\hat{a}^{\text{out}}|B^{+}\rangle &= 0 \\ {}_{lm\omega P}\hat{a}^{\text{down}}|B^{+}\rangle &= 0 \end{aligned} \tag{6.3.2}$$

The Bogolubov transformation between the pair of operators  ${}_{lm\omega P}\hat{a}^{\text{in}}$  and  ${}_{lm\omega P}\hat{a}^{\text{up}}$  and the pair  ${}_{lm\omega P}\hat{a}^{\text{down}}$  and  ${}_{lm\omega P}\hat{a}^{\text{out}}$  is non-trivial: the expression for  ${}_{lm\omega P}\hat{a}^{\text{in}\dagger} [{}_{lm\omega P}\hat{a}^{\text{up}\dagger}]$  in terms of ‘out’ and ‘down’ operators contains  ${}_{l,-m,-\omega,P}\hat{a}^{\text{down}\dagger} [{}_{l,-m,-\omega,P}\hat{a}^{\text{out}\dagger}]$  for modes in the superradiant regime. This implies that the past Boulware state contains both outgoing and downgoing superradiant particles, and is therefore not empty at  $\mathcal{I}^{+}$  and  $\mathcal{H}^{+}$ . This flux of particles out to  $\mathcal{I}^{+}$  corresponds to the Starobinskiĭ-Unruh effect. Similarly, the future Boulware state contains ingoing and upgoing superradiant particles, and is therefore not empty at  $\mathcal{I}^{-}$  and  $\mathcal{H}^{-}$ . Because of the fact that  ${}_{lm\omega P}\hat{a}^{\text{up}}$ , when expressed in terms of ‘out’ and ‘down’ operators, contains the creator operator  ${}_{l,-m,-\omega,P}\hat{a}^{\text{out}\dagger}$ , it is not possible to construct a state which is empty at both  $\mathcal{I}^{-}$  and  $\mathcal{I}^{+}$ , like the Boulware vacuum in the Schwarzschild space-time.

From the definitions (6.3.1) and (6.3.2) together with the relations (3.2.43), the past and future Boulware states are obtainable one from the other under the transformation  $(t, \phi) \rightarrow (-t, -\phi)$ . Because the two states are not equivalent, it follows that neither is invariant under this symmetry of the Kerr (and Kerr-Newman) space-time.

Several attempts have been made to construct a state which is stable and is also empty at both  $\mathcal{I}^{+}$  and  $\mathcal{I}^{-}$ . Matacz, Davies and Ottewill [63] considered

### 6.3. Boulware vacuum

---

a highly relativistic rotating star by assuming that the space-time outside the star at a radius  $r_* = x$  is given by the Kerr metric and requiring the scalar modes to vanish at the surface  $r_* = x$  of the star. The radius  $r_* = x$  is outside the horizon but close enough to it that there is an ergosphere. They then find that the state empty at  $\mathcal{I}^-$  is related to the state empty at  $\mathcal{I}^+$  by a trivial Bogolubov transformation, so that the state is indeed empty at both  $\mathcal{I}^-$  and  $\mathcal{I}^+$ . It is also invariant under the symmetry  $(t, \phi) \rightarrow (-t, -\phi)$  of the space-time. This result, however, was proved under the explicit assumption of the absence of solutions with complex frequencies. They say that if solutions with complex frequencies were to exist, then their result would not be valid. Furthermore, Friedman [36] proved that any stationary and asymptotically flat space-time which has an ergosphere but no event horizon is classically unstable to scalar perturbations. It is straightforward to show that Friedman's result is applicable to the model of a star in [63] and therefore solutions with complex frequencies do exist. Kang [55] has shown that the response function of an Unruh 'particle detector' is unstable if modes with complex frequency exist. The state defined by [63] is therefore unstable.

Winstanley [93] has constructed a state in Kerr with the defining features of the Boulware vacuum in Schwarzschild by using a variant of the  $\eta$  formalism (which employs non-standard commutation relations for the creation and annihilation operators) introduced by Frolov and Thorne [37]. This state  $|B_{\mathcal{I}}\rangle$  is defined as the one satisfying

$$\begin{aligned} {}_{lm\omega P}\hat{a}^{\text{in}}|B_{\mathcal{I}}\rangle &= 0 \\ {}_{lm\omega P}\hat{a}^{\text{up}}|B_{\mathcal{I}}\rangle &= 0 \quad \text{for } \omega > 0 \\ {}_{lm\omega P}\hat{a}^{\text{up}\dagger}|B_{\mathcal{I}}\rangle &= 0 \quad \text{for } \omega < 0 \end{aligned} \tag{6.3.3}$$

Defining the state as in (6.3.3) is equivalent to defining it as

$$\begin{aligned} {}_{lm\omega P}\hat{a}^{\text{in}}|B_{\mathcal{I}}\rangle &= 0 \\ {}_{lm\omega P}\hat{a}^{\text{out}}|B_{\mathcal{I}}\rangle &= 0 \end{aligned} \tag{6.3.4}$$

The state  $|B_{\mathcal{I}}\rangle$  is therefore empty at both  $\mathcal{I}^+$  and  $\mathcal{I}^-$  and it is invariant under



## 6.4. Hartle-Hawking state

---

$(t, \phi)$  reversal. Winstanley has also proved that the RSET when the field is in this state goes asymptotically to zero as  $O(r^{-3})$  for  $r \rightarrow +\infty$ . Therefore  $|B_{\mathcal{I}}\rangle$  possesses some of the characteristic properties that the Boulware state possesses in the Schwarzschild space-time. It still remains to be checked that this state is regular everywhere. The formalism in [37] which Winstanley used to construct this state, however, introduces irregularities in the Hartle-Hawking case, as we shall see in the next section.

Finally, one can similarly define a state as the one that satisfies

$$\begin{aligned} {}_{lm\omega P}\hat{a}^{\text{up}}|B_{\mathcal{H}}\rangle &= 0 \\ {}_{lm\omega P}\hat{a}^{\text{down}}|B_{\mathcal{H}}\rangle &= 0 \end{aligned} \tag{6.3.5}$$

This state is then empty at both  $\mathcal{H}^+$  and  $\mathcal{H}^-$  and is invariant under  $(t, \phi)$  reversal.

## 6.4 Hartle-Hawking state

The defining features of a Hartle-Hawking state is that it possesses the symmetries of the space-time and that it is regular everywhere, including on both the past and the future event horizons. Kay and Wald [56] have proven that for any globally hyperbolic space-time which has a Killing field with a bifurcate Killing horizon there can be at most one state with the above features. Kay and Wald have further shown that for the Kerr space-time this state does not exist. The Rindler and the Schwarzschild space-times are covered by Kay and Wald's theorem. In the Rindler space-time this state is clearly the Minkowski vacuum.

### Schwarzschild space-time

In the Schwarzschild space-time the state  $|H\rangle$  is defined as the one that corresponds to quantizing the field with upgoing normal modes which on  $\mathcal{H}^-$  have positive frequency with respect to the Kruskal co-ordinate  $U \equiv -e^{-\kappa+u}$  and with ingoing normal modes which on  $\mathcal{H}^+$  have positive frequency with respect to the Kruskal co-ordinate  $V \equiv e^{\kappa+v}$ .

## 6.4. Hartle-Hawking state

---

The state  $|H\rangle$  is then the one that has the mentioned Hartle-Hawking features in the Schwarzschild space-time. Indeed, Candelas [13] showed that the state defined in the above manner is regular on both the past and future horizons. He also found that the RSET at infinity when the field is in the  $|H\rangle$  state corresponds to that of a bath of black body radiation at the black hole temperature  $T_H$ . The Hartle-Hawking state models a black hole in unstable thermal equilibrium with an infinite distribution at the Hawking temperature.

From the above results and from the previous section we know that  $\langle \hat{T}_{\alpha\beta} \rangle^{H-B}$  is thermal both for  $r \rightarrow r_+$  and for  $r \rightarrow +\infty$ . Christensen and Fulling conjecture that this is the case everywhere. However, Jensen, McLaughlin and Ottewill [52] numerically show that  $\langle \hat{T}_{\alpha\beta} \rangle^{H-B}$  deviates from isotropic, thermal form as one moves away from the horizon.

We can establish a direct correspondence between observers and states in different space-times. Candelas showed that the RSET close to the horizon when the field is in the  $|B\rangle$  state diverges like minus the stress tensor of black body radiation at the black hole temperature, and that it must also be equal to  $-\langle \hat{T}_{\alpha\beta} \rangle_{\text{SO}}^H$ , due to (6.2.17) and to the regularity of  $|H\rangle$ . Analogously, Unruh [90] showed that in flat space-time and when the field is in the Minkowski vacuum, a Rindler observer RO will also see a bath of black body radiation at the Hawking temperature of a black hole with surface gravity  $\kappa_+ = a\alpha$ , where  $a$  is the RO's acceleration and  $\alpha$  is the lapse function in Rindler space. We can therefore establish a correspondence  $\text{RO} \leftrightarrow \text{SO}$  and also  $|M\rangle \leftrightarrow |H\rangle$ ; see also [49]. The correspondence between  $|M\rangle$  and  $|H\rangle$  is related to the fact that they are both regular close to the horizon of their respective space-times. We can then also establish a correspondence between the RO's own vacuum,  $|F\rangle$ , and the SO's own vacuum,  $|B\rangle$ , related to the fact that they are both divergent close to the horizon of their respective space-times. Finally, from the  $|M\rangle \leftrightarrow |H\rangle$  correspondence we can also establish a correspondence between the inertial observers in flat space-time and the freely-falling observers in Schwarzschild.

### Kerr space-time

With the variant of the  $\eta$  formalism mentioned in the previous section, Frolov and Thorne [37] define a new “Hartle-Hawking” state  $|FT\rangle$  invariant under the symmetries of the Kerr space-time. They go on to prove that the RSET when the field is in the  $|FT\rangle$  state is finite at the horizon but that, at least for arbitrarily slow rotation, it is equal to the stress tensor of a thermal distribution at the Hawking temperature rigidly rotating with the horizon. This suggests that it becomes irregular wherever  $\chi$  is not timelike, that is on and outside the speed-of-light surface. Ottewill and Winstanley [72], however, proved that although  $|FT\rangle$  has a Feynman propagator with the correct properties for regularity on the horizons, its two-point function is actually pathological almost everywhere, not just outside the speed-of-light surface. Only at the axis of symmetry, where all the modes in the two-point function for the scalar field are evaluated for  $\tilde{\omega} = \omega$  (i.e.,  $m = 0$ ), it does not suffer from this pathology.

Frolov and Thorne claim that close to the horizon ZAMOs make measurements relative to an unspecified Boulware vacuum. They also claim that, when the field is in the state  $|FT\rangle$ , ZAMOs measure close to the horizon a stress tensor equal to that of a thermal distribution at the Hawking temperature rigidly rotating with the horizon.

Duffy [32] modified the Kerr space-time by introducing a mirror and constructed a state  $|H_{\mathcal{M}}\rangle$  for the scalar field that is invariant under the isometries of the modified space-time. He then showed that  $|H_{\mathcal{M}}\rangle$  is regular everywhere in the modified space-time if, and only if, the mirror removes the region outside the speed-of-light surface. He constructed another state  $|B_{\mathcal{M}}\rangle$  invariant under the isometries of the modified space-time and empty on both the past and future horizons. This is the state that RROs make measurements relative to in the modified space-time. He also numerically showed that when the field is in the  $|H_{\mathcal{M}}\rangle$  state the stress tensor measured by a RRO is, close to the horizon, that of a thermal distribution at the Hawking temperature rigidly rotating with the

horizon.

Finally, CCH defined a new Hartle-Hawking-type state, which we will hereafter denote by  $|CCH^-\rangle$ . This state is obtained by thermalizing the ‘in’ and ‘up’ modes with respect to their natural energy. Ottewill and Winstanley [72] showed that this state is, however, not invariant under the symmetry transformation  $(t, \phi) \rightarrow (-t, -\phi)$  of the space-time. They further argued that the RSET when the scalar field is in the  $|CCH^-\rangle$  state is regular on the future horizon but irregular on the past horizon. We must note that these results were derived in [72] based on a stress-energy tensor for which the  $t\theta$ - and  $\phi\theta$ -components are identically zero. We shall see in Section 6.7 that although this is indeed the case for the scalar field, which is the case they considered, this is most probably not true for the electromagnetic field. A similar state could be constructed by applying the transformation  $(t, \phi) \rightarrow (-t, -\phi)$  to the state  $|CCH^-\rangle$ . This state, suitably named  $|CCH^+\rangle$ , would then be irregular on the future horizon and regular on the past horizon. In Section 6.8 we will investigate the form close to the horizon of  $\left\langle \hat{T}^\mu{}_\nu \right\rangle_{\text{ren}}^{CCH^--B^-}$  for electromagnetism.

## 6.5 Unruh state

### Schwarzschild space-time

Unruh [90] constructed a state  $|U^-\rangle$  in the Schwarzschild space-time that would model the state of a black hole at late times. With this purpose he replaced the stellar collapse by certain boundary conditions at  $\mathcal{H}^-$ . He then expanded the scalar field in modes that are positive frequency with respect to the proper time  $t$  of inertial observers in  $\mathcal{I}^-$  and modes that are positive frequency with respect to the proper time of inertial observers close to  $\mathcal{H}^-$ . Unruh showed that an inertial observer falling into  $\mathcal{H}^-$  will see no particles flowing out of the black hole but he will see particles flowing in, when the field is in the  $|U^-\rangle$  state.

## 6.6. Expectation value of the stress tensor

---

Unruh and later Candelas [13] (aided by the regularity of  $|H\rangle$  at the horizon) showed that  $|U^-\rangle$  is regular on  $\mathcal{H}^+$ , but is irregular on  $\mathcal{H}^-$ . Candelas also showed that the RSET when the field is in the  $|U^-\rangle$  state corresponds to a flux of thermal radiation at the Hawking temperature outgoing at  $\mathcal{I}^+$ . This radiation is the Hawking radiation discussed in Section 1.4.

### Kerr space-time

It is possible to construct a state  $|U^-\rangle$  in Kerr with the same positive-frequency mode definitions as for the Unruh state in Schwarzschild. This state, like  $|U^-\rangle$  in Schwarzschild, is empty at  $\mathcal{I}^-$  but is thermally populated at the Hawking temperature at  $\mathcal{I}^+$ , corresponding to the Hawking radiation. It is clearly not invariant under  $(t, \phi) \rightarrow (-t, -\phi)$ , like  $|U^-\rangle$  in Schwarzschild. The state  $|U^-\rangle$  is referred to as the *past Unruh state*. However, since in the Kerr space-time there is no Hartle-Hawking-type state regular on both the past and future horizons, it is a difficult task to prove any properties of the state  $|U^-\rangle$  near the horizon. Duffy [32], however, obtained numerical results which indicate that this state is regular on the future horizon.

The expressions for the expectation value of the stress-energy tensor as measured by various observers that we have discussed in the present and in the two previous sections are summarized in Table 6.1. This table also summarizes the thermal behaviour that some of these expectation values possess proven so far in the literature.

## 6.6 Expectation value of the stress tensor

In this section we give the expectation values of a quadratic operator and of the stress-energy tensor when the field is in various physical states, as given by CCH. To our knowledge, these important expressions for the electromagnetic field in the Kerr space-time have only been given so far by CCH. These are the

## 6.6. Expectation value of the stress tensor

---

Space-time	
Flat	$\langle \hat{T}_{\alpha\beta} \rangle_{\text{RO}}^{\Psi} = \langle \hat{T}_{\alpha\beta} \rangle_{\text{ren}}^{\Psi-F}$ $\langle \hat{T}_{\alpha\beta} \rangle_{\text{RO}}^M = T_{\alpha\beta}^{\text{th}}$
Schwarzschild	$\langle \hat{T}_{\alpha\beta} \rangle_{\text{SO}}^{\Psi} = \langle \hat{T}_{\alpha\beta} \rangle_{\text{ren}}^{\Psi-B}$ $\langle \hat{T}_{\alpha\beta} \rangle_{\text{SO}}^H \rightarrow -\langle \hat{T}_{\alpha\beta} \rangle_{\text{ren}}^B \rightarrow T_{\alpha\beta}^{\text{th}} \quad (r \rightarrow r_+)$
Kerr	$\langle \hat{T}_{\alpha\beta} \rangle_{\text{RRO}}^{\Psi} = \langle \hat{T}_{\alpha\beta} \rangle_{\text{ren}}^{\Psi-B_{\mathcal{H}}}$
Modified Kerr	$\langle \hat{T}_{\alpha\beta} \rangle_{\text{RRO}}^{\Psi_{\mathcal{M}}} = \langle \hat{T}_{\alpha\beta} \rangle_{\text{ren}}^{\Psi-B_{\mathcal{M}}}$ $\langle \hat{T}_{\alpha\beta} \rangle_{\text{RRO}}^{H_{\mathcal{M}}} \rightarrow -\langle \hat{T}_{\alpha\beta} \rangle_{\text{ren}}^{B_{\mathcal{M}}} \rightarrow T_{\alpha\beta}^{(\text{th},\text{RR})} \quad (r \rightarrow r_+)$

Table 6.1: Expectation value of the stress-energy tensor as measured by various observers in different space-times and their thermal behaviour in certain states. The states  $|\Psi\rangle$  and  $|\Psi_{\mathcal{M}}\rangle$  represent any state in the corresponding space-times. The stress-energy tensor  $T_{\alpha\beta}^{(\text{th},\text{RR})}$  corresponds to a rigidly-rotating thermal distribution at the Hawking temperature and its form is given in (6.8.2).

## 6.6. Expectation value of the stress tensor

---

expressions that we initially used in our numerical calculations. We felt forced to review them, however, and that is addressed later in Section 6.9.

The following expressions are given by CCH where  $\hat{Q}$  is any quadratic operator in the field and its derivatives and  $Q$  is its classical counterpart:

$$\begin{aligned} \langle B^- | \hat{Q} | B^- \rangle &= \\ &= \sum_{lmP} \left\{ \int_0^\infty d\tilde{\omega} Q[lm\omega\phi_h^{\text{up}}, lm\omega\phi_h^{\text{up}*}] + \int_0^\infty d\omega Q[lm\omega\phi_h^{\text{in}}, lm\omega\phi_h^{\text{in}*}] \right\} \end{aligned} \quad (6.6.1a)$$

$$\begin{aligned} \langle U^- | \hat{Q} | U^- \rangle &= \\ &= \sum_{lmP} \left\{ \int_0^\infty d\tilde{\omega} \coth\left(\frac{\pi\tilde{\omega}}{\kappa}\right) Q[lm\omega\phi_h^{\text{up}}, lm\omega\phi_h^{\text{up}*}] + \int_0^\infty d\omega Q[lm\omega\phi_h^{\text{in}}, lm\omega\phi_h^{\text{in}*}] \right\} \end{aligned} \quad (6.6.1b)$$

$$\begin{aligned} \langle CCH^- | \hat{Q} | CCH^- \rangle &= \sum_{lmP} \left\{ \int_0^\infty d\tilde{\omega} \coth\left(\frac{\pi\tilde{\omega}}{\kappa}\right) Q[lm\omega\phi_h^{\text{up}}, lm\omega\phi_h^{\text{up}*}] + \right. \\ &\quad \left. + \int_0^\infty d\omega \coth\left(\frac{\pi\omega}{\kappa}\right) Q[lm\omega\phi_h^{\text{in}}, lm\omega\phi_h^{\text{in}*}] \right\} \end{aligned} \quad (6.6.1c)$$

From the above equations (6.6.1), the expressions for the expectation value of the stress-energy tensor when the field is in different states follow:

$$\begin{aligned} \langle B^- | \hat{T}_{\mu\nu} | B^- \rangle &= \\ &= \sum_{lmP} \left\{ \int_0^\infty d\tilde{\omega} T_{\mu\nu}[lm\omega\phi_h^{\text{up}}, lm\omega\phi_h^{\text{up}*}] + \int_0^\infty d\omega T_{\mu\nu}[lm\omega\phi_h^{\text{in}}, lm\omega\phi_h^{\text{in}*}] \right\} \end{aligned} \quad (6.6.2a)$$

$$\begin{aligned} \langle U^- | \hat{T}_{\mu\nu} | U^- \rangle &= \\ &= \sum_{lmP} \left\{ \int_0^\infty d\tilde{\omega} \coth\left(\frac{\pi\tilde{\omega}}{\kappa}\right) T_{\mu\nu}[lm\omega\phi_h^{\text{up}}, lm\omega\phi_h^{\text{up}*}] + \int_0^\infty d\omega T_{\mu\nu}[lm\omega\phi_h^{\text{in}}, lm\omega\phi_h^{\text{in}*}] \right\} \end{aligned} \quad (6.6.2b)$$

$$\begin{aligned} \langle CCH^- | \hat{T}_{\mu\nu} | CCH^- \rangle &= \sum_{lmP} \left\{ \int_0^\infty d\tilde{\omega} \coth\left(\frac{\pi\tilde{\omega}}{\kappa}\right) T_{\mu\nu}[lm\omega\phi_h^{\text{up}}, lm\omega\phi_h^{\text{up}*}] + \right. \\ &\quad \left. + \int_0^\infty d\omega \coth\left(\frac{\pi\omega}{\kappa}\right) T_{\mu\nu}[lm\omega\phi_h^{\text{in}}, lm\omega\phi_h^{\text{in}*}] \right\} \end{aligned} \quad (6.6.2c)$$

We use the obvious notation that  $Q[lm\omega\phi_h^\bullet, lm\omega\phi_h^{\bullet*}]$  and  $T_{\mu\nu}[lm\omega\phi_h^\bullet, lm\omega\phi_h^{\bullet*}]$  denote

## 6.6. Expectation value of the stress tensor

---

the general expressions for  $Q$  and the stress-energy tensor (6.1.11) respectively, where the scalars  $\phi_h$  have been replaced by the modes  ${}_{lm\omega}\phi_h^\bullet$ . We will also use the symbol  ${}_{lm\omega}T_{\mu\nu}^\bullet$  to refer to  $T_{\mu\nu} [{}_{lm\omega}\phi_h^\bullet, {}_{lm\omega}\phi_h^{\bullet*}]$ .

CCH's original expressions contained the symbols  $Q [u_{\omega lmP}^\bullet, u_{\omega lmP}^{\bullet*}]$  and  $T_{\mu\nu} [u_{\omega lmP}^\bullet, u_{\omega lmP}^{\bullet*}]$ , which we have respectively replaced in the expressions (6.6.1) and (6.6.2) above by  $Q [{}_{lm\omega}\phi_h^\bullet, {}_{lm\omega}\phi_h^{\bullet*}]$  and  $T_{\mu\nu} [{}_{lm\omega}\phi_h^\bullet, {}_{lm\omega}\phi_h^{\bullet*}]$ . Note that the above expressions (6.6.1) and (6.6.2) without these replacements are indeed valid for the scalar field case.

CCH did not give an expression for the expectation value of the stress tensor when the field is in the state  $|FT\rangle$ , as this state was only defined later. We give here an expression for this expectation value obtained by direct generalization from the corresponding one for the scalar field as in the case of the states in (6.6.2):

$$\begin{aligned} \langle FT | \hat{T}_{\mu\nu} | FT \rangle = & \sum_{lmP} \left\{ \int_0^\infty d\tilde{\omega} \coth \left( \frac{\pi\tilde{\omega}}{\kappa} \right) T_{\mu\nu} [{}_{lm\omega}\phi_h^{\text{up}}, {}_{lm\omega}\phi_h^{\text{up}*}] \right. \\ & \left. + \int_0^\infty d\omega \coth \left( \frac{\pi\tilde{\omega}}{\kappa} \right) T_{\mu\nu} [{}_{lm\omega}\phi_h^{\text{in}}, {}_{lm\omega}\phi_h^{\text{in}*}] \right\} \end{aligned} \quad (6.6.3)$$

We will only use this expression in Section 6.9.1. We shall show in that section that CCH's expressions (6.6.2) are incorrect. We obtain the corrected expressions and give them in (6.9.29).

Graphs 6.1–6.3 have been obtained with these corrected expressions. We plot the  $r\theta$ -component of the stress tensor for the difference between the  $|U^- \rangle$  and the  $|B^- \rangle$  states. This is the only component that is not plotted in later sections. A plot of the same component for the difference between the  $|CCH^- \rangle$  and the  $|B^- \rangle$  states is identical to Figure 6.1 for the range of  $r$  displayed. The components for the difference between  $|CCH^- \rangle$  and  $|U^- \rangle$  are trivially obtained by subtracting the previous two differences between states. We have included the  $r\theta$ - and  $t\phi$ -components for the difference between  $|CCH^- \rangle$  and  $|U^- \rangle$ .



## 6.6. Expectation value of the stress tensor

---

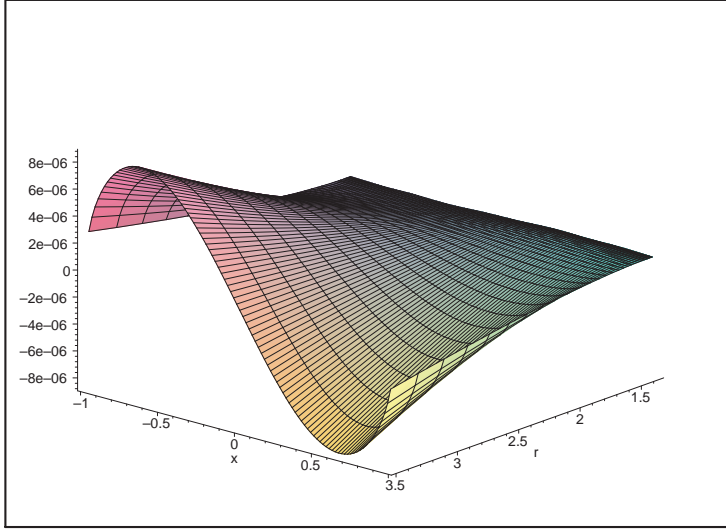


Figure 6.1:  $\frac{1}{4\pi}\Delta^2 \left\langle \hat{T}_{r\theta} \right\rangle^{U^- - B^-}$

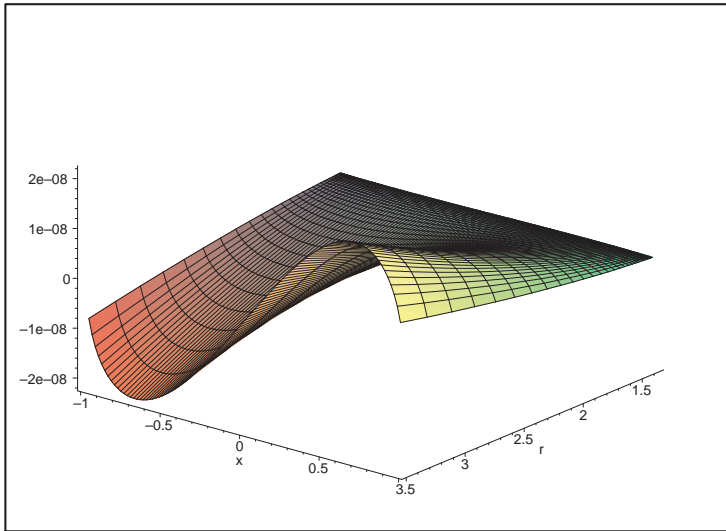


Figure 6.2:  $\frac{1}{4\pi}\Delta^2 \left\langle \hat{T}_{r\theta} \right\rangle^{CCH^- - U^-}$

## 6.6. Expectation value of the stress tensor

---

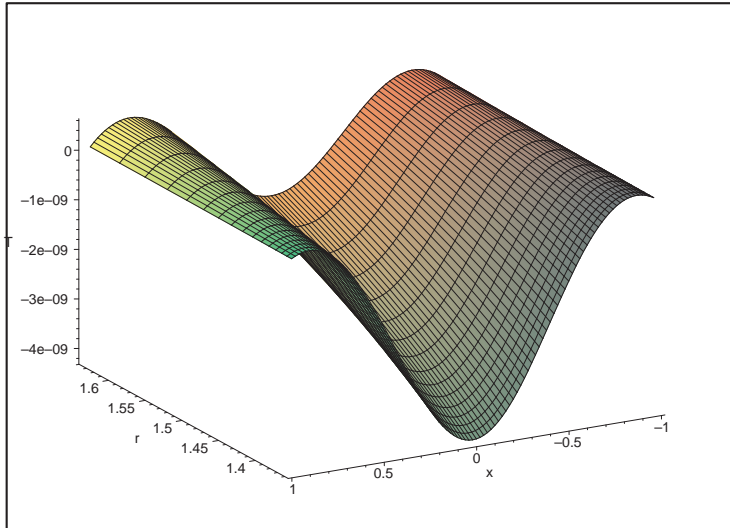


Figure 6.3:  $\frac{1}{4\pi} \langle \hat{T}_{t\phi} \rangle^{CCH^- - U^-}$

## 6.7 Luminosity

The total energy flux at infinity per unit solid angle is given by

$$\frac{dE}{dt d\Omega} = \lim_{r \rightarrow +\infty} r^2 T^r_t \quad (6.7.1)$$

Let  $E^{(\text{inc})}$  and  $E^{(\text{ref})}$  denote, respectively, the energy incident and the energy reflected by the black hole at infinity. The corresponding incident and reflected energy fluxes at infinity per unit solid angle are then calculated with (6.7.1) including in the NP scalars only the ingoing (i.e., incident) and outgoing (i.e., reflected) parts, respectively, of the radial functions  ${}_h R^{\text{in}}$ . The expressions at radial infinity of the corresponding NP scalars are denoted by  $\phi_h^{(\text{in,inc})}$  and  $\phi_h^{(\text{in,ref})}$  respectively. The following expressions can be immediately checked:

$$\frac{dE^{(\text{inc})}}{dt d\Omega} = \frac{r^2}{8\pi} \left| \phi_{-1}^{(\text{in,inc})} \right|^2 \quad (6.7.2a)$$

$$\frac{dE^{(\text{ref})}}{dt d\Omega} = \frac{r^2}{2\pi} \left| \phi_{+1}^{(\text{in,ref})} \right|^2 \quad (6.7.2b)$$

Let  $E^{(\text{tra})}$  denote the energy going down across the event-horizon of the black hole. If there is a flux of energy across the 2-surface element formed by the intersection of an element of the horizon with two surfaces of constant  $v$  separated by  $dv$ , then the change in energy of the black hole is

$$dE^{(\text{tra})} = T_\mu{}^\nu \xi^\mu d^3\Sigma_\nu \quad (6.7.3)$$

where  $d^3\Sigma_\nu$  is the 3-surface element of the horizon, normal to the inward radial direction of the Kerr system  $\{v, r, \theta, \bar{\phi}\}$ . It can be checked that the corresponding flux of energy per unit solid angle is

$$\frac{dE^{(\text{tra})}}{dt d\Omega} = \frac{\Delta^2}{8\pi(r_+^2 + a^2)} \frac{\omega}{\bar{\omega}} \left| \phi_{-1}^{(\text{in,tra})} \right|^2 \quad (6.7.4)$$

where  $\phi_{-1}^{(\text{in,tra})}$  refers to the inclusion in the NP scalar of only the transmitted part close to the horizon of the radial function  ${}_{+1} R^{\text{in}}$ .

The wronskian relations in Table 3.1 relate the above energy fluxes. Indeed these wronskian relations correspond to the conservation of energy law that equates

## 6.7. Luminosity

the net flux of energy coming in from infinity to the net flux of energy going down into the black hole:

$$\frac{dE^{(\text{inc})}}{dt} - \frac{dE^{(\text{ref})}}{dt} = \frac{dE^{(\text{tra})}}{dt} \quad (6.7.5)$$

The *reflection coefficient*  $\mathbb{R}_{lm\omega}$  and the *transmission coefficient*  $\mathbb{T}_{lm\omega}$  of an incoming wave mode are defined as the following flux ratios:

$$\mathbb{R}_{lm\omega} \equiv \frac{dE_{lm\omega}^{(\text{ref})}/dt}{dE_{lm\omega}^{(\text{inc})}/dt} \quad (6.7.6a)$$

$$\mathbb{T}_{lm\omega} \equiv \frac{dE_{lm\omega}^{(\text{tra})}/dt}{dE_{lm\omega}^{(\text{inc})}/dt} \quad (6.7.6b)$$

The transmission coefficient  $\mathbb{T}_{lm\omega}$  is also commonly interpreted as the absorption probability for an incoming wave mode and is then denoted by  $\Gamma_{lm\omega}$ . The conservation of energy law (6.7.5) can then be re-expressed as

$$\mathbb{R}_{lm\omega} = 1 - \mathbb{T}_{lm\omega} = 4 \frac{\left| {}_{lm\omega}\phi_{+1}^{(\text{in,ref})} \right|^2}{\left| {}_{lm\omega}\phi_{-1}^{(\text{in,inc})} \right|^2} \quad (6.7.7)$$

where we have made use of expressions (6.7.2).

By using the asymptotic expressions for the NP scalars together with the relations (3.2.34) and (3.2.28) and the wronskians in Table 3.1 we immediately find various, equivalent expressions for the reflection and absorption coefficients:

$$\mathbb{T}_{lm\omega} = 1 - \mathbb{R}_{lm\omega} = 1 - |A_{lm\omega}^{\text{in}}|^2 = \frac{-i}{2^4 \omega^3} W[Y_{+1}^{\text{in}}, Y_{-1}^{\text{in}*}]_{lm\omega} \quad (6.7.8)$$

We use the obvious notation that subindices outside the square brackets of the wronskian apply to the radial functions inside the brackets. It is clear that the coefficients of the radial function  $X_{lm\omega}$ , rather than those of  ${}_h R_{lm\omega}$ , are the natural ones in the description of the scattering of wave modes. As anticipated in Section 3.2,  $|A_{lm\omega}^{\text{in}}|^2$  is the fractional gain or loss of energy of an incoming wave mode. We know that for superradiant wave modes this quantity is greater than one and therefore the reflection coefficient  $\mathbb{R}_{lm\omega}$  is also greater than one while the transmission coefficient  $\mathbb{T}_{lm\omega}$  is negative for these modes.

## 6.7. Luminosity

The conservation equations  $\nabla_\nu T_\mu{}^\nu = 0$  can alternatively be written [31] as

$$\partial_\nu (T_\mu{}^\nu \sqrt{-g}) = \frac{1}{2} \sqrt{-g} (\partial_\mu g_{\alpha\beta}) T^{\alpha\beta} \quad (6.7.9)$$

Assuming that the stress-energy tensor is independent of  $t$  and  $\phi$ , like the Kerr metric (and the Kerr-Newman solution), the  $\mu = t$  and  $\mu = \phi$  components of equations (6.7.9) become

$$\partial_r (\Sigma \sin \theta T_t{}^r) + \partial_\theta (\Sigma \sin \theta T_t{}^\theta) = 0 \quad (6.7.10a)$$

$$\partial_r (\Sigma \sin \theta T_\phi{}^r) + \partial_\theta (\Sigma \sin \theta T_\phi{}^\theta) = 0 \quad (6.7.10b)$$

After integrating these equations over  $r$  the result is:

$$T_{tr} = \frac{K(\theta)}{\Delta} - \frac{1}{\Delta \sin \theta} \partial_\theta \left( \sin \theta \int_{r_+}^r dr' T_{t\theta} \right) \quad (6.7.11a)$$

$$T_{\phi r} = \frac{L(\theta)}{\Delta} - \frac{1}{\Delta \sin \theta} \partial_\theta \left( \sin \theta \int_{r_+}^r dr' T_{\phi\theta} \right) \quad (6.7.11b)$$

where  $K(\theta)$  and  $L(\theta)$  are arbitrary functions. The function  $K(\theta)$  is related to the *luminosity*, which is defined as the instantaneous flux of energy per unit time. The luminosity when the field is in the state  $|\Psi\rangle$  is given by

$$\frac{dM}{dt} = \Delta \int_S d\Omega \langle \hat{T}_{tr} \rangle_{\text{ren}}^\Psi \quad (6.7.12)$$

where the surface  $S$  can be any surface of constant  $t$  and  $r$ . A non-zero value for the luminosity when the field is in the past Boulware state in a background possessing an ergosphere is a manifestation of the Starobinskiĭ-Unruh effect. Analogously, a non-zero value for the luminosity when the field is in the past Unruh state in such a background is a manifestation of the Hawking radiation. In the forthcoming the subindex  $A$  refers to either  $t$  or  $\phi$  and the subindex  $X$  to either  $r$  or  $\theta$ .

In order to compare some spin-1 results with the corresponding spin-0 results we shall briefly outline the latter. Consequently, the present and following paragraphs only apply to the scalar case. On the one hand, it can be proved that, for spin-0, it is  $T_{A\theta}(x, x') = 0$  for any points  $x$  and  $x'$ . On the other hand,

Frolov and Thorne [37] prove that  $T_{AX}^{\text{div}} = 0$  for spin-0 whenever the separation between the points  $x$  and  $x'$  is the particular choice that they both lie in the same two-dimensional surface  $\Sigma \equiv \{t, \phi\}$ , i.e.,  $x = (t, r_*, \theta, \phi)$  and  $x' = (t' = t, r'_*, \theta', \phi' = \phi)$ . Combining both results it follows that  $\left\langle \hat{T}_{A\theta} \right\rangle_{\text{ren}}^{\Psi} = 0$  for spin-0, where  $|\Psi\rangle$  is any state among  $|B^{\pm}\rangle$ ,  $|U^{-}\rangle$ ,  $|CCH^{-}\rangle$  or  $|FT\rangle$ .

Equations (6.7.11) give

$$\left. \begin{aligned} T_{tr} &= \frac{K(\theta)}{\Delta} \\ T_{\phi r} &= \frac{L(\theta)}{\Delta} \end{aligned} \right\} \quad \text{if } T_{A\theta} = 0 \quad (6.7.13)$$

so that, in particular, equations (6.7.13) apply to the RSET when the scalar field is in any of the above-mentioned states. It may indeed be calculated directly from the expression for the spin-0 stress-energy tensor that all the radial dependence of  $\Delta_{lm\omega} T_{tr}$  can be expressed as a radial wronskian. It can also be checked that  ${}_{lm\omega} T_{tr}^{\text{in}} = -{}_{lm\omega} T_{tr}^{\text{up}}$  for spin-0 so that the only contribution to the luminosity in the past Boulware vacuum comes from the superradiant modes:

$$\Delta \left\langle \hat{T}_{tr} \right\rangle_{\text{ren}}^{B^{-}} = -2 \sum_{l=1}^{\infty} \sum_{m=1}^l \int_0^{m\Omega_+} d\omega \Delta_{lm\omega} T_{tr}^{\text{up}} \quad \text{for } s = 0 \quad (6.7.14)$$

It is immediately apparent that for the spin-1 case the task to prove analytically whether  $\Delta T_{tr}$  is constant in  $r$  or not is much more arduous than for spin-0. In the expression for  ${}_{lm\omega} T_{tr}$  both terms with  ${}_{-1}S_{lm\omega}^2$  and other terms with  ${}_{+1}S_{lm\omega}^2$  appear in it. As a matter of fact, when evaluated at the axis of symmetry  $\theta = 0$  or  $\pi$ , only one term of the first type and one of the second type appear. Furthermore, neither of these two terms is constant in  $r$ . It is therefore apparent that if we wish to prove that  $\Delta T_{tr}$  is constant in  $r$ , or otherwise, we must then somehow relate  ${}_{-1}S_{lm\omega}^2$  to  ${}_{+1}S_{lm\omega}^2$ . It follows from the symmetries (4.2.1) that we can only relate one spherical function to the other at the same point by applying the transformation  $(m, \omega) \rightarrow (-m, -\omega)$  to one of them. The change in sign of  $m$  can be overturned due to the symmetric sum in  $m$  in the Fourier sums (6.6.2). The change in sign of  $\omega$ , however, is a problem when trying to relate

a term with  $_{-1}S_{lm\omega}^2$  to a term with  $_{+1}S_{lm\omega}^2$  due to the non-symmetric nature under  $(m, \omega) \rightarrow (-m, -\omega)$  of the integrals over  $\omega$  or  $\tilde{\omega}$  for all states involved in (6.6.2). The use of (4.2.3a) does not help either since it introduces an undesirable derivative in  $\theta$ , which could not be cancelled out.

We encounter a similar problem when trying to prove whether  $T_{t\theta}$  is zero or not. Since we do not know whether it is zero or not we cannot see either from (6.7.11a) that  $\Delta T_{tr}$  is constant in  $r$ , as we did for spin-0.

In the case  $a = 0$ , since the spin-weighted spherical harmonics do not depend on  $\omega$ , we only need a change in the sign of  $m$  to relate the two types of terms in  $\Delta_{lm\omega} T_{tr}$ . Indeed, use of (4.1.13) allows us to prove that  $\sum_m \Delta_{lm\omega} T_{tr}$  is constant in  $r$  and that  $\sum_m {}_{lm\omega} T_{tr}^{\text{up}} = -\sum_m {}_{lm\omega} T_{tr}^{\text{in}}$  in the Schwarzschild background.

The solution to this deadlock for the spin-1 case in the Kerr background consists in integrating over the solid angle. This allows us to relate a term with  $\int d\Omega {}_{-1}S_{lm\omega}^2$  to a term with  $\int d\Omega {}_{+1}S_{lm\omega}^2$ , when both types of terms appear in  $\int d\Omega \Delta_{lm\omega} T_{tr}$ . This is in accord with the fact that if we integrate the conservation equation (6.7.11a) over the solid angle we immediately obtain that

$$\int d\Omega \Delta T_{tr} = \int d\Omega K(\theta) = \text{const.} \quad (6.7.15)$$

Indeed, we analytically calculated  $\int d\Omega \Delta \left\langle \hat{T}_{tr} \right\rangle^{U-}$  in the above manner and found that it is constant and in agreement with Page's [73] expression. Since the calculations were not immediate, we will give here a brief outline. For each term in (6.1.11) for  ${}_{lm\omega} T_{tr}$  that contains  ${}_{lm\omega} \phi_0$  we choose to use one particular expression for this NP scalar out of the two in (2.8.10). The expression we choose for  ${}_{lm\omega} \phi_0$  in each term is the one that uses the same  ${}_h S_{lm\omega}$  and different  ${}_h R_{lm\omega}$  from those, as given by (2.8.9), appearing in the other NP scalar in that term. The reason for this choice is two-fold. One, so that we can later easily identify the wronskian expressions (3.2.51). Secondly, so that we can directly compare these terms containing  ${}_{lm\omega} \phi_0$  with the ones containing  $|{}_{lm\omega} \phi_{\pm 1}|^2$ , since then both types of terms involve  ${}_{\mp 1} S_{lm\omega}^2$ . For each term in  ${}_{lm\omega} T_{tr}$  we then factor out parts which

## 6.7. Luminosity

are functions of  $r$  only. We identify and group terms such that their factorized parts containing  $\theta$  are equal (bar a sign) after being integrated over the solid angle and the symmetry (4.2.1a) is used. The result after also including the complex conjugate part is that all terms can be grouped together with common factor either  $\left[ {}_{-1}R_{lm\omega}^* \mathcal{D}_0^\dagger (\Delta_{+1} R_{lm\omega}) - \Delta_{+1} R_{lm\omega} \mathcal{D}_{0-1}^\dagger R_{lm\omega}^* \right] + c.c.$ , which is zero from (3.2.51), or else  $\left[ {}_{-1}R_{lm\omega}^* \mathcal{D}_0^\dagger (\Delta_{+1} R_{lm\omega}) - \Delta_{+1} R_{lm\omega} \mathcal{D}_{0-1}^\dagger R_{lm\omega}^* \right] - c.c..$  The factor multiplying the latter can be simplified to eventually yield the desired result:

$$\int d\Omega \Delta_{lm\omega} T_{tr}^{\text{up}} = - \int d\Omega \Delta_{lm\omega} T_{tr}^{\text{in}} = \frac{-1}{4\pi} \omega \mathbb{T}_{lm\omega} \quad (6.7.16)$$

where we have included the constants of normalization (6.2.13).

We can now give simple expressions for the luminosity when the electromagnetic field is in the past Boulware state and in the past Unruh state:

$$\left. \frac{dM}{dt} \right|_{B^-} = \frac{1}{2\pi} \sum_{l=1}^{\infty} \sum_{m=1}^{+l} \sum_{P=\pm 1} \int_0^{m\Omega_+} d\omega \omega \mathbb{T}_{lm\omega} \quad (6.7.17a)$$

$$\left. \frac{dM}{dt} \right|_{U^-} = \frac{1}{2\pi} \sum_{l=1}^{\infty} \sum_{m=-l}^{+l} \sum_{P=\pm 1} \int_0^{\infty} d\omega \frac{\omega \mathbb{T}_{lm\omega}}{e^{2\pi\tilde{\omega}/\kappa} - 1} \quad (6.7.17b)$$

The former corresponds to the Starobinskiĭ-Unruh radiation and the latter to the Hawking radiation. Since only superradiant modes are being included in the Starobinskiĭ-Unruh radiation (6.7.17a) and the transmission coefficient  $\mathbb{T}_{lm\omega}$  is negative for these modes, there is a constant outflow of energy from the black hole when the field is in the past Boulware state.

We numerically evaluated (6.7.17) for the case  $Q = 0$  and  $a = 0.95M$ . The results, compared against values in the literature are:

$$M^2 \left. \frac{dM}{dt} \right|_{B^-} = -4.750 * 10^{-4} \quad (\text{spin-1}) \quad (6.7.18a)$$

$$M^2 \left. \frac{dM}{dt} \right|_{B^-} = -5.01 * 10^{-5} \quad (\text{spin-0, Duffy}) \quad (6.7.18b)$$



in the past Boulware state, and

$$M^2 \left. \frac{dM}{dt} \right|_{U^-} = -1.1714 * 10^{-3} \quad (\text{spin-1}) \quad (6.7.19a)$$

$$M^2 \left. \frac{dM}{dt} \right|_{U^-} = -1.18 * 10^{-3} \quad (\text{spin-1, Page}) \quad (6.7.19b)$$

in the past Unruh state. The value (6.7.18b) for the scalar field is calculated by Duffy [32] and we have calculated (6.7.19b) from splining Page's [73] numerical results. Both of them have also been calculated for  $Q = 0$  and  $a = 0.95M$ .

The above results for the expectation value of the stress-energy tensor for a spin-1 field have been obtained using CCH's expressions (6.6.2). We now investigate what effect it has in these results the use of the correction (6.9.29) to CCH's expressions. The difficulty we encountered above when trying to see whether  $T_{t\theta}$  is zero and whether  $\Delta T_{tr}$  is constant in  $r$  does not exist when calculating the expectation value of these components in the past Boulware and past Unruh states using expressions (6.9.29). Indeed, due to the symmetry (4.2.1a) we can now relate terms in each of these components that contain  $_{-1}S_{lm\omega}^2 + \mathcal{P}_{-1}S_{lm\omega}^2$  to terms that contain  $_{+1}S_{lm\omega}^2 + \mathcal{P}_{+1}S_{lm\omega}^2$ . The calculation of  $\Delta ({}_{lm\omega}T_{tr} + \mathcal{P}_{lm\omega}T_{tr})$  follows through in a very similar manner to the calculation of  $\int d\Omega \Delta_{lm\omega}T_{tr}$  described above and the result is:

$$\begin{aligned} \Delta ({}_{lm\omega}T_{tr}^{\text{up}} + \mathcal{P}_{lm\omega}T_{tr}^{\text{up}}) &= \\ &= \frac{\mathbb{T}_{lm\omega}}{4\pi^2\Sigma} \left\{ -\omega\Sigma ({}_{-1}S_{lm\omega}^2 + {}_{+1}S_{lm\omega}^2) + \frac{a^3 \cos\theta \sin^2\theta}{\Sigma} ({}_{-1}S_{lm\omega}^2 - {}_{+1}S_{lm\omega}^2) + \right. \\ &\quad \left. + a \sin\theta ({}_{-1}S_{lm\omega} \partial_{\theta-1} S_{lm\omega} - {}_{+1}S_{lm\omega} \partial_{\theta+1} S_{lm\omega}) \right\} \end{aligned} \quad (6.7.20)$$

The corresponding result for the 'in' modes is equal to (6.7.20) with a change of sign, by virtue of (6.7.8) and the property (3.2.53).

Even if we used equation (4.2.3c) to rid of the derivatives in (6.7.20), we would not be able to express its last term in terms of  $_{-1}S_{lm\omega}^2$  and  $_{+1}S_{lm\omega}^2$  only. It follows that  $\Delta ({}_{lm\omega}T_{tr} + \mathcal{P}_{lm\omega}T_{tr})$  is not constant in  $r$  and therefore neither is  $\Delta \left\langle \hat{T}_{tr} \right\rangle_{\text{ren}}^{B^-}$  nor  $\Delta \left\langle \hat{T}_{tr} \right\rangle_{\text{ren}}^{U^-}$ . Similarly, a calculation of  $({}_{lm\omega}T_{t\theta} + \mathcal{P}_{lm\omega}T_{t\theta})$  shows

## 6.8. RSET close to the horizon in the Boulware vacuum

---

that it is not zero and therefore neither  $\langle \hat{T}_{t\theta} \rangle_{\text{ren}}^{B^-}$  nor  $\langle \hat{T}_{t\theta} \rangle_{\text{ren}}^{U^-}$  are zero. However, since  $\int d\Omega \mathcal{P}f(\theta) = \int d\Omega f(\theta)$ , the results obtained above involving integration over the solid angle, i.e., equations (6.7.17)–(6.7.19), remain unaltered by the correction (6.9.29).

Indeed, Graphs 6.4–6.11 numerically corroborate the above conclusions. Graphs 6.4 and 6.5 show that neither  $\Delta \langle \hat{T}_{tr} \rangle^{U^- - B^-}$  nor  $\Delta \langle \hat{T}_{tr} \rangle^{CCH^- - U^-}$  are constant in  $r$ . Graphs 6.8–6.11 show that neither  $\langle \hat{T}_{A\theta} \rangle_{\text{ren}}^{U^- - B^-}$  nor  $\langle \hat{T}_{A\theta} \rangle_{\text{ren}}^{CCH^- - U^-}$  are zero. Graphs 6.6–6.7, however, seem to indicate that both  $\Delta \langle \hat{T}_{r\phi} \rangle^{CCH^- - U^-}$  and  $\Delta \langle \hat{T}_{r\phi} \rangle^{U^- - B^-}$  might actually be constant in  $r$ .

## 6.8 RSET close to the horizon in the Boulware vacuum

Candelas and Deutsch [15] consider flat space-time in the presence of an accelerating barrier with acceleration  $a_B^{-1}$ . They then calculate the spin-1 RSET in the tetrad of an accelerating observer RO with local acceleration  $\xi^{-1}$ . In the limit  $\xi/a_B \rightarrow \infty$  the vacuum state above the accelerating mirror approximates the Fulling vacuum  $|F\rangle$ . The result is

$$\begin{aligned} \langle T^{\bar{\mu}}_{\bar{\nu}} \rangle_{\text{ren}}^F &\sim -\frac{1}{\pi^2 \xi^4} \int_0^\infty dx \frac{x^3 + x}{e^{2\pi x} - 1} \text{diag} \left( -1, \frac{1}{3}, \frac{1}{3}, \frac{1}{3} \right) = \\ &= \frac{-11}{240\pi^2 \xi^4} \text{diag} \left( -1, \frac{1}{3}, \frac{1}{3}, \frac{1}{3} \right) \quad (\xi/a_B \rightarrow \infty) \end{aligned} \quad (6.8.1)$$

where the bars on the indices indicate RO tetrad. Expression (6.8.1) is equivalent to minus the stress-energy tensor for thermal radiation at a temperature of  $(2\pi\xi)^{-1}$ . We saw in Section 6.4 that in Schwarzschild space-time, analogously to (6.8.1) in flat space, the RSET close to the horizon when the field is in the Boulware vacuum diverges like minus the stress tensor of black body radiation at the black hole temperature. It is therefore reasonable to expect that if there existed

## 6.8. RSET close to the horizon in the Boulware vacuum

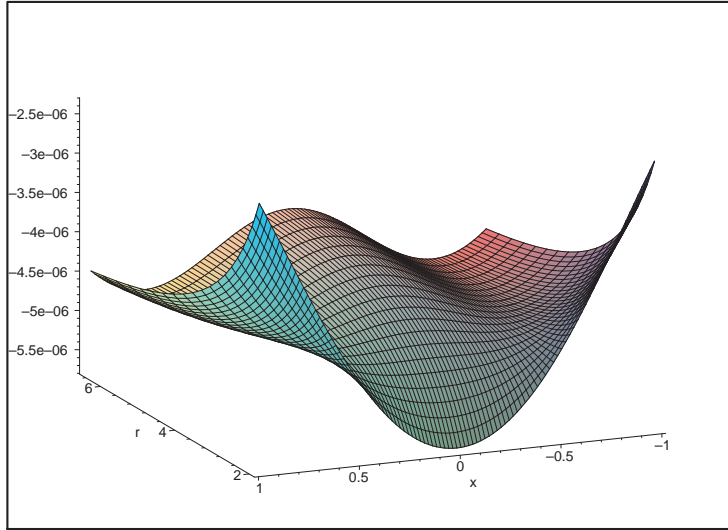


Figure 6.4:  $\frac{1}{4\pi}\Delta\langle\hat{T}_{tr}\rangle^{U^- - B^-}$

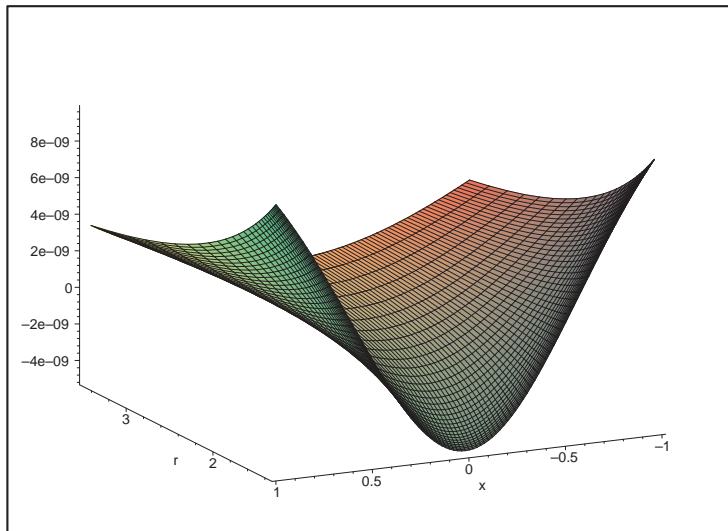


Figure 6.5:  $\frac{1}{4\pi}\Delta\langle\hat{T}_{tr}\rangle^{CCH^- - U^-}$

## 6.8. RSET close to the horizon in the Boulware vacuum

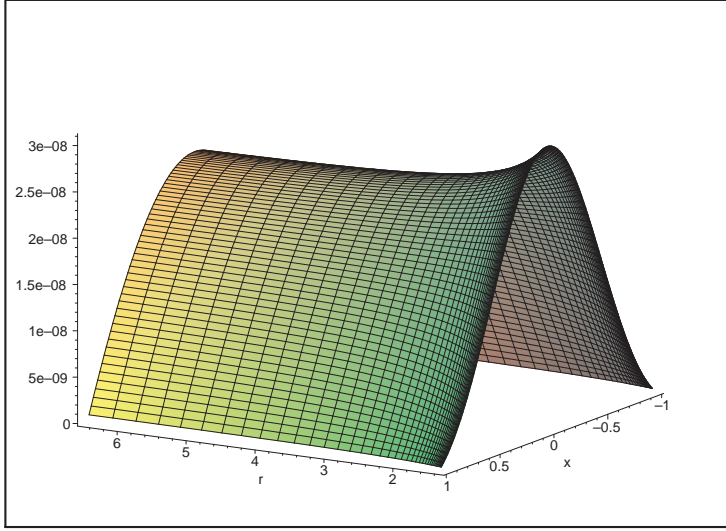


Figure 6.6:  $\frac{1}{4\pi}\Delta\langle\hat{T}_{r\phi}\rangle^{CCH^--U^-}$

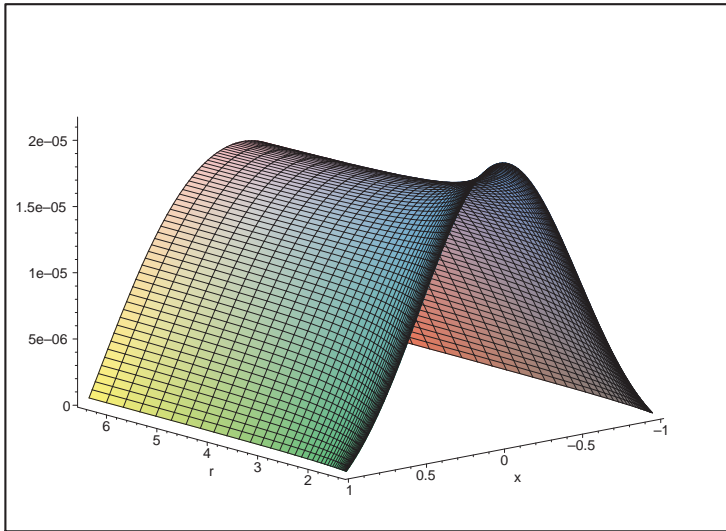


Figure 6.7:  $\frac{1}{4\pi}\Delta\langle\hat{T}_{r\phi}\rangle^{U^--B^-}$

## 6.8. RSET close to the horizon in the Boulware vacuum

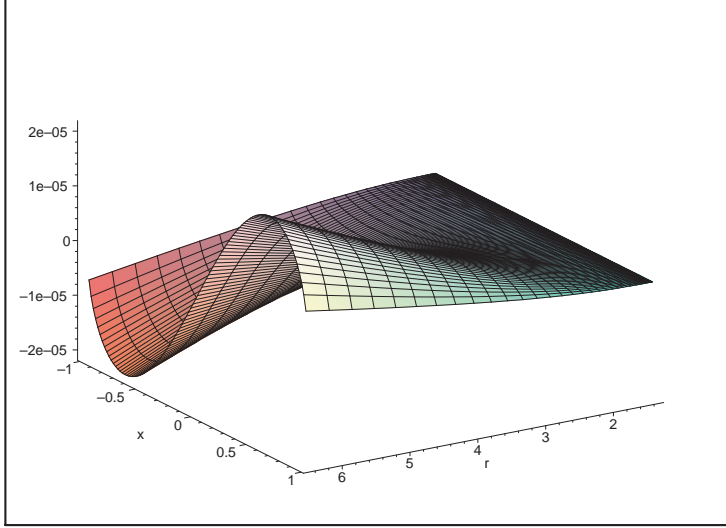


Figure 6.8:  $\frac{1}{4\pi}\Delta^2\langle\hat{T}_{t\theta}\rangle^{U^-B^-}$ . Note that the viewing angle in this and the following graphs is different from that of the previous graphs in order to make more visible the region far from the horizon.

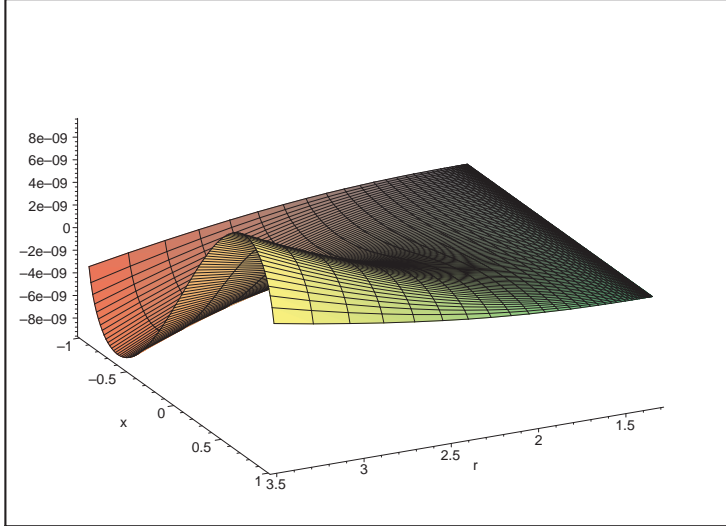


Figure 6.9:  $\frac{1}{4\pi}\Delta^2\langle\hat{T}_{t\theta}\rangle^{CCH^-U^-}$

## 6.8. RSET close to the horizon in the Boulware vacuum

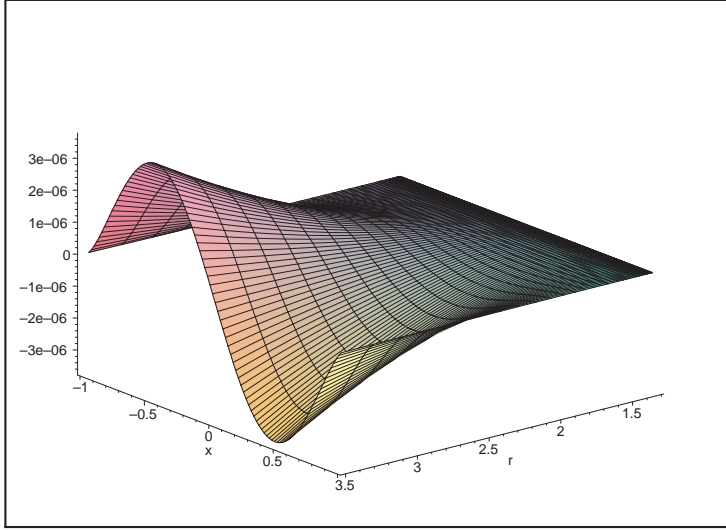


Figure 6.10:  $\frac{1}{4\pi}\Delta^2 \langle \hat{T}_{\theta\phi} \rangle^{U^- - B^-}$

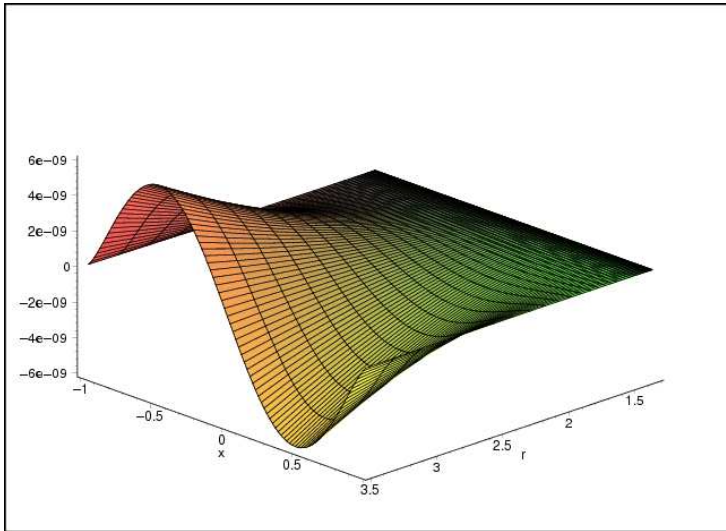


Figure 6.11:  $\frac{1}{4\pi}\Delta^2 \langle \hat{T}_{\theta\phi} \rangle^{CCH^- - U^-}$

## 6.8. RSET close to the horizon in the Boulware vacuum

---

a state in Kerr with the defining features that the Boulware vacuum possesses in Schwarzschild, then the RSET close to the horizon when the field were in this vacuum, would diverge like minus the stress tensor of black body radiation at the black hole temperature rotating with the horizon. The past Boulware vacuum is not invariant under  $(t, \phi)$  reversal because of the existence of the Starobinskiĭ-Unruh radiation. However, the stress tensor components  $tr$  and  $r\phi$ , which correspond to the Starobinskiĭ-Unruh radiation, are expected (from Section 6.7) to have a divergence of one lower leading order than that of the diagonal components as the horizon is approached. It is with this understanding that we say that a state is isotropic at the horizon and that, in particular, the past Boulware vacuum might be isotropic. It is obvious that to next order in  $\Delta$  the past Boulware vacuum cannot be isotropic, but  $\left\langle \hat{T}^\mu_\nu \right\rangle_{\text{ren}}^{CCH^- - B^-}$  might be since  $|CCH^- \rangle$  is not invariant under  $(t, \phi)$  reversal either.

CCH claim that the RSET of the electromagnetic field in the past Boulware vacuum close to the horizon differs from that of minus the stress-energy tensor of a thermal distribution rotating at the angular velocity of a Carter observer by a factor which is a function of  $\theta$ . In the present section, we will show that CCH's result is due to a flawed assumption in the asymptotic behaviour of the SWSH. We will show this by re-calculating their result using the assumptions we believe they used. The numerical results back up the fact that the mentioned RSET is (minus) thermal at the horizon.

We also saw in Section 6.4 that Frolov and Thorne claim that close to the horizon ZAMOs measure a thermal stress tensor which is rigidly rotating with the horizon when the field is in the  $|FT\rangle$  state. That is, they argue that  $\left\langle \hat{T}^\mu_\nu \right\rangle_{\text{ren}}^{FT-B}$  (where  $|B\rangle$  is an unspecified Boulware-type state) is thermal close to the horizon, and isotropic in the frame of a RRO. Duffy, in turn, shows that close to the horizon RROs measure a thermal state which is rigidly rotating with the horizon when the field is in the  $|H_{\mathcal{M}}\rangle$  state in the Kerr space-time modified with the introduction of a mirror. That is to say, close to the horizon  $\left\langle \hat{T}^\mu_\nu \right\rangle_{\text{ren}}^{H_{\mathcal{M}}-B_{\mathcal{M}}}$  is thermal and

## 6.8. RSET close to the horizon in the Boulware vacuum

isotropic in the frame of a RRO. Finally, as mentioned above, CCH claim that  $\left\langle \hat{T}^\mu{}_\nu \right\rangle_{\text{ren}}^{CCH^- - B^-}$  is, bar a factor, thermal at the horizon and isotropic in the Carter tetrad. Of course, the angular velocity at the horizon of a Carter observer, a RRO and a ZAMO is  $\omega = \Omega_+$  for them all, so that CCH's result does not actually distinguish between these observers.

Ottewill and Winstanley [71] have proved that if a certain stress-energy tensor is thermal and rigidly-rotating with the horizon everywhere, then it is divergent on the speed-of-light surface in the Boyer-Lindquist co-ordinates, which are regular on this surface. This implies that if  $\left\langle \hat{T}^\mu{}_\nu \right\rangle_{\text{ren}}^{CCH^- - B^-}$  were thermal and rigidly-rotating with the horizon everywhere then the state  $|CCH^- \rangle$  would have to be irregular on the speed-of-light surface. In the present section we will numerically investigate the rate of rotation of the thermal distribution in question.

The stress-energy tensor of a spin-1 thermal distribution at the Hawking temperature rigidly rotating with the horizon is given by

$$T^{(\text{th,RR})\mu}{}_\nu = \frac{11T^4\pi^2}{45} \left[ \delta^\mu_\nu - 4 \frac{\chi^\mu \chi_\nu}{\chi^\rho \chi_\rho} \right] \quad (6.8.2)$$

where

$$T \equiv \frac{\kappa_+}{2\pi} \frac{1}{\sqrt{-\chi^\rho \chi_\rho}} \quad (6.8.3)$$

is the local temperature. Note that this stress-energy tensor is obviously isotropic in the frame of a RRO, but it is not in the rigidly-rotating co-ordinate system  $\{t_+, r, \theta, \phi_+\}$ , which is not adapted to a RRO.

In primed co-ordinates, which are adapted to a RRO, the rigidly-rotating thermal stress tensor becomes

$$T^{(\text{th,RR})\mu'}{}_{\nu'} = \frac{11(r_+ - r_-)^4}{2^8 \cdot 3^2 \cdot 5\pi^2} \frac{1}{\Delta^2 \Sigma^2} \text{diag} \left( -1, \frac{1}{3}, \frac{1}{3}, \frac{1}{3} \right) \quad (6.8.4)$$

in the Kerr space-time.

CCH calculate an expression for the RSET close to the horizon when the electromagnetic field is in the past Boulware state. They make the assumption that



## 6.8. RSET close to the horizon in the Boulware vacuum

the RSET close to the horizon when the field is in this state is more irregular than when it is in the  $|CCH^-\rangle$  state and therefore approximate

$$\left\langle \hat{T}^\mu{}_\nu \right\rangle_{\text{ren}}^{B^-} \sim \left\langle \hat{T}^\mu{}_\nu \right\rangle_{\text{ren}}^{B^-} - \left\langle \hat{T}^\mu{}_\nu \right\rangle_{\text{ren}}^{CCH^-} = \left\langle \hat{T}^\mu{}_\nu \right\rangle^{B^-} - \left\langle \hat{T}^\mu{}_\nu \right\rangle^{CCH^-} \quad (r \rightarrow r_+) \quad (6.8.5)$$

They can then use their expressions (6.6.2), and it is clear that only the ‘up’ modes are involved in the calculation. Their result, when the components of the stress tensor are put in the Carter orthonormal tetrad (1.3.4) is:

$$\begin{aligned} \left\langle \hat{T}^{\hat{\mu}}{}_{\hat{\nu}} \right\rangle_{\text{ren}}^{B^-} &\sim -\frac{8M^3 r_+}{\pi^2 \Delta^2 \Sigma} \int_0^\infty d\tilde{\omega} \frac{\tilde{\omega}(\tilde{\omega}^2 + \kappa^2)}{e^{2\pi\tilde{\omega}/\kappa} - 1} \text{diag} \left( -1, \frac{1}{3}, \frac{1}{3}, \frac{1}{3} \right) = \\ &= -\frac{1}{r_+} \frac{11(r_+ - r_-)^4}{2^8 \cdot 3^2 \cdot 5\pi^2} \frac{1}{\Delta^2 \Sigma (2Mr_+)} \text{diag} \left( -1, \frac{1}{3}, \frac{1}{3}, \frac{1}{3} \right) \end{aligned} \quad (6.8.6)$$

where the hats on the indices indicate adaptation to the Carter orthonormal tetrad. This expression and the expected result, minus (6.8.4), differ in a factor of  $r_+(2Mr_+)/\Sigma$ . We proceed to reproduce CCH’s expression to explain this disagreement.

We believe that CCH followed Candelas [13] method for spin-0 to obtain asymptotic expansions for the radial solutions for spin-1 close to the horizon. This is the method that we developed in Section 3.5. Armed with the asymptotics of that section, we can proceed to calculate the different components of the stress-energy tensor. In order to do that, we are first going to separately calculate the asymptotic expressions for the various terms that occur in the classical stress-energy tensor (6.1.11).

As mentioned in Section 3.5, for the asymptotic behaviour we are seeking here we can replace the spin-weighted spheroidal harmonics  ${}_h S_{lm}$  by the spin-weighted spherical harmonics  ${}_h Y_{lm}$ . We can then make use of (4.1.12), which immediately leads to

$$\sum_{m=-l}^l {}_{lm\omega} \phi_h^{\text{up}} {}_{lm\omega} \phi_{h'}^{up*} \rightarrow 0 \quad (l \rightarrow +\infty, r \rightarrow r_+) \quad \text{when } h \neq h' \quad (6.8.7)$$

The asymptotic calculation of the term  $|{}_{lm\omega} \phi_0^{\text{up}}|^2$  requires a more careful treatment. We observed in Section 3.5 that the large- $l$  modes dominate the Fourier

## 6.8. RSET close to the horizon in the Boulware vacuum

series for the ‘up’ radial solution close to the horizon. Using (2.8.10) and replacing  $\sum_{l=0}^{\infty}$  with  $\int_0^{\infty} dl$  as we are only interested in the behaviour for  $l \rightarrow +\infty$ , we have

$$\begin{aligned} \sum_{l,m,P} |{}_{lm\omega}\phi_0^{\text{up}}|^2 &\sim \int_0^{\infty} dl \frac{|N_{+1}^{\text{up}}|^2}{2^2 \Sigma^2} \left[ \left| (\rho^{-1} \mathcal{D}_0^\dagger + 1) (\Delta_{+1} R_{lm\omega}^{\text{up}}) \right|^2 \sum_{m=-l}^l \left| \mathcal{L}_{1-1}^\dagger Y_{lm} \right|^2 + \right. \\ &+ a^2 \sin^2 \theta \left| \mathcal{D}_0^\dagger (\Delta_{+1} R_{lm\omega}^{\text{up}}) \right|^2 \sum_{m=-l}^l |{}_{-1}Y_{lm}|^2 + \\ &\left. + \text{terms with } \sum_{m=-l}^l ({}_0Y_{lm-1} Y_{lm}^* + {}_{-1}Y_{lm0} Y_{lm}^*) \right] \quad (l \rightarrow +\infty, r \rightarrow r_+) \end{aligned} \quad (6.8.8)$$

Using equations (4.1.4), (4.1.7a), (4.1.13) and (4.1.12) and the fact that of the two independent variables  $\tilde{\omega}$  and  $m$ ,  ${}_h R_{lm\omega}^{\text{up}}$  depends only on  $\tilde{\omega}$  in the limit ( $l \rightarrow +\infty, r \rightarrow r_+$ ), whereas  ${}_h Y_{lm}$  depends only on  $m$ , equation (6.8.8) can be simplified to

$$\sum_{l,m,P} |{}_{lm\omega}\phi_0^{\text{up}}|^2 \sim \frac{1}{2^3 \pi \Sigma} \int_0^{\infty} dl l^3 |N_{+1}^{\text{up}}|^2 \left| \mathcal{D}_0^\dagger (\Delta_{+1} R_{lm\omega}^{\text{up}}) \right|^2 \quad (l \rightarrow +\infty, r \rightarrow r_+) \quad (6.8.9)$$

where we have also used the fact that

$$|N_{+1}^{\text{up}}|^2 \mathcal{D}_0^\dagger (\Delta_{+1} R_{lm\omega}^{\text{up}}) \gg |N_{+1}^{\text{up}}|^2 \Delta_{+1} R_{lm\omega}^{\text{up}} \quad (l \rightarrow +\infty, r \rightarrow r_+) \quad (6.8.10)$$

as can be seen from (3.5.15) and (3.5.18). We then substitute (3.5.16), (3.5.17), and (3.5.20) in the above equation and approximate  ${}_1 B_{lm\omega} \sim l^2$ . The next integral, found in [40], is needed:

$$\int_0^{\infty} dl l^3 K_{iq}^2(2lx^{1/2}) = \frac{q^2(1+q^2) |\Gamma(iq)|^2}{3 \cdot 2^4 x^2} \quad (6.8.11)$$

We finally obtain

$$\sum_{l,m,P} |{}_{lm\omega}\phi_0^{\text{up}}|^2 \sim \frac{Mr_+ \tilde{\omega} |\Re|^2}{6\pi^2 \Sigma \Delta^2} \quad (l \rightarrow +\infty, r \rightarrow r_+) \quad (6.8.12)$$

The other terms in the expression for the stress-energy tensor can be obtained in a similar manner, but they are easier to calculate. We will therefore only give

## 6.8. RSET close to the horizon in the Boulware vacuum

the final results:

$$\sum_{l,m,P} |{}_{lm\omega}\phi_{-1}^{\text{up}}|^2 \sim \frac{2Mr_+\tilde{\omega}|\Re|^2}{3\pi^2\Delta^3} \quad (l \rightarrow +\infty, r \rightarrow r_+) \quad (6.8.13a)$$

$$\sum_{l,m,P} |{}_{lm\omega}\phi_{+1}^{\text{up}}|^2 \sim \frac{Mr_+\tilde{\omega}|\Re|^2}{6\pi^2\Sigma^2\Delta} \quad (l \rightarrow +\infty, r \rightarrow r_+) \quad (6.8.13b)$$

We can now use equations (6.8.7), (6.8.12) and (6.8.13) together with the quantum expressions (6.8.5) and (6.6.2) to reproduce equation 3.7 in CCH. We obtain

$$\begin{aligned} \left\langle \hat{T}^\mu{}_\nu \right\rangle_{\text{ren}}^{B^-} &\sim \left\langle \hat{T}^\mu{}_\nu \right\rangle^{B^- - CCH^-} \sim \frac{-8M^3r_+^3}{3\pi^2\Delta^2\Sigma^2} \int_0^\infty \frac{d\tilde{\omega}\tilde{\omega}(\tilde{\omega}^2 + \kappa^2)}{e^{2\pi\tilde{\omega}/\kappa} - 1} \times \\ &\times \begin{pmatrix} -3(r_+^2 + a^2) - a^2 \sin^2 \theta & 0 & 0 & 4a \sin^2 \theta (r_+^2 + a^2) \\ 0 & \Sigma & 0 & 0 \\ 0 & 0 & \Sigma & 0 \\ -4a & 0 & 0 & (r_+^2 + a^2) + 3a^2 \sin^2 \theta \end{pmatrix} \quad (r \rightarrow r_+) \end{aligned} \quad (6.8.14)$$

in Boyer-Lindquist co-ordinates.

This is exactly equation 3.7 in CCH except for the fact that (6.8.14) contains a factor  $r_+^3$  instead of a  $r_+$  in CCH. We believe that the discrepancy is due to a typographical error in CCH since otherwise the stress-energy tensor would not have the correct units. We have also checked that equation (6.8.14), when the tensor indices are adapted to the Carter orthonormal tetrad, produces the result (6.8.6) above. Again, the discrepancy with respect to (6.8.6) is only in the power of  $r_+$ . It seems that, despite the discrepancy in the power of  $r_+$ , this is the method that CCH used to calculate their expression (6.8.6). However, as we pointed out in Section 3.5, this asymptotic analysis is only valid when both  $\omega$  and  $m$  are kept bounded since otherwise we would not be able to replace the spin-weighted spheroidal harmonics by the spin-weighted spherical harmonics. In the analysis we have just carried out  $\omega$  and  $m$  do not both remain bounded in general. The only points in the Kerr space-time where both remain bounded are the points along the axis  $\theta = 0$  or  $\pi$  since, there, the Newman-Penrose scalars  ${}_{lm\omega}\phi_h$  are only non-zero for  $m = \pm 1, 0$  and thus  $m$  is bounded. The frequency  $\omega$  is then also

## 6.8. RSET close to the horizon in the Boulware vacuum

---

kept bounded because the factor in the integrand diminishes exponentially with  $\tilde{\omega}$  and thus the contribution is only important when  $\tilde{\omega}$  is bounded. Equations (6.8.14) and (6.8.6) are therefore only valid at the axis. An asymptotic behaviour of the ‘up’ radial solutions uniform both in  $l$  and  $\tilde{\omega}$  is required.

Another issue is the fact that the state  $|CCH^-\rangle$  has been used in (6.8.5) as a Hartle-Hawking state, regular on both the past and future horizons. We know from Kay and Wald’s work that there exists no such state on the Kerr space-time satisfying its isometries. Since  $|CCH^-\rangle$  is not invariant under  $(t, \phi)$  reversal it is not covered by Kay and Wald’s result and thus it might be regular on both  $\mathcal{H}^-$  and  $\mathcal{H}^+$ . We saw that Ottewill and Winstanley [72] argued that in the scalar case this state is irregular on  $\mathcal{H}^-$  and regular on  $\mathcal{H}^+$ . Even if that were also the case for spin-1, using  $|CCH^-\rangle$  in the preceding calculation could still be acceptable if the divergence of  $|CCH^-\rangle$  close to  $r_+$  is of a smaller order than that of  $|B^-\rangle$ . In the Schwarzschild background Candelas has shown that the Unruh state is irregular on  $\mathcal{H}^-$ , regular on  $\mathcal{H}^+$  and that the order of its divergence close to  $r_+$  is smaller than that of the Boulware state. It is therefore reasonable to expect that the order of the divergence of  $|CCH^-\rangle$  close to  $r_+$  in the Kerr background is smaller than that of the past Boulware state. Indeed, our numerical data indicate that the approximation in (6.8.5) is correct.

Graphs 6.12–6.18 show that the RSET when the field is in the past Boulware vacuum approaches a thermal distribution rotating with the horizon rather than CCH’s result (6.8.14). The red lines in the graphs correspond to the thermal stress tensor (6.8.2) rotating with the horizon evaluated at  $r = r_+ \simeq 1.3122$ . The black lines are also located at  $r = r_+$  and correspond to CCH’s result (6.8.14). It can be seen in the graphs that as  $r$  becomes closer to the horizon,  $\left\langle \hat{T}_{\mu\nu} \right\rangle_{\text{ren}}^{CCH^--B^-}$  approaches the thermal stress tensor (6.8.2) (red line) rather than CCH’s corrected equation (6.8.14) (black line). At the poles, however, it can be straight-forwardly checked analytically that the two coincide, as expected. Only for the  $rr$ -component, which is the only component that diverges

## 6.8. RSET close to the horizon in the Boulware vacuum

---

like  $O(\Delta^{-3})$  close to the horizon, we did not seem to be able to obtain a clear plot.

Within the range of  $r$  considered in Graphs 6.12–6.18 (except 6.16) for the difference between the states  $|CCH^- \rangle$  and  $|B^- \rangle$  of the various expectation values, the corresponding plots for the difference between the states  $|U^- \rangle$  and  $|B^- \rangle$  are identical. This is the expected behaviour since for small radius  $r$  the ‘up’ modes dominate in these RSETs. Graph 6.16 includes the two differences for the  $\theta\theta$ -component of the stress-energy tensor up to a value of  $r$  large enough so that the two differences become clearly distinct.

In following with the notation used in (1.3.1) and the one used so far for tensor components in Boyer-Lindquist co-ordinates, we use the obvious notation of ‘ $(\alpha\beta)$ -component’ to refer to the stress-energy tensor component  $T_{\mu\nu}e_{(\alpha)}{}^\mu e_{(\beta)}{}^\nu$  in the tetrad of a stationary observer. Since the angular velocities of a RRO, ZAMO and Carter observer all equal  $\Omega_+$  at the horizon, each one of the diagonal components of a stress tensor for a thermal distribution will be the same in any of the three tetrads adapted to these observers. The  $(r\theta)$ -component will also be the same in any of the three tetrads since the tetrad vectors  $e_{(r)}$  and  $e_{(\theta)}$  do not depend on the rate of rotation. The  $(t\phi)$ -component, however, vanishes to leading order for the radial functions as  $r \rightarrow r_+$ . To the next leading order for the radial functions this component does depend on the rate of rotation of the stationary observer that the tetrad is adapted to. Graphs 6.19–6.20 for  $\left\langle \hat{T}_{t+\phi+} \right\rangle_{\text{ren}}^{B^-}$  show that the rate of rotation of the thermal distribution approaches, to next order in  $\Delta$ , that of a RRO, rather than that of a ZAMO or a Carter observer. This result tallies with Duffy [32]’s results for the spin-0 case in the Kerr space-time modified with a mirror when the field is in the  $|H_{\mathcal{M}} \rangle$  state. He also numerically shows that  $\left\langle \hat{T}_{\mu\nu} \right\rangle^{U^- - B^-}$  is, close to the horizon and for the scalar field, thermal and rotating at the rate of a RRO to  $O(\Delta)$  in the angular frequency. We calculated and plotted  $\left\langle \hat{T}_{t+\phi+} \right\rangle_{\text{ren}}^{U^- - B^-}$  and it fully coincided with  $\left\langle \hat{T}_{t+\phi+} \right\rangle_{\text{ren}}^{CCH^- - B^-}$  in the region of Graphs 6.19–6.20, which is why we do not include them. We conclude

---

## 6.9. Symmetry $(\theta, \phi) \rightarrow (\pi - \theta, \phi + \pi)$

that the rate of rotation close to the horizon for the difference between the states  $|U^- \rangle$  and  $|B^- \rangle$  is also that of a RRO, in agreement with Duffy's results.

An alternative technique for investigating what is the rate of rotation of the thermal distribution at the horizon is as follows. We find what is the frequency  $\omega = \omega_{\text{ZEFO}}$  of rotation of the tetrad frame (1.3.1) such that  $T_{(t\phi)} = 0$ , where the term ZEFO stands for *zero energy flux observer*. The answer is

$$\omega_{\text{ZEFO}} = \frac{-2C}{B + \sqrt{B^2 - 4AC}} \quad (6.8.15)$$

where

$$\begin{aligned} A &= g_{\phi\phi}T_{t\phi} - g_{t\phi}T_{\phi\phi} \\ B &= g_{\phi\phi}T_{tt} - g_{tt}T_{\phi\phi} \\ C &= g_{t\phi}T_{tt} - g_{tt}T_{t\phi} \end{aligned} \quad (6.8.16)$$

We then plot  $\omega_{\text{ZEFO}}$  where  $T_{\mu\nu}$  is replaced by  $\langle \hat{T}_{\mu\nu} \rangle_{\text{ren}}^{CCH^- - B^-}$  in (6.8.16). This plot is compared against that of the angular velocities of a RRO, ZAMO and Carter observer in Figure 6.21. We also plotted  $\omega_{\text{ZEFO}}$  where  $T_{\mu\nu}$  is replaced by  $\langle \hat{T}_{\mu\nu} \rangle_{\text{ren}}^{U^- - B^-}$  and it fully coincided with the corresponding one for  $\langle \hat{T}_{\mu\nu} \rangle_{\text{ren}}^{CCH^- - B^-}$  in the region of Figure 6.21.

Graphs 6.22–6.26 show the behaviour of the various modes as the horizon is approached. Most of the features described in their captions are explained by the horizon asymptotics developed in Section 3.5.

## 6.9 Symmetry $(\theta, \phi) \rightarrow (\pi - \theta, \phi + \pi)$

When we initially used the expressions (6.6.2) given by CCH for the calculation of the difference in the RSET when the field is in two different states, we found to our surprise that the results were not symmetric under the parity operation  $\mathcal{P} : (\theta, \phi) \rightarrow (\pi - \theta, \phi + \pi)$ . Analytically, there was a strong indication that the results were not symmetric under  $\mathcal{P}$ , although it was hard to prove the lack of

## 6.9. Symmetry $(\theta, \phi) \rightarrow (\pi - \theta, \phi + \pi)$

---

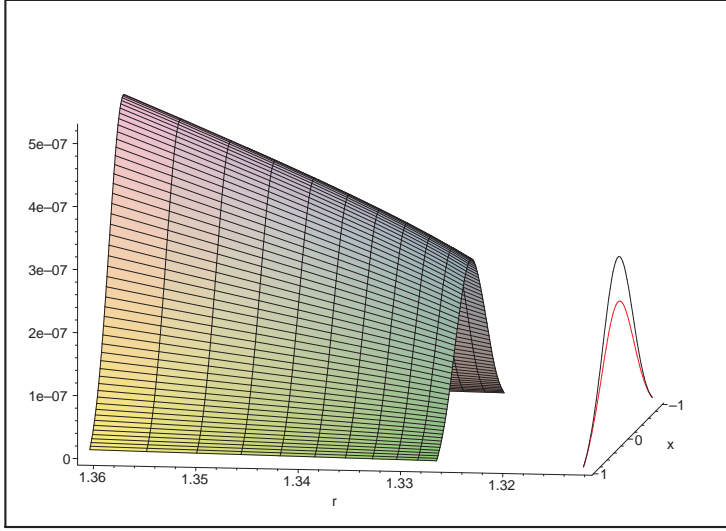


Figure 6.12:  $\frac{1}{4\pi}\Delta^2 \langle \hat{T}_{tt} \rangle^{CCH^- - B^-}$

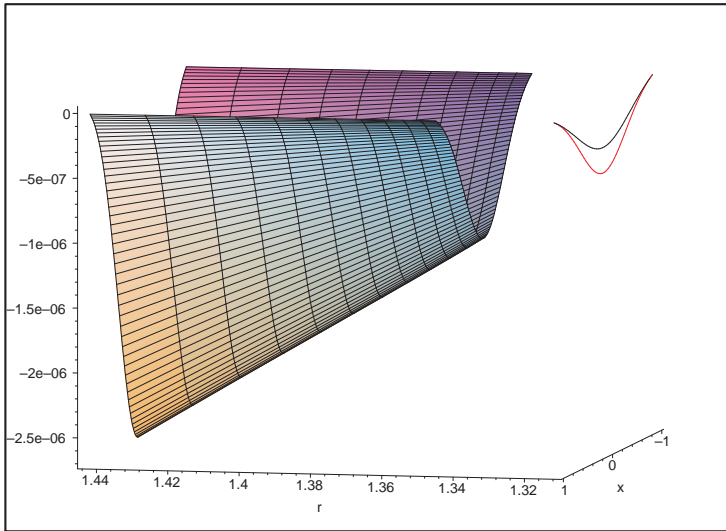


Figure 6.13:  $\frac{1}{4\pi}\Delta^2 \langle \hat{T}_{t\phi} \rangle^{CCH^- - B^-}$

## 6.9. Symmetry $(\theta, \phi) \rightarrow (\pi - \theta, \phi + \pi)$

---

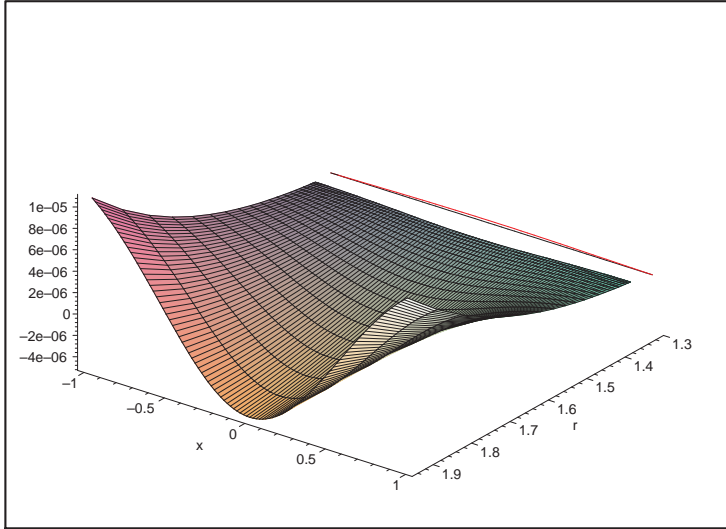


Figure 6.14:  $\frac{1}{4\pi}\Delta^3 \left\langle \hat{T}_{rr} \right\rangle^{CCH^- - B^-}$



## 6.9. Symmetry $(\theta, \phi) \rightarrow (\pi - \theta, \phi + \pi)$

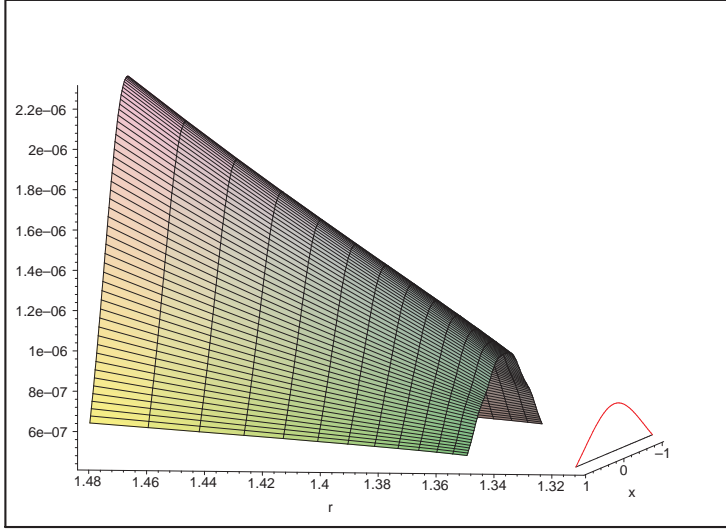


Figure 6.15:  $\frac{1}{4\pi}\Delta^2 \langle \hat{T}_{\theta\theta} \rangle^{CCH^- - B^-}$

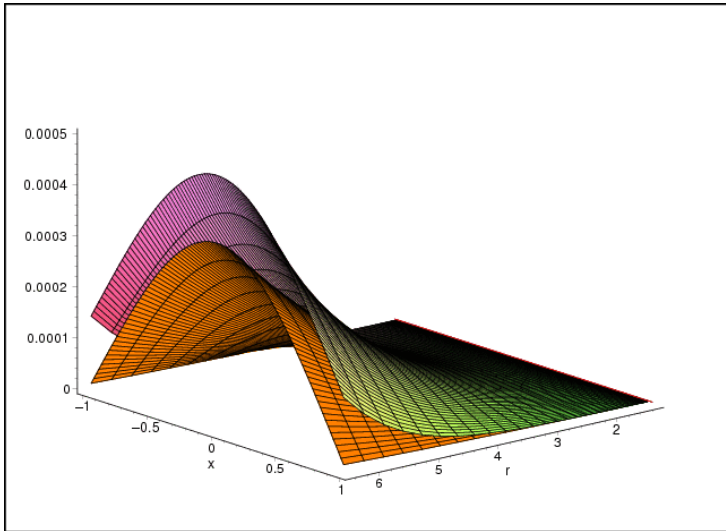


Figure 6.16:  $\frac{1}{4\pi}\Delta^2 \langle \hat{T}_{\theta\theta} \rangle^{CCH^- - B^-}$  and  $\frac{1}{4\pi}\Delta^2 \langle \hat{T}_{\theta\theta} \rangle^{U^- - B^-}$  (orange)

## 6.9. Symmetry $(\theta, \phi) \rightarrow (\pi - \theta, \phi + \pi)$

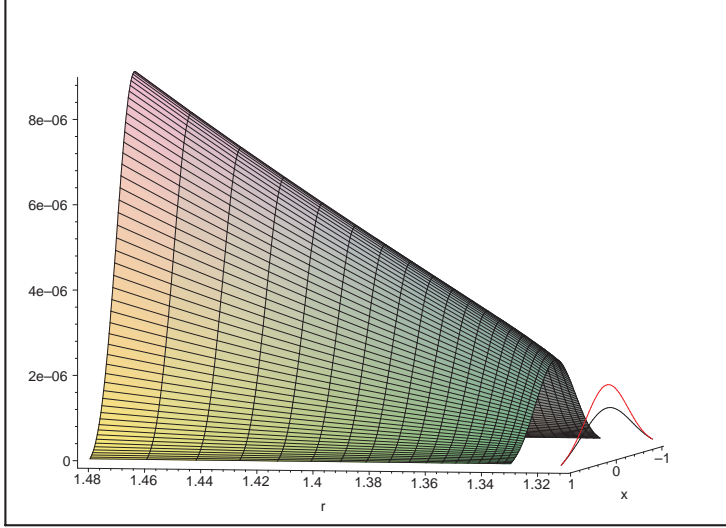


Figure 6.17:  $\frac{1}{4\pi} \Delta^2 \langle \hat{T}_{\phi\phi} \rangle^{CCH^- - B^-}$

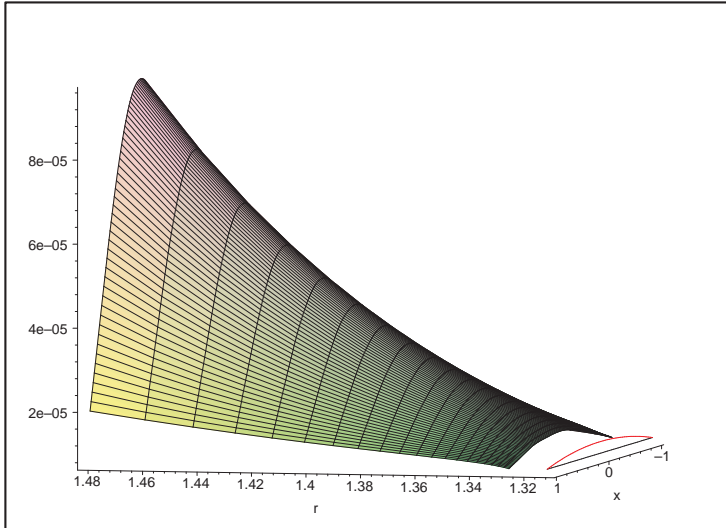


Figure 6.18:  $\frac{\Sigma \Delta^2}{4\pi \sin^2 \theta} \langle \hat{T}_{\phi\phi} \rangle^{CCH^- - B^-} + \frac{11(r_+ - r_-)^4 M r_+ a^2 \sin^2 \theta}{2^9 \cdot 3^2 \cdot 5 \pi^3}$  (so that CCH's expression is constant in  $\theta$ )

## 6.9. Symmetry $(\theta, \phi) \rightarrow (\pi - \theta, \phi + \pi)$

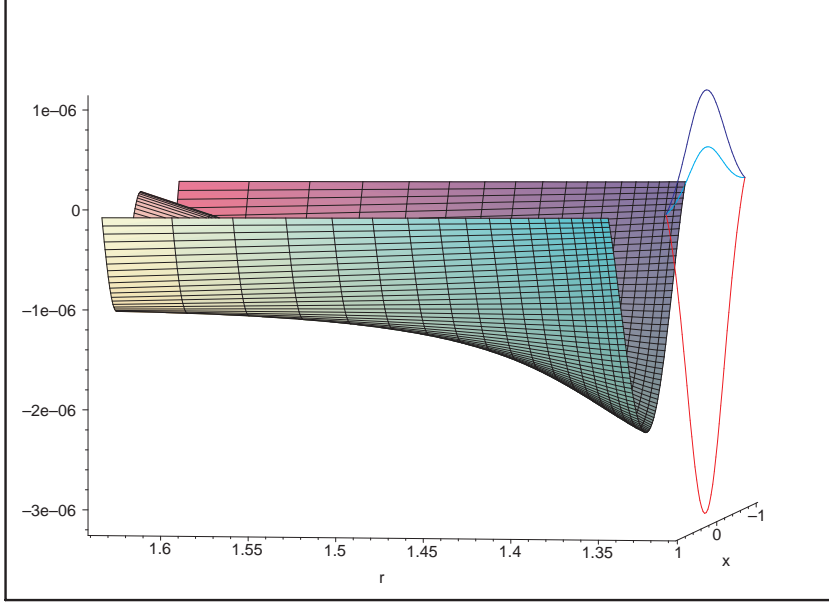


Figure 6.19:  $\frac{1}{4\pi}\Delta\langle\hat{T}_{t+\phi+}\rangle^{CCH^- - B^-}$ ,  $\frac{1}{4\pi}\Delta T_{t+\phi+}^{(\text{th,RR})}$  (red),  $\frac{1}{4\pi}\Delta T_{t+\phi+}^{(\text{th,ZAMO})}$  (blue) and  $\frac{1}{4\pi}\Delta T_{t+\phi+}^{(\text{th,Carter})}$  (cyan).

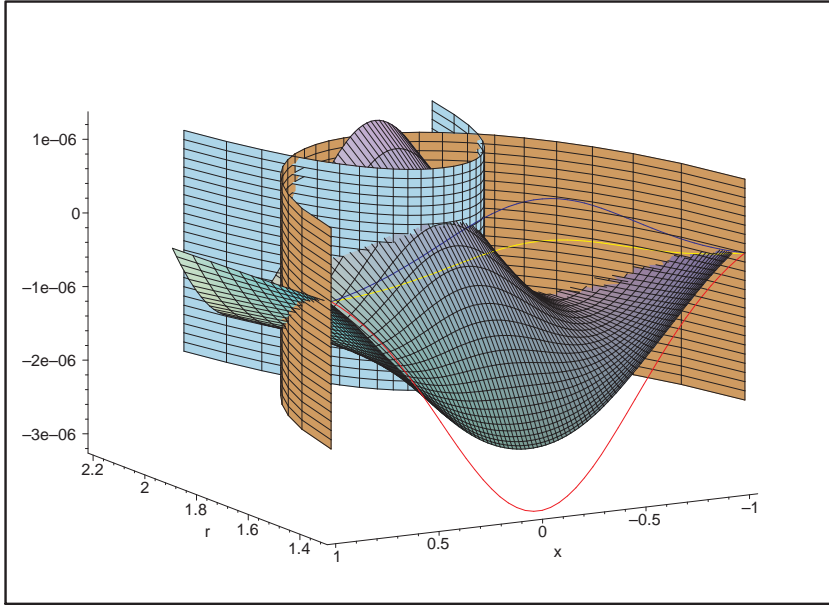


Figure 6.20:  $\frac{1}{4\pi}\Delta\langle\hat{T}_{t+\phi+}\rangle^{CCH^- - B^-}$ ,  $\frac{1}{4\pi}\Delta T_{t+\phi+}^{(\text{th,RR})}$  (red),  $\frac{1}{4\pi}\Delta T_{t+\phi+}^{(\text{th,ZAMO})}$  (blue) and  $\frac{1}{4\pi}\Delta T_{t+\phi+}^{(\text{th,Carter})}$  (yellow). The light blue and brown surfaces correspond to the speed-of-light and the static limit surfaces respectively.

## 6.9. Symmetry $(\theta, \phi) \rightarrow (\pi - \theta, \phi + \pi)$

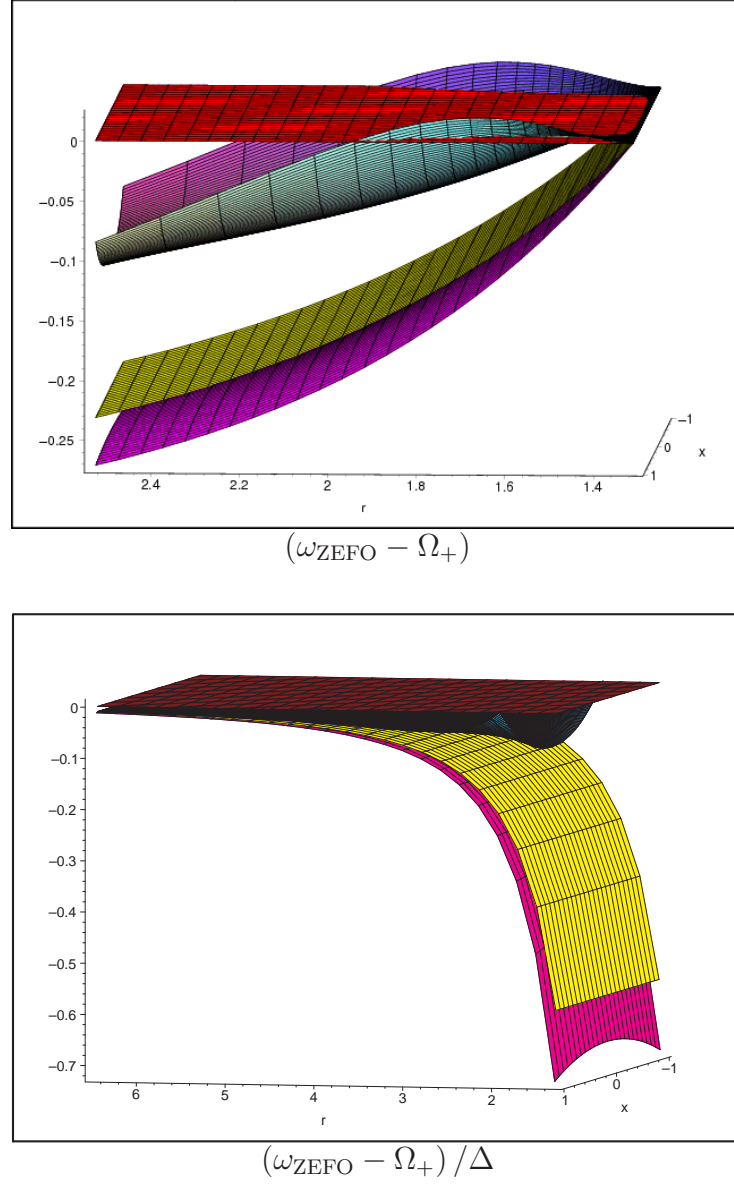


Figure 6.21: Plots of  $(\omega_{\text{ZEFO}} - \Omega_+)$  and  $(\omega_{\text{ZEFO}} - \Omega_+) / \Delta$  (dark surfaces) where  $T_{\mu\nu}$  is replaced by  $\langle \hat{T}_{\mu\nu} \rangle_{\text{ren}}^{CCH^- - B^-}$  in (6.8.15), together with the corresponding plots with the angular velocities of a RRO (red), ZAMO (magenta) and Carter observer (yellow).

## 6.9. Symmetry $(\theta, \phi) \rightarrow (\pi - \theta, \phi + \pi)$

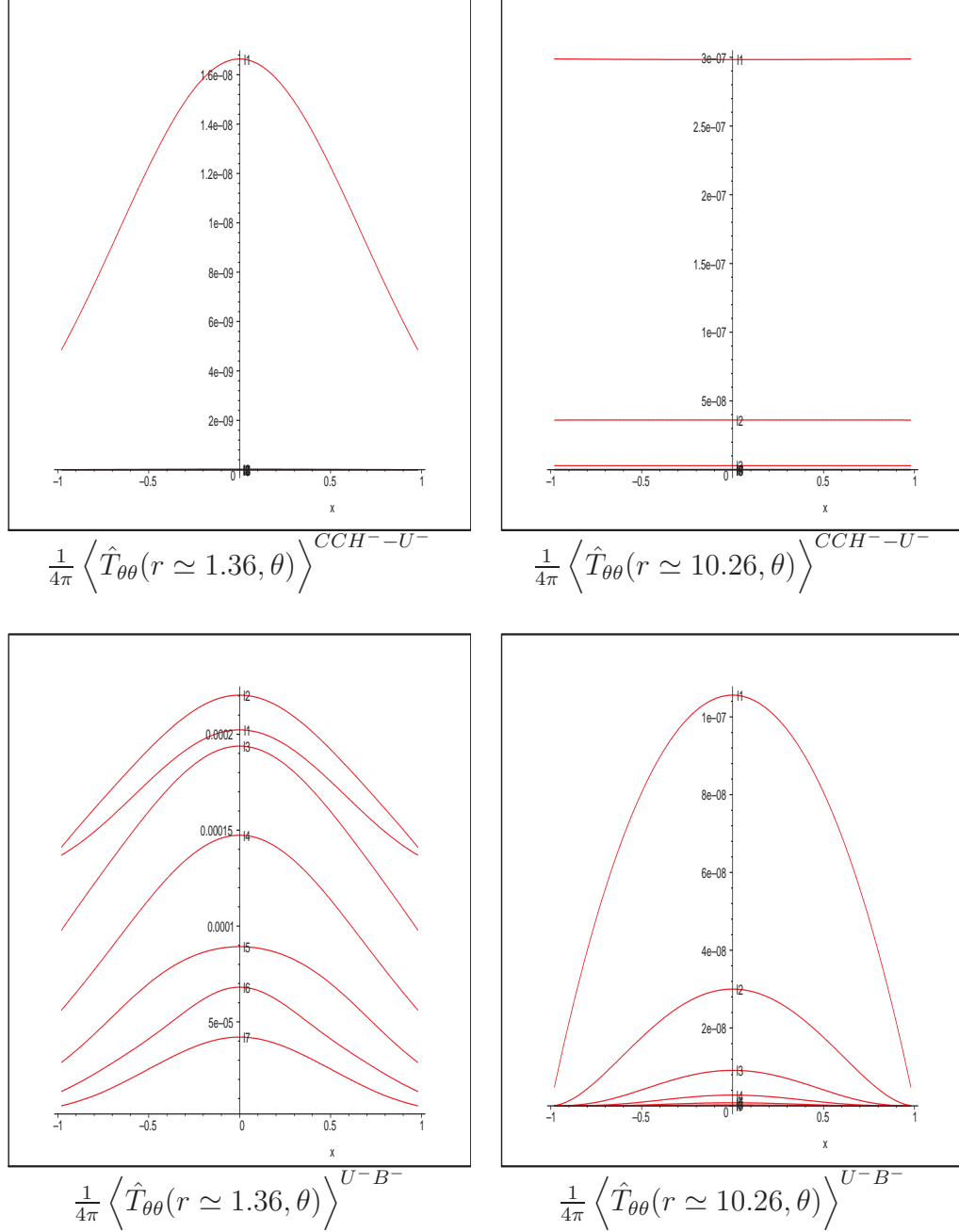
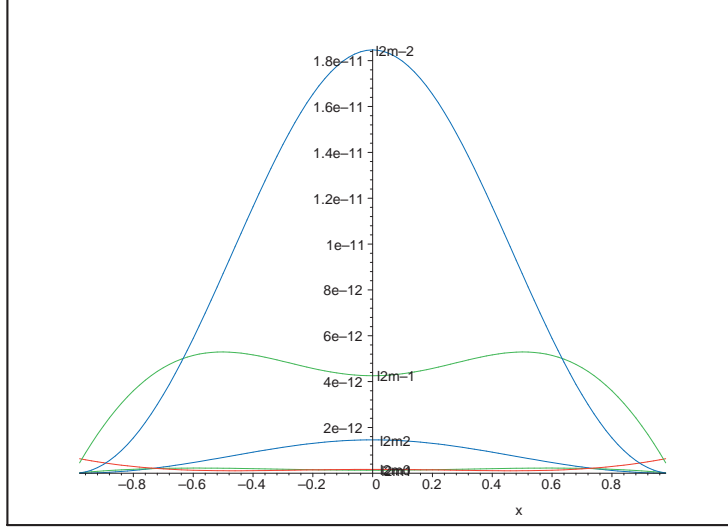


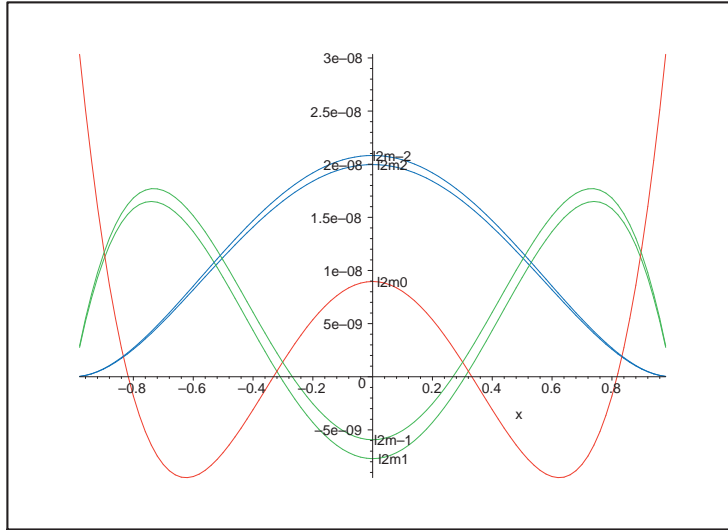
Figure 6.22: The sum over  $l$  has not been performed. For each value of  $l$  the sum  $\sum_{m=-l}^l$  has been performed. In the case of  $\langle \hat{T}_{\theta\theta} \rangle^{CCH^- - U^-}$  the low- $l$  modes clearly dominate close to the horizon. On the other hand, the high- $l$  modes dominate close to the horizon in the case of  $\langle \hat{T}_{\theta\theta} \rangle^{U^- - B^-}$ .

## 6.9. Symmetry $(\theta, \phi) \rightarrow (\pi - \theta, \phi + \pi)$

---



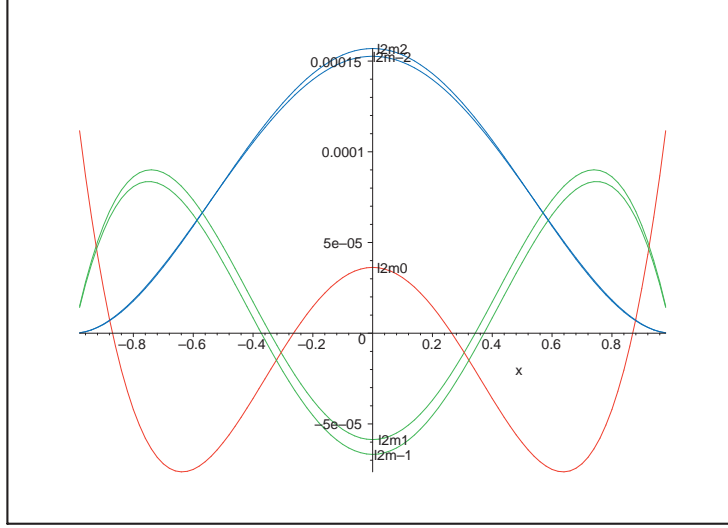
$l = 2$  at  $r \simeq 1.36$



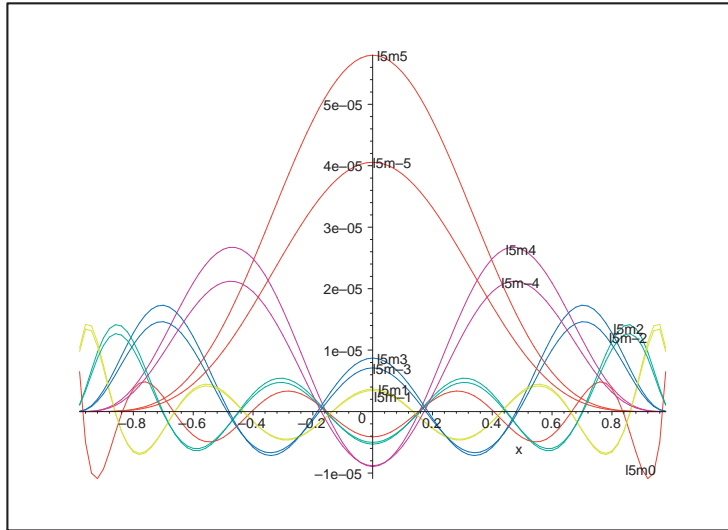
$l = 2$  at  $r \simeq 10.26$

Figure 6.23:  $\frac{1}{4\pi} \langle \hat{T}_{\theta\theta} \rangle^{CCH^- - U^-}$  where the sums over  $l$  and  $m$  have not been performed. The graphs for the modes with  $(l, |m|)$  and with  $(l, -|m|)$  are very similar in shape. Close to the horizon the ones with  $(l, -|m|)$  dominate.

## 6.9. Symmetry $(\theta, \phi) \rightarrow (\pi - \theta, \phi + \pi)$



$l = 2$  at  $r \simeq 1.36$



$l = 5$  at  $r \simeq 1.36$

Figure 6.24:  $\frac{1}{4\pi} \langle \hat{T}_{\theta\theta} \rangle^{U^- - B^-}$  where the sums over  $l$  and  $m$  have not been performed. The graphs for the modes with  $(l, |m|)$  and with  $(l, -|m|)$  are very similar in shape and magnitude, both close and far from the horizon.

## 6.9. Symmetry $(\theta, \phi) \rightarrow (\pi - \theta, \phi + \pi)$

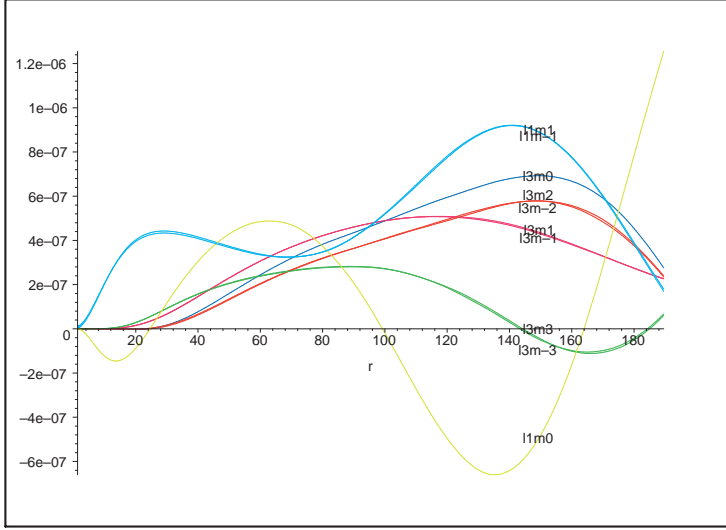


Figure 6.25:  $\frac{1}{4\pi} \langle \hat{T}_{\theta\theta}(r, \theta = \pi/2) \rangle^{CCH^- - U^-}$  for  $l = 1, 3$  and  $m = -l \rightarrow l$ . The modes  $(l, |m|)$  and  $(l, -|m|)$  are paired up far from the horizon, where they intertwine. One set does not dominate over the other in that region. Low- $l$  modes dominate over high- $l$  ones close to the horizon but neither set dominates far from the horizon.

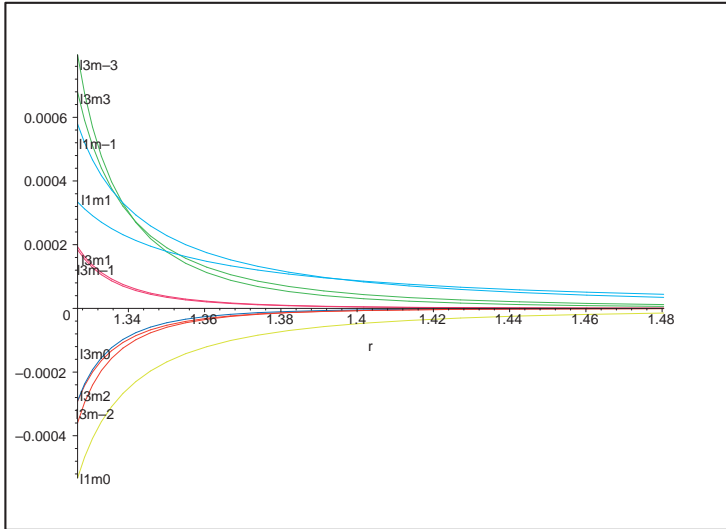


Figure 6.26:  $\frac{1}{4\pi} \langle \hat{T}_{\theta\theta}(r, \theta = \pi/2) \rangle^{U^- - B^-}$  for  $l = 1, 3$  and  $m = -l \rightarrow l$ . Modes  $(l, -|m|)$  dominate over  $(l, |m|)$  much closer to the horizon than they do for the ‘in’ modes case. High- $l$  modes dominate over low- $l$  ones close to the horizon.



---

## 6.9. Symmetry $(\theta, \phi) \rightarrow (\pi - \theta, \phi + \pi)$

---

symmetry. Numerically, the results obtained were clearly not symmetric under the parity operation.

In the first subsection of this last section we analytically prove that the results obtained using CCH's expressions (6.6.2) are not symmetric under  $\mathcal{P}$ . In the second subsection we find that the reason for this lack of symmetry is that expressions (6.6.2) are not correct, and we find the correct expressions. In the third and last subsection we give a physical interpretation of the different sets of terms in the expressions for the expectation value of the stress-energy tensor in various states.

Even though the full parity operation involves a transformation in both angular variables  $\theta$  and  $\phi$ , it is clear that we only need to consider the transformation in  $\theta$  as regards to the stress-energy tensor.

### 6.9.1 Lack of symmetry

The invariance under the transformation  $(\theta \rightarrow \pi - \theta)$  is straight-forwardly satisfied on the Schwarzschild background by the RSET of a field of any spin when the field is in any of the states in expressions (6.6.2). The reason for this invariance in the Schwarzschild background is that when  $a = 0$ , the angular function does not depend on  $\omega$  and the radial function does not depend on  $m$ . Therefore, applying the transformation  $(\theta \rightarrow \pi - \theta)$  on any mode in (6.6.2) is equivalent to performing  $(m \rightarrow -m)$  only, by virtue of the relations (3.1.3b) and (4.2.1b) and the reality of the stress tensor. The sum over  $m$  appearing in (6.6.2) then guarantees the invariance of those expressions under  $(\theta \rightarrow \pi - \theta)$ , and therefore under  $\mathcal{P}$ .

Such a straight-forward reasoning does not follow in the Kerr background because applying the parity operation on the expressions (6.6.2) implies a change in the sign of  $\omega$  as well as in the sign of  $m$ . Whereas the sum over  $m$  is symmetric with respect to  $m = 0$ , the integration over the frequency is not symmetric with

## 6.9. Symmetry $(\theta, \phi) \rightarrow (\pi - \theta, \phi + \pi)$

---

respect to  $\omega = 0$ . In order to investigate the symmetry, or otherwise, under  $\mathcal{P}$  of the expectation values (6.6.2) on the Kerr background, we will calculate these expectation values evaluated at the point  $(r, \theta)$  minus their value at the point  $(r, \pi - \theta)$ . This procedure is obviously not useful for those components of the stress-energy tensor such that one index is  $\theta$  and the other one is not. For these components, the symmetry under parity should be investigated by adding the value of the expectation value at  $(r, \theta)$  to that at  $(r, \pi - \theta)$ .

The classical stress-energy tensor (6.1.11) is made up of the sum of various terms that are quadratic in the field. We conveniently gather these terms into groups that appear when expressing the stress-energy tensor in Boyer-Lindquist co-ordinates. We then calculate the difference between the value at  $(r, \theta)$  and the value at  $(r, \pi - \theta)$  of these groups of terms, mode by mode. The following are useful expressions for some of such differences:

$$\begin{aligned} \frac{|_{lm\omega}\phi_{-1}(r, \theta)|^2}{4} + \frac{|_{lm\omega}\phi_{+1}(r, \theta)|^2}{\Delta^2 \Sigma^2} - [\theta \rightarrow \pi - \theta] = \\ = \frac{-iK}{2B\Delta^2} ({}_{+1}S_{lm\omega}^2 - {}_{-1}S_{lm\omega}^2) W[Y_{+1}, Y_{-1}^*]_{lm\omega} \end{aligned} \quad (6.9.1a)$$

$$\begin{aligned} \frac{|_{lm\omega}\phi_{-1}(r, \theta)|^2 \Delta}{4\Sigma} - \frac{|_{lm\omega}\phi_{+1}(r, \theta)|^2 \Sigma}{\Delta} - [\theta \rightarrow \pi - \theta] = \\ = \frac{\Delta}{4\Sigma} ({}_{+1}S_{lm\omega}^2 - {}_{-1}S_{lm\omega}^2) \left( |{}_{+1}R_{lm\omega}|^2 + \frac{\Sigma^4}{\Delta^2} |{}_{-1}R_{lm\omega}|^2 \right) \end{aligned} \quad (6.9.1b)$$

$$\begin{aligned} |_{lm\omega}\phi_0(r, \theta)|^2 - [\theta \rightarrow \pi - \theta] = \\ = \frac{-iaW[Y_{+1}, Y_{-1}^*]_{lm\omega}}{2\Sigma^2 {}_1B_{lm\omega}^2} \left[ 2 \cos \theta (\mathcal{L}_{1-1}^\dagger S_{lm\omega})(\mathcal{L}_{1+1} S_{lm\omega}) + \right. \\ \left. + \sin \theta ({}_{+1}S_{lm\omega}(\mathcal{L}_{1-1}^\dagger S_{lm\omega}) + {}_{-1}S_{lm\omega}(\mathcal{L}_{1+1}^\dagger S_{lm\omega})) \right] \end{aligned} \quad (6.9.1c)$$

$${}_{lm\omega}\phi_{+1}(r, \theta) {}_{lm\omega}\phi_{-1}^*(r, \theta) \frac{1}{\rho^2} - [\theta \rightarrow \pi - \theta] = 0 \quad (6.9.1d)$$

We are adopting the notation that the symbol  $[\theta \rightarrow \pi - \theta]$  at the end of an expression represents all the previous terms in that expression being evaluated at  $\pi - \theta$  instead of  $\theta$ . Note that we are not using any particular boundary conditions for the radial functions. We therefore do not include any constants of normalization

## 6.9. Symmetry $(\theta, \phi) \rightarrow (\pi - \theta, \phi + \pi)$

---

and will only include them when we wish to calculate the expectation value of the stress-energy tensor.

An outline of two useful properties that some of these groups of terms possess is given in Table 6.2. When the stress-energy tensor is expressed in Boyer-Lindquist co-ordinates and its value at  $(r, \pi - \theta)$  is subtracted from the one at  $(r, \theta)$ , there exist two other groups of terms apart from those in (6.9.1) which we have included in Table 6.2 but which do not possess any of the two properties in question. Table 6.3 shows which groups of terms appear for each component of the stress tensor.

We calculate in this subsection the expectation value of any quadratic operator when the field is in a certain state of interest with CCH's expressions (6.6.1). In order to evaluate the difference in the RSET in a particular state between the points  $(r, \theta)$  and  $(r, \pi - \theta)$ , we also need to know how  $T_{\mu\nu}^{\text{div}}$  behaves under  $(\theta \rightarrow \pi - \theta)$ . Since  $T_{\mu\nu}^{\text{div}}$  is a purely geometrical object and the metric is invariant under  $\mathcal{P}$ , this divergent stress tensor must also be invariant under  $\mathcal{P}$ . This invariance implies that

$$\left\langle \hat{T}_{\mu\nu}(r, \theta) \right\rangle^{\Psi} - (-1)^{\vartheta} \left\langle \hat{T}_{\mu\nu}(r, \pi - \theta) \right\rangle^{\Psi} = \left\langle \hat{T}_{\mu\nu}(r, \theta) \right\rangle_{\text{ren}}^{\Psi} - (-1)^{\vartheta} \left\langle \hat{T}_{\mu\nu}(r, \pi - \theta) \right\rangle_{\text{ren}}^{\Psi} \quad (6.9.2)$$

where  $\Psi$  represents any state. The variable  $\vartheta$  is defined so that  $(-1)^{\vartheta}$  is equal to -1 if one index of the component of the stress tensor is  $\theta$  and the other one is not, and it is equal to +1 otherwise.

By virtue of the symmetries (6.2.5b) and the property (3.2.53), the expectation value in certain states of operators corresponding to the groups of terms for which the radial functions only appear as part of a wronskian will adopt a particularly simple form. This is the case for the groups of terms (a) and (c) in Table 6.2. Table 6.4 shows the form of the expectation value of such operators when the electromagnetic field is in various states when expressions (6.6.2) and (6.6.3) are used.

	has $(+1S_{lm\omega}^2 - -1S_{lm\omega}^2)$ ?	has $W[Y_{+1}, Y_{-1}^*]_{lm\omega}$ ?
(a) $\frac{ lm\omega\phi_{-1} ^2}{4} + \frac{ lm\omega\phi_{+1} ^2}{\Delta^2\Sigma^2} - [\theta \rightarrow \pi - \theta]$	Y	Y
(b) $\frac{ lm\omega\phi_{-1} ^2\Delta}{4\Sigma} - \frac{ lm\omega\phi_{+1} ^2\Sigma}{\Delta} - [\theta \rightarrow \pi - \theta]$	Y	N
(c) $ lm\omega\phi_0 ^2 - [\theta \rightarrow \pi - \theta]$	N	Y
(d) $lm\omega\phi_{+1} \quad lm\omega\phi_{-1}^* \frac{1}{\rho^2} - [\theta \rightarrow \pi - \theta]$	0	
(e) $lm\omega\phi_0 \quad lm\omega\phi_{-1}^* \frac{\Delta}{\Sigma} + 2lm\omega\phi_{+1} \quad lm\omega\phi_0^* - [\theta \rightarrow \pi - \theta]$	N	N
(f) $-lm\omega\phi_0 \quad lm\omega\phi_{-1}^* \frac{\Delta}{\Sigma} + 2lm\omega\phi_{+1} \quad lm\omega\phi_0^* - [\theta \rightarrow \pi - \theta]$	N	N

Table 6.2: This table indicates which of the groups of terms appearing in  $lm\omega T_{\mu\nu}(r, \theta) - [\theta \rightarrow \pi - \theta]$  in Boyer-Lindquist co-ordinates contain the factors  $(+1S_{lm\omega}^2 - -1S_{lm\omega}^2)$  and  $W[Y_{+1}, Y_{-1}^*]_{lm\omega}$

## 6.9. Symmetry $(\theta, \phi) \rightarrow (\pi - \theta, \phi + \pi)$

---

$T_{\mu\nu}$
$t\phi, tt, \phi\phi$ : (a),(c),(d),(e)
$tr, r\phi$ : (b),(f)
$t\theta, \theta\phi$ : (d),(e)
$rr$ : (a),(c)
$\theta\theta$ : (c),(d)
$r\theta$ : (f)

Table 6.3: Groups of terms in Table 6.2 that appear in the expression for  ${}_{lm\omega}T_{\mu\nu}(r, \theta) - [\theta \rightarrow \pi - \theta]$  for each one of the components in Boyer-Lindquist co-ordinates.

$ \Psi\rangle$	$\langle \hat{Q} \rangle^\Psi$
$ B^-\rangle$	0
$ FT\rangle$	$-2 \sum_{m=1}^l \int_0^{m\Omega_+} d\omega \coth(\frac{\pi\tilde{\omega}}{\kappa})$
$ CCH^-\rangle$	$-2 \sum_{m=1}^l \int_0^{m\Omega_+} d\omega \coth(\frac{\pi\tilde{\omega}}{\kappa}) + \sum_{m=-l}^l \int_0^\infty d\omega [\coth(\frac{\pi\tilde{\omega}}{\kappa}) - \coth(\frac{\pi\omega}{\kappa})]$
$ U^-\rangle$	$-2 \sum_{m=1}^l \int_0^{m\Omega_+} d\omega \coth(\frac{\pi\tilde{\omega}}{\kappa}) + \sum_{m=-l}^l \int_0^\infty d\omega [\coth(\frac{\pi\tilde{\omega}}{\kappa}) - 1]$

Table 6.4:  $\hat{Q}$  is any quadratic operator in the field and its derivatives such that all the radial functions content of its classical counterpart  $Q[{}_{lm\omega}\phi_h^\bullet, {}_{lm\omega}\phi_h^{\bullet*}]$  can be expressed as a wronskian. For clarity,  $\sum_{lP}$  has been omitted from the sums and  $Q[{}_{lm\omega}\phi_h^{\text{up}}, {}_{lm\omega}\phi_h^{\text{up}*}]$  from all integrands.

## 6.9. Symmetry $(\theta, \phi) \rightarrow (\pi - \theta, \phi + \pi)$

We now proceed to analytically prove the lack of symmetry under parity of the RSET for the easiest case. Tables 6.2 and 6.3 reveal that the easiest component of the RSET for which to investigate the symmetry under parity is the  $\theta\theta$ -component. The easiest point where to evaluate the stress-energy tensor is at the axis of symmetry. We are therefore going to calculate  ${}_{lm\omega}T_{\theta\theta}(r, \theta = 0) - {}_{lm\omega}T_{\theta\theta}(r, \theta = \pi)$ , which only involves term (c) in Table 6.2.

From equations (4.2.7) and (2.7.10a) it follows that

$$\mathcal{L}_n^{\{\dagger\}} S_{lm\omega} \sim 2^{(\beta-1/2)} {}_h a_{n=0,lm\omega} (2\alpha \pm m + n) (1-x)^{(\alpha-1/2)} \quad (x \rightarrow +1) \quad (6.9.3a)$$

$$\mathcal{L}_n^{\{\dagger\}} S_{lm\omega} \sim 2^{(\alpha-1/2)} {}_h b_{n=0,lm\omega} (-2\beta \pm m - n) (1+x)^{(\beta-1/2)} \quad (x \rightarrow -1) \quad (6.9.3b)$$

We insert these equations into the two equivalent expressions for  ${}_{lm\omega}\phi_0$  given in (2.8.10). These expressions refer to either ‘in’ or ‘up’ modes and we will temporarily follow the same normalization as in [20]. This normalization is obtained by replacing  ${}_{+1}R_{lm\omega}^{\text{in}}$  by  $-2\sqrt{2\pi} {}_{+1}R_{lm\omega}$  and  ${}_{-1}R_{lm\omega}^{\text{in}}$  by  $-\sqrt{2\pi} {}_{-1}R_{lm\omega}/{}_1B_{lm\omega}$ . Alternatively, this normalization can be obtained from an expression for ‘up’ modes by replacing  ${}_{+1}R_{lm\omega}^{\text{up}}$  by  $-2\sqrt{2\pi} {}_{+1}R_{lm\omega}/{}_1B_{lm\omega}$  and  ${}_{+1}R_{lm\omega}^{\text{up}}$  by  $-\sqrt{2\pi} {}_{+1}R_{lm\omega}/{}_1B_{lm\omega}^2$ . We will later restore the appropriate factors. We can then deduce the behaviour at the axis of  ${}_{lm\omega}\phi_0$  in this normalization:

$$\begin{aligned} {}_{lm\omega}\phi_0 \left( r, \theta = \begin{Bmatrix} 0 \\ \pi \end{Bmatrix} \right) &\sim \\ &\sim \frac{(\pm |m \pm 1| + m \pm 1) 2^{(|m \mp 1|/2-1)} {}_{+1} \left\{ \begin{smallmatrix} a \\ b \end{smallmatrix} \right\}_{n=0,lm\omega} (1 \mp x)^{(|m \pm 1|-1)/2}}{(r \mp ia)^2 {}_1B_{lm\omega}} \times \\ &\quad \times [(r \mp ia) \mathcal{D}_0 - 1] {}_{-1}R_{lm\omega} = \\ &= \frac{-(\pm |m \mp 1| - m \pm 1) 2^{(|m \pm 1|/2-1)} {}_{-1} \left\{ \begin{smallmatrix} a \\ b \end{smallmatrix} \right\}_{n=0,lm\omega} (1 \mp x)^{(|m \mp 1|-1)/2}}{(r \mp ia)^2 {}_1B_{lm\omega}} \times \\ &\quad \times [(r \mp ia) \mathcal{D}_0^\dagger - 1] (\Delta_{+1} R_{lm\omega}) \quad (x \rightarrow \pm 1) \end{aligned} \quad (6.9.4)$$

By looking at the coefficient and the exponent of  $(1 \mp x)$  in (6.9.4) we can see that  ${}_{lm\omega}\phi_0$  is only non-zero at  $\theta = 0, \pi$  if  $m = 0$ . The value of this NP scalar in

## 6.9. Symmetry $(\theta, \phi) \rightarrow (\pi - \theta, \phi + \pi)$

that case is

$$\begin{aligned} {}_{l,m=0,\omega}\phi_0\left(r, \theta = \begin{Bmatrix} 0 \\ \pi \end{Bmatrix}\right) &= \frac{\pm 2_{+1} \left\{ \begin{smallmatrix} a \\ b \end{smallmatrix} \right\}_{n=0,l,m=0,\omega}}{\sqrt{2}(r \mp ia)^2 {}_1B_{lm\omega}} [(r \mp ia) \mathcal{D} - 1] {}_{-1}R_{l,m=0,\omega} = \\ &= \frac{\mp 2_{-1} \left\{ \begin{smallmatrix} a \\ b \end{smallmatrix} \right\}_{n=0,l,m=0,\omega}}{\sqrt{2}(r \mp ia)^2 {}_1B_{lm\omega}} [(r \mp ia) \mathcal{D}^\dagger - 1] (\Delta_{+1} R_{l,m=0,\omega}) \end{aligned} \quad (6.9.5)$$

Proceeding now similarly to the way we did to obtain (6.9.1c), we have that at the axis of symmetry

$$\begin{aligned} &|{}_{l,m=0,\omega}\phi_0(r, \theta = 0)|^2 - |{}_{l,m=0,\omega}\phi_0(r, \theta = \pi)|^2 = \\ &= \frac{-4iaW[Y_{+1}, Y_{-1}^*]_{l,m=0,\omega} (-1a_{n=0,l,m=0,\omega} + 1a_{n=0,l,m=0,\omega})}{(r^2 + a^2)^2 {}_1B_{l,m=0,\omega}^2} \end{aligned} \quad (6.9.6)$$

is satisfied.

As we have seen, Table 6.4 applies to the term  $|{}_{lm\omega}\phi_0(r, \theta = 0)|^2 - |{}_{lm\omega}\phi_0(r, \theta = \pi)|^2$ , and thus to  ${}_{lm\omega}T_{\theta\theta}(r, \theta = 0) - {}_{lm\omega}T_{\theta\theta}(r, \theta = \pi)$ . Since this term is zero at the axis for  $m \neq 0$ , this table shows that the  $\theta\theta$ -component of the RSET when the field is in the states  $|FT\rangle$  or  $|CCH^-\rangle$  (as well, of course, as in the state  $|B^-\rangle$ ) is invariant under parity at the axis. Only in the state  $|U^-\rangle$  this component might not be invariant at the axis. From (6.1.11), (6.9.6) and Table 6.4 we can finally find a simple expression for the difference in the  $\theta\theta$ -component of the RSET in the past Unruh state evaluated at  $\theta = 0$  and at  $\theta = \pi$ . This expression, where we now include the constant of normalization and we restore the appropriate factors for the ‘in’ and ‘up’ modes, is:

$$\begin{aligned} &\left\langle \hat{T}_{\theta\theta}(r, \theta = 0) \right\rangle_{\text{ren}}^{U^-} - \left\langle \hat{T}_{\theta\theta}(r, \theta = \pi) \right\rangle_{\text{ren}}^{U^-} = \\ &= \sum_{l=0}^{\infty} \int_0^{\infty} d\omega \left[ \coth\left(\frac{\pi\omega}{\kappa}\right) - 1 \right] \times \\ &\quad \times \frac{-2^3 ia |N_{+1}^{\text{up}}|^2 W[Y_{+1}^{\text{up}}, Y_{-1}^{\text{up}*}]_{l,m=0,\omega} (-1a_{n=0,l,m=0,\omega} + 1a_{n=0,l,m=0,\omega})}{(r^2 + a^2)^2 {}_1B_{l,m=0,\omega}^2} = \\ &= \sum_{l=0}^{\infty} \int_0^{\infty} d\omega \left[ \coth\left(\frac{\pi\omega}{\kappa}\right) - 1 \right] \times \\ &\quad \times \frac{2^3 ia |N_{+1}^{\text{up}}|^2 W[Y_{+1}^{\text{up}}, Y_{-1}^{\text{up}*}]_{l,m=0,\omega} + 1a_{n=0,l,m=0,\omega}^2}{(r^2 + a^2)^2 {}_1B_{l,m=0,\omega}^2} \frac{\sqrt{-1\lambda_{l,m=0,\omega} + 2a\omega}}{\sqrt{-1\lambda_{l,m=0,\omega} - 2a\omega}} \end{aligned} \quad (6.9.7)$$

## 6.9. Symmetry $(\theta, \phi) \rightarrow (\pi - \theta, \phi + \pi)$

---

where in the last step we have made use of (4.2.12).

From Table 3.1 we can see that  $iW[Y_{+1}^{\text{up}}, Y_{-1}^{\text{up}*}]_{l,m=0,\omega} = \frac{{}_1B_{l,m=0,\omega}^2}{\omega} |-1R_{l,m=0,\omega}^{\text{up,tra}}|^2 \geq 0$  as long as  $\omega \geq 0$ , and therefore the integrand in (6.9.7) is non-negative for  $\omega \geq 0$ .

Proceeding similarly for the other groups of terms in Table 6.2, we can see that (e) and (f) will be zero at the axis after summing over  $m$  since  ${}_{lm\omega}\phi_{-1}$ ,  ${}_{lm\omega}\phi_0$  and  ${}_{lm\omega}\phi_{+1}$  are only non-zero at  $\theta = \left\{\frac{0}{\pi}\right\}$  when  $m = \left\{\frac{-1}{+1}\right\}$ ,  $\left\{\frac{0}{0}\right\}$  and  $\left\{\frac{+1}{-1}\right\}$  respectively. This result is obviously equally valid if the expectation value of the quadratic term at the point  $\pi - \theta$  is added, rather than subtracted, to that at the point  $\theta$ , so that this result is also useful for those components of the stress tensor such that one index is  $\theta$  and the other one is not.

On the other hand, we are not able to prove whether the groups of terms (a) and (b) are zero or not at the axis. The reason is the presence of the factor  $({}_{+1}S_{lm\omega}^2 - {}_{-1}S_{lm\omega}^2)$ : after the summation over  $m$  we have two separate terms, one for the mode  $m = +1$  and the other for the mode  $m = -1$ . It is not possible to combine together these two modes using the symmetries (4.2.1) of the angular function unless the transformation ( $\omega \rightarrow -\omega$ ) is also applied.

A summary of the analytical results relating to the symmetry under  $\mathcal{P}$  of the Boyer-Lindquist components of the RSET in various states of interest when expressions (6.6.2) and (6.6.3) are used, is as follows:

- $\left\langle \hat{T}_{rr} \right\rangle_{\text{ren}}^{B^-}$  and  $\left\langle \hat{T}_{\theta\theta} \right\rangle_{\text{ren}}^{B^-}$  are both symmetric under  $\mathcal{P}$  everywhere, and  $\left\langle \hat{T}_{tt} \right\rangle_{\text{ren}}^{B^-}$ ,  $\left\langle \hat{T}_{t\phi} \right\rangle_{\text{ren}}^{B^-}$  and  $\left\langle \hat{T}_{\phi\phi} \right\rangle_{\text{ren}}^{B^-}$  are symmetric under  $\mathcal{P}$  at the axis.
- $\left\langle \hat{T}_{r\theta} \right\rangle_{\text{ren}}^{\Psi}$ ,  $\left\langle \hat{T}_{t\theta} \right\rangle_{\text{ren}}^{\Psi}$ ,  $\left\langle \hat{T}_{\phi\theta} \right\rangle_{\text{ren}}^{\Psi}$  where  $|\Psi\rangle$  may be any one state among  $|B^- \rangle$ ,  $|FT\rangle$ ,  $|CCH^- \rangle$ ,  $|U^- \rangle$  are all symmetric under  $\mathcal{P}$  at the axis.
- $\left\langle \hat{T}_{\theta\theta} \right\rangle_{\text{ren}}^{\Psi}$  where  $\Psi$  may be any one state among  $|B^- \rangle$ ,  $|FT\rangle$ ,  $|CCH^- \rangle$  are all symmetric under  $\mathcal{P}$  at the axis.
- $\left\langle \hat{T}_{\theta\theta} \right\rangle_{\text{ren}}^{U^-}$  is not symmetric under  $\mathcal{P}$  at the axis.



## 6.9. Symmetry $(\theta, \phi) \rightarrow (\pi - \theta, \phi + \pi)$

---

To conclude this subsection, we consider two analytic results in the literature for which the electromagnetic RSET on the Kerr background exhibits an invariance under parity.

One result is, of course, CCH's asymptotic result (6.8.14), which we know is only valid at the poles. We have already seen in Section 6.8 that the replacement of spheroidal functions by spherical functions together with the use of the asymptotic behaviour (3.5.10) at the horizon for the radial functions leads to stress-energy tensor components for the 'up' modes that are symmetric under  $\mathcal{P}$  to leading order. Indeed, if the wronskian is calculated with the asymptotics at the horizon for the 'up' radial functions, its leading order behaviour is zero. Therefore, groups of terms (a) and (c) in Table 6.2 for the 'up' modes are zero to leading order at the horizon. The group of terms (b) is zero to leading order at the poles for the 'up' modes because the spheroidal functions can be replaced by spherical functions. All the groups of terms in Table 6.2 for the 'up' modes are therefore either identically zero or zero to leading order at the poles. It follows that the leading order at the poles of all components of the stress-energy tensor for the 'up' modes are symmetric under parity.

This means that  $\left\langle \hat{T}_{\theta\theta} \right\rangle_{\text{ren}}^{U-}$  is symmetric under  $\mathcal{P}$  at the poles. However, since there is no divergence along the axis off the horizon, modes other than those with  $l \rightarrow +\infty$  contribute to (6.9.7), making it non-zero. Even though  $\left\langle \hat{T}_{\theta\theta} \right\rangle_{\text{ren}}^{U-}$  is symmetric under  $\mathcal{P}$  at the poles, it is not symmetric along the axis off the horizon.

The other result we wish to mention was obtained by Frolov and Zel'nikov [38]. They calculated the electromagnetic RSET at the pole ( $r = r_+, \theta = 0$ ) when the field is in the state  $|FT\rangle$ . We used their method to obtain the same result at the other pole, ( $r = r_+, \theta = \pi$ ). The electromagnetic RSET when the field is in the state  $|FT\rangle$  is therefore symmetric under parity at the poles. The result they find at the pole is finite and we therefore cannot apply the same reasoning as above. We have seen that the  $r\theta$ ,  $t\theta$ ,  $\phi\theta$  and  $\theta\theta$  components should all be symmetric at

## 6.9. Symmetry $(\theta, \phi) \rightarrow (\pi - \theta, \phi + \pi)$

---

the axis when the field is in the state  $|FT\rangle$  but unfortunately we do not have an explanation for the symmetry of the other components at the axis.

We include one graph for one of the components, the  $tr$ -component, for the difference in the RSET between the past Unruh and past Boulware states as an example of the clear lack of symmetry under the parity operation for most components. Graph 6.27 has been obtained using the expressions in (6.6.2).

### 6.9.2 New expressions for the quantization of the field

Having proved that CCH's expressions (6.6.2) lead to expectation values of the stress-energy tensor which are not invariant under the parity operation, in the present subsection we will find the reason for this asymmetry.

Note that, from (6.2.5a), the potential mode  ${}_{lm\omega P}A_\mu^\bullet$  is indeed an eigenfunction of the parity operator. However, the general solution  $A_\mu^\bullet$ , for which no boundary conditions have been specified, is not:

$$\mathcal{P}A_\mu^\bullet = \sum_{lmP} \int_{-\infty}^{+\infty} d\omega^\bullet P_{lm\omega P} a_{lm\omega P}^\bullet A_\mu^\bullet \neq \pm \sum_{lmP} \int_{-\infty}^{+\infty} d\omega^\bullet {}_{lm\omega P}a_{lm\omega P}^\bullet A_\mu^\bullet = \pm A_\mu^\bullet \quad (6.9.8)$$

Similarly, from (6.2.5b), one NP scalar mode is complex-conjugated (and  $m$  and  $\omega$  change sign) under the parity operation but the general solution is not:

$$\begin{aligned} \mathcal{P}\phi_h^\bullet &= (-1)^{h+1} \sum_{lmP} \int_{-\infty}^{+\infty} d\omega^\bullet P_{lm\omega P} a_{lm\omega P}^{\bullet*} \phi_h^{\bullet*} \neq \\ &\neq \pm \sum_{lmP} \int_{-\infty}^{+\infty} d\omega^\bullet {}_{lm\omega P}a_{lm\omega P}^{\bullet*} \phi_h^{\bullet*} = \pm \phi_h^{\bullet*} \end{aligned} \quad (6.9.9)$$

We will now call  ${}_{lm\omega P}\Phi_h^\bullet$  the integrand in (6.2.8). We immediately have that

$$\begin{aligned} \mathcal{P}{}_{lm\omega P}\Phi_h^\bullet &= (-1)^{h+1} P_{lm\omega P} \Phi_h^{\bullet*} \\ \mathcal{P}({}_{lm\omega P}\Phi_h^\bullet {}_{l'm'\omega'P'}\Phi_{h'}^{\bullet*} + c.c.) &= (-1)^{h+h'} PP' ({}_{lm\omega P}\Phi_h^{\bullet*} {}_{l'm'\omega'P'}\Phi_{h'}^\bullet + c.c.) \end{aligned} \quad (6.9.10)$$

and therefore the latter is an eigenfunction of the parity operator.

## 6.9. Symmetry $(\theta, \phi) \rightarrow (\pi - \theta, \phi + \pi)$

---

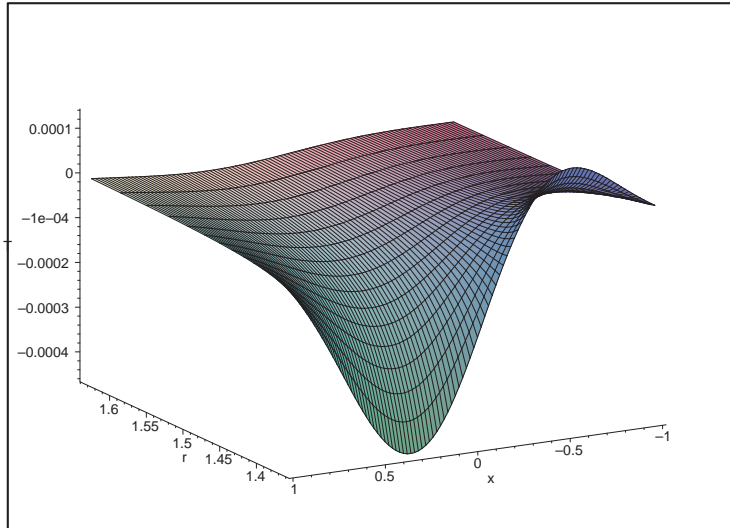


Figure 6.27:  $\frac{1}{4\pi} \langle \hat{T}_{tr} \rangle^{U^-B^-}$

## 6.9. Symmetry $(\theta, \phi) \rightarrow (\pi - \theta, \phi + \pi)$

We look next at the quantized expressions, obtained by promoting the coefficients  ${}_{lm\omega P}a^\bullet$  and  ${}_{lm\omega P}a^{\bullet*}$  to operators. There is, however, an operator-ordering ambiguity in the transition. The classical term  $(\phi_h \phi_{h'}^* + c.c.)$  should be quantized to the symmetrized form  $(\hat{\phi}_h \hat{\phi}_{h'}^\dagger + \hat{\phi}_{h'}^\dagger \hat{\phi}_h)/2 + h.c.$ , where the symbol ‘ $h.c.$ ’ stands for hermitian conjugate. There is no physical reason why the classical term  $(\phi_h \phi_{h'}^* + c.c.)$  should be quantized to one particular choice between  $(\hat{\phi}_h \hat{\phi}_{h'}^\dagger + h.c.)$  and  $(\hat{\phi}_{h'}^\dagger \hat{\phi}_h + h.c.)$ . However, in the expression that CCH give for the electromagnetic stress-energy tensor operator, the choice of one option over the other seems to have been arbitrarily taken for each of the various quadratic terms appearing in it- the correct, symmetrized form was not used for any of the terms. Furthermore, we shall see that CCH have used the first option over the second one and over the symmetrized form when calculating the expression for the expectation value of a general quadratic operator in the field in the past Boulware state. In the analogous expression for the past Unruh state neither of the two options nor the symmetrized form was used.

We look at what is the result of using separately each one of the two options, i.e., each one of the two quadratic terms in the symmetrized form. It follows from (6.9.10) that

$$\begin{aligned} \mathcal{P} {}_{lm\omega P} \hat{\Phi}_h^\bullet &= (-1)^{h+1} P {}_{lm\omega P} \hat{\Phi}_h^{\bullet\dagger} \\ \mathcal{P} \left( {}_{lm\omega P} \hat{\Phi}_h^\bullet {}_{l'm'\omega' P'} \hat{\Phi}_{h'}^{\bullet\dagger} + h.c. \right) &= \mathcal{P} \left( {}_{lm\omega P} \hat{\Phi}_h^\bullet {}_{l'm'\omega' P'} \hat{\Phi}_{h'}^{\bullet\dagger} + {}_{l'm'\omega' P'} \hat{\Phi}_{h'}^\bullet {}_{lm\omega P} \hat{\Phi}_h^{\bullet\dagger} \right) = \\ &= (-1)^{h+h'} P P' \left( {}_{lm\omega P} \hat{\Phi}_h^\bullet {}_{l'm'\omega' P'} \hat{\Phi}_{h'}^{\bullet\dagger} + {}_{l'm'\omega' P'} \hat{\Phi}_{h'}^{\bullet\dagger} {}_{lm\omega P} \hat{\Phi}_h^\bullet \right) \end{aligned} \quad (6.9.11)$$

In the past Boulware state we have

$$\langle B^- | \left( \hat{\phi}_h^\bullet \hat{\phi}_{h'}^{\bullet\dagger} + h.c. \right) | B^- \rangle = \sum_{lmP} \int_0^{+\infty} d\omega^\bullet ({}_{lm\omega} \phi_h^\bullet {}_{lm\omega} \phi_{h'}^{\bullet*} + c.c.) \quad (6.9.12)$$

whereas

$$\begin{aligned} \langle B^- | \left( \hat{\phi}_{h'}^{\bullet\dagger} \hat{\phi}_h^\bullet + h.c. \right) | B^- \rangle &= (-1)^{h+h'} \sum_{lmP} \int_0^{+\infty} d\omega^\bullet \left[ \mathcal{P} ({}_{lm\omega} \phi_{h'}^\bullet {}_{lm\omega} \phi_h^{\bullet*}) + c.c. \right] = \\ &= (-1)^{h+h'} \mathcal{P} \left( \langle B^- | \left( \hat{\phi}_h^\bullet \hat{\phi}_{h'}^{\bullet\dagger} + h.c. \right) | B^- \rangle \right) \end{aligned} \quad (6.9.13)$$

## 6.9. Symmetry $(\theta, \phi) \rightarrow (\pi - \theta, \phi + \pi)$

---

We can see from (6.2.5b) that the two options (6.9.12) and (6.9.13) will in principle give different results. It is the first option, (6.9.12), that CCH used to obtain their expression (6.6.1a). We have seen, however, that in the Schwarzschild space-time the two coincide (except for a possible different sign) since the transformation  $(\omega \rightarrow -\omega)$  is not required in the symmetry (6.2.5b).

The expectation value in the state  $|B^-\rangle$  of one of the two terms  $\hat{\phi}_h^\bullet \hat{\phi}_{h'}^{\bullet\dagger}$  and  $\hat{\phi}_{h'}^{\bullet\dagger} \hat{\phi}_h^\bullet$  is derived from that of the other term by operating with  $\mathcal{P}$  and multiplying by  $(-1)^{h+h'}$ , but only if each term is added to its own hermitian conjugate. Therefore the quantum-mechanical symmetrization guarantees that the expectation value in the state  $|B^-\rangle$  of a hermitian, quadratic operator will be invariant (bar a sign) under parity. The sign  $(-1)^{h+h'}$  is precisely the same sign appearing in (6.1.12). This implies that if the quadratic terms in the expression (6.1.11) are quantum-mechanically symmetrized when promoting the NP scalars to operators, then the expectation value in the state  $|B^-\rangle$  of the stress-energy tensor will be invariant under parity.

In order to calculate the expectation value of the quadratic terms  $\hat{\phi}_h^\bullet \hat{\phi}_{h'}^{\bullet\dagger}$  and  $\hat{\phi}_{h'}^{\bullet\dagger} \hat{\phi}_h^\bullet$  in the past Unruh state we are going to make use of the expression calculated in [37] which gives the past Unruh state in terms of the past Boulware state:

$$|U^-\rangle = \prod_{lm\tilde{\omega}P} C_{lm\omega P} \exp(e^{-\pi\tilde{\omega}/\kappa_+} {}_{lm\omega P}\hat{a}^{\text{up}\dagger} {}_{lm\omega P}\hat{a}^{\text{up}\dagger}) |B^-\rangle \quad (6.9.14)$$

where  $C_{lm\omega P}$  are normalization constants and  ${}_{lm\omega P}\hat{a}^{\text{up}\dagger}$  are creation operators in region  $I^*$  of the extended Kerr space-time.

We will also make use of the following expression in [81]:

$$S(r, \phi) = (\cosh r)^{-1} e^{-\hat{a}_+^\dagger \hat{a}_-^\dagger e^{2i\phi} \tanh r} e^{-(\hat{a}_+^\dagger \hat{a}_+ + \hat{a}_-^\dagger \hat{a}_-) \ln(\cosh r)} e^{\hat{a}_+ \hat{a}_- e^{-2i\phi} \tanh r} \quad (6.9.15)$$

where  $S(r, \phi)$  is the two-mode squeeze operator

$$S(r, \phi) = e^{r(\hat{a}_+ \hat{a}_- e^{-2i\phi} - \hat{a}_+^\dagger \hat{a}_-^\dagger e^{2i\phi})} \quad (6.9.16)$$

and the independent operators  $\hat{a}_+$  and  $\hat{a}_-$  satisfy the standard commutation

## 6.9. Symmetry $(\theta, \phi) \rightarrow (\pi - \theta, \phi + \pi)$

relations. By using (6.9.15) and (6.9.16) we can re-express (6.9.14) as

$$|U^-\rangle = \exp \left\{ \sum_{lmP} \int_0^\infty d\tilde{\omega} \left[ \ln C_{lm\omega P} + \ln(\cosh r_{\tilde{\omega}}) \right] \right\} e^{-\hat{A}} |B^-\rangle \quad (6.9.17)$$

with

$$\hat{A} \equiv \sum_{lmP} \int_0^\infty d\tilde{\omega} r_{\tilde{\omega}} ({}_{lm\omega P} \hat{a}^{\text{up}\dagger} {}_{lm\omega P} \hat{a}^{\text{up}\dagger} - {}_{lm\omega P} \hat{a}^{\text{up}} {}_{lm\omega P} \hat{a}^{\text{up}}) \quad (6.9.18)$$

and

$$r_{\tilde{\omega}} \equiv -\tanh^{-1} (e^{-\pi\tilde{\omega}/\kappa_+}) \quad (6.9.19)$$

Since  $(e^{\hat{A}})^\dagger = e^{-\hat{A}}$ , the normalization  $\langle U^- | U^- \rangle = 1$  implies

$$\exp \left\{ \sum_{lmP} \int_0^\infty d\tilde{\omega} \left[ \ln C_{lm\omega P} + \ln C_{lm\omega P}^* + 2 \ln(\cosh r_{\tilde{\omega}}) \right] \right\} = 1 \quad (6.9.20)$$

Using now the Baker-Campbell-Hausdorff equation ([62])

$$e^{\xi\hat{P}} \hat{Q} e^{-\xi\hat{P}} = \hat{Q} + \xi[\hat{P}, \hat{Q}] + \frac{\xi^2}{2!}[\hat{P}, [\hat{P}, \hat{Q}]] + \frac{\xi^3}{3!}[\hat{P}, [\hat{P}, [\hat{P}, \hat{Q}]]] + \dots \quad (6.9.21)$$

where  $\hat{P}$  and  $\hat{Q}$  are any two operators and  $\xi$  is a parameter, we can find that

$$e^{\hat{A}} {}_{lm\omega P} \hat{a}^{\text{up}} e^{-\hat{A}} = {}_{lm\omega P} \hat{a}^{\text{up}} \cosh r_{\tilde{\omega}} + {}_{lm\omega P} \hat{a}^{\text{up}\dagger} \sinh r_{\tilde{\omega}} \quad (6.9.22)$$

and finally

$$\langle U^- | {}_{lm\omega P} \hat{a}^{\text{up}\dagger} {}_{l'm'\omega'P'} \hat{a}^{\text{up}} | U^- \rangle = \frac{1}{2} \left[ \coth \left( \frac{\pi\tilde{\omega}}{\kappa_+} \right) - 1 \right] \delta(\omega - \omega') \delta_{ll'} \delta_{mm'} \delta_{PP'} \quad (6.9.23a)$$

$$\langle U^- | {}_{lm\omega P} \hat{a}^{\text{up}\dagger} {}_{l'm'\omega'P'} \hat{a}^{\text{up}\dagger} | U^- \rangle = 0 \quad (6.9.23b)$$

$$\langle U^- | {}_{lm\omega P} \hat{a}^{\text{up}} {}_{l'm'\omega'P'} \hat{a}^{\text{up}} | U^- \rangle = 0 \quad (6.9.23c)$$

With the above results we find that

$$\begin{aligned} \langle U^- | \hat{\phi}_h^{\text{up}} \hat{\phi}_{h'}^{\text{up}\dagger} | U^- \rangle &= \\ &= \frac{1}{2} \sum_{lmP} \int_0^\infty d\tilde{\omega} \left\{ \left[ {}_{lm\omega} \phi_h^{\text{up}} {}_{lm\omega} \phi_{h'}^{\text{up}*} + (-1)^{h+h'} \mathcal{P}({}_{lm\omega} \phi_h^{\text{up}*} {}_{lm\omega} \phi_{h'}^{\text{up}}) \right] \coth \left( \frac{\pi\tilde{\omega}}{\kappa_+} \right) + \right. \\ &\quad \left. + \left[ {}_{lm\omega} \phi_h^{\text{up}} {}_{lm\omega} \phi_{h'}^{\text{up}*} - (-1)^{h+h'} \mathcal{P}({}_{lm\omega} \phi_h^{\text{up}*} {}_{lm\omega} \phi_{h'}^{\text{up}}) \right] \right\} = \\ &= (-1)^{h+h'} \mathcal{P} \left( \langle U^- | \hat{\phi}_h^{\text{up}\dagger} \hat{\phi}_{h'}^{\text{up}} | U^- \rangle \right) \end{aligned} \quad (6.9.24)$$

## 6.9. Symmetry $(\theta, \phi) \rightarrow (\pi - \theta, \phi + \pi)$

---

Note the minus sign in the second term in (6.9.24). Its presence may seem a bit surprising at first but, as we shall now see, it is precisely this sign that causes the expectation value of the stress-energy tensor in the past Unruh state to adopt a more familiar form by having all ‘up’ terms multiplied by a coth factor. This is already clear from looking at (6.9.24) and realizing that when quantum-symmetrizing the classic expression  $\phi_h^{\text{up}} \phi_{h'}^{\text{up}*}$  the terms without a coth factor will cancel out.

For the ‘in’ modes we have

$$\langle U^- | \hat{\phi}_h^{\text{in}} \hat{\phi}_{h'}^{\text{in}\dagger} | U^- \rangle = \sum_{lmP} \int_0^\infty d\omega_{lm\omega} \phi_h^{\text{in}} \phi_{h'}^{\text{in}*} = (-1)^{h+h'} \mathcal{P} \left( \langle U^- | \hat{\phi}_h^{\text{in}\dagger} \hat{\phi}_{h'}^{\text{in}} | U^- \rangle \right) \quad (6.9.25)$$

The following identities are therefore immediately satisfied

$$\begin{aligned} \left\langle \left[ \hat{\phi}_h^\bullet, \hat{\phi}_{h'}^{\bullet\dagger} \right] \right\rangle^{U^-} &= \left\langle \left[ \hat{\phi}_h^\bullet, \hat{\phi}_{h'}^{\bullet\dagger} \right] \right\rangle^{B^-} = \\ &= \sum_{lmP} \int_0^\infty d\omega^\bullet \left[ {}_{lm\omega} \phi_h^\bullet {}_{lm\omega} \phi_{h'}^{\bullet*} - (-1)^{h+h'} \mathcal{P} ({}_{lm\omega} \phi_h^{\bullet*} {}_{lm\omega} \phi_{h'}^\bullet) \right] \end{aligned} \quad (6.9.26)$$

and therefore

$$\left\langle \left[ \hat{\phi}_h^\bullet, \hat{\phi}_{h'}^{\bullet\dagger} \right] \right\rangle^{U^- - B^-} = 0 \quad (6.9.27)$$

as it should be.

When the classical term  $(\phi_h \phi_{h'}^* + c.c.)$  is quantized to the symmetrized term  $(\hat{\phi}_h \hat{\phi}_{h'}^\dagger + \hat{\phi}_{h'}^\dagger \hat{\phi}_h) / 2 + h.c..$  it gives the following real, parity-invariant expressions

## 6.9. Symmetry $(\theta, \phi) \rightarrow (\pi - \theta, \phi + \pi)$

---

in the past Boulware and past Unruh states:

$$\begin{aligned}
 & \left\langle \frac{\hat{\phi}_h \hat{\phi}_{h'}^\dagger + \hat{\phi}_{h'}^\dagger \hat{\phi}_h}{2} + h.c. \right\rangle^{B^-} = \\
 & = \frac{1}{2} \sum_{lmP} \left( \int_0^\infty d\tilde{\omega} \left[ {}_{lm\omega}\phi_h^{\text{up}} {}_{lm\omega}\phi_{h'}^{\text{up}*} + (-1)^{h+h'} \mathcal{P}({}_{lm\omega}\phi_h^{\text{up}} {}_{lm\omega}\phi_{h'}^{\text{up}*}) \right] + \right. \\
 & \quad \left. + \int_0^\infty d\omega \left[ {}_{lm\omega}\phi_h^{\text{in}} {}_{lm\omega}\phi_{h'}^{\text{in}*} + (-1)^{h+h'} \mathcal{P}({}_{lm\omega}\phi_h^{\text{in}} {}_{lm\omega}\phi_{h'}^{\text{in}*}) \right] \right) + c.c.
 \end{aligned} \tag{6.9.28a}$$

$$\begin{aligned}
 & \left\langle \frac{\hat{\phi}_h \hat{\phi}_{h'}^\dagger + \hat{\phi}_{h'}^\dagger \hat{\phi}_h}{2} + h.c. \right\rangle^{U^-} = \\
 & = \frac{1}{2} \sum_{lmP} \left( \int_0^\infty d\tilde{\omega} \left[ {}_{lm\omega}\phi_h^{\text{up}} {}_{lm\omega}\phi_{h'}^{\text{up}*} + (-1)^{h+h'} \mathcal{P}({}_{lm\omega}\phi_h^{\text{up}} {}_{lm\omega}\phi_{h'}^{\text{up}*}) \right] \coth\left(\frac{\pi\tilde{\omega}}{\kappa}\right) + \right. \\
 & \quad \left. + \int_0^\infty d\omega \left[ {}_{lm\omega}\phi_h^{\text{in}} {}_{lm\omega}\phi_{h'}^{\text{in}*} + (-1)^{h+h'} \mathcal{P}({}_{lm\omega}\phi_h^{\text{in}} {}_{lm\omega}\phi_{h'}^{\text{in}*}) \right] \right) + c.c.
 \end{aligned} \tag{6.9.28b}$$

Note that in the above expressions we have been able to complex conjugate the mode functions that are operated on by  $\mathcal{P}$  because of the existence of the  $+c.c.$  terms. This immediately leads to the following real, parity-invariant expressions for the stress-energy tensor in the past Boulware and past Unruh states:

$$\begin{aligned}
 & \langle B^- | \hat{T}_{\mu\nu} | B^- \rangle = \\
 & = \frac{1}{2} \sum_{lmP} \left( \int_0^\infty d\tilde{\omega} \left\{ T_{\mu\nu} [{}_{lm\omega}\phi_h^{\text{up}}, {}_{lm\omega}\phi_h^{\text{up}*}] + (-1)^\vartheta \mathcal{P}(T_{\mu\nu} [{}_{lm\omega}\phi_h^{\text{up}}, {}_{lm\omega}\phi_h^{\text{up}*}]) \right\} + \right. \\
 & \quad \left. + \int_0^\infty d\omega \left\{ T_{\mu\nu} [{}_{lm\omega}\phi_h^{\text{in}}, {}_{lm\omega}\phi_h^{\text{in}*}] + (-1)^\vartheta \mathcal{P}(T_{\mu\nu} [{}_{lm\omega}\phi_h^{\text{in}}, {}_{lm\omega}\phi_h^{\text{in}*}]) \right\} \right)
 \end{aligned} \tag{6.9.29a}$$

$$\begin{aligned}
 & \langle U^- | \hat{T}_{\mu\nu} | U^- \rangle = \frac{1}{2} \sum_{lmP} \\
 & \left( \int_0^\infty d\tilde{\omega} \coth\left(\frac{\pi\tilde{\omega}}{\kappa_+}\right) \left\{ T_{\mu\nu} [{}_{lm\omega}\phi_h^{\text{up}}, {}_{lm\omega}\phi_h^{\text{up}*}] + (-1)^\vartheta \mathcal{P}(T_{\mu\nu} [{}_{lm\omega}\phi_h^{\text{up}}, {}_{lm\omega}\phi_h^{\text{up}*}]) \right\} + \right. \\
 & \quad \left. + \int_0^\infty d\omega \left\{ T_{\mu\nu} [{}_{lm\omega}\phi_h^{\text{in}}, {}_{lm\omega}\phi_h^{\text{in}*}] + (-1)^\vartheta \mathcal{P}(T_{\mu\nu} [{}_{lm\omega}\phi_h^{\text{in}}, {}_{lm\omega}\phi_h^{\text{in}*}]) \right\} \right)
 \end{aligned} \tag{6.9.29b}$$



## 6.9. Symmetry $(\theta, \phi) \rightarrow (\pi - \theta, \phi + \pi)$

Note that the sign  $(-1)^\vartheta$  appears in the above expressions instead of  $(-1)^{h+h'}$  by virtue of the change under the parity operation of the coefficients of the quadratic field operators that appear in the expression for the stress-energy tensor, as seen in (6.1.12).

This is in sharp contrast with the expressions given by CCH. The expressions for the stress-energy tensor given by CCH, i.e., (6.6.2a) and (6.6.2b), are not invariant under parity. They are equivalent to (6.9.29) if  $\mathcal{P}(l_{m\omega}\phi_h^\bullet l_{m\omega}\phi_{h'}^{\bullet*}) = (-1)^{h+h'} l_{m\omega}\phi_h^\bullet l_{m\omega}\phi_{h'}^{\bullet*} \forall h, h'$ , which we have proved in this chapter that it is not the case. The general expressions (6.6.1) for a quadratic operator  $\hat{Q}$  given by CCH, when applied to the cases  $\hat{\phi}_h \hat{\phi}_{h'}^\dagger$  and  $\hat{\phi}_h^\dagger \hat{\phi}_{h'}$ , yield the surprising result:

$$\begin{aligned} \left\langle \left[ \hat{\phi}_h^\bullet, \hat{\phi}_{h'}^{\bullet\dagger} \right] \right\rangle^{U^- - B^-} &= \\ &= \sum_{lmP} \int_0^\infty d\tilde{\omega} \left\{ \left[ \coth \left( \frac{\pi\tilde{\omega}}{\kappa_+} \right) - 1 \right] [l_{m\omega}\phi_h^{\text{up}} l_{m\omega}\phi_{h'}^{\text{up}*} - \mathcal{P}(l_{m\omega}\phi_h^{\text{up}} l_{m\omega}\phi_{h'}^{\text{up}*})] \right\} \end{aligned} \quad (6.9.30)$$

which is not generally zero, as proved in the previous subsection.

To our knowledge, this is the first time that the expressions (6.9.29) for the expectation value of the stress-energy tensor when the electromagnetic field is in the past Boulware and past Unruh states have been given.

By comparing the expectation values in (6.6.2) with their symmetrized versions in (6.9.29) for the past Boulware and past Unruh states, we can give an analogous symmetrized version for the state  $|CCH^- \rangle$ :

$$\begin{aligned} \langle CCH^- | \hat{T}_{\mu\nu} | CCH^- \rangle &= \frac{1}{2} \sum_{lmP} \\ &\left( \int_0^\infty d\tilde{\omega} \coth \left( \frac{\pi\tilde{\omega}}{\kappa_+} \right) \left\{ T_{\mu\nu} [l_{m\omega}\phi_h^{\text{up}}, l_{m\omega}\phi_h^{\text{up}*}] + (-1)^\vartheta \mathcal{P}(T_{\mu\nu} [l_{m\omega}\phi_h^{\text{up}}, l_{m\omega}\phi_h^{\text{up}*}]) \right\} + \right. \\ &\left. + \int_0^\infty d\omega \coth \left( \frac{\pi\omega}{\kappa_+} \right) \left\{ T_{\mu\nu} [l_{m\omega}\phi_h^{\text{in}}, l_{m\omega}\phi_h^{\text{in}*}] + (-1)^\vartheta \mathcal{P}(T_{\mu\nu} [l_{m\omega}\phi_h^{\text{in}}, l_{m\omega}\phi_h^{\text{in}*}]) \right\} \right) \end{aligned} \quad (6.9.31)$$

### 6.9.3 Polarization

In this last subsection we will give a physical interpretation of the non-parity term and the parity term appearing in the expressions (6.9.29) and (6.9.31) for the expectation value of the stress-energy tensor in different states. We denote by parity term in a certain expression a term that explicitly contains the parity operator  $\mathcal{P}$ , and by non-parity term one in the same expression that does not explicitly contain this operator.

It is clear from the classical expression (2.4.21c) for the ‘upgoing gauge’ potential  ${}_{lm\omega}A^{\text{up}\mu}$  that this potential only contains the null vectors  $\mathbf{n}$  and  $\mathbf{m}$ . The parity term  $P\mathcal{P}{}_{lm\omega}A^{\text{up}\mu}$  in (6.2.2), because of the transformations (1.3.13) of the null base under parity, contains the vectors  $\mathbf{n}$  and  $\mathbf{m}^*$ . The potential  ${}_{lm\omega P}A^{\text{up}\mu}$  therefore contains the vectors  $\mathbf{n}$ ,  $\mathbf{m}$  and  $\mathbf{m}^*$ . However, as we saw in Section 2.3, only two of them are physically significant. Indeed, we know that the parity term is a pure gauge and therefore the contribution to the physical quantities from the term with  $\mathbf{m}^*$  in the potential is zero. Only the terms with  $\mathbf{n}$  and  $\mathbf{m}$  in the ‘upgoing’ potential contribute to physical quantities.

In particular, it is immediate from expressions (2.4.2) for the Maxwell scalars that only the term in the potential  ${}_{lm\omega P}A^{\text{up}\mu}$  that contains the vector  $\mathbf{m}$  contributes to  ${}_{lm\omega}\phi_{+1}^{\text{up}}$  whereas only the term with  $\mathbf{n}$  contributes to  ${}_{lm\omega}\phi_{-1}^{\text{up}}$ . Both, terms with  $\mathbf{n}$  and terms with  $\mathbf{m}$ , contribute to  ${}_{lm\omega}\phi_0^{\text{up}}$ .

It is in the limit for large  $r$  that the physical meaning of the various vectors becomes clear. We know that in flat space-time an electric field mode of positive frequency that is proportional to the vector  $(\hat{\mathbf{e}}_\theta + i\hat{\mathbf{e}}_\phi)[(\hat{\mathbf{e}}_\theta - i\hat{\mathbf{e}}_\phi)]$  possesses a positive[negative] angular momentum and we thus say that it is positively[negatively] polarized. If the mode is instead of negative frequency, the sign of the angular momentum changes and then an electric field mode proportional to  $(\hat{\mathbf{e}}_\theta + i\hat{\mathbf{e}}_\phi)[(\hat{\mathbf{e}}_\theta - i\hat{\mathbf{e}}_\phi)]$  is said to be negatively[positively] polarized. Therefore, according to (4.1.14), an electric and a magnetic field modes of positive frequency

## 6.9. Symmetry $(\theta, \phi) \rightarrow (\pi - \theta, \phi + \pi)$

---

that are proportional to the vector  $\mathbf{m}[\mathbf{m}^*]$  correspond, in the flat space limit, to a positive[negative] polarization, whereas the vectors  $\mathbf{l}$  and  $\mathbf{n}$  correspond both to neutral polarization. This implies that the positive-frequency modes  ${}_{lm\omega}\phi_{-1}^{\text{up}}$ ,  ${}_{lm\omega}\phi_{+1}^{\text{up}}$  and  ${}_{lm\omega}\phi_0^{\text{up}}$  are obtained from terms in the potential that, in the flat space limit, are neutrally-, positively- and both neutrally- and positively- polarized respectively. As we have seen, the parity term in the potential in (6.2.2), which is of the opposite polarization to that of the non-parity term, does not contribute to any NP scalar mode because it is pure gauge. This does not mean that the opposite polarization to that of the non-parity term in the potential does not contribute to the NP scalars. Indeed, it does contribute through the negative-frequency modes when the integration is over all frequencies, as in (6.2.3). In the expression (6.2.7) for the potential or (6.2.8) for the NP scalars, in which we have rid of the negative-frequency modes, the opposite polarization appears via the complex-conjugate term or the parity-term respectively.

Even though all three Maxwell scalars appear in the classical expression for the electromagnetic stress tensor, due to their different asymptotic behaviour (2.7.27) for large  $r$ , the terms in the stress tensor (6.1.11) with  ${}_{lm\omega}\phi_{+1}^{\text{up}}$  predominate in this limit. That is, the radiation field components of the stress tensor  $T^{\text{up}\mu\nu}$  are calculated in the flat space limit from modes in the potential (6.2.3) which for positive[negative] frequency correspond to a positive[negative] polarization. Note that the complex-conjugation of NP scalars in the stress tensor does not change the polarization of the field since it is merely a consequence of the fact that the null tetrad contains complex vectors, and does not imply the complex-conjugation of the tensor field components  $F_{\mu\nu}$ .

We give here expressions for the ‘upgoing’ potential modes in the limit for large  $r$ . We wish, however, to obtain expressions for the fields that are real mode by mode. We will therefore not calculate the potential modes  ${}_{lm\omega P}A^{\text{up}\mu}$  from expressions (2.7.15), since the transformation  $(m, \omega) \rightarrow (-m, -\omega)$  has been applied to the complex-conjugated term in (2.7.14b). Even though the potential is

## 6.9. Symmetry $(\theta, \phi) \rightarrow (\pi - \theta, \phi + \pi)$

obviously real, the potential modes  ${}_{lm\omega P}A^{\text{up}\mu}$  are not. Instead, we will calculate potential modes that are real mode by mode by applying equation (2.4.20) mode by mode. We denote these modes by  ${}_{lm\omega P}A'^{\text{up}\mu}$ . From equations (6.2.2), (2.4.21c) and (3.2.27b) it then follows that

$$\begin{aligned} {}_{lm\omega P}A'^{\text{up}\mu} &\equiv \left( \Pi_j^{\dagger\alpha} {}_{lm\omega} \varphi_j \right)^* + \Pi_j^{\dagger\alpha} {}_{lm\omega} \varphi_j \rightarrow -\frac{\omega i |N_{+1}^{\text{up}}|}{\sqrt{2}r} \times \\ &\times \left[ {}_{-1}Y_{{}_{lm\omega+1}} R_{{}_{lm\omega}}^{\text{up,tra}} e^{-i\omega(t-r)} (\hat{e}_\theta + i\hat{e}_\phi) - {}_{-1}Y_{{}_{lm\omega+1}}^* R_{{}_{lm\omega}}^{\text{up,tra}*} e^{+i\omega(t-r)} (\hat{e}_\theta - i\hat{e}_\phi) \right] \\ &\hspace{15em} (r \rightarrow +\infty) \end{aligned} \quad (6.9.32)$$

where we have used the fact that in flat space we can replace  ${}_h Z_{{}_{lm\omega}}$  by  ${}_h Y_{{}_{lm\omega}}$ . The difference between  ${}_{lm\omega P}A^{\text{up}\mu}$  and  ${}_{lm\omega P}A'^{\text{up}\mu}$  lies only on a sign factor and a change of sign in  $(m, \omega)$  on the second term. We know, however, that the second term is pure gauge mode by mode and it therefore does not contribute to the NP scalars. The electric and magnetic fields that correspond to the above potential follow through trivially when  $a = 0$ :

$$\begin{aligned} {}_{lm\omega P}\mathbf{E}^{\text{up}} &= -\nabla {}_{lm\omega P}A'^{\text{up}0} - \frac{\partial {}_{lm\omega P}\mathbf{A}'^{\text{up}}}{\partial t} = \frac{\omega^2 |N_{+1}^{\text{up}}|}{\sqrt{2}r} \times \\ &\times \left[ {}_{-1}Y_{{}_{lm\omega+1}} R_{{}_{lm\omega}}^{\text{up,tra}} e^{-i\omega(t-r)} (\hat{e}_\theta + i\hat{e}_\phi) + {}_{-1}Y_{{}_{lm\omega+1}}^* R_{{}_{lm\omega}}^{\text{up,tra}*} e^{+i\omega(t-r)} (\hat{e}_\theta - i\hat{e}_\phi) \right] \\ {}_{lm\omega P}\mathbf{B}^{\text{up}} &= \nabla \times {}_{lm\omega P}\mathbf{A}'^{\text{up}} = \frac{-\omega^2 i |N_{+1}^{\text{up}}|}{\sqrt{2}r} \times \\ &\times \left[ {}_{-1}Y_{{}_{lm\omega+1}} R_{{}_{lm\omega}}^{\text{up,tra}} e^{-i\omega(t-r)} (\hat{e}_\theta + i\hat{e}_\phi) - {}_{-1}Y_{{}_{lm\omega+1}}^* R_{{}_{lm\omega}}^{\text{up,tra}*} e^{+i\omega(t-r)} (\hat{e}_\theta - i\hat{e}_\phi) \right] \end{aligned} \quad (6.9.33)$$

where  ${}_{lm\omega P}A'^{\text{up}} = \left( {}_{lm\omega P}A'^{\text{up}0}, {}_{lm\omega P}\mathbf{A}'^{\text{up}} \right)$ . It is worth noting that even though the second term in either (2.4.20) or (2.7.14b) does not contribute to the NP scalars it does contribute to the fields. The reason is that the NP scalars must be calculated from real fields. It does not make physical sense to consider the contribution to the NP scalars from a non-real field, such as the second term in the above expressions for the field. We say that this term is ‘pure gauge’ in the sense that it does not contribute to the NP scalars even if it does contribute to the physical fields so as to make them real. The angular functions can be expressed

## 6.9. Symmetry $(\theta, \phi) \rightarrow (\pi - \theta, \phi + \pi)$

---

in terms of the orbital angular momentum acting on the spherical harmonics as

$$\pm_1 Y_{lm\omega} = -[l(l+1)]^{-1/2} (\hat{\mathbf{e}}_\theta \pm i\hat{\mathbf{e}}_\phi) \mathbf{L} Y_{lm\omega} \quad (6.9.34)$$

where we have made use of the relationships (4.1.7) and (4.1.20). The large- $r$  asymptotics for the NP Maxwell scalars in terms of the electric and magnetic fields are easily obtained:

$$\begin{aligned} \phi_{-1} &\rightarrow -\frac{1}{\sqrt{2}} (\mathbf{E} + \mathbf{B}i) (\hat{\mathbf{e}}_\theta + i\hat{\mathbf{e}}_\phi) \quad (r \rightarrow +\infty) \\ \phi_0 &\rightarrow \frac{1}{2} (\mathbf{E} + \mathbf{B}i) \hat{\mathbf{e}}_r \quad (r \rightarrow +\infty) \\ \phi_{+1} &\rightarrow \frac{1}{2\sqrt{2}} (\mathbf{E} + \mathbf{B}i) (\hat{\mathbf{e}}_\theta - i\hat{\mathbf{e}}_\phi) \quad (r \rightarrow +\infty) \end{aligned} \quad (6.9.35)$$

It is clear that the parity and non-parity terms correspond to opposite polarizations both for the potential (6.9.32) and the fields (6.9.33). It is also clear that the only contribution to  $\phi_{+1}^{\text{up}}$  from the ‘upgoing’ electric and magnetic fields comes from the non-parity term. To leading order in  $r$  for the electric and magnetic fields both  $\phi_{-1}^{\text{up}}$  and  $\phi_0^{\text{up}}$  vanish, in agreement with (2.7.27). To next order in  $r$ , expressions (6.9.33) and (6.9.35) must be calculated to include lower order terms and it is therefore not valid to conclude from them that the only contribution to  $\phi_{-1}^{\text{up}}$  and  $\phi_0^{\text{up}}$  comes from negatively- and neutrally- polarized terms respectively. We have indeed seen in the beginning of this subsection that this is not the case. Finally, it is also manifest from the above asymptotic expressions that the positive- and the negative- frequency modes of the potential (6.2.3) have opposite polarization. Indeed, since the negative-frequency ones correspond to the positive-frequency, complex-conjugated term in (6.2.7), the term with  $(\hat{\mathbf{e}}_\theta + i\hat{\mathbf{e}}_\phi)$  in the fields (6.9.33), which is the only term that contributes to the NP scalars and which is positively-polarized, is complex-conjugated to a negatively-polarized term with  $(\hat{\mathbf{e}}_\theta - i\hat{\mathbf{e}}_\phi)$ .

The reasoning used so far for the ‘upgoing gauge’ potential can be applied in the same manner to the ‘ingoing gauge’ potential  ${}_{lm\omega}A^{\text{in}\mu}$ . In this case, the potential contains one term with the vector  $\mathbf{l}$ , which is the only one that contributes to

## 6.9. Symmetry $(\theta, \phi) \rightarrow (\pi - \theta, \phi + \pi)$

---

${}_{lm\omega}\phi_{+1}^{\text{in}}$ , and one term with the vector  $\mathbf{m}^*$ , which is the only one that contributes to  ${}_{lm\omega}\phi_{-1}^{\text{in}}$ . Like in the ‘upgoing gauge’ case, both terms contribute to  ${}_{lm\omega}\phi_0^{\text{up}}$ , and the parity term (containing  $\mathbf{l}$  and  $\mathbf{m}$ ) does not contribute to any of the NP scalars. The scalar  ${}_{lm\omega}\phi_{-1}^{\text{in}}$  is the one that diminishes more slowly in the limit for large  $r$ . The radiative components of the classical stress tensor  $T^{\text{in}\mu\nu}$  is thus calculated in the flat space limit from modes in the potential (6.2.3) that for positive[negative] frequency correspond to negative[positive] polarization.

It is clear that the two terms in the asymptotic expression (6.9.32) for the ‘upgoing’ potential are both derived from the modes of the null tetrad component  $A_m^{\text{up}}$ . Similarly, the only asymptotic contribution to the ‘ingoing’ potential comes from  $A_{m^*}^{\text{in}}$ . We can thus say that  $A_m$  and  $A_{m^*}$  are the asymptotically gauge independent parts of  $A_\mu$ .

So far in this subsection we have looked at the physical meaning of the different terms in classical expressions only. We are now in a position to understand the physical meaning of the terms in the quantum field theory expressions. The positive frequency modes in (6.2.3) correspond to the non-parity term in the expression (6.2.8) for the NP scalar and, ultimately, give rise to the non-parity term in the expectation value of the stress tensor (6.9.29). Similarly, the negative frequency modes in (6.2.3) give rise to the parity term in the NP scalars and the parity term in the expectation value of the stress tensor. We therefore reach the conclusion that the non-parity terms in expressions (6.9.29) for the expectation value of the stress tensor correspond in the flat space limit to one specific polarization (positive in the ‘up’ case and negative in the ‘in’ case) and that the corresponding parity terms in the same expressions correspond to the opposite polarization. Both the contribution from the positive-polarization terms and from the negative-polarization terms are separately real, as it should be. We also know, from the beginning of Subsection 6.9.1, that in the spherically-symmetrical case  $a = 0$ , the contribution to the expectation value of the stress tensor from the positive-polarization terms is identical to the one from the negative-polarization

## 6.9. Symmetry $(\theta, \phi) \rightarrow (\pi - \theta, \phi + \pi)$

---

terms, as one would expect.

The notable exception to this picture are the ‘up’ superradiant modes. Indeed, these modes have a sign of  $\omega$  opposite to the non-superradiant modes in the same term in the expectation value, whether the parity term or the non-parity term. The polarization of the ‘up’ superradiant modes is therefore the opposite to the non-superradiant modes in the same term, that is, it is negative if part of the non-parity term and positive if part of the parity term. Note, however, that the ‘in’ superradiant modes have the same sign of  $\omega$  (positive), and therefore the same polarization, as the non-superradiant modes in the same term in the expectation value.

When CCH only include non-parity terms in their expressions (6.6.2) they are only including one polarization and leaving out the other one for the ‘in’ modes. For the ‘up’ modes, they are only including one polarization for the non-superradiant modes and the opposite polarization for the superradiant modes. In particular, when subtracting the expectation value of the stress tensor in the past Boulware state from the one in the past Unruh state, only ‘up’ modes are needed. Neglecting the parity terms is in this case equivalent to neglecting negative polarization non-superradiant modes as well as positive polarization superradiant modes. That is the case in the calculation of  $\left\langle \hat{T}^\mu_\nu \right\rangle_{\text{ren}}^{B^-}$  close to the horizon in Section 6.8 but, as explained in Subsection 6.9.1, in this limit the non-parity and the parity terms coincide.

It is interesting to group the terms with the same polarization in the expectation value of the stress energy tensor. Of course, in the case of the difference between the states  $|CCH^-\rangle$  and  $|U^-\rangle$ , which only has contribution from the ‘in’ modes, the sum of the positive polarization terms coincides with the direct evaluation of CCH’s expressions (6.6.2). The negative polarization contribution can be obtained by applying the transformation  $x \rightarrow -x$ . We include the plots of the tensor components corresponding to the fluxes of energy and angular momentum from the positive polarization terms in Figures 6.28–6.29. The evaluation of

## 6.9. Symmetry $(\theta, \phi) \rightarrow (\pi - \theta, \phi + \pi)$

---

the positive polarization contribution to the difference in the expectation value of the stress energy tensor between the states  $|U^-\rangle$  and  $|B^-\rangle$  requires carefully adding the contribution of the superradiant modes to the appropriate polarization. We calculated the positive polarization contribution to these differences of expectation values and plot them in Figures 6.30–6.31. The corresponding negative polarization contribution is, again, obtained by applying the transformation  $x \rightarrow -x$ . The interest of these graphs lies in the region far from the horizon. Close to the horizon the irregularity of the state  $|B^-\rangle$  dominates and thermality guarantees symmetry with respect to the equator.



## 6.9. Symmetry $(\theta, \phi) \rightarrow (\pi - \theta, \phi + \pi)$

---

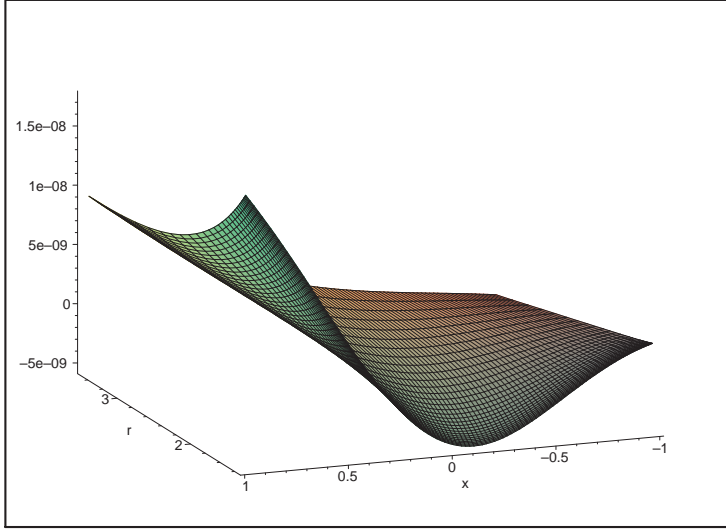


Figure 6.28: Positive polarization terms of  $\frac{1}{4\pi} \Delta \langle \hat{T}_{tr} \rangle^{CCH^- - U^-}$

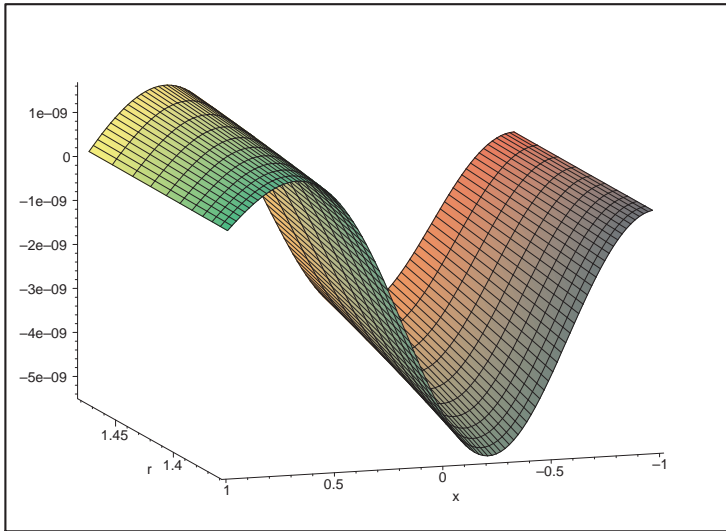


Figure 6.29: Positive polarization terms of  $\frac{1}{4\pi} \langle \hat{T}_{t\phi} \rangle^{CCH^- - U^-}$

## 6.9. Symmetry $(\theta, \phi) \rightarrow (\pi - \theta, \phi + \pi)$

---

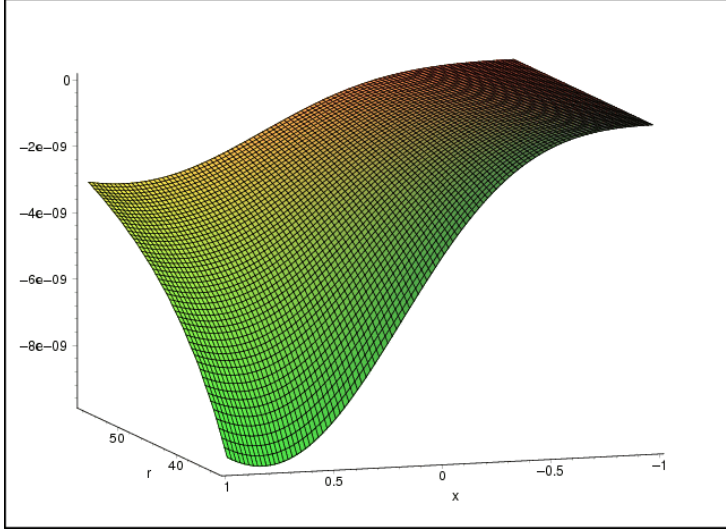


Figure 6.30: Positive polarization terms of  $\frac{1}{4\pi} \langle \hat{T}_{tr} \rangle^{U^- - B^-}$

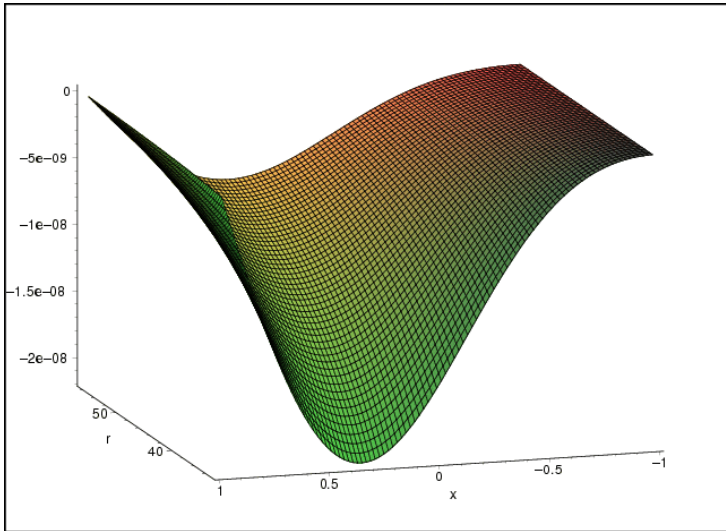


Figure 6.31: Positive polarization terms of  $\frac{1}{4\pi} \langle \hat{T}_{t\phi} \rangle^{U^- - B^-}$

# Conclusions

## Results

In this thesis we have aimed to give a precise and complete account of the quantum theory of linear spin-1 perturbations of the Kerr and Kerr-Newman space-times. This is a scarce subject in the literature compared to the volume of work on the scalar field in the Kerr space-time or on the electromagnetic field in the Schwarzschild space-time, precisely because it is considerably more difficult to deal with.

In Chapter 2 we gave a full account of the classical theory on a Type-D background where  $\kappa = \sigma = \nu = \lambda = 0$ , based on the elegant and compact formalism introduced by Wald. We also showed that the ingoing and upgoing gauge electromagnetic potentials can both be naturally expressed in terms of one single Newman-Penrose Maxwell scalar,  $\phi_0$ . It is therefore possible to reduce the quantization of the electromagnetic theory to that of a simpler, complex scalar theory. Unfortunately, we showed that this was not viable in the Kerr space-time when using either the Kinnersley or the Carter null tetrads since the field equation for  $\phi_0$  is not separable in either case. It is however possible to do so in the Reissner-Nordström space-time.

In Chapter 3 we studied the solution to the radial Teukolsky equation, corresponding to the decoupling of the field equations for the other two Newman-Penrose scalars,  $\phi_{+1}$  and  $\phi_{-1}$ , in the Kerr-Newman space-time. The radial

Teukolsky equation has a long-range potential, behaving as  $1/r$  for large  $r$ . Its solution cannot be expressed in terms of any standard functions and must be solved numerically. We considered the various alternative methods that convert the radial equation into one with a short-range potential. We numerically integrated the equation and compared our numerical results against those in the literature. We also completed an analysis of the behaviour of the general-spin radial solution close to the horizon following a study by Candelas that he only developed for spin-0. The chapter ended with a study of the asymptotics for small frequency based on a method presented by Page.

The solution of the angular Teukolsky equation was the topic of the following chapter. We presented the background research on these solutions and on their limiting cases of either spin-0 in Kerr space-time or else general spin in the Schwarzschild space-time. We numerically solved the angular equation for the spin-1 case in the Kerr-Newman space-time and presented the results.

Chapter 5 was dedicated to the asymptotic analysis of the angular solution in the limit of large frequency and fixed  $m$ . The study was based on a paper by Breuer, Ryan and Waller. Their analysis, however was incomplete and partly flawed. They wrongly imposed a regularity condition on the solution and they also ignored the asymptotic solution that is valid in the region far from the boundary points. These are the reasons why they could not determine the parameter  $\gamma$  on which the asymptotic behaviour crucially depends. In this chapter we made the appropriate corrections to their paper and gave a complete account of the large frequency asymptotics with fixed  $m$  of the eigenvalue and the angular solution for general spin in the Kerr-Newman space-time. Such an account has not been presented in the literature before.

The last chapter undertook the quantization of the electromagnetic field on the Kerr background. It starts with a revision of the results in the literature related to the construction of physical states in the Kerr background that have the same defining features as the Boulware, Hartle-Hawking or Unruh states in the

Schwarzschild background. We quantized the electromagnetic field following a canonical quantization method presented by Candelas, Chrzanowski and Howard (CCH) which they used for the electromagnetic and gravitational fields. We calculated, both analytically and numerically, the luminosity of a black hole when the electromagnetic field is in the past Boulware vacuum and when it is in the past Unruh state. We compared the results against related ones in the literature and exposed some of the algebraic complications existing in the calculation of stress-energy tensor components for spin-1. We also calculated the expectation value of the renormalized stress-energy tensor (RSET) close to the horizon when the field is in the past Boulware vacuum. This calculation was prompted by a result in CCH which did not agree with the expected result that it should correspond to minus the stress-energy tensor of a thermal distribution at the Hawking temperature rigidly rotating with the horizon. Our numerical calculations agree with the latter rather than with CCH's result. We showed that the error in their calculation was caused by the fact that their asymptotic approximation of the radial and angular functions close to the horizon was not uniform in  $\tilde{\omega}$ . We further showed that the rate of rotation close to the horizon of the mentioned thermal distribution approaches that of a RRO rather than that of a ZAMO or a Carter observer.

We initially used expressions in CCH for the expectation value of the stress-energy tensor when the field is in the  $|B^- \rangle$ ,  $|CCH^- \rangle$  or  $|U^- \rangle$  states. Both analytically and numerically they led to the surprising result that the difference of the RSET between two of the previous states was not invariant under the parity transformation  $(\theta, \phi) \rightarrow (\pi - \theta, \phi + \pi)$ . We found that the reason for this asymmetry was the non-symmetrization of the quantum operators. We obtained the correct expressions, which are invariant under the parity transformation. We finally showed that the non-parity and the parity terms appearing in these corrected expressions correspond to two opposite polarizations, except for the case of the 'up' superradiant modes which have opposite polarization to the 'up' non-superradiant modes in the same term.

## Future work

We have seen that the reduction in the Kerr or Kerr-Newman backgrounds of the quantization of the electromagnetic theory to a complex scalar theory is not possible using the Kinnersley or Carter null tetrads due to the non-separability of the equations for  $\phi_0$ . However, by making full use of the three classes of rotation of the NP frame it might be possible to find another null tetrad for which the corresponding equation for  $\phi_0$  is separable. Alternatively, it might be possible to prove either that such a tetrad does exist or else that it does not; we are not aware of the existence of such a theorem. In any case, it is possible to separate the equation for  $\phi_0$  in the Reissner-Nordström space-time. We intend to develop the quantization of the electromagnetic field in this space-time treating it as a complex scalar field.

We have obtained an asymptotic analysis of the radial solution close to the horizon and of the angular solution for large frequency and fixed  $m$ . The asymptotic analysis of the angular solution that would allow us to obtain asymptotic results for the RSET in different physical states close to the horizon is one that is uniform in  $m$ . A possible approach for obtaining this asymptotic analysis uniform in  $m$  consists in performing an asymptotic analysis of the angular solution for large frequency and large  $m$  and then matching this analysis with the one for large frequency and fixed  $m$ . This is still an open problem.

In this thesis we have described the algebraic difficulties that calculations for the spin-1 field imply in relation to those for the spin-0 field. We believe, however, that with the insight we have gained into these calculations for the spin-1 field, a similar analysis of the stress-energy tensor to that carried out in [72] for the spin-0 field in terms of general physical principles is ready to be performed for spin-1. Such an analysis would be very interesting in order to further our knowledge of the properties -regularity and symmetries in particular- of the different physical states in the Kerr-Newman space-time.

Finally, one of our initial aims was to investigate the extreme charged Kerr-Newman black hole. Even though we gradually diverted from this aim as we encountered various challenges, our analysis and programs only require minor modifications to produce results for the extreme charged Kerr-Newman black hole. This black hole has recently acquired relevant importance, particularly in light of the result ([3]) that its geometry close to the horizon has similar properties to the  $AdS_2 \times S^2$  geometry. Some asymptotically anti-de-Sitter space-times have the interesting property that they can be in stable equilibrium with a thermal distribution ([43], [46]). The space-time corresponding to the geometry of a Kerr-Newman black hole embedded in the anti-de-Sitter universe is an example of these space-times. These space-times are recently of huge interest because of a conjectured correspondence between gravity in the anti-de-Sitter universe and conformal field theory on its boundary- the AdS/CFT correspondence. We believe that a great part of our analysis and our programs can be adapted for investigation of such space-times.

# Appendix A

## Radial numerics

The following are the values of the coefficients  ${}_i c_{lm\omega}$  that appear in the asymptotic expansion (3.3.1) of the radial function  $X_{lm\omega}^{\text{up}*}/B_{lm\omega}^{\text{up}*}$  in the limit  $r_* \rightarrow +\infty$ :

$${}_1 c_{lm\omega} = -\frac{i(-{}_1\lambda_{lm\omega} + 2am\omega)}{2\omega} \quad (\text{A.0.1a})$$

$${}_2 c_{lm\omega} = \frac{(-{}_1\lambda_{lm\omega} + 2am\omega)}{4\omega^2} - iamM \quad (\text{A.0.1b})$$

$$\begin{aligned} {}_3 c_{lm\omega} = & -\frac{M-{}_1\lambda_{lm\omega}}{2\omega^2} - \frac{i}{24\omega^3} ({}_1\lambda_{lm\omega}^2 + 4a\omega m-{}_1\lambda_{lm\omega} + 4a\omega m + 32am\omega^3 M^2 - \\ & - 8a^3\omega^3 m - 3\kappa - 4a^2\omega^2 - 4\omega^2-{}_1\lambda_{lm\omega} a^2 - 8a\omega^3 Q^2 m) \end{aligned} \quad (\text{A.0.1c})$$

$$\begin{aligned} {}_4 c_{lm\omega} = & \frac{1}{16\omega^4} (2-{}_1\lambda_{lm\omega}^2 + 4-{}_1\lambda_{lm\omega}\omega^2 Q^2 + 4m^2 a^2 \omega^2 + 8-{}_1\lambda_{lm\omega} m a \omega - 8a^3 \omega^3 m - \\ & - 4a^2 \omega^2 - 4a^2 \omega^2-{}_1\lambda_{lm\omega} + 4\omega a m - 3\kappa) - \frac{i}{16\omega^4} (-M\omega-{}_1\lambda_{lm\omega}^2 - \\ & - 16\omega^4 M Q^2 a m + 4\omega^3 M a^2 - 16M a^3 \omega^4 m + 32am M^3 \omega^4 - 4am M \omega^2 + \\ & + 10M\omega\kappa) \end{aligned} \quad (\text{A.0.1d})$$



---


$$\begin{aligned}
{}_5c_{lm\omega} = & \frac{1}{80\omega^5} \left( -80\omega^2 M_{-1} \lambda_{lm\omega} a m + 80\omega^3 {}_{-1}\lambda_{lm\omega} a^2 M + 80\omega^3 a^2 M + 130M\omega\kappa - \right. \\
& -40M_{-1} \lambda_{lm\omega}^2 \omega - 80M\omega^2 a m \left. \right) - \frac{i}{80\omega^5} \left( -8a^2\omega^2 + 2{}_{-1}\lambda_{lm\omega}^2 + 30\kappa - \right. \\
& -4\omega^2 {}_{-1}\lambda_{lm\omega} a^2 + 16a^4\omega^4 - 15\kappa {}_{-1}\lambda_{lm\omega} - 40a^3\omega^3 m - 8a^2\omega^4 Q^2 + \\
& + 24a^2\omega^2 m^2 + 20\omega^2 \kappa a^2 - 30\omega^2 \kappa Q^2 + 8a\omega^3 Q^2 m + 4a\omega m {}_{-1}\lambda_{lm\omega} - \\
& -50a\omega m \kappa + 16a^5\omega^5 m + 8a^4\omega^4 {}_{-1}\lambda_{lm\omega} - 4a^2\omega^2 {}_{-1}\lambda_{lm\omega}^2 + 2\omega^2 {}_{-1}\lambda_{lm\omega}^2 Q^2 + \\
& + {}_{-1}\lambda_{lm\omega}^3 - 16a^3\omega^3 m {}_{-1}\lambda_{lm\omega} + 8a^2\omega^2 m^2 {}_{-1}\lambda_{lm\omega} + 6a\omega m {}_{-1}\lambda_{lm\omega}^2 + \\
& + 32a^3\omega^5 Q^2 m - 192M^2 a^3\omega^5 m + 8a\omega m + 16\omega^5 Q^4 a m - \\
& \left. -192Q^2\omega^5 M^2 a m + 256M^4\omega^5 a m - 60\omega^2 M^2 \kappa \right)
\end{aligned}
\tag{A.0.1e}$$

$$\begin{aligned}
{}_6c_{lm\omega} = & -\frac{1}{48\omega^6} \left( 24Q^2\omega^4 {}_{-1}\lambda_{lm\omega} a^2 + 54\omega^2 Q^2 \kappa - 30\omega^2 \kappa a^2 + 24a^4\omega^4 m^2 + \right. \\
& + 48\omega^4 M^2 a^2 - 24\omega^2 M^2 {}_{-1}\lambda_{lm\omega}^2 - 24a\omega m {}_{-1}\lambda_{lm\omega}^2 + 48a^3\omega^3 m {}_{-1}\lambda_{lm\omega} + \\
& + 84\omega a m \kappa + 210\omega^2 M^2 \kappa - 8a^3\omega^3 m^3 - 36a^2\omega^2 m^2 {}_{-1}\lambda_{lm\omega} + 12a^2\omega^2 {}_{-1}\lambda_{lm\omega}^2 - \\
& -12a^4\omega^4 {}_{-1}\lambda_{lm\omega} - 12\omega^2 {}_{-1}\lambda_{lm\omega}^2 Q^2 - 24a^5\omega^5 m + 24a^2\omega^4 Q^2 - 24a^4\omega^4 - \\
& -24Q^2\omega^3 {}_{-1}\lambda_{lm\omega} a m + 27\kappa {}_{-1}\lambda_{lm\omega} - 12{}_{-1}\lambda_{lm\omega} a\omega m - 4{}_{-1}\lambda_{lm\omega}^3 - \\
& -24\omega^3 Q^2 a m - 48\omega^3 M^2 a m - 48\omega^2 a^2 m^2 - 12a\omega m + 12a^2\omega^2 + 72\omega^3 a^3 m + \\
& + 12\omega^2 {}_{-1}\lambda_{lm\omega} a^2 - 45\kappa - 3{}_{-1}\lambda_{lm\omega}^2 \left. \right) + \frac{i}{48\omega^6} \left( 256a^3\omega^6 M^3 m - 256\omega^6 M^5 a m - \right. \\
& -138M\omega^2 a m \kappa - 63M\omega\kappa {}_{-1}\lambda_{lm\omega} + 96M\omega^3 \kappa a^2 - 42M\omega^3 \kappa Q^2 + \\
& + 32M\omega^2 a m - 6M a^2 {}_{-1}\lambda_{lm\omega}^2 \omega^3 + 6m a {}_{-1}\lambda_{lm\omega}^2 M\omega^2 + 2{}_{-1}\lambda_{lm\omega}^3 M\omega + \\
& + 231M\omega\kappa + 24a^4 M\omega^5 + 24M\omega^3 a^2 m^2 + 256Q^2\omega^6 M^3 a m - \\
& -96Q^2\omega^6 M a^3 m - 48Q^4\omega^6 M a m - 48a^5 M\omega^6 m - 8M {}_{-1}\lambda_{lm\omega} a^2\omega^3 + \\
& \left. + 8M {}_{-1}\lambda_{lm\omega} a\omega^2 m - 32a^2\omega^3 M - 48M a^3\omega^4 m + 8M {}_{-1}\lambda_{lm\omega}^2 \omega \right)
\end{aligned}
\tag{A.0.1f}$$

The following table shows the values of the radial functions  ${}_{-1}R_{2,-2,-0.5}^{\text{chandr}}$  from TableV in Chandrasekhar's [20] Appendix and  ${}_{-1}R_{2,-2,-0.5}^{\text{sym,num}}$  calculated with Fortran90 program RADDRV2KN.F described in Section 3.3.

Table A.1: Radial functions and their derivatives for  $h = -1$ ,  $Q = 0$ ,  $a = 0.95$ ,  $l = 2$ ,  $m = -2$ ,  $\omega = -0.5$ . Within each cell for the radial functions and for the derivatives the top value corresponds to the real part and the bottom value to the imaginary part.

$r/M$	${}_{-1}R_{2,-2,-0.5}^{\text{chandr}}$	${}_{-1}R_{2,-2,-0.5}^{\text{sym,num}}$	$\frac{\text{d-}{}_1R_{2,-2,-0.5}^{\text{chandr}}}{\text{dr}}$	$\frac{\text{d-}{}_1R_{2,-2,-0.5}^{\text{sym,num}}}{\text{dr}}$
2.1	1.2003	1.20026785136567	2.18133	2.18334724475591
	-0.10873	-0.10875922190824	-1.2468	-1.24677817342713
2.2	1.4350	1.43492663358771	2.5017	2.50176744330508
	-0.24999	-0.25002380500959	-1.5818	-1.58179707611184
2.3	1.6992	1.69915736492414	2.7757	2.77575249647072
	-0.42574	-0.42576456994030	-1.9361	-1.93613390496899
2.4	1.9887	1.98869418055624	3.0079	3.00797480302144
	-0.63781	-0.63783865284620	-2.3080	-2.30801570052304
2.5	2.2994	2.29938556170459	3.1991	3.19916057586282
	-0.88783	-0.88785789689252	-2.6946	-2.69460457858789
2.6	2.6272	2.62716311795229	3.3492	3.34919957529641
	-1.1771	-1.17714459161815	-3.0926	-3.09264287195368
2.7	2.9679	2.96782782649048	3.4575	3.45746844788633
	-1.5066	-1.50664472608102	-3.4985	-3.49853230609708
2.8	3.3173	3.31722704239298	3.5234	3.52337153886738
	-1.8770	-1.87698636533703	-3.9087	-3.90869011633273
2.9	3.6711	3.67107176062917	3.5463	3.54629329952196
	-2.2884	-2.28840304104407	-4.3194	-4.31941466954318
3.0	4.0251	4.02503739941419	3.5258	3.52580194116473
	-2.7407	-2.74076500607478	-4.7270	-4.72703002192608
3.1	4.3748	4.37477566784955	3.4617	3.46169488540498
	-3.2336	-3.23358278453457	-5.1279	-5.12790900693526

---

3.2	4.7160	4.71592778158095	3.3540	3.35402047306941
	-3.7660	-3.76600886397982	-5.5185	-5.51848547182964
3.3	5.0442	5.04413646655539	3.2031	3.20308181562904
	-4.3368	-4.33681855987963	-5.8953	-5.89525158089140
3.4	5.3551	5.35511788785783	3.0095	3.00948363393847
	-4.9445	-4.94448127866285	-6.2549	-6.25483895346162
3.5	5.6447	5.64463977090707	2.7741	2.77408878295112
	-5.5871	-5.58710647199081	-6.5940	-6.59396595505323
3.6	5.9086	5.90858014436306	2.4980	2.49803814126054
	-6.2625	-6.26248554733942	-6.9095	-6.90949152985754
3.7	6.1430	6.14293415562655	2.1827	2.18273401664141
	-6.9681	-6.96812791317567	-7.1984	-7.19842063374193
3.8	6.3439	6.34387247839626	1.8298	1.82983839651524
	-7.7012	-7.70119148771223	-7.4579	-7.45791354146316
3.9	6.5077	6.50771674910113	1.4412	1.44124730666313
	-8.4586	-8.45862800399240	-7.6853	-7.68530442839311
4.0	6.6310	6.6310	1.0191	1.01908734960253
	-9.2371	-9.2371	-7.8781	-7.87810703311225
4.1	6.7105	6.71049567442221	0.56571	0.56570603328326
	-10.0330	-10.03301997548350	-8.0341	-8.03403834407662
4.2	6.7432	6.74317769234848	0.83637	0.08363318452101
	-10.8430	-10.84260964545399	-8.1510	-8.15099433940105
4.3	6.7264	6.72632534827829	-0.042439	-0.42440357766359
	-11.6620	-11.66187058988782	-8.2272	-8.22710903213187
4.4	6.6576	6.65754159377316	-0.09555	-0.95549606758222
	-12.4870	-12.48661417641590	-8.2608	-8.26076519166212
4.5	6.5346	6.53458927651571	-1.5066	-1.50663575355877

---

	-13.3130	-13.31255141698046	-8.2505	-8.25048650875395
4.6	6.3557	6.35565169996788	-2.0746	-2.07464130742694
	-14.1350	-14.13520779834626	-8.1951	-8.19509763948480
4.7	6.1192	6.11911479670302	-2.6562	-2.65625398486783
	-14.9500	-14.95002770851276	-8.0937	-8.09358159395761
4.8	5.8241	5.82397789741934	-3.2480	-3.24805124849254
	-15.7520	-15.75237325602916	-7.9455	-7.94536770095228
4.9	5.4694	5.46938483164315	-3.8466	-3.84658353999649
	-16.5380	-16.53754452954476	-7.7500	-7.74998554852685
5.0	5.0547	5.05467081851123	-4.4484	-4.44837518344008
	-17.3010	-17.30079952288854	-7.5071	-7.50709894810016
5.1	4.5797	4.57969767206908	-5.0499	-5.04986329143664
	-18.0370	-18.03737403247108	-7.2168	-7.21674248154373
5.2	4.0448	4.04462210157875	-5.6475	-5.64747476292679
	-18.7430	-18.74251756497168	-6.8793	-6.87915515030467
5.3	3.4505	3.45026879397524	-6.2376	-6.23760299462583
	-19.4120	-19.41162505323660	-6.4952	-6.49506253045761
5.4	2.7977	2.79759552270645	-6.8167	-6.81668061192606
	-20.0400	-20.04007705958522	-6.0653	-6.06525657188396
5.5	2.0876	2.08760103455425	-7.3812	-7.38118691076062
	-20.6230	-20.62321598203533	-5.5906	-5.59052672884331
5.6	1.3220	1.32190457349643	-7.9277	-7.92764415522192
	-21.1570	-21.15664442715797	-5.0722	-5.07211926348503
5.7	0.50282	0.50271763626229	-8.4527	-8.45263822831099
	-21.6360	-21.63621445472158	-4.5118	-4.51170165964859
5.8	-0.36768	-0.36768764471486	-8.9528	-8.95282258003868
	-22.0580	-22.05775138133475	-3.9110	-3.91093638972109

---

---

5.9	-1.2868	-1.28682498342566	-9.4250	-9.42493652904060
	-22.4170	-22.41718655405400	-3.2716	-3.27161266174137
6.0	-2.2516	-2.25163946019482	-9.8659	-9.86586697577774
	-22.7110	-22.71085893051983	-2.5960	-2.59593849391648
6.1	-3.2589	-3.25887087136051	-10.2730	-10.27260628469677
	-22.9350	-22.93522595577702	-1.8863	-1.88623285460110
6.2	-4.3049	-4.30492749584150	-10.6420	-10.64231072724808
	-23.0870	-23.08705554175912	-1.1451	-1.14504283409244
6.3	-5.3860	-5.38600209115882	-10.9720	-10.97226665323438
	-23.1630	-23.16328981815513	-0.37505	-0.37503743621995
6.4	-6.4980	-6.49797039906948	-11.2600	-11.25994137512047
	-23.1610	-23.16120229611491	0.42089	0.42089987073883
6.5	-7.6365	-7.63650873314380	-11.5030	-11.50295464488002
	-23.0780	-23.07828061195214	1.2397	1.23977308060567
6.6	-8.7970	-8.79701255583228	-11.6990	-11.69920334879844
	-22.9130	-22.91253679020954	2.0784	2.07837074709545
6.7	-9.9747	-9.97471998568154	-11.8470	-11.84673549848341
	-22.6620	-22.66217107792423	2.9334	2.93340696991069
6.8	-11.1650	-11.16467396352343	-11.9440	-11.94373627176464
	-22.3260	-22.32556159484567	3.8015	3.80149794211117
6.9	-12.3620	-12.36170540720160	-11.9890	-11.98854519165635
	-21.9020	-21.90131337097084	4.6791	4.67914339708598
7.0	-13.5610	-13.56055044001096	-11.9800	-11.97988874356997
	-21.3900	-21.38872477349637	5.5627	5.56273274110761

# Bibliography

- [1] Milton Abramowitz and Irene A. Stegun. *Handbook of Mathematical Functions*. Dover Publications, Inc., New York, USA, ninth edition, 1965.
- [2] James M. Bardeen, B. Carter, and S.W. Hawking. The four laws of black hole mechanics. *Commun. Math. Phys.*, 31:161–170, 1973.
- [3] James M. Bardeen and Gary T. Horowitz. The extreme Kerr throat geometry: A vacuum analog of  $AdS_2 \times S^2$ . *Phys. Rev. D*, 60:104030, 1999.
- [4] Carl M. Bender and Steven A. Orszag. *Advanced mathematical methods for scientists and engineers*. McGraw-Hill, 1978.
- [5] Emanuele Berti, Vitor Cardoso, and Shijun Yoshida. Highly damped quasinormal modes of Kerr black holes: A complete numerical investigation. *Phys. Rev. D*, 69:124018, 2004.
- [6] S.K. Bose. Studies in the Kerr-Newman metric. *J. Math. Phys.*, 16(4):772–775, 1975.
- [7] Robert H. Boyer and Richard W. Lindquist. Maximal analytic extension of the Kerr metric. *J. Math. Phys.*, 8(2):265–281, 1967.
- [8] R.A. Breuer, M.P. Ryan Jr, and S. Waller. Some properties of spin-weighted spheroidal harmonics. *Proc. R. Soc. Lond. A*, 358:71–86, 1977.
- [9] Reinhard A. Breuer. Gravitational perturbation theory and synchrotron radiation. *Lecture Notes in Physics*, 44, 1975.

- [10] M.R. Brown and Adrian C. Ottewill. The energy momentum operator in curved space-time. *Proc. R. Soc. Lond. A*, 389:379–403, 1983.
- [11] H. Buchholz. *The Confluent Hypergeometric Function*. Springer Tracts in Natural Philosophy, 1969.
- [12] William B. Campbell. Tensor and spinor spherical harmonics and the spin- $s$  harmonics  ${}_sy_{lm}(\theta, \phi)$ . *J. Math. Phys.*, 12(8):1763–1770, 1971.
- [13] Philip Candelas. Vacuum polarization in Schwarzschild spacetime. *Phys. Rev. D*, 21(8):2185–2202, 1980.
- [14] Philip Candelas, P. Chrzanowski, and K. W. Howard. Quantization of electromagnetic and gravitational perturbations of a Kerr black hole. *Phys. Rev. D*, 24(2):297–304, 1981.
- [15] Philip Candelas and David Deutsch. On the vacuum stress induced by uniform acceleration or supporting the ether. *Proc. R. Soc. Lond. A*, 354:79–99, 1977.
- [16] B. Carter. Hamilton-Jacobi and Schrodinger separable solutions of Einstein’s equations. *Commun. Math. Phys.*, 10:280–210, 1968.
- [17] B. Carter. In B. DeWitt and C. DeWitt, editors, *Black Holes*, New York, USA, 1973. Gordon and Breach.
- [18] B. Carter. Mathematical foundations of the theory of relativistic stellar and black hole configurations. In B. Carter and J.B. Hartle, editors, *Gravitation in Astrophysics. Cargèse 1986*, New York, USA, 1987. Plenum Press and NATO Scientific Affairs Division.
- [19] Brandon Carter. Global structure of the Kerr family of gravitational fields. *Phys. Rev.*, 174(5):1559–1571, 1968.
- [20] S. Chandrasekhar. *The Mathematical Theory of Black Holes*. Oxford University Press, Oxford, UK, second edition, 1992.

- [21] S. M. Christensen. Regularization, renormalization, and the covariant geodesic point separation. *Phys. Rev. D*, 17(4):946–963, 1978.
- [22] S. M. Christensen and S. A. Fulling. Trace anomalies and the Hawking effect. *Phys. Rev. D*, 15(8):2088–2104, 1977.
- [23] D. Christodoulou. Reversible and irreversible transformations in black hole physics. *Phys. Rev. Lett.*, 25:1596–1597, 1970.
- [24] D. Christodoulou and R. Ruffini. Reversible transformations of a charged black hole. *Phys. Rev. D*, 4:3552–3555, 1971.
- [25] Paul L. Chrzanowski. Vector potential and metric perturbations of a rotating black hole. *Phys. Rev. D*, 11(8):2042–2062, 1975.
- [26] Paul L. Chrzanowski, Richard A. Matzner, Vernon D. Sandberg, and Michael P. Ryan Jr. Zero-mass plane waves in nonzero gravitational backgrounds. *Phys. Rev. D*, 14(2):317–326, 1976.
- [27] Paul L. Chrzanowski and C.W. Misner. Geodesic synchrotron radiation in the Kerr geometry by the method of asymptotically factorized Green’s functions. *Phys. Rev. D*, 10(6):1701–1721, 1974.
- [28] Jeffrey M. Cohen and Lawrence S. Kegeles. Electromagnetic fields in curved spaces: A constructive procedure. *Phys. Rev. D*, 10(4):1070–1084, 1974.
- [29] Stephen L. Detweiler. On the equations governing the electromagnetic perturbations of the Kerr black hole. *Proc. R. Soc. Lond. A*, 349:217–230, 1976.
- [30] Stephen L. Detweiler. On resonant oscillations of a rapidly rotating black hole. *Proc. R. Soc. Lond. A*, 352:381–395, 1977.
- [31] P.A.M. Dirac. *General Theory of Relativity*. Wiley, New York, 1975.
- [32] Gavin Duffy. *Scalar Quantum Field Theory on the Kerr Black Hole Background*. PhD thesis, University College Dublin, 2002.



- [33] A. Erdélyi, W. Magnus, F. Oberhettinger, and F.G. Tricomi. *Higher Transcendental Functions*. Bateman Manuscript Project, 1953.
- [34] Edward D. Fackerell and Robert G. Grossman. Spin-weighted angular spheroidal functions. *J. Math. Phys.*, 18(9):1849–1854, 1977.
- [35] C. Flammer. *Spheroidal Wave Functions*. Stanford University Press, 1957.
- [36] John L. Friedman. Ergosphere instability. *Commun. Math. Phys.*, 63:243–255, 1978.
- [37] Valery P. Frolov and Kip S. Thorne. Renormalized stress-energy tensor near the horizon of a slowly evolving rotating black hole. *Phys. Rev. D*, 39(8):2125–2154, 1989.
- [38] Valery P. Frolov and A. I. Zel’nikov. Vacuum polarization of the electromagnetic field near a rotating black hole. *Phys. Rev. D*, 32(12):3150–3163, 1985.
- [39] J.N. Goldberg, A.J. MacFarlane, E.T. Newman, F. Rohrlich, and E.C.G. Sudarshan. Spin- $s$  spherical harmonics and  $\bar{\partial}$ . *J. Math. Phys.*, 8(11):2155–2161, 1967.
- [40] I. S. Gradshteyn and I. M. Ryzhik. *Table of Integrals, Series and Products*. Academic Press, San Diego, fifth edition, 1995.
- [41] W. Gropp, E. Lusk, and A. Skjellum. *Using MPI. Portable Parallel Programming with the Message Passing Interface*. The MIT Press, Cambridge, Massachusetts, second edition, 1999.
- [42] P.G. Grove and Adrian C. Ottewill. Notes on ‘particle detectors’. *J. Phys. A*, 16:3905–3920, 1983.
- [43] S. W. Hawking and Don N. Page. Thermodynamics of black holes in anti-de Sitter space. *Commun. Math. Phys.*, 87:577–587, 1983.

- [44] Stephen W. Hawking. Gravitational radiation from colliding black holes. *Phys. Rev. Lett.*, 26:1344–1346, 1971.
- [45] Stephen W. Hawking. Particle creation by black holes. *Commun. Math. Phys.*, 43:199–220, 1975.
- [46] Stephen W. Hawking, C.J. Hunter, and M.M. Taylor-Robinson. Rotation and the AdS/CFT correspondence. *Phys. Rev. D*, 59:064005, 1999.
- [47] S. Hod. Bohr’s correspondence principle and the area spectrum of quantum black holes. *Phys. Rev. Lett.*, 81:4293–4296, 1998.
- [48] James R. Ipser. Electromagnetic test fields around a Kerr-metric black hole. *Phys. Rev. Lett.*, 27(8):529–531, 1971.
- [49] Werner Israel. Thermo-field dynamics of black holes. *Phys. Lett. A*, 57(2):107–110, 1976.
- [50] Werner Israel. Third law of black hole dynamics: A formulation and proof. *Phys. Rev. Lett.*, 57:397–399, 1986.
- [51] Bruce P. Jensen, John G. McLaughlin, and Adrian C. Ottewill. Renormalized electromagnetic stress tensor for an evaporating black hole. *Phys. Rev. D*, 43(12):4142–4144, 1991.
- [52] Bruce P. Jensen, John G. McLaughlin, and Adrian C. Ottewill. Anisotropy of the quantum thermal state in Schwarzschild space-time. *Phys. Rev. D*, 45(8):3002–3005, 1992.
- [53] Bruce P. Jensen, John G. McLaughlin, and Adrian C. Ottewill. One-loop quantum gravity in Schwarzschild space-time. *Phys. Rev. D*, 51(10):5676–5697, 1995.
- [54] Bruce P. Jensen, John G. McLaughlin, and Adrian C. Ottewill. Renormalized electromagnetic energy density on the horizon of a Kerr black hole. *Class. Quantum. Grav.*, 5:L187–L189, 1999.

- [55] Gungwon Kang. Quantum aspects of ergoregion instability. *Phys. Rev. D*, 55:7563–7573, 1997.
- [56] Bernard S. Kay and Robert M. Wald. Theorems on the uniqueness and thermal properties of stationary, nonsingular, quasifree states on spacetimes with a bifurcate Killing horizon. *Physics Reports*, 207(2):49–136, 1991.
- [57] Roy. P. Kerr and A. Schild. A new class of vacuum solutions of the Einstein field equations. In *Proceedings of the Galileo Galilei Centenary Meeting on General Relativity, Problems of Energy and Gravitational Waves*, pages 222–233, Florence, 1965. Comitato Nazionale per le Manifestazione Celebrative.
- [58] William Kinnersley. Type D vacuum metrics. *J. Math. Phys.*, 10:1195–1203, 1969.
- [59] W. Kundt and A. Thompson. Le tenseur de Weyl et une congruence associée de géodésiques isotropes sans distorsion. *C.R. Acad. Sci. Paris*, 254:4257–4259, 1962.
- [60] W. Kundt and M. Trümper. Beiträge zur theorie der gravitationsstrahlungsfelder. *Akad. Wiss. Lit. Mainz, Abhandl. Math.-Nat. Kl.*, 12:965–1000, 1962.
- [61] E. W. Leaver. Solutions to a generalized spheroidal wave equation: Teukolsky’s equations in general relativity, and the two-center problem in molecular quantum mechanics. *J. Math. Phys.*, 27(5):1238–1265, 1986.
- [62] William H. Louisell. *Quantum Statistical Properties of Radiation*. Wiley-Interscience, 1990.
- [63] A. L. Matacz, P. C. W. Davies, and Adrian C. Ottewill. Quantum vacuum instability near rotating stars. *Phys. Rev. D*, 47(4):1557–1562, 1993.
- [64] John Gerard McLaughlin. *Renormalisation of the energy-momentum stress tensor for quantum fields on a curved background*. PhD thesis, University of Oxford, 1990.

- [65] Josef Meixner and Friedrich Wilhelm Schäfke. *Mathieusche Funktionen und Sphäroidfunktionen mit Anwendungen auf Physikalische und Technische Probleme*. Springer-Verlag, 1954.
- [66] Charles W. Misner, Kip S. Thorne, and John Archibald Wheeler. *Gravitation*. W.H. Freeman, San Francisco, 1973.
- [67] E.T. Newman, E. Couch, K. Chinnapared, A. Exton, A. Prakash, and R. Torrence. Metric of a rotating, charged mass. *J. Math. Phys.*, 6(6):918–919, 1965.
- [68] Ezra T. Newman and A.I. Janis. Note on the Kerr spinning-particle metric. *J. Math. Phys.*, 6(6):915–917, 1966.
- [69] Ezra T. Newman and Roger Penrose. An approach to gravitational radiation by a method of spin coefficients. *J. Math. Phys.*, 3(3):566–578, 1962.
- [70] Ezra T. Newman and Roger Penrose. Note on the Bondi-Metzner-Sachs group. *J. Math. Phys.*, 7:863–870, 1966.
- [71] Adrian C. Ottewill and Elizabeth Winstanley. Divergence of a quantum thermal state on Kerr space-time. *Phys. Lett. A*, 273:149–152, 2000.
- [72] Adrian C. Ottewill and Elizabeth Winstanley. Renormalized stress tensor in Kerr space-time: General results. *Phys. Rev. D*, 62(8):084018, 2000.
- [73] Don N. Page. Particle emission rates from a black hole: II. massless particles from a rotating hole. *Phys. Rev. D*, 14(12):3260–3273, 1976.
- [74] Don N. Page. Particle emission rates from a black hole: Massless particles from an uncharged, nonrotating hole. *Phys. Rev. D*, 13(2):198–205, 1976.
- [75] R. Penrose. Gravitational collapse: The role of general relativity. *Rev. del Nuovo Cimento*, 1:252–276, 1969.

- [76] William H. Press and Saul A. Teukolsky. Perturbations of a rotating black hole. II. Dynamical stability of the Kerr metric. *The Astrophysical Journal*, 185:649–673, 1973.
- [77] William H. Press, Saul A. Teukolsky, William T. Vetterling, and Brian P. Flannery. *Numerical Recipes in Fortran*. Cambridge University Press, Cambridge, second edition, 1992.
- [78] Richard H. Price. Nonspherical perturbations of relativistic gravitational collapse. II. integer-spin, zero-rest-mass fields. *Phys. Rev. D*, 5:2439–2454, 1972.
- [79] I. Robinson and A. Schild. Generalization of a theorem by Goldberg and Sachs. *J. Math. Phys.*, 4:484–489, 1963.
- [80] Misao Sasaki and Takashi Nakamura. Gravitational radiation from a Kerr black hole. I. *Progress of Theoretical Physics*, 67(6):1788–1809, 1982.
- [81] Bonny L. Schumaker and Carlton M. Caves. New formalism for two-photon quantum optics. II. Mathematical foundation and compact notation. *Phys. Rev. A*, 31(5):3093–3111, 1985.
- [82] Edward Seidel. A comment on the eigenvalues of the spin-weighted spheroidal functions. *Class. Quantum. Grav.*, 6:1057–1062, 1989.
- [83] A. A. Starobinskiĭ. Amplification of waves during reflection from a rotating black hole. *Zh. Eksp. Theor. Fiz.*, 64:48–57, 1973.
- [84] A. A. Starobinskiĭ and S. M. Churilov. Amplification of electromagnetic and gravitational waves scattered by a rotating black hole. *Zh. Eksp. Theor. Fiz.*, 65:3–11, 1973.
- [85] J.M. Stewart. On the stability of Kerr’s space-time. *Proc. R. Soc. Lond. A*, 344:65–79, 1975.

- [86] Saul A. Teukolsky. Rotating black holes: Separable wave equations for gravitational and electromagnetic perturbations. *Phys. Rev. Lett.*, 29(16):1114–1118, 1972.
- [87] Saul A. Teukolsky. Perturbations of a rotating black hole. I. Fundamental equations for gravitational, electromagnetic, and neutrino-field perturbations. *The Astrophysical Journal*, 185:635–647, 1973.
- [88] Saul A. Teukolsky and William H. Press. Perturbations of a rotating black hole. III. Interaction of the hole with gravitational and electromagnetic radiation. *The Astrophysical Journal*, 193:443–461, 1974.
- [89] William G. Unruh. Second quantization in the Kerr metric. *Phys. Rev. D*, 10(10):3194–3205, 1974.
- [90] William G. Unruh. Notes on black-hole evaporation. *Phys. Rev. D*, 14(4):870–891, 1976.
- [91] Robert M. Wald. Construction of solutions of gravitational, electromagnetic, or other perturbation equations from solutions of decoupled equations. *Phys. Rev. Letters*, 41(4):203–206, 1978.
- [92] Robert M. Wald. *General Relativity*. The University of Chicago Press, Chicago and London, 1984.
- [93] Elizabeth Winstanley. Quantum field theory on black hole backgrounds. First year dissertation, Oxford University, 1993.
- [94] Ya. B. Zel’dovich. The generation of waves by a rotating body. *ZhETF Pis. Red.*, 14:270–, 1971.

# Errata

The following are corrections to the printed version of the Ph.D. thesis.

- In Eqs. (2.7.19), (2.8.1), (2.8.2), (6.2.9) (6.2.10), (6.2.12) (6.9.10), (6.9.11) and (6.9.23) the index  $w$  should be  $\omega$ .

## Chapter 1

- On Pages 18, 20 (twice) and 21, “Schwarzschild” has been misspelled as “Schwarzcild”.

## Chapter 2

- The factor  $\cos^2 \theta$  in the Teukolsky equation (2.7.2) should be  $\cot^2 \theta$  instead.
- The power of  $\rho^*$  in Eq. (2.7.24) should be  $(\pm 1 - 1)$ , so that the equation should read:

$${}_{lm\omega}A_\beta = -\Pi_{\mp 1\beta}{}^{\dagger*} \rho^{*(\pm 1 - 1)}{}_{\mp 1} R_{lm\omega}{}_{\pm 1} Z_{lm\omega} e^{-i\omega t}$$

## Chapter 3

- There are two wrong signs and a power of two missing in the values of  $a_D$  and  $b_D$  in Eq. (3.2.4). It should read:

$$a_D = -\frac{2}{\Delta^2} [2K^2 - \Delta(iK' + {}_{-1}\lambda_{lm\omega})]$$
$$b_D = -\frac{4iK}{\Delta}$$

- There is a minus sign missing in the potential (3.2.20), in the first term of the right hand side on the second line. It should read:

$$\begin{aligned}
 {}_{-1}\mathcal{U} = & -\frac{[-\omega(r^2 + a^2) + am]^2}{(r^2 + a^2)^2} + \frac{\Delta_{-1}\lambda_{lm\omega}}{(r^2 + a^2)^2} - \frac{\Delta(\Delta r^2 + 4Ma^2r - Q^2(a^2 - r^2))}{(r^2 + a^2)^4} - \\
 & - \frac{\Delta[\Delta(10r^2 + 2\nu^2) - (r^2 + \nu^2)(11r^2 - 10rM + \nu^2)]}{(r^2 + a^2)^2[(r^2 + \nu^2)^2 + \eta\Delta]} + \\
 & + \frac{12\Delta r(r^2 + \nu^2)^2[\Delta r - (r^2 + \nu^2)(r - M)]}{(r^2 + a^2)^2[(r^2 + \nu^2)^2 + \eta\Delta]^2} - \frac{\Delta(r - M)^2\eta[2(r^2 + \nu^2)^2 - \eta\Delta]}{(r^2 + a^2)^2[(r^2 + \nu^2)^2 + \eta\Delta]^2}
 \end{aligned}$$

- The variable  $\tilde{\omega}$  used for the first time on Page 74 is not defined anywhere. For an uncharged matter field in a Kerr-Newman black hole it is defined as  $\tilde{\omega} \equiv \omega - m\Omega_+$ .

- The normalization used in Table 3.1 has not been indicated.

It is:  ${}_{-1}R_{lm\omega}^{\text{in,inc}} = {}_{-1}R_{lm\omega}^{\text{up,inc}} = 1$ .

- On Page 95 it should say  ${}_hZ_{lm\omega} \rightarrow {}_hY_{lm}$  rather than  ${}_hS_{lm} \rightarrow {}_hY_{lm}$ .
- Eq. (3.5.12) should read:

$$I_{\tilde{\omega}} \equiv e^{-i\tilde{\omega}r_+} (4M\kappa_+)^{-\frac{i\tilde{\omega}}{2\kappa_+}} (-4M\kappa_-)^{-\frac{i\tilde{\omega}}{2\kappa_-}}$$

- There is a missing subscript in the normalization constant in Eq. (3.5.15):

$$|N_{-1}^{\text{up}}|_h R_{lm\omega}^{\text{up}} \rightarrow A_h N x^{-1/2} K_{h+iq}(2lx^{1/2}) \quad (l \rightarrow +\infty, r \rightarrow r_+, lx^{1/2} \text{ finite})$$

- There is a factor  $|N_{-1}^{\text{up}}|$  missing in Eqs. (3.5.18) and (3.5.20). They should respectively read:

$$\begin{aligned}
 & \frac{|N_{-1}^{\text{up}}|}{A_h N} \mathcal{D}_0^\dagger (\Delta_h R_{lm\omega}^{\text{up}}) \rightarrow \\
 & \rightarrow (r_+ - r_-) x^{-h/2} \left[ \left( -\frac{h}{2} + 1 + i\frac{q}{2} \right) K_{h+iq}(2lx^{1/2}) + lx^{1/2} K'_{h+iq}(2lx^{1/2}) \right] \\
 & \quad (l \rightarrow +\infty, r \rightarrow r_+, lx^{1/2} \text{ finite})
 \end{aligned}$$

and

$$\frac{|N_{-1}^{\text{up}}|}{A_h N} \mathcal{D}_0^\dagger (\Delta_{+1} R_{lm\omega}^{\text{up}}) \rightarrow -\frac{(r_+ - r_-)}{2x^{1/2}} K_{iq} \quad (l \rightarrow +\infty, r \rightarrow r_+)$$



## Chapter 4

- Eq. (4.1.6) should read:

$${}_hE_{lm} \equiv {}_hE_{lm\omega=0} = l(l+1).$$

- There is a typo in Eq. (4.2.11). The term  $n(n+1)$  should be replaced by  $n(n-1)$  so that the equation reads

$$\begin{aligned} {}_h\left\{\begin{matrix} a \\ b \end{matrix}\right\}_{n+1,lm\omega} &= \frac{1}{2(n+1)\left(n+1+2\left\{\begin{matrix} \alpha \\ \beta \end{matrix}\right\}\right)} \left\{ \left[ 2n(\alpha+\beta+1) - \right. \right. \\ &\quad \left. \left. - ({}_hE_{lm\omega} - (\alpha+\beta)(\alpha+\beta+1) + c^2 \mp 2ch) + n(n-1) \right] {}_h\left\{\begin{matrix} a \\ b \end{matrix}\right\}_{n,lm\omega} + \right. \\ &\quad \left. + 2c(c \mp h) {}_h\left\{\begin{matrix} a \\ b \end{matrix}\right\}_{n-1,lm\omega} - c^2 {}_h\left\{\begin{matrix} a \\ b \end{matrix}\right\}_{n-2,lm\omega} \right\}, \quad \forall n \in \mathbb{N} \end{aligned}$$

## Chapter 5

- There is a factor  $u$  missing in the third line of Eq. (5.3.1). It should read

$$\begin{aligned} &u \frac{d^2 {}_hy_{lm\omega}}{du^2} + (2\alpha+1) \frac{d {}_hy_{lm\omega}}{du} - \\ &\quad - \frac{1}{4} \left[ u + 2h - \frac{1}{c} (c^2 - (\alpha+\beta)(\alpha+\beta+1) + {}_hE_{lm\omega}) \right] {}_hy_{lm\omega} - \\ &\quad - \frac{1}{4c} \left[ u^2 \frac{d^2 {}_hy_{lm\omega}}{du^2} + 2(\alpha+\beta+1)u \frac{d {}_hy_{lm\omega}}{du} - \left( \frac{1}{4}u^2 + hu \right) {}_hy_{lm\omega} \right] = 0 \end{aligned}$$

## Chapter 6

- We are using rationalized units (i.e., the Maxwell equations are given by Eq. (2.3.1) and the stress-energy tensor by Eq. (6.1.11)). There is therefore an incorrect factor of  $4\pi$  in Eqs. (6.7.2) and (6.7.4). Furthermore, the derivative sign  $d$  in the numerator of the left hand side of these equations should be a second derivative sign  $d^2$ . These equations should respectively read

$$\begin{aligned} \frac{d^2 E^{(\text{inc})}}{dtd\Omega} &= \frac{r^2}{2} \left| \phi_{-1}^{(\text{in,inc})} \right|^2 \\ \frac{d^2 E^{(\text{ref})}}{dtd\Omega} &= 2r^2 \left| \phi_{+1}^{(\text{in,ref})} \right|^2 \end{aligned}$$

and

$$\frac{d^2 E^{(\text{tra})}}{dt d\Omega} = \frac{\Delta^2}{2(r_+^2 + a^2)} \frac{\omega}{\tilde{\omega}} \left| \phi_{-1}^{(\text{in,tra})} \right|^2$$

- Above Eq. (6.8.7) the spin-weighted spheroidal harmonics should be denoted by  ${}_h Z_{lm\omega}$ , not by  ${}_h S_{lm}$ .
- On Page 214, where it says "Graphs 6.19–6.20 for  $\left\langle \hat{T}_{t_+\phi_+} \right\rangle_{\text{ren}}^{B^-} \dots$ " it should instead say "Graphs 6.19–6.20 for  $\left\langle \hat{T}_{t_+\phi_+} \right\rangle_{\text{ren}}^{CCH^- - B^-} \dots$ ".
- The variable  $B$  in Eq. (6.9.1a) should be  ${}_1 B_{lm\omega}$ .
- The terms ‘positive’ and ‘negative’ referring to the polarization should be swapped everywhere in Section 6.9.3, except for in the very last paragraph and in its corresponding Figs. (6.28)–(6.31). As an example, the fourth paragraph of Section 6.9.3 should start as: "It is in the limit for large  $r$  that the physical meaning of the various vectors becomes clear. We know that in flat space-time an electric field mode of positive frequency that is proportional to the vector  $(\hat{e}_\theta + i\hat{e}_\phi)[(\hat{e}_\theta - i\hat{e}_\phi)]$  possesses a negative[positive] angular momentum and we thus say that it is negatively[positively] polarized.". This is because a time dependence  $e^{+i\omega t}$  is assumed. The reason for this confusion arose because of the non-standard notational change in the sign of  $(m, \omega)$  in Eq. (2.7.13). The sign of  $(m, \omega)$  in the right hand side of Eqs. (6.9.32) and (6.9.33) should be changed so that they read

$$\begin{aligned} {}_{lm\omega P} A'^{\text{up}\mu} &\equiv \left( \Pi_j^{\dagger\alpha} {}_{lm\omega} \varphi_j \right)^* + \Pi_j^{\dagger\alpha} {}_{lm\omega} \varphi_j \rightarrow -\frac{\omega i |N_{+1}^{\text{up}}|}{\sqrt{2}r} \times \\ &\times \left[ {}_{-1} Y_{l-m-\omega+1} R_{l-m-\omega}^{\text{up,tra}} e^{+i\omega(t-r)} (\hat{e}_\theta + i\hat{e}_\phi) - {}_{-1} Y_{l-m-\omega+1}^* R_{l-m-\omega}^{\text{up,tra}*} e^{-i\omega(t-r)} (\hat{e}_\theta - i\hat{e}_\phi) \right] \\ &\quad (r \rightarrow +\infty) \end{aligned}$$

and

$$\begin{aligned}
{}_{lm\omega P}\mathbf{E}^{\text{up}} &= -\nabla {}_{lm\omega P}A'^{\text{up}0} - \frac{\partial {}_{lm\omega P}\mathbf{A}'^{\text{up}}}{\partial t} = \frac{\omega^2 |N_{+1}^{\text{up}}|}{\sqrt{2}r} \times \\
&\times \left[ {}_{-1}Y_{l-m-\omega+1} R_{l-m-\omega}^{\text{up,tra}} e^{+i\omega(t-r)} (\hat{\mathbf{e}}_\theta + i\hat{\mathbf{e}}_\phi) + {}_{-1}Y_{l-m-\omega+1}^* R_{l-m-\omega}^{\text{up,tra}*} e^{-i\omega(t-r)} (\hat{\mathbf{e}}_\theta - i\hat{\mathbf{e}}_\phi) \right] \\
{}_{lm\omega P}\mathbf{B}^{\text{up}} &= \nabla \times {}_{lm\omega P}\mathbf{A}'^{\text{up}} = \frac{-\omega^2 i |N_{+1}^{\text{up}}|}{\sqrt{2}r} \times \\
&\times \left[ {}_{-1}Y_{l-m-\omega+1} R_{l-m-\omega}^{\text{up,tra}} e^{+i\omega(t-r)} (\hat{\mathbf{e}}_\theta + i\hat{\mathbf{e}}_\phi) - {}_{-1}Y_{l-m-\omega+1}^* R_{l-m-\omega}^{\text{up,tra}*} e^{-i\omega(t-r)} (\hat{\mathbf{e}}_\theta - i\hat{\mathbf{e}}_\phi) \right]
\end{aligned}$$

respectively.

## Bibliography

- The year in [54] should be 1988, not 1999.